Spring 1981

Usage and Limitations of Characteristic Vector Analysis of Remote Sensing Multispectral Data for the Identification and Quantification of Water Quality Parameters

Theodore A. Talay
Old Dominion University

USAGE AND LIMITATIONS OF CHARACTERISTIC VECTOR ANALYSIS OF REMOTE SENSING MULTISPECTRAL DATA FOR THE IDENTIFICATION AND QUANTIFICATION OF WATER QUALITY PARAMETERS

by

Theodore A. Talay

B.A.E. June 1967, Rensselaer Polytechnic Institute
M.A.E. February 1970, Rennsselaer Polytechnic Institute

A Dissertation Submitted to the Faculty of
Old Dominion University in Partial Fulfillment of the
Requirements for the Degree of

DOCTOR OF PHILOSOPHY

CIVIL ENGINEERING

OLD DOMINION UNIVERSITY

May 1981

Approved by:

Chin Y. Kuo (Director)

ABSTRACT

USAGE AND LIMITATIONS OF
CHARACTERISTIC VECTOR ANALYSIS OF REMOTE SENSING
MULTISPECTRAL DATA FOR THE IDENTIFICATION
AND QUANTIFICATION OF WATER QUALITY PARAMETERS

Theodore A. Talay
Old Dominion University, 1981
Director: Dr. Chin Y. Kuo

Recent applications of the technique of characteristic vector analysis to remote-sensing water color data has met with varying degrees of success. It is apparent from these experiments that a more thorough understanding of the informational capability of characteristic vector analysis is needed before the technique is applied in general. The objective of this investigation is to examine how characteristic vector analysis resolves total radiance signals measured by a remote sensor into eigenvectors and associated scalar coefficients, and their relationships to the identification and quantification of the in-situ water constituents. To realize this objective, technique operation is checked against a progression of hypothetical test cases and a limited number of laboratory data sets. As a result of this investigation, an improved understanding of technique usage and limitations has been obtained in the areas of optical physics, in terms of constituent-water interactions, and environmental effects, in terms of measurement noise and atmospherics.

Under ideal conditions, characteristic vector analysis has the potential of identifying and quantifying individual constituents in water, even when in mixtures, with a minimum of surface truth data. Exact constituent identification, using characteristic vectors, and quantification, by scaling of scalar coefficients, is possible when the study constituents have a linear radiance-concentration relationship, superimpose linearly in mixtures, and the measured radiance spectra are devoid of measurement noise and atmospheric effects. As these conditions are relaxed, technique limitations and inexact solutions are encountered.

From hypothetical test cases and laboratory data sets, it is concluded that the technique is also applicable for constituents which have a radiance-concentration relationship nonlinearity that is independent of wavelength. For accurate relative quantification in the absence of surface truth data, prior knowledge of the form of the nonlinearity is required. Technique operation on wavelength-dependent nonlinear constituents is inexact and represents a limitation on its proper usage.

It is concluded that nonlinear superposition of constituents in mixtures imposes an additional limitation on the use of the technique in quantifying constituents. Without prior knowledge of the form of the nonlinear superposition process, observed convergence or divergence of calculated scalar coefficients may result in a misinterpretation of constituent concentrations.

From hypothetical test cases, it is concluded that the effects of random noise on technique identification and quantification depend on the degree of random noise, the form of radiance-concentration relationships of constituents and their interactions, and the spectral similarity of constituents in mixtures. True random noise does not affect general constituent identification, but specific sample point identification and quantification are degraded.

Atmospheric interference will affect technique operation unless proper mission planning is used to fix influential variables and minimize their effects on measured signal variability. Even under controlled conditions, a horizontally-homogeneous atmosphere will modify characteristic vectors of constituents but not affect relative quantification provided atmosphere-modified comparison characteristic vectors are used in the analysis. Horizontally-variable atmospheres impose a significant limitation on exact technique operation. Conditions favoring a variable atmosphere such as data collection at high altitudes or for long flight lines should be avoided.

This study demonstrates the usefulness of the technique of characteristic vectors when properly applied to remote-sensing multispectral data. Laboratory testing of constituents of foremost interest in remote sensing is required, however, to determine ones likely to be analyzed successfully using the technique, and those that possess limiting factors concerning wavelength-dependencies, interactions, or spectral similarities to other constituents.

ACKNOWLEDGEMENTS

I wish to acknowledge the aid freely given by a number of individuals that contributed immeasureably to this study. My sincere appreciation goes to the director of my Ph.D. committee, Dr. Chin Y. Kuo, whose sustained interest and encouragement were important driving forces behind this research. In addition, were the helpful suggestions and review by the other members of my committee including Dr. William Drewry, Dr. Robert Cheng, and Dr. George Ofelt. At Langley Research Center, my special thanks go to my immediate supervisor, Dr. Janet Campbell and Mr. Lamont Poole for allowing me to tap their statistical expertise, and Dr. Charles H. Whitlock who provided many helpful suggestions during the course of this investigation. I am especially grateful to my wife, Linda, whose typing skills and patience were critical elements needed for the completion of this effort.

Theodore A. Talay

Norfolk, Virginia

November, 1980

TABLE OF CONTENTS

CHAPTER I

INTRODUCTION

Man and nature both impact the Earth's water environment. Man utilizes lakes, rivers, estuaries, and oceans as sources of water, food, transportation, and recreation. Often, these same waters become a sink for man's wastes as well. By natural processes, also, significant sediment loadings enter these waters. The pollution and sediment loads can seriously affect marine productivity in the coastal waters. Control of pollution and a detailed knowledge of marine productivity require an extensive, effective monitoring system. Conventional in-situ monitoring efforts often are slow, sparse, and costly. Remote sensing has significant advantages over in-situ techniques in monitoring the quality and productivity of inland and coastal waters. Not only are the requirements of personnel, instrumentation, and boats reduced or eliminated, but the broad synoptic coverage of large areas provides considerably more data than could be collected otherwise. With this growth in information capability, however, go the problems of interpreting the remote-sensing data in terms of constituents in the water and their concentrations.

Generally, the use of water quality remote-sensing data has fallen into two broad categories: (1) the identification and classification of water pollutants and features, and (2) the quantification of water quality parameters. In the first instance, a usual approach is to

obtain training sets of spectral signatures based on a priori knowledge of the geographic area, surface truth, or upwelling spectral signatures from laboratory tests. The signatures can then be compared to the remotely-sensed data to spectrally identify pollutants and features for the entire data field. For quantification of water quality parameters, statistical techniques such as regression analysis (in one of many forms) may be used to correlate collected in-situ surface truth measurements of specific parameters and the remotely-sensed spectral data. The developed algorithm, if statistically significant, may then be applied to the entire data field, mapping out the desired parameter concentration.

This dissertation is concerned with the use of characteristic vector analysis applied to multispectral data, a technique which basically can perform both the objectives of identification and quantification, the latter with a minimum of surface truth data. While characteristic vector analysis has been used before in the form of principal components analysis in widely-varying disciplines, it has only recently been applied to the water color problem. Mueller (1973, 1976), Grew (1977a, 1977b), Philpot and Klemas (1979), have applied the technique to ocean color spectra with varying degrees of success. However, it is apparent by these studies, that a more complete understanding of the informational capability of characteristic vector analysis is needed before it is applied in general. Specifically, this study focuses on the characteristic vector analysis technique for resolution of total radiation signals into eigenvectors and associated

scalar coefficients and how these are related to known constituent spectra and constituent concentrations, respectively. A major objective of this study is to examine the optical physics and environmental conditions for which the technique is most applicable in the identification and quantification of water constituents. Test cases, including hypothetical and laboratory experiment data sets, are used to derive and demonstrate the limitations and conditions of applicability.

CHAPTER II

RADIATIVE TRANSFER AND REMOTE SENSORS

Remote sensing of water represents the acquisition of information about water properties from measurements made at a distance. The physical basis of remote sensing lies in the ability to measure the electromagnetic or light variations caused by the absorption and scattering of light by substances dissolved and suspended in water. For this discussion, a solar energy spectrum is considered as input at the top of the atmosphere. The spectrum is modified by the atmosphere before its entry into the water.

The absorption and scattering of light in pure water is wavelength dependent with blue wavelengths of light scattered the most, whereas absorption is dominant in the red and infrared regions of the spectrum. Dissolved sea salts appear to have little effect on these absorption and scattering optical processes (Jerlov 1976). Other dissolved substances, however, may cause considerable changes in water absorption properties. For example, gelbstoffe (yellow substances) and humus compounds in marine waters considerably modify water color. Particulates or suspended materials in highly variable concentrations in water cause an increase in the multiple-scattering processes. Scattering in water

is influenced by the wavelength of the incident light, the particle shapes and particle size distributions, and the refractive index of the particulates (Kuo and Cheng 1976).

The light which is scattered back towards the water surface, the inherent upwelling spectral radiance, is the information-bearing signal of interest, a signal modified by the particular water constituents present. At the atmosphere-water interface a modification of the upwelled signal by the reflectivity and refractive index of the interface occurs resulting in an upwelled water radiance emergent from the water surface as shown in figure 1. While this upwelled radiance contains useful information about the water column, other components, shown in figure 1, act to obscure the signal in its passage or transfer to the altitude of the remote sensor. These include (1) reflected sunlight and skylight from off the water surface, (2) path radiance due to sunlight and skylight scattered into the path of sight between the water surface and the remote sensor, (3) bottom reflected radiance, and (4) a transmission loss through the atmosphere as the upwelled radiance transfers to the altitude of the remote sensor. These components and effects are, in general, a function of wavelength, solar and remote-sensor geometry, atmospheric aerosol composition and distributions, surface reflectances, and sea state.

Passive remote-sensing systems, such as cameras, radiometers, spectrometers, and multispectral scanners measure these modified solar spectra over a scene of interest. Broad-band photographic and radiometer systems measure the spectra over broad ranges of wavelengths

and thus tend to integrate out subtle spectral changes that may relate to changes in water properties. Filters are added to photographic systems for multispectral coverage. Spectrometers add a dispersing element to the radiometer system so that the sensed radiation is measured as a function of wavelength. In laboratory usage, the spectrometer can make very precise spectral measurements over preselected wavelength ranges. Aircraft-mounted, the spectrometer sees only the target towards which it is pointed with the result that radiance spectra are obtained along a line of flight. To obtain data over an area-wide scene of interest, the aircraft must fly staggered, repetitive flight lines to sample the entire scene. To solve this problem, optical-mechanical scanners image the entire scene by scanning perpendicular to the flight path of the aircraft. A scene is formed by the line-by-line build up of data as the flight line progresses. Multispectral scanners are optical-mechanical scanners that measure the upwelling spectra in discrete bands or wavelength ranges. They are widely-used research and application instruments providing the advantages of both narrow band spectral resolution plus wide area spectral coverage. Table 1 lists several multispectral scanner systems now in use or development for both aircraft and satellites along with the wavelength bands used, swath width (total surface width of scan perpendicular to the flight path), and minimum surface resolution element size. The aircraft-mounted scanners (NASA's Ocean Color Scanner, Multichannel Ocean Color Sensor, Test Bed Aircraft Multispectral Scanner, and the Bendix Modular Multispectral Scanner) have been widely used in research

and development work to derive algorithms to extract water property information from the remotely-sensed signals and also to provide reference data to correlate with satellite data during analysis. These aircraft-mounted scanners have good surface resolutions because of the low altitudes at which they are flown. The numerous narrow bands allow for study of spectral changes in the visible and near infrared, characteristic of variable constituent concentrations. The surface swath widths are adequate for lakes, rivers, estuaries, and near coastal-zone feature coverage. For general coastal zone and ocean coverage, however, satellite-mounted multispectral scanners, at higher altitudes (table 1), provide a much larger swath width or spatial coverage.

Although the multispectral scanners on LANDSATS 1, 2, and 3 were not intended for use in water observations due to the low instrument sensitivities and wide bands selected for land use, nonetheless, variations in sediment, chlorophyll, and ocean waste dumps are evident in the imagery. The proposed LANDSAT D multispectral scanner will have somewhat narrower bandwidths and better resolution than the earlier LANDSATS. The Coastal Zone Color Scanner on the Nimbus 7 satellite has a coarser surface resolution (800 m vs. 70 m for LANDSAT) but benefits from a higher spectral resolution (20 nm bandwidths vs. 100 nm for the early LANDSATS), broader swath width, and sensitivities set for the lower reflectances typical of water scenes.

CHAPTER III

DATA INTERPRETATION TECHNIQUES

Before the data acquired by a remote sensor can be utilized in final form in its intended manner by a user agency, it must undergo an analysis procedure. As indicated in figure 2, the analysis procedure involves the preprocessing and interpretation of data in either a photo image or digitized form as acquired, for example, by a camera or multispectral scanner system. The preprocessing step is used to geometrically correct the data and also filter out noise and atmospheric effects. Next, data interpretation techniques are used to take the preprocessed data and convert this into a described image or data product. For data utilization, this may be in the form of maps, tables, histograms, or other statistical representations of the original scene. It is not the objective of this dissertation to detail the available preprocessing techniques or the particular formats of image description. Instead, this section will briefly review some of the more popular data interpretation techniques used to classify and quantify the remotely-sensed data in terms of surface features or properties. Also, the corrections for noise and atmospheric effects will not be considered, at this point, a critical part of the preprocessing, as these components will be studied in later chapters in a sensitivity analysis of the characteristic vector analysis technique.

Aerial photography represents the earliest form of remote sensing. Used originally for mapmaking and reconnaissance purposes, most interpretation was performed manually. This required a degree of sophistication in terms of skills of the photointerpreter in classifying features into similar groupings based on size, shape, texture, shadow and other distinquishing key information. During the 1960's newer photographic methods were utilized to detect and document water pollution. Strandberg (1966) showed for various film/filter combinations, it was possible to record various pollutants entering various water masses. Yost and Wanderoth (1967) described a four band multispectral camera system covering the wavelength range 360 to 980 nm. Representing a four-fold increase in amounts of data to be analyzed, the photointerpretation technique utilized a viewer to produce false color enhancements of subtle reflectance differences in water by color additive techniques. This represented a semi-automatic approach to the interpretation process. James and Burgess (1970) demonstrated the use of the photodensitometer to digitize aerial photographs and produced a computer-generated contour map of ocean outfall waste concentrations. Klooster and Sherz (1973) also digitized image brightness using a densitometer and using a correlation curve between turbidity and image brightness could specify a turbidity value anywhere within the scene.

With the advent of multispectral scanners, such as those listed in table 1, a tremendous growth in the amount of digitized data available nearly precludes any manual interpretation of the data except for the most rudimentary descriptions. For example, each LANDSAT scene contains

over 7 million pixels or picture elements in each of four bands which obviously can only be handled efficiently by computer processing. Because of these vast amounts of data to be analyzed (with spectral, spatial, and sometimes temporal degrees of freedom), most multispectral scanner studies are approached in a statistical manner. Additionally, a computer allows the use of more complex models and higher-order statistical interpretation of the data.

Multispectral Classification Techniques

Much of the multispectral scanner data acquired by aircraft and satellites have been utilized with respect to land use and it is natural to expect the development of statistical techniques adapted to this type of application. The usual requirement is to classify multispectral imagery data into a number of distinct classes or categories. Quantification then consists of determining the area extent of the land use type (e.g., wheat fields, conifer forests, urban developments, etc.) by a product of the total picture elements (pixels) per class and the ground resolution area per pixel. This type of "spatial quantification" is distinct from what is termed quantification in this dissertation - the concentrations of water parameters for single or multiple constituent waters.

Classification algorithms are performed in the supervised or unsupervised modes. In the supervised classification mode, the user designates certain collections of data points as training samples, representative of the classes of interest. The computer is then programmed to classify

unknown data points in the scene to classes according to how close, spectrally, the points come to the designated training sample classes. One major problem of this mode is to obtain training samples truly representative, in a spectral sense, of the classes of interest. In the unsupervised classification mode, no training sample data are used. Instead, a clustering algorithm is used to divide or "cluster" the image elements based on inherent spectral differences, thus forming individual, but unknown, classes. A cluster may exhibit small spectral differences from point to point, but separate class clusters should be well separated. It is up to the user, in the unsupervised mode, to decide whether these class clusters correspond to any features of interest (e.g., wheat fields, forests, clean water, etc.). Often, superfluous classes are generated which may have no interest to the user.

Numerous methods have been developed to classify unknown data points according to the training samples or clusters generated by the above procedures. In figure 3, for example, class data points corresponding to forest, bare soil, and water areas are plotted based on the measured multispectral scanner radiance returns for the two wavelengths or bands X_1 and X_2. It is expected that there are some minor in-class spectral differences resulting in the scatter of data points within classes, but a separation, due to major spectral differences, between classes. An unknown data element, $U(X_1,X_2)$ can be classified by (1) a "nearest neighbor" algorithm - finding the minimum distance from U to the nearest class sample point, (2) the nearest mean vector algorithm - finding the mean value of each class and then classifying

$U(X_1,X_2)$ according to a minimum distance to the nearest mean, and (3) a Gaussian maximum-likelihood classifier which assigns probability density functions to each training set or cluster and assigns unknown elements to the highest probability classes. The maximum-likelihood classifying algorithm has been widely used in Earth resources surveys. A recent study (Scholz et al 1979) indicates that there was little difference in classifications for several data sets among these classification algorithms (and others examined in the study) if the same training sample statistics were used.

In this simple example, and others to follow, only two wavelengths have been used to plot the image elements. As table 1 indicates most multispectral scanners have $n \geq 4$ bands or wavelengths. In general, then, the clusters will exist in an n-dimensional "hyperspace" which cannot be displayed efficiently but may be interpreted by a computer.

More recent interpretation techniques for classification include the use of canonical analysis and principal components analysis (Jenson and Waltz 1979). The objective of canonical analysis is to make the classes or categories as separate as possible while making each individual class or category as homogeneous as possible. Mathematically, this involves maximizing the among-category covariance matrix and minimizing the within-category covariance matrix. Geometrically, canonical analysis represents a rotation, translation, and scaling of the original wavelengths axes to produce new axes to satisfy the above mathematical statement. Figure 4(a) (after Podwysocki et al 1977) shows the mean values (as centerpoints) and density distributions

(depicted by ellipses) of the classes shown in figure 3. Along axis X_1 classes A+C and B+C are separable whereas A+B are not, and along axis X_2 A+B and B+C are separable but A+C are not. Figure 4(b) shows the same clusters after canonical rotation, translation, and scaling of the axes. The previous elliptical density distributions are now spherical because of the axes scaling. The original X_1, X_2 axes are shown only for reference purposes. In the new axes system (Y_1, Y_2) all classes are separable along each axis and one has a maximum separability between the classes. Podwysocki et al (1977) applied this technique to LANDSAT data to discriminate between igneous, metamorphic, and sedimentary rock types. Canonical analysis produced black and white and color pictures with greater spectral separation for some rock types than resulted from using other classification techniques. Although producing enhanced pictures, the authors concluded this technique involved much more work.

Principal components analysis has been more widely used than canonical analysis and more examples are available in the literature. Principal components analysis is a unique transformation belonging to the general class of factor analysis techniques that analyze correlations within a set of variables. This will be explained in more detail later in this chapter. Figure 5 shows, in simple geometric terms, the use of the technique in a two variable system (radiances at two wavelengths or bands as the axes variables).

Radiance values from different spectral bands on multispectral scanners typically exhibit a significant amount of redundancy, that is,

interband correlations. Often, the highest intercorrelations occur with adjacent bands. When plotted in figure 5, a sampling of data points from a multispectral scanner image shows a rather elliptical distribution. If the wavelength bands were totally correlated, the data points would lie along a line but if the bands were totally uncorrelated the data set would form a circular homogeneous pattern. Principal components analysis involves a translation and rotation of the axes (X_1,X_2) to new axes positions (Y_1,Y_2) such that the first axis, Y_1, the first principal component (or first eigenvector direction), lies along the direction of maximum data variance (the major axis of the ellipse). The remaining variance in this two-dimensional case is explained by the second axis, Y_2, or principal component (second eigenvector direction) orthogonal to the first axis, and along the minor axis of the ellipse. The principal components are simply linear compounds of the original wavelengths or bands, but optimized in terms of explaining the observed variance. For an n-band case with the data plotted in "hyperspace," succeeding principal axes explain, in a hierarchial fashion, maximum amounts of remaining variance until all of the original variance is explained. This requires n principal components or eigenvectors for n bands. However, because of redundancy (intercorrelations) between bands, it is usually observed that much less than n principal components or eigenvectors are needed to explain most of the total data variance. Truncating the higher-order principal components, one effectively has compressed nearly all of the data set variance into a few principal components. It is this

property that makes principal components analysis attractive to computer classification studies.

Ready and Wintz (1973) applied the principal component transformation (also known as the Karhunen-Loeve transformation) to six-band aircraft and three-band satellite multispectral data over agricultural land. Results show that for the six-band multispectral data, three principal components contained 97% of the original data variance while for the three-band data case, two principal components contained 93% of the total data variance. Additionally, computer classification of the data into classes using a maximum-likelihood algorithm operating on the first few principal components produced better classification accuracies than using the same number of original spectral bands. Results indicated a higher signal-to-noise (S/N) ratio for the principal components than for the original spectral bands. As a result, images derived from the principal components appeared enhanced with less noise evident.

Algazi (1973) used principal components analysis to reduce the dimensionality of LANDSAT-1 (ERTS-1) multispectral data from four bands to three principal components. The objective was to produce optimum color images by assigning the three principal components to the three primary colors - red, blue, and green, and producing a composite image by juxtaposition of the three subimages. For three different data sets tested, three principal components accounted for more than 99% of the total variance in each of the data sets. The principal components composite image formed showed significantly more detail than a composite image formed by using three of the original spectral bands. An

interesting refinement was to apply principal components analysis separately to land and water within one image. Significantly different principal components were obtained for the two spectral classes.

Taylor (1973) used a principal components analysis for LANDSAT-1 images taken over southern Canada. The final objective was, like Algazi (1973), to map the first three principal components onto a color space for image enhancement. However, Taylor used as color dimensions "brightness," "redness-greenness," and "blueness-yellowness." A significant development was Taylor's suggestion that one need not necessarily limit oneself to the eigenvector directions from a principal components analysis (directions for maximizing explained variance), but one can further "rotate the space in any arbitrary way, to suit particular needs." In particular, one rotation of the axes might optimally display forests, another rotation provide the best discrimination of agricultural lands, etc. This represents an early reference in remote-sensing literature to a "characteristic vector" approach that searches for an underlying structure producing the variance in multispectral data.

Fontanel et al (1975) applied a principal components analysis to a LANDSAT image of southern France. The technique was applied first to all the four-band data directly and second, separately to six classes of data as generated by a Gaussian maximum-likelihood classifier. The first two principal components, in each case, were used to generate a two-color composite image. Results showed that using principal

components analysis after a multispectral classification algorithm produced enhanced details of features not revealed in a conventional application of principal components analysis of the unclassified data.

Murai (1976) performed a principal component analysis of LANDSAT imagery from two different dates over the inland sea of Japan. The analysis showed that the first principal component was associated with turbid water, whereas the second principal component was associated with organic matter in the water. Each principal component was divided into five ranks according to the "scores" of the principal components. These scores may be considered multipliers of the eigenvectors necessary to reconstitute the original data matrix. After forming a twenty-five element matrix of the ranks from the principal components, the author assigned each matrix element to one of five classes of water ranging from very clear to highly polluted. A computer-generated dot map, based on this classification algorithm, was drawn to display the five water classes for the inland sea.

Williams and Borden (1977) subjected multidate LANDSAT imagery of the Washington, DC, area to a principal components analysis. Four-band LANDSAT data from two dates (one spring, one fall) were merged and considered as an eight-band data set. Five principal components explained 99% of the total data variance. Classification accuracies using the transformed data were significantly increased.

Lodwick (1979) also applied a principal components analysis to multidate LANDSAT imagery for a study area in Australia. Performed

separately for each date, the analysis showed two principal components sufficient to explain most of the data variance. Variations of the first principal component, from date to date, were related to variations in solar/land geometries, whereas second principal component variations were related to seasonal-climatic or man-induced effects.

Other varied applications of principal components analysis may be found in the literature. Boland (1976) developed a trophic classification parameter for lakes using principal components; Podwysocki et al (1977) applied the technique for discrimination of rock and soil types using LANDSAT imagery; Santisteban and Munoz (1977) applied the technique in a conventional manner for LANDSAT imagery from central Spain for geological discriminations; and Abotteen (1978) used the technique on multiple LANDSAT imagery to improve agricultural crop classification.

Multispectral Quantification Techniques

The preceding discussion demonstrated a variety of classification techniques developed for multispectral radiance data, mainly for land use situations. In water quality studies, however, the concern is not just in identifying or classifying water quality parameters, but also in estimating their concentrations. Particularly difficult is the problem of two or more constituents coexisting or mixed in water. The resulting observed spectral radiance is some composite signal derived from the individual constituent signals. Many of the classification techniques discussed assign mixture image elements to a class of highest probability or to a catch-all unclassified category.

In the latter case, the concentrations of the individual constituents in the image element are undetermined. Fortunately, other statistical methods exist for handling the mixture problem. One large class of such methods is known as regression analysis.

Regression Analysis

The objective of regression analysis is to optimize simple predetermined relations between parameter concentrations and observed remote-sensing radiance spectra. The usual approach is to correlate, in a least-squares manner, the radiance values from one or more wavelengths (or bands) with the concentrations of a particular water quality parameter measured in-situ (i.e., surface truth measurements). If the regression equation derived is a "good" fit (high correlation, low standard error), the assumption is it can be applied to other points in the remote-sensing image where no surface truth exists to estimate the particular water parameter concentrations. By using color coding or contouring, a computer can be used to map out the concentration levels of the parameter for the entire scene.

Whitlock (1977a) and Whitlock and Kuo (1979) provide a detailed discussion of the use of linear multiple regression analysis for remote-sensing water parameter quantification. The following discussion summarizes this, and other forms of regression analysis.

The usual form of the regression analysis approach is a linear equation of the form:

$$C = \alpha + \sum_{j=1}^{n} \beta_j L_j + \varepsilon \qquad (3\text{-}1)$$

where:

C = water constituent concentration

L = radiance at wavelength (or band) j

α = intercept coefficient

β = regression coefficient at wavelength j

ε = error in the estimation of C

n = maximum number of bands used in the regression

The coefficients α, β_j are determined by a least-squares regression analysis as the best straight-line fit to the measured data. If only one band ($n = 1$) is used in the analysis, the regression is termed linear regression, while for multiple bands ($n > 1$) the regression is termed linear multiple regression. Sometimes a bivariate relationship is more aptly described by a curve. Regression methods for fitting a curve are called curvilinear or polynomial regression (Nie et al 1975) and have the form:

$$C = \alpha + \beta_1 L_j^1 + \beta_2 L_j^2 + \ldots + \beta_d L_j^d + \varepsilon \qquad (3\text{-}2)$$

where:

d = the degree of the polynomial

j = wavelength or band j

The addition of more terms in the polynomial equation will serve to increase the correlation obtained; it is up to the researcher to decide if the added terms are meaningful in a physical sense or just serve well in a particular data set.

In some instances, it is observed that the underlying multivariate relationship takes on forms which are easily restated or transformed into a linear form. For example:

$$C = \alpha + \beta_1(L_1/L_2) + \varepsilon \tag{3-3}$$

$$C = \alpha + \beta_1(e^{L_1}) + \varepsilon \tag{3-4}$$

$$C = \alpha + \beta_1(1/L_1) + \varepsilon \tag{3-5}$$

are all amenable to linear regression analysis if the independent variable is calculated first as stated by the functions in parentheses.

The quantification of water quality constituents by regression analysis of the forms just discussed has been somewhat inconsistent and unreliable from a survey of the literature (Whitlock 1977a). Various reasons exist for this inconsistency including (1) the choice of an incorrect form of the multivariate relationship relating the water parameter concentrations and radiances, (2) surface truth collected at widely-variant times with respect to the remote-sensing overpass (hydraulically inappropriate sampling); surface truth measurements not uniformly dispersed over the range of concentrations in the scene nor sampled in all water mass types within the scene; inconsistent handling and analysis of water samples, (3) remote-sensing data collected at

varying solar-remote sensor geometries, atmospheric conditions, water surface conditions (waves, whitecaps), (4) the presence of unknown water constituents and surface contaminants (oil films, foams), (5) bottom reflections within the scene, (6) unknown vertical concentration gradients in the water column for the parameters of interest, and (7) varying degrees of noise and operating characteristics of different remote sensors.

Acknowledging these inconsistencies and assumptions, researchers still have been able, in some instances, to achieve reasonable intra-scene results. For example, Johnson and Bahn (1977) in a study of the James River, using linear multiple regression analysis, developed expressions for sediment, chlorophyll-a, Secchi depth, inorganic NO_3, inorganic NO_2, acidity, and salinity with correlation coefficients ranging from 0.87 to 0.99 (where 1.00 is total correlation). Maps of constituent concentration levels for the study appeared reasonable.

On the other hand, results to date have demonstrated that regression equations derived for one scene are inappropriate when applied for predictive purposes to interscene images (spatially and temporally independent). Thus, one of the primary requirements of regression analysis is a source of good surface truth measurements from scene to scene for research and development of expressions for an automatic data processing system. For application purposes, however, where the time and expense of collecting such surface truth may be at a premium, the desirable situation would be the instance where little or no surface truth is required and water quality constitutent concentrations

are inferred by operation on the remote-sensing data. This type of analysis has been used in classification studies outlined earlier as principal components analysis. Recently, this factor analysis technique has been applied directly to the study of water color (Mueller 1973, 1976; Grew 1977a, 1977b; Klemas et al 1978a, 1978b; Philpot and Klemas, 1979) for classification and, to some degree, quantification studies.

Characteristic Vector Analysis

Factor analysis is a general term for a variety of procedures developed for the purpose of analyzing the intercorrelations within a set of variables (Cooley 1962). If the objective of the analysis is to extract the maximum variance from a set of responses and perform a data compression, the technique is generally referred to as principal components analysis. In the literature, however, the transformation is variously referred to as the principal-component transformation, Karhunen-Loeve transformation, eigenvector transformation, the Hotelling transformation (Ready and Wintz 1973) and characteristic vector analysis (Simonds 1962). If the objective of the analysis is to search for some underlying structure or variables presumed to have caused the observed variance in the original data set, the technique is referred to by Harman (1967) as multiple-factor analysis. In principle, this search for structure may involve a rotation of the axes defined by a principal-components analysis. Mueller (1973, 1976) and Grew (1977a, 1977b) both address this "search for structure" objective and refer to it as a "characteristic vector analysis." In

order to maintain a consistency in terminology for water-color work, this dissertation uses "characteristic vector analysis" whether or not a rotation of the principal axes is performed. Eigenvectors defined by a principal components transformation, if directly associated with particular inherent structure, are termed characteristic vectors. As Mueller (1976) notes, this use of characteristic vector nomenclature "better connotes the role that these vectors play in characterizing the variational structure of a sample of spectral observations."

Characteristic vector analysis has been used frequently in statistical analysis of multivariate response data. The underlying technique, as principal components analysis, was first developed by Hotelling in 1933 (Harman, 1967) and used in such diverse fields as the optical and photographic sciences (Morris and Morrissey 1954; Simonds 1962; Friederichs and Scarpace 1977), meteorology (Hardy and Walton 1978), soils analysis (Condit 1970, 1972), nearshore bathymetry (Hayden et al 1975), daylight spectral energy (Condit and Grum 1964) in addition to the references cited earlier in this chapter on principal components analysis for classification purposes and water-color studies.

Simonds (1962), cited by many references, presents a particularly good presentation of the characteristic vector analysis method as applied to photographic and optical curve response data. The discussion includes a fully worked out step-by-step numerical example. Simonds' approach is to show that a set of response curves may be represented by a mean curve plus varying proportions of several eigenvectors or

characteristic curves. This means any particular response curve, L_j, may be expressed as:

$$L_j = \bar{L}_j + \sum_{k=1}^{p} Y_k v_{kj} \qquad (3\text{-}6)$$

where:

L_j = jth component of the response vector

$\bar{L}_j$ = jth component of the mean vector of the response curves

v_{kj} = jth component of the kth eigenvector

Y_k = scalar coefficient corresponding to the kth eigenvector

j = 1, 2, ... , n is index of n variables defining the response curves

k = 1, 2, ..., p is index of retained eigenvectors

$p \leq n$ is the number of eigenvectors retained in the analysis.

Depending upon the particular method used to normalize the eigenvectors, the scalar coefficients are variously referred to as the principal component values, scalar multiples or multipliers, weightings or weighting coefficients. Chapter IV considers the normalization methods in more detail.

Mueller (1973, 1976) apparently was the first to apply a characteristic vector analysis directly to the study of ocean-water color. Ocean color spectra were measured off the coast of Oregon using a 55-band spectrometer at wavelengths every five nanometers apart between 422 and 692 nm. A total of 31 of the collected spectra were subjected

to a characteristic vector analysis. Mathematically, 55 eigenvectors would be necessary to explain all the observed data variance if the data in all bands (or wavelengths) were uncorrelated. But, as in the land use applications discussed earlier, interband correlations of the data result in much fewer eigenvectors explaining most of the observed data variance. Mueller found that four eigenvectors were sufficient to explain over 99% of the total data variance and, in fact, only two were needed to explain over 95% of the total sample variance.

Mueller felt that the transparency of sea water may be related to the principal component values, Y_k ($k = 1,2,3,4$), calculated. Linear multiple regression was used to relate Secchi depth and phytoplankton pigment concentrations to the principal components. Results show Secchi depth related to the first two principal components, whereas phytoplankton pigment concentration was related to the first three principal components. The Secchi-depth regression equation was considered satisfactory, but the phytoplankton regression equation was considered poor. Mueller attributed this to a nonlinearity that exists between the phytoplankton concentrations and principal components and neglect of certain other optically important substances in the water. Mueller also cautioned about applying these low-altitude flight results to a higher altitude where atmospheric effects are not negligible.

Other authors also considered the possibility that the scalar coefficients, Y_k, may be related directly to inherent variables or a basic underlying structure causing the observed data set variance.

Hayden et al (1975) studied nearshore bathymetry along the Atlantic and Gulf Coasts of the United States. Bathymetric profiles (running in an offshore direction) from 504 sites were subjected to a characteristic vector analysis. Three eigenvectors accounted for over 95% of the total variance. The scalar coefficients or "weightings" (called scalar multiples by Simonds (1962) and related to the principal component values of Mueller (1973)) from the second and third eigenvectors were plotted versus one another. Four general classes of inshore bar-trough morphology were then defined corresponding to the four quadrants of the weightings plot or "scatter" diagram. Regions of the Atlantic and Gulf Coasts were classified according to where individual profile weighting points fell on this diagram. The important concept developed here was the use of weightings to describe the morphology variations which, after all, represent the cause of the data variance.

Kitchen (1977) applied characteristic vector analysis to particle-size distributions from water samples obtained off the Oregon coast. Particle-size distributions were given as particle counts for each of 12 size classes or intervals. For 263 sample distributions, characteristic vector analysis indicated two eigenvectors sufficient to explain 92% of the data set variance. The "weighting factors" (called scalar multiples by Simonds (1962)) associated with the first two eigenvectors, were related to particulate carbon and chlorophyll-a concentrations by linear multiple regression. Good regression equations resulted leading to the conclusion that large volumes of suspended particulates were due to phytoplankton. This study was significant

in its attempt to directly relate eigenvector weighting factors (obtained from particle size distributions) to constituents of the water samples.

Grew (1977a, 1977b) has demonstrated the most detailed use, to date, of the characteristic vector analysis technique as applied to ocean color spectra obtained from remote-sensing aircraft flights. He also appears to be the only author, in this field, to point out the advantages of an axes rotation to identify water constituents and the possibility that scalar multiple values are related to the water constituent concentrations. Data sets investigated included spectra from algae, sediment, acid waste, sewage sludge, and oil in water. The data sets were collected using a 20-band multispectral scanner (MOCS - see table 1) at an altitude of 5.33 km.

Grew, using an independent "signature extraction" technique, had obtained spectral signatures (radiance spectra) for sediment, algae and acid. The objective of his analysis was to use characteristic vector analysis on flight data obtained off the coast of New Jersey (in the New York Bight area) to match these spectral signatures either directly with, or by a transformation (by axes rotation) of the calculated eigenvectors thereby confirming the constituents' presence in the over-flown water.

A first flight data set of spectra subjected to a characteristic vector analysis, was collected in a region of known variability in chlorophyll-a (found in algae) and turbidity. Two eigenvectors accounted for 97% of the total data set variance. The second eigenvector appeared similar,

spectrally, to the algae spectral signature used for comparison, but the first eigenvector appeared more like a "composite" vector of both algae and sediment. Grew plotted the scalar multiples of these two vectors versus one another (each point on the plot representing a measured spectra) and connected the points together in the order they were collected along the flight line. A pattern emerged which suggested an axes rotation to line up the pattern with the axes. This axis rotation transforms both the scalar multiples and the eigenvectors. After rotation, the first transformed eigenvector, or characteristic vector, matched closely the "sediment" signature derived independently while the second transformed eigenvector appeared as a "composite" signature. Grew demonstrated it was possible to get both the "algae" and "sediment" signatures to appear as transformed vectors if the axes rotation is oblique (axes do not remain orthogonal). Although little surface truth was available, Grew presented graphical evidence to suggest the associated scalar multiples, obtained after this oblique rotation, may be directly related to algae related chlorophyll-a and sediment concentrations. However, this conclusion is complicated by a plot showing "algae" characteristic vectors changing shape over three ranges of chlorophyll-a concentrations. Therefore, it remained a question whether the scalar multiples alone, or in conjunction with varying characteristic vectors for a constituent, are related to the constituent concentrations.

Acid waste dumps were overflown on several occasions. For one data case, confined to one specific dump region, one eigenvector accounted for 99% of the total data variance suggesting that the

associated scalar multiples may be related to acid waste concentrations. Another data case involved several dump regions, presumably acid dumps of differing "ages" (time from dump into the water). A characteristic vector analysis showed two vectors accounting for over 99% of the data variance. Interestingly, when the associated scalar multiples for the two vectors were plotted versus one another, several linear features or "linear clusters" emerged each of which corresponded to separate dump regions. This led to a separate characteristic vector analysis for each dump region independently. The results showed eigenvectors differing for each dump region strongly suggesting the acid waste dumps change spectrally with age of dump. Grew suggested that "care must be taken in selecting algorithms for quantifying the dump" where the dump varies significantly with age.

A separate characteristic vector analysis of an acid dump flown two years earlier than the previous data produced a first eigenvector, or characteristic vector, similar to one found in another of the data sets. This was evidence that, for dumps of about the same age, characteristic vectors are appreciably the same. It is suggested that the scalar multiples for dump regions of a fixed age may quantify the concentrations of the acid waste, but surface truth would be needed for verification.

Other pollutants were also studied. Characteristic vector analysis of a sewage sludge dump showed a vector (after axes rotation) similar to sediment. This suggests that sewage sludge and sediment may be difficult to distinguish. A final data set considered was oil on

water, but this set was complicated by cloud shadows. Nevertheless, a characteristic vector analysis was conducted with the first eigenvector associated with the sunlight-shadow variations (99% of the variance of the data set explained) whereas the second eigenvector was associated with oil spectra variations (0.05% variance explained). The fact that the oil was distinguishable was considered promising.

Grew concluded from his analyses that (1) like Mueller (1973, 1976), ocean color data can be reconstructed from a few eigenvectors, (2) in some cases the eigenvectors, before or after an axes rotation, were similar to those spectral signatures extracted by another technique (algae, sediment, acid waste) and represented "characteristic vectors" of the constituents, (3) "linear clusters" appearing on scalar multiple plots may be associated with a particular constituent or, as in the case of acid waste, differing ages of the acid waste dump, (4) the characteristic vectors differed for acid waste if the ages of the dumps were different (but essentially the same if the ages were the same), (5) the characteristic vectors for "algae" were different over several ranges of concentration of the algae, and (6) quantification of constituents may be possible using associated scalar multiples and/or the shapes of the characteristic vectors for particular concentration ranges.

Recent studies by Klemas et al (1978a, 1978b) and Philpot and Klemas (1979) applied an "eigenvector" analysis to LANDSAT multispectral scanner data. The first studies (Klemas et al 1978a, 1978b) applied the analysis to LANDSAT scenes, from off the Delaware coast, which contained

iron-acid waste, sediment, clouds and clear water targets. Eigenvectors for each of the features were obtained from training sample areas in the images. These eigenvectors then were the characteristic vectors of these classes (but containing atmospheric effects and instrument noise). Classification of all pixels within the LANDSAT scenes was accomplished by a scheme which determined how close individual data points approached each class axis (eigenvector direction) and assigning the pixels to the class of closest approach. Data points were unclassified if they failed to approach any characteristic vector class axis within a preset two or three standard deviations limit about any axis. Results were good in distinguishing between clouds, acid waste, and background water (few pixels were classified as sediment).

Some consideration was given to quantification of individual parameters by defining displacements of points along the characteristic vector directions from a clear water origin, in units of standard deviation along the axis. This principle is analogous to defining the scalar multiple values used by Simonds (1962) and Grew (1977a, 1977b). However no applied results are given.

This study also raised some of the more pressing problems associated with an eigenvector analysis including (1) recognizing in the study that the atmosphere had changed from day-to-day which would require atmospheric corrections to the radiance spectra to account for characteristic vector temporal variations, (2) recognizing that the constituents in water may not have linear radiance-concentration

relationships and (3) recognizing the uncertainty of the classification scheme developed when two or more constituents are mixed in the water column.

Philpot and Klemas (1979) refined the earlier analyses of Klemas et al (1978a, 1978b) and applied the eigenvector classification method to acid waste and sewage sludge plumes in the New York Bight region. Clouds were also present. Results showed characteristic vectors associated with clouds were clearly different than those for sewage sludge and acid waste, but that the sewage sludge and acid waste characteristic vectors were so similar as to be indistinguishable - especially for low concentrations of the constituents in water. Also, there was enough day-to-day variability in the vectors in addition to the spectral similarities as to make a semiautomatic classification system unlikely at present.

Quantification of acid waste based on the LANDSAT imagery was considered in this study by relationship to distances along the acid waste characteristic vector direction referenced to a clear water origin. Such distances were measured in units of standard deviations along the vector. Up to two standard deviations from the clear water origin, low concentrations were presumed to exist, and beyond two standard deviations, data for the acid wastes would correspond to high concentrations. Mapping results showed a gross characterization of the acid waste plume into these two levels of quantification, but no surface truth was available for verification.

Acid-waste dump age was considered (already pointed out by Grew, 1977b) as a cause of characteristic vector variability. The age was related to the settling of the dump particulates into the water column, expressed as a "mean depth." It was hypothesized that while concentrations of a constituent are implied by the displacement distance along a vector direction, the vector direction itself may shift due to a change in the "mean depth" of the constituent (for example, acid waste settling with time). This temporal change would further complicate the classification schemes developed in these studies. This latest study further concludes that there are limits to the spectral separability of substances in water and that random noise may degrade the classification accuracies further.

Considering the cited characteristic vector investigations, it may be concluded that while identification and classification of constituents using characteristic vectors has been demonstrated, the quantification of these constituents has only been inferred in most cases. This is due to (1) the lack of adequate surface truth measurements of constituent concentrations to verify the relations between "scalar multiples" or "principal components distances" and constituent concentrations, and (2) unexplained variabilities in the flight data spectra, not accounted for by constituent concentration variations, but more likely associated with atmospheric variability and instrument noise in the remote sensor. These investigations have also recognized the added problems in interpretation caused by nonlinearity of the constituent radiance-concentration relationship, mixtures of

constituents in water, similarity of spectra from different constituents, and temporal variations in the spectra of individual constituents.

One might expect that these factors, working singly or in combination, may make it difficult to understand the general relationships that exist between characteristic vectors and associated scalar coefficients derived from remote-sensing data and particular constituents and their concentrations that exist in the water. This weakness led the author to approach the problem from a more fundamental analysis viewpoint of determining relationships based on sets of hypothetical data.

Characteristic vector analysis is allowed to operate on ideal data sets (noiseless, no atmospheric effects) of dissimilar and similar hypothetical constituents. The objective is to determine how the scalar coefficients associated with the characteristic vectors for the constituents are related to constituent concentrations for single and multiple constituents in water. The analysis then proceeds to relax the assumptions of linearity of constituents and linear superposition of mixtures of constituents to examine the sensitivity of the scalar coefficient - concentration relations to these changes. A limited number of laboratory tank test results are incorporated in this analysis to help verify the conclusions drawn. Instrument noise and atmospheric effects, as might be found in real data cases, are added in to the hypothetical data sets as a further sensitivity analysis of the scalar coefficient - constituent concentration relationships. The ultimate objective is to examine optical physics (constituent-water interactions)

and environment conditions (noise and atmospherics) for which the characteristic vector analysis technique is most applicable for use.

CHAPTER IV

THEORY OF CHARACTERISTIC VECTOR ANALYSIS

A Geometric Interpretation

In Chapter III it was demonstrated how radiance data measured by a two-band multispectral scanner, $L(X_1,X_2)$, might be interpreted by a principal components analysis. Figure 5 depicted, for data with a degree of interband correlation, a new axes system, (Y_1,Y_2), located by a translation and rotation of the original axes (X_1,X_2). The eigenvector directions, specifying the principal axes (or components), have the unique properties that along the first axis direction, a maximum percentage of the original total data variance is explained, while the second axis, orthogonal to the first, explains any remaining variance.

How is this measured radiance distribution to be interpreted physically? Such a distribution may be associated with the presence of a single constituent (or water quality parameter) in water with spatially variable concentrations. The distribution of the constituent concentrations is, in some manner, related to the distribution of the data along the first principal axis which, in turn, is related to the scalar coefficients associated with the first eigenvector as given in equation (3-6). A major objective of this dissertation is to explore these relationships such that the scalar coefficients may be used to determine constituent concentrations. Data dispersion along the second principal axis assuming a linear radiance-concentration

relationship may be attributed to "noise" from the scanner system or random atmospheric effects over the remote-sensing scene. If these noise and atmospheric effects are initially removed from the data before a principal components analysis, then all the radiance data points would ideally lie along the first principal axis, and the first eigenvector would represent a defining "characteristic vector" for that constituent. All data variance (100%) is explained ideally by the first eigenvector, and no variance remains to be explained by the second eigenvector.

Consider a case of two spatially-independent and spectrally dissimilar constituents in water. With no noise or atmospheric effects present, a two-band plot of the radiance data may appear as shown in figure 6(a). Lines drawn through the data distributions merge at a point representing the spectrum of the background water where both constituent concentrations are zero. Principal components analysis applied to the entire data, collectively, yields the principal axes shown in figure 6(b). The first eigenvector direction explains a maximum amount of data variance which, for this case, lies somewhere between the "directions" suggested by the individual constituent data distributions. The second eigenvector direction, orthogonal to the first, explains the remaining data variance. Neither eigenvector could be considered "characteristic" of either constituent.

One alternative is to apply a principal components analysis to the spectra of the individual data sets, as suggested by examination of figure 6(a). For the situation of two spatially-independent constituents, separate principal components analysis produces the two "characteristic

vectors" as shown in figure 6(c). Each vector explains 100% of the data variance observed for each constituent and these vectors are spectrally dissimilar. Fontanel et al (1975) discovered that detail-enhanced color images resulted for LANDSAT four-band spectral data when principal components analyses were applied to separate class features after a classification algorithm rather than applying the principal components analysis on the collective unclassified data. By obtaining characteristic vectors for each class separately, one maximizes the data variance explained for that feature class and enhances the class detail when displayed in image form.

An alternative exists for obtaining the constituent characteristic vectors from the original principal axes of the collective data set (figure 6(b)). This involves a rotation of the principal axes such that one or the other axis "aligns" in the directions as suggested by the original data distributions. Axis Y_1 would line up with one constituent's data distribution if rotated through an angle θ_1, and axis Y_2 line up with the other constituent's distribution if rotated through an angle θ_2. Certain criteria, however, remain to be developed to determine how these rotations are executed.

Characteristic vector descriptions of single constituent and spatially-independent multiple constituent data sets have been discussed. A more sophisticated problem case is that of multiple constituents that are "spatially-coincident" or are mixed in water. Figure 7(a) represents how such radiance data (measured spectra from background waters, regions of two individual constituents, and regions

of two constituents mixed together in water) might appear on a two-band plot. Figure 7(b) shows the principal axes for the entire data set. The variance explained is partitioned among the two axes directions, with the maximum amount explained, as usual, by the first eigenvector direction. In such a situation, the data distribution does not directly suggest a "simple structure" such as was obtained in figure 6(c). Thus it is uncertain what the orientation of the principal axes means in relation to the constituents. As will be seen in this chapter, however, a search for simple structure may be initiated with a free-rotation of the principal axes.

The concepts developed for a two-band case can be extended to a three-band multispectral scanner. Figure 8(a) depicts how three-band spectral data might appear, each point representing one measured spectrum, $L(X_1,X_2,X_3)$, when plotted in wavelength space. When a degree of intercorrelation between the bands exists, the plotted data appears as an ellipsoidal distribution, with the ellipsoidal axes of differing lengths. A principal components analysis defines three eigenvector directions placing the principal axes in an ordered sequence of decreasing amounts of total variance explained as shown in figure 8(a).

If, as has already been demonstrated for the two-band case, the ellipsoidal distribution of data points represents a single constituent, then, for a linear radiance-concentration relationship, the second and third eigenvector directions may be related to system noise and atmospheric variations. In such an ideal situation, the data appears

distributed along a single characteristic vector direction as shown in figure 8(b).

Interpretation of cases of spatially-independent and mixed constituents in water for the three-band case are analogous to the two-band scanner cases although one works in a wavelength space. Ideal radiance data for spatially-independent constituents and mixtures of two constituents in three-band space are shown respectively as figures 9(a) and 9(b). A principal components analysis produces an orthogonal set of three axes or eigenvectors as shown. Since all radiance data for the two cases lie in a plane defined by the characteristic vectors v_A and v_B (linear, additive mixtures), the first two principal axes lie also in this plane and explain 100% of the observed data variance. In such cases, the third principal axes is superfluous. In n-band space, in fact, the third through nth principal axes become superfluous since no variance remains to be explained. It is noteworthy that, in general, the plane formed by the two constituents and mixture points will lie out-of-plane of any two of the original wavelength axes $(X_1, X_2, \ldots, X_n)$. Rotation angles θ_1 and θ_2 as originally defined in figure 6(b) still apply to the plane of the radiance data, whether it exists in three-band or n-band space.

Extending the analogies to n-band scanner data, when $n > 3$, it becomes difficult to display efficiently "hyperellipsoid" data distributions and principal axes in "hyperspace." It becomes a necessity to utilize high speed computers to calculate and store the required vector-coefficient information when n becomes large.

Characteristic Vector Analysis of n-band Data

Characteristic vector analysis of n-band multispectral scanner radiance data may be considered to proceed in three stages. In stage one, the variance-covariance matrix (henceforth "covariance matrix") for the n-band measured spectra is calculated. In stage two, a principal components analysis operates on this covariance matrix to calculate up to n eigenvalues (or roots) and eigenvectors. Associated with each eigenvector (or principal axis direction) are sets of calculated scalar coefficients necessary to reconstitute the original data matrix. In the third stage, a free-rotation of the principal axes is executed transforming both the eigenvectors and sets of associated scalar coefficients in a search for simple structure, i.e., the characteristic vectors of particular constituents.

Stage 1. - The Covariance Matrix

Consider an aircraft overflying a water scene and measuring upwelling radiance spectra using an n-band (wavelength) multispectral scanner. Within a specific spatial domain, m spectra of the form $L(X_1, X_2, \ldots X_n)$ are collected for analysis. The matrix of spectral data is given by:

$$L = \begin{bmatrix} L_{11} & \cdots & L_{1j} & \cdots & L_{1n} \\ \vdots & & \vdots & & \vdots \\ L_{i1} & \cdots & L_{ij} & & \vdots \\ \vdots & & & & \vdots \\ L_{m1} & \cdots & \cdots & \cdots & L_{mn} \end{bmatrix} \qquad (4\text{-}1)$$

where:

$i = 1,2,\ldots m$ $\quad m$ = total number of spectra

$j = 1,2,\ldots n$ $\quad n$ = total number of bands

A mean spectrum for the data set is formed from columnwise averages of L:

$$\bar{L} = [\bar{L}_1, \bar{L}_2 \ldots\ \bar{L}_j \ldots\ \bar{L}_n] \tag{4-2a}$$

where

$$\bar{L}_j = \frac{1}{m} \sum_{i=1}^{m} L_{ij} \tag{4-2b}$$

Consider the distribution of spectral data points for a three-band scanner as given in figure 8(a). A first step in obtaining the principal axes was the translation of the original wavelength axes to the mean spectrum point. This is accomplished by subtracting the mean spectrum (eq. (4-2a)) from the original spectral data matrix given by equation (4-1). The resulting matrix is referred to as the mean-corrected spectra data matrix, P, given by:

$$P = \begin{bmatrix} L_{11} - \bar{L}_1 \ldots L_{1j} - \bar{L}_j \ldots L_{1n} - \bar{L}_n \\ \vdots \\ L_{i1} - \bar{L}_1 \ldots L_{ij} - \bar{L}_j \\ \vdots \\ L_{m1} - \bar{L}_1 \ldots\ldots\ldots\ldots L_{mn} - \bar{L}_n \end{bmatrix} \tag{4-3a}$$

with individual elements given by:

$$P_{ij} = L_{ij} - \bar{L}_j \tag{4-3b}$$

The variance-covariance matrix, S_X, is formed by premultiplying P by its transpose, P', and dividing by (m-1) as:

$$S_X = \frac{1}{(m-1)} (P'P)_X \tag{4-4}$$

where the subscript X refers to the original wavelength axes system. Performing the indicated operations using equation (4-3a), an $n \times n$ matrix is formed:

$$S_X = \begin{bmatrix} s_{11} & s_{12} & \cdots & s_{1n} \\ s_{21} & s_{22} & \cdots & s_{2n} \\ \cdot & \cdot & & \cdot \\ \cdot & \cdot & & \cdot \\ \cdot & \cdot & & \cdot \\ s_{n1} & s_{n2} & \cdots & s_{nn} \end{bmatrix} \tag{4-5}$$

whose elements are given by:

$$s_{jk} = \frac{1}{(m-1)} (p'p)_{jk} = \frac{1}{(m-1)} \sum_{i=1}^{m} (L_{ij} - \bar{L}_j)(L_{ik} - \bar{L}_k) \tag{4-6}$$

where $(p'p)_{jk}$ are elements of the $(P'P)_X$ matrix.

Along the diagonal, $j = k$, and the variances of the original axes variables $(X_1, X_2, \ldots, X_n)$ are:

$$s_{jj} = \frac{1}{(m-1)} (p'p)_{jj} = \frac{1}{(m-1)} \sum_{i=1}^{m} (L_{ij} - \bar{L}_j)^2 \qquad (4\text{-}7)$$

The $(P'P)_X$ and covariance matrices are symmetric or:

$$(p'p)_{jk} = (p'p)_{kj} \qquad (4\text{-}8)$$

and

$$s_{jk} = s_{kj} \qquad (4\text{-}9)$$

The total data set variance is simply the sum of the diagonal elements of S_X also referred to as the trace (tr) of S_X:

$$\text{tr } S_X = \frac{1}{(m-1)} \text{tr } (P'P)_X = \sum_{j=1}^{n} s_{jj} = \frac{1}{(m-1)} \sum_{j=1}^{n} (p'p)_{jj} \qquad (4\text{-}10)$$

It is useful also to calculate the correlation matrix, R, whose elements are related to the elements of the covariance matrix, S_X, by:

$$r_{ij} = \frac{s_{ij}}{\sqrt{s_{ii}\, s_{jj}}} \qquad (4\text{-}11)$$

The resulting $n \times n$ correlation matrix is symmetric $(r_{ij} = r_{ji})$ and has the form:

$$R = \begin{bmatrix} 1.00 & r_{12} & \cdots & r_{1n} \\ r_{21} & 1.00 & \cdots & r_{2n} \\ \cdot & \cdot & & \cdot \\ \cdot & \cdot & & \cdot \\ r_{n1} & r_{n2} & \cdots & 1.00 \end{bmatrix} \qquad (4\text{-}12)$$

Stage 2. - Principal Components Analysis

As suggested in figure 8(a), once an original set of axes $(X_1, X_2, \ldots, X_n)$ has been translated to the mean spectrum point, a rotation of these axes is performed in hyperspace. The objective is a new set of axes $(Y_1, Y_2, \ldots, Y_n)$, known as the principal axes, which seek to explain, in an ordered sequence, maximum amounts of total data set variance (equation (4-10)). Mathematically, to find the principal axes directions, the eigenvalues and eigenvectors of the covariance matrix, S_X, would at this point be calculated. However, since the $(P'P)_X$ matrix differs from S_X only by a constant factor, (m-1), one can operate directly on this matrix instead. As discussed later, this also has additional benefits in plotting the scalar coefficients. For this dissertation, the eigenvalues and eigenvectors of $(P'P)_X$ are calculated directly from:

$$v_k \, (P'P)_X = \lambda_k \, v_k \qquad (4\text{-}13)$$

where:

v_k = kth eigenvector

λ_k = eigenvalue of the kth eigenvector

$k = 1,2,\ldots,p$

$p \leq n$

The eigenvalues, λ_k, obtained should zero the determinant given by:

$$\left| (P'P)_x - \lambda_k \, I \right| = 0 \qquad (4\text{-}14)$$

where I = the identity matrix.

Appendix C describes an iterative method, used by Simonds (1962), to converge on a sequence of eigenvectors and eigenvalues. As a result of this analysis the $(P'P)_X$ matrix of the original data set is transformed into a $(P'P)_Y$ matrix of the principal components given by:

$$(P'P)_Y = \begin{bmatrix} \lambda_1 & & & 0 \\ & \lambda_2 & & \\ & & \ddots & \\ 0 & & & \lambda_n \end{bmatrix} \qquad (4\text{-}15)$$

where the eigenvalues of $(P'P)_Y$ are ordered such that

$$\lambda_1 > \lambda_2 > \ldots > \lambda_n \tag{4-16}$$

It is noteworthy that in this principal axes system, the interband correlations, r_{ij} $(i \neq j)$, equal zero. Furthermore, the total system data variance is unchanged in the new axes system and is related to the trace of the new $(P'P)_Y$ matrix as:

$$\text{tr } S_X = \frac{1}{(m-1)} \text{tr } (P'P)_Y = \frac{1}{(m-1)} (\lambda_1 + \lambda_2 + \ldots + \lambda_n) \tag{4-17}$$

The percentage of the total system variance explained by the kth eigenvector is given by l_k:

$$l_k = \frac{\lambda_k}{\text{tr } (P'P)_X} \cdot 100 \tag{4-18}$$

The eigenvectors calculated for the matrix $(P'P)_X$ are of the form:

$$v_k = (v_{k1}, v_{k2}, \ldots, v_{kj}, \ldots, v_{kn}) \tag{4-19}$$

Thus, an n-band scanner will yield eigenvectors which have n-components. In principle, one can always calculate up to $k = n$ separate eigenvectors, but because their contributions to the total data set are ordered by the values of the eigenvalues it is usually found that fewer than n vectors are needed to explain most of the data variance

observed. As described earlier, for example, Mueller (1973, 1976) found four eigenvectors ($k = 1,2,3,4$) sufficient to describe over 99% of the total data variance in ocean color spectra using a 55-band spectrometer ($n=55$).

The eigenvectors calculated by a principal components analysis can be normalized in two ways. As presented in Appendix C, Simonds (1962) and Grew (1977a, 1977b) normalize the eigenvectors to the corresponding eigenvalues as:

$$\sum_{j=1}^{n} v_{kj}^2 = \lambda_k \qquad j = 1,2,\ldots,n \tag{4-20}$$

In this system (System I), the vector magnitude is proportional to the data standard deviation $\left(\sigma_k = \sqrt{\frac{\lambda_k}{m-1}}\right)$.

Mueller (1973, 1976), Klemas et al (1978a, 1978b) and Philpot and Klemas (1979) normalize the eigenvectors to unity (System II), or:

$$\sum_{j=1}^{n} v_{kj}^2 = 1 \qquad j = 1,2,\ldots,n \tag{4-21}$$

The eigenvector components in the two systems are related by

$$(v_{kj})_I = \sqrt{\lambda_k}\,(v_{kj})_{II} \tag{4-22}$$

The original data matrix, L, given by equation (4-1) may be reconstituted from:

$$L_{ij} = \bar{L}_j + \sum_{k=1}^{p} Y_{ki} \, v_{kj} \qquad (4\text{-}23)$$

where:

v_{kj} = jth component of kth eigenvector

Y_{ki} = ith spectra scalar coefficient for kth eigenvector

$i = 1,2,\ldots,m$

$j = 1,2,\ldots,n$

$k = 1,2,\ldots,p \qquad p \leq n$

There are sets of m scalar coefficients for each of the p eigenvectors retained in the analysis. In System I (Simonds (1962)) they are calculated from:

$$(Y_{ki})_I = \sum_{j=1}^{n} \frac{(v_{kj})_I}{\lambda_k} P_{ij} \qquad (4\text{-}24a)$$

and have the property (for operations performed on the $(P'P)_X$ matrix),

$$\sum_{i=1}^{m} (Y_{ki})_I^2 = 1 \qquad (4\text{-}24b)$$

whereas in System II (Mueller (1973, 1976)) they are:

$$(Y_{ki})_{II} = \sum_{j=1}^{n} (v_{kj})_{II} P_{ij} \qquad (4\text{-}25a)$$

which have the property,

$$\sum_{i=1}^{m} (Y_{ki})^2_{II} = \lambda_k \qquad (4\text{-}25b)$$

The scalar coefficients in the two systems are related by:

$$(Y_{ki})_I = (Y_{ki})_{II} / \sqrt{\lambda_k} \qquad (4\text{-}26)$$

$(Y_{ki})_{II}$ are referred to as values of the principal components (Mueller (1973, 1976)). Scaled by the square root of the eigenvalues along the principal axes, these principal component values become $(Y_{ki})_I$ and are referred to as scalar multiples by Simonds (1962) and Grew (1977a, 1977b). The scalar multiple system is used in this dissertation because of its clearer display in plotting in cases of constituents with similar spectral characteristics. On the other hand, the eigenvectors scaled to unity (System II) are also used within the analysis to facilitate vector comparisons from data set to data set. Whatever system of scalar coefficients and eigenvectors is used, they yield the same product summation given in equation (4-23).

In summary, a principal components analysis has yielded a set of k principal axes whose directions in n-space are specified by the eigenvectors, v_k. The data variance along the kth eigenvector is related to the eigenvalue by $\lambda_k/(m - 1)$. Scalar coefficients (principal component values or scalar multiples) specify the particular positions of the m spectra data points along these axes. The principal axes are hierarchically ordered in terms of total data variance explained.

Stage 3. - Rotation of Principal Axes

The eigenvectors representing the principal axes provide the most efficient representation of the original data (in terms of variance distribution), but as Simonds (1962) notes, there is "no certainty that there will be a simple relationship between the vector data and the underlying causal variables of the situation." Initially, one must assume that, as figure 6 suggests, there is a characteristic vector for each of the water constituents producing variance in the data set. These vectors, uniquely oriented in n-space, are <u>not</u>, in general, equal to the principal axes eigenvectors. The suggestion is that the principal axes be rotated, in some manner, to search for these characteristic vectors. Once the variance-maximization criteria of principal components analysis are abandoned, an infinite number of alternative sets of new axes (linear combinations of the original axes) are available for use by rotational transformations.

Consider a situation where two constituents determine an observed distribution. Under ideal, noisefree conditions, two eigenvectors corresponding to two principal axes explain 100% of the total variance. In such a case, equation (4-23) becomes (with $p = 2$) for wavelength j of a spectrum:

$$L_j = \bar{L}_j + Y_1 v_{1j} + Y_2 v_{2j} \tag{4-27}$$

and

$$l_1 + l_2 = 100\%$$

If the principal axes are rotated rigidly through an angle θ, then equation (4-27) becomes:

$$L_j = \bar{L}_j + Y_1' v_{1j}' + Y_2' v_{2j}' \tag{4-28}$$

where the vector components, v_{kj}', and scalar coefficients, Y_k', in the new axes system are related to those values in the old system by (Harman (1967)):

$$\begin{aligned} v_{1j}' &= v_{1j} \cos\theta + v_{2j} \sin\theta \\ v_{2j}' &= -v_{1j} \sin\theta + v_{2j} \cos\theta \end{aligned} \tag{4-29}$$

and similarly,

$$Y_1' = Y_1 \cos\theta + Y_2 \sin\theta$$
$$Y_2' = -Y_1 \sin\theta + Y_2 \cos\theta \qquad (4\text{-}30)$$

One may easily verify that the products of the vectors and coefficients are equal in each system,

$$Y_1' v_1' + Y_2' v_2' = Y_1 v_1 + Y_2 v_2 \qquad (4\text{-}31)$$

by substituting equations (4-29), (4-30) into equation (4-31) and using the identity $\cos^2\theta + \sin^2\theta = 1$.

Figure 9 showed how the principal axes might appear for an ideal two-constituent data case. It is evident that the characteristic vectors for these constituents are not orthogonal. In fact, the more similar the spectra of these constituents become, the more closely these characteristic vectors approach each other's direction in space. In general, no single rotation of orthogonal axes through a single angle θ will align transformed principal axes (Y_1', Y_2') along <u>both</u> data distribution directions. An oblique transformation (included angle between axes, ϕ) of the principal axes to accomplish such an alignment is suggested. It is not evident, however, that the oblique angle, ϕ, between axes will be known beforehand.

An alternative to the oblique axes transformation is the successive use of orthogonal axes transformations. For the general case of two constituents with nonorthogonal characteristic vectors, two rigid rotations of the principal axes are executed. Axes (Y_1,Y_2) are rotated through angle θ_1 to produce transformed axes (Y_1',Y_2') where the transformed eigenvector, v_1', for axis Y_1' is aligned along the characteristic vector direction of the first constituent, v_A. A second rotation through angle θ_2 produces transformed axes (Y_1'',Y_2'') where the transformed eigenvector, v_2'', for axis Y_2'' is aligned along the characteristic vector direction of the second constituent, v_B. Simple geometry shows the oblique axis angle, ϕ, related to these rotations, given by:

$$\phi = 90^\circ + (\theta_2 - \theta_1) \tag{4-32}$$

Once the characteristic vector directions have been isolated, the rotation angles θ_1 and θ_2 are known. A direct transformation of the scalar coefficients from the principal axes system, Y_1 and Y_2, into the oblique axes system of the characteristic vectors, Y_1',Y_2'', is possible using the transformation equations:

$$Y_1' = \frac{1}{\cos(\theta_1 - \theta_2)} [Y_1 \cos\theta_2 + Y_2 \sin\theta_2] \tag{4-33}$$

and,

$$Y_2'' = \frac{1}{\cos(\theta_1 - \theta_2)} [-Y_1 \sin \theta_1 + Y_2 \cos \theta_1] \qquad (4\text{-}34)$$

This method of transformation is used in this dissertation. The exact criteria, with examples, for rotating through angles θ_1 and θ_2 are considered in Chapter V.

One may proceed to examine a case where three constituents (causal variables) determine the radiance distribution in a data set. For linear, additive constituents with a noisefree environment, the original data spectra may be reconstituted exactly from:

$$L_j = \bar{L}_j + Y_1 v_{1j} + Y_2 v_{2j} + Y_3 v_{3j} \qquad (4\text{-}35)$$

In n-band space, all principal axes beyond the first three are superfluous as all data variance is explained by the first three axes. Consider three-band space. One can rotate the three principal axes rigidly through space to a new orientation that attempts to explain an inherent structure rather than maximization of variance. For the final orientation:

$$L_j = \bar{L}_j + Y_1' v_{1j}' + Y_2' v_{2j}' + Y_3' v_{3j}' \qquad (4\text{-}36)$$

The rotations necessary to transform the eigenvectors and scalar coefficients as

$$(v_{1j}, v_{2j}, v_{3j}) \rightarrow (v'_{1j}, v'_{2j}, v'_{3j})$$

and (4-37)

$$(Y_1, Y_2, Y_3) \rightarrow (Y'_1, Y'_2, Y'_3)$$

are more complex than the planar case just presented. Harman (1967) discusses the problem and shows that for three or more dimensions, one can rotate any pair of axes while holding the other axes fixed. To reach a final orientation in three-dimensional space requires three successive planar transformations and, in principle, the total transformation is a product of the three planar transformations. In matrix form, one may express this transformation as:

$$T = T_1 \cdot T_2 \cdot T_3 \qquad (4\text{-}38)$$

where each orthogonal matrix on the right is an $n \times n$ identity matrix except for the matrix components given by:

$$t_{ii} = \cos \theta_{ij}$$

$$t_{ji} = \sin \theta_{ij} \qquad (4\text{-}39)$$

$$t_{ij} = -\sin \theta_{ij}$$

$$t_{jj} = \cos \theta_{ij}$$

where θ_{ij} is the angle through which axes i and j are rotated. The order of rotation is important. Thus one should rotate axes pair (Y_1,Y_2) through angle θ_{12}, transformed axes (Y_1',Y_3') through angle θ_{13}, and transformed axes (Y_2'',Y_3'') through angle θ_{23}. The result is a new orientation in space with transformed axes (Y_1''',Y_2''',Y_3''').

As with the two-constituent case, however, the real data distributions may suggest that the three causal variables constituting the data variance observed as represented in three-band space by three nonorthogonal characteristic vectors. No final orientation of transformed orthogonal axes will determine these vectors simultaneously. Computers allow for a high-speed "search" for the proper orientation of each of these nonorthogonal vectors, or axes, using the principal axes as a starting point. Three orientation angles are necessary to define each of the transformed axes. In principle, these angles can be used to directly transform the scalar coefficients from the principal axes system directly into the nonorthogonal system, similar to the two-dimensional transformations developed in equations (4-33) and (4-34).

The preceeding arguments may be extended to n-band hyperspace for radiance distributions caused by up to n constituents. However, the transformations into orthogonal or nonorthogonal characteristic vector hyperspaces become complex. In the interest of brevity, this dissertation is confined to situations of one and two constituents in water. Demonstrative three constituent cases are presented, however, where applicable.

This chapter has presented the three-stage calculations necessary to isolate constituent characteristic vectors and the coordinate systems that the vectors define based on the rotational transformation of principal axes. The next chapter introduces several hypothetical constituents used throughout the remainder of this study. Characteristic vector analysis will be applied to these constituents under certain assumptions of constituent linearity and noisefree environment. The relationship between the constituent concentrations and transformed scalar coefficients are a primary objective of this analysis.

CHAPTER V

ADDITIVE, LINEAR IDEAL CONSTITUENTS

To understand the consequences of applying characteristic vector analysis to actual remote-sensing radiance data, an isolation-sensitivity procedure is followed. Characteristic vector analysis is applied to ideal model constituents considered to be free (or isolated) from all atmospheric and sensor system noise effects. The model constituents have an upwell radiance-concentration relationship which varies in a linear manner. Upwell radiance from individual constituents mixed in water are additive, i.e., superimpose linearly with water and with each other in mixtures. Later chapters investigate the sensitivities of the characteristic vector analysis results as the additive, linear, ideal assumptions are relaxed.

Hypothetical Constituents

The model used for linear constituents has the form:

$$L_{ij} = B_j + M_j C_i \qquad (5\text{-}1)$$

where:

L_{ij} = upwell radiance for jth wavelength (band) of ith spectral curve

B_j = base water radiance for jth wavelength

M_j = proportionality constant for jth wavelength (band)

C_i = constituent concentration in water corresponding to ith spectral curve

The base water spectrum, B_j, is, in general, variable with wavelength. It may be a spectrum for pure water, or represent water with several constituents which do not vary over the scene of interest. As long as $B(\lambda)$ superimposes linearly with variable constituent spectra, it may be subtracted out to yield base-water corrected spectra. In general, M also is a function of wavelength. Although the choice of $M(\lambda)$ is arbitrary, simple functions reduce computational complexities and aid in computer program debugging. The choices for $M(\lambda)$ included a half-sine and full-sine wave with a wavelength range of 400 to 1000 nanometers (nm) to encompass most of the ranges of the scanners presented in table 1. While a normalized or nondimensional wavelength scale could have been used, it was decided to relate as such as possible to real world operations. The "shape factors" used were:

$$M_{\substack{\text{half} \\ \text{sine}}}(\lambda) = .2 \sin \left[\frac{\pi}{600} (\lambda - \lambda_o)\right] \tag{5-2}$$

and

$$M_{\substack{\text{full} \\ \text{sine}}}(\lambda) = .2 \sin \left[\frac{2\pi}{600} (\lambda - \lambda_o)\right] \tag{5-3}$$

where

λ = wavelength (nm)

λ_o = phase difference (nm)

When λ_o = 400 nm, both forms start at zero at λ = 400 nm. Constituent A was defined as the half sine wave when λ_o = 400 nm, and constituent B, the full sine wave when λ_o = 400 nm. Base-water corrected spectral curves for both constituents are given by:

$$L_{Ai}(\lambda) = .2 \sin \left[\frac{\pi}{600} (\lambda - 400)\right] C_{Ai} \qquad (5\text{-}4)$$

and

$$L_{Bi}(\lambda) = .2 \sin \left[\frac{2\pi}{600} (\lambda - 400)\right] C_{Bi} \qquad (5\text{-}5)$$

Consider the concentrations given by $C_A = C_B$ = (0, 10, 20, 30, 40) where the units are arbitrary. Figure 10 shows the resultant base-water corrected radiance spectra for these two constituents. Constituent A is not unlike the radiance spectra for some sediment types tested in a series of water tank experiments by Whitlock et al (1977a). Such sediment spectra show peak radiance values in midrange wavelengths whereas the radiances fall off at the low and high ends of the investigated wavelength range. Constituent B has characteristics of an algae or phytoplankton spectrum, including reflective and absorbtive ranges of wavelengths, and a hinge point (null point) (Duntley et al (1974)) which is insensitive to concentration changes. Constituent C is reserved for any variations in constituents A and B

that incorporate a phase difference ($\lambda_o > 400$ nm). When ($\lambda_o = 450$ nm), the half-sine wave is displaced by 50 nm to the right as shown in figure 11 representing a linear constituent with radiance distributions in water very similar to constituent A.

Individual Constituents

A characteristic vector analysis computer program was applied to the base-water corrected constituents A, B, and C, considering each five-spectra family (m=5), shown in figures 10 and 11 individually. Radiance data were input at nine wavelengths (n=9) every 50 nm for 500 nm $\leq \lambda \leq$ 900 nm. Although many more wavelengths could have been used, it was felt nine were sufficient to define general curve shapes and keep the matrix operations simple. Table 2 presents spectra for a number of cases presented in this chapter. For the individual constituent cases, spectra sets (1, 6, 7, 8, 9), (1, 2, 3, 4, 5), and (26, 27, 28, 29, 30) were used for constituents A, B, and C, respectively. Table 3 are the correlation matrices (eqs. (4-11) and (4-12)) for the three constituents. For this linear model, there are total interband correlations for all bands ($r_{ij} = \pm 1.000$).

The mean spectra, $\overline{L}$, defined by equations (4-2), for the three constituents are presented in table 4 and as figure 12(a). The figure curves represent extrapolations and interpolations of the nine-wavelength calculations. The mean spectra are shapewise similar to the family of curves from which they were derived. As discussed earlier a base or background water spectra has been subtracted out of all spectra.

If present, this spectrum would appear as added to all these mean spectra curves. Only one eigenvector ($k = 1$) is required to explain 100% of the total data variance for each constituent. This is because there are no noise or atmospheric effects present to scatter the data (a geometric interpretation is fig. 8 extended to a nine-band hyperspace). The nine-band first eigenvectors for each constituent are listed in table 4 for the vectors normalized to the eigenvalues (System I), and normalized to unity (System II). Figure 12(b) presents the vectors normalized to unity. It comes as no surprise that the vectors for A and C look like half-sine waves, and the vector for B looks like a full-sine wave. The base-water corrected spectral families are characterized by these vectors. The vectors explain all the observed data variation and are in the direction of the line of the data distributions in nine-band space. Henceforth, they are referred to as the characteristic vectors for the constituents, v_A, v_B, v_C.

Consider the scalar coefficients defined by equations (4-24) or (4-25). As suggested by equation (4-23), when added to the mean spectra, the product of the scalar coefficients and characteristic vectors will reconstitute the constituent spectral families. Combining equations (5-1) and (4-23) for a single constituent (e.g., constituent A) one obtains:

$$L_{Aij} = B_j + M_j C_{Ai} = \bar{L}_{Aj} + Y_{Ai} v_{Aj} \qquad (5\text{-}6)$$

Rearranging, one obtains:

$$Y_{Ai} = a_j + b_j C_{Ai} \qquad (5\text{-}7)$$

where:

$$a_j = (B_j - \bar{L}_{Aj}) / v_{Aj}$$

$$b_j = M_j / v_{Aj}$$

For ideal, linear, additive constituents, a_j and b_j are independent of wavelength. Thus, the scalar coefficients are indeed linearly related to the constituent concentrations. This is a fundamental argument - that the scalar coefficients may be used to determine the original concentrations. In actual practice, a_j and b_j would be unknowns. This would require a minimum of two surface truth samples to establish the absolute quantification relationship between scalar coefficients and constituent concentrations. Relative quantification, however, may be accomplished for linear constituents without surface truth. From equation (5-7) it is evident that a concentration increment $\Delta C = C_2 - C_1$ and a scalar coefficient increment $\Delta Y = Y_2 - Y_1$ are directly related by

$$\Delta Y = b \, \Delta C \qquad (5\text{-}8)$$

Table 5 presents the scalar coefficients (scalar multiples - System I, principal component values - System II) which, combined with the vectors presented in table 4, reconstitute the half-sine and full-sine wave constituent families. The linear relationship between the constituent concentrations and scalar coefficients is obvious as are the proportional increments.

A region of water where spectra for a variable constituent have been collected can be transformed into a scalar coefficient map. Without using surface truth, from equations (5-7) and (5-8), a map of such scalar coefficients, contoured at fixed ΔY increments, reveals (a) the regions of relative high and low constituent concentrations, (b) that the distance gradients of the scalar coefficients, $\Delta Y/\Delta X$ where ΔX = distance between contour levels, indicates regions of large or small concentration gradients, and (c) that the shapes formed by the contour lines of the scalar coefficients are directly related to the pattern of constituent concentrations in the water.

It is useful, when a base water exists in the scene of data, to scale the scalar coefficients for relative quantification. For the base water spectra, where the constituent concentration is zero $(C_A = 0)$, using equation (5-7)

$$Y_A(C_A = 0) = a \qquad (5\text{-}9)$$

where a is constant for linear constituents. This scalar coefficient value, corresponding to a zero concentration of the constituent, is

subtracted from the set of calculated values and the result divided by the range of the scalar coefficients

$$h_i = \frac{Y_{Ai} - Y_A(C_A = 0)}{\text{range } Y_{Ai}} \tag{5-10}$$

This will henceforth be referred to as "linear scaling" of the scalar coefficients. Using the scalar multiple values, $(Y_{Ai})_I$, from table 5 as an example:

Concentration A (arbitrary units)	$(Y_{Ai})_I$	h_i
0	-0.632	0.00
10	-0.316	0.25
20	0.000	0.50
30	0.316	0.75
40	0.632	1.00

where:

$(Y_A(C_A = 0)) = -0.632$

range $(Y_{Ai})_I = 1.264$

The use of scaled, scalar coefficients for relative quantification is especially useful in contour plotting quantification levels in a scene of data. As noted by equations (4-24b) and (4-25b), in System I the sum of the squares of the scalar multiples is unity, whereas in System II, the sum of the squares of the principal component values is

the eigenvalue. The eigenvalues calculated for these examples were $(\lambda_1)_A = 234.641$, $(\lambda_1)_B = 220.000$, $(\lambda_1)_C = 227.321$, which may be used with the coefficients in table 5 to confirm these properties.

In summary, for an ideal, linear constituent spectral family, a characteristic vector analysis confirms that one eigenvector is sufficient to explain all observed data variance in the spectra. This eigenvector (first principal axis direction), or characteristic vector, is shapewise similar to the base-water corrected constituent spectral signature. The scalar coefficients associated with the vector are directly proportional to the original constituent concentrations. Any base-water spectrum added influences only the mean spectra calculations.

Spatially-Independent Constituents

Consider a situation where constituents A, B, and C have been dumped in an ocean waste disposal area by several ships in the form of three line dumps as shown in figure 13. An aircraft-mounted remote sensor is flown over the scene collecting radiance spectra which, for this discussion, are noisefree with no atmospheric effects. Over the background ocean waters all spectra are constant, representing a base water that may be subtracted from all collected spectra, to yield zero radiance spectra over the background waters, and base-water corrected spectra over the line dumps.

Two flight lines are shown, D - D' and E - E', crossing pairs of line dumps A and B, A and C. Generally, as a line dump is overflown, one observes spectra corresponding to increasing concentrations of the

line dump constituent approaching the center of the plume, and spectra corresponding to decreasing concentrations as the sensor passes the center (Ohlhorst 1979). The spectral shapes measured for the three plumes are all different. Consider using only the collected spectra represented by the following concentration data matrices:

C_A

C_B or C_C	0	10	20	30	40
0	x	x	x	x	x
10	x				
20	x				
30	x				
40	x				

where:

x indicates a measured spectrum

C_A, C_B, C_C = concentrations for constituents A, B, C (arbitrary units)

Repeated spectra, missing spectra, or spectra for intermediate concentrations are not considered presently. For flight line D - D' there are nine collected spectra numbers (1 - 9) from table 2. For flight line E - E', the nine collected spectra for constituents A and C correspond to spectra numbers (6 - 9, 26 - 30) from table 2. These two cases, of nine spectral curves each, were input to the characteristic

vector analysis program. Table 6 shows the interband correlations for each combination of spectra. Constituents A and B were chosen to be dissimilar in spectral characteristics, whereas constituents A and C were considered similar. This is confirmed by the significantly higher interband correlations observed for A and C compared to those for A and B.

Results of the analyses conducted are presented as figures 14 through 17. Figure 14(a) shows the mean vector for the spectra set of constituents A and B. It represents a weighted average of the mean vectors for constituents A and B presented in figure 12(a). The two unit eigenvectors, v_1 and v_2, shown in figure 14(b), describe the directions in nine-band space for the first two principal axes. These vectors account for 100% of the total data set variance. The two eigenvalues and percentage of total variance described by each eigenvector (eq. (4-18)) are:

Constituents A and B

$\lambda_1 = 682.209$ $\quad l_1 = 79.441\%$

$\lambda_2 = 176.558$ $\quad l_2 = 20.559\%$

Neither eigenvector, v_1 or v_2, correspond to the characteristic vectors, v_A or v_B, given as figure 12(b). Figure 15 presents the scalar coefficients (the scalar multiples in (a) and the principal component values in (b)). Two linear features are present, converged at the zero base-water spectrum, and directly proportional to the concentration of each constituent noted on the figures.

Figures 16 and 17 present, respectively, the mean vector, two eigenvectors, and associated scalar coefficients for constituents A and C. In this case, the two eigenvalues and percentage of variance explained by each eigenvector are:

Constituents A and C

$\lambda_1 = 356.023$ $\quad l_1 = 96.500\%$

$\lambda_2 = 12.914$ $\quad l_2 = 3.500\%$

Constituents A and C are spectrally more similar than constituents A and B. The mean vector, for example, as a weighted average of the mean vectors $\overline{L}_A$ and $\overline{L}_C$, in figure 12(a), also appears as a half-sine wave, peaking at 725 nm, midway between the mean vector maximums of the individual constituents. The characteristic vectors for constituents A and C, v_A and v_C, are oriented very nearly in the same direction in hyperspace with data variance along these directions. The first principal axis eigenvector, v_1, aligns in much this same direction and explains 96.5% of the total data variance. Its shape, given as figure 16(b), is similar, but not identical to either v_A or v_C. By characteristic vector analysis, v_2 is defined as orthogonal to v_1. This second principal axis eigenvector points in a hyperspace direction much different than v_A or v_C explaining why its shape in figure 16(b) is very much unlike v_A and v_C and accounts for only the 3.5% of remaining data set variance.

The scalar multiples (fig. 17(a)) for constituents A and C plot very much like those for A and B. Presented as principal component

values, however, in figure 17(b), the spectra similarity results in a narrow "V" plot with small included angle, consistent with the characteristic vector directions in space. In mixture situations, discussed later, one has many spectra points plotted within this narrow field making graphical interpretation difficult. Also, the axes scales vary widely from case to case. Although either scalar coefficient system is valid for use, for visual clarity in plots, the scalar multiple system is primarily used in succeeding discussions. Transformation to the principal component value system is always possible using equation (4-26).

In neither of the cases just presented did the principal axes eigenvectors calculated correspond exactly to the individual constituent characteristic vectors. The search for structure is accomplished by the multiple use of orthogonal axes transformations suggested in Chapter IV and utilizing equations (4-29), (4-30), (4-33) and (4-34). Consider the case of two spatially-independent constituents, say A and B. Since v_A and v_B are not, in general, orthogonal whereas v_1 and v_2 must be, two rotations through angles θ_1 and θ_2 are necessary. The general procedure is to:

(1) rotate through angle θ_1 such that the transformed first principal axis eigenvector is the same as the characteristic vector for one of the constituents, i.e., $v_1' = v_A$ or $v_1' = v_B$;

(2) perform a rotation through angle θ_2 (based on the original axes position) such that the second principal axis eigenvector is the same as the characteristic vector for the remaining constituent, i.e., $v_2'' = v_B$ or $v_2'' = v_A$;

(3) use equations (4-33) and (4-34) to directly transform the scalar coefficients (Y_{1i}, Y_{2i}) into the oblique system (Y'_{1i}, Y''_{2i}). For ideal hypothetical constituents the vector comparisons will be exact, but under less-than-ideal conditions the comparisons are only approximate. The criteria used to decide when $v'_1 \rightarrow v_A$ (or v_B) and $v''_2 \rightarrow v_B$ (or v_A) optimally is a least squares for the n-wavelengths used. For example,

$$\min \sum_{j=1}^{n} (v'_{1j} - v_{Aj})^2 \quad \text{infers} \quad \theta_1 \tag{5-11}$$

$$\min \sum_{j=1}^{n} (v''_{2j} - v_{Bj})^2 \quad \text{infers} \quad \theta_2 \tag{5-12}$$

These minimums are zero under ideal conditions. These criteria are used in all succeeding analyses in this dissertation. The following point should be made at this time. A strong case is being presented for the necessity of acquiring characteristic vectors for use as comparison vectors. Whereas in regression analysis surface truth is compared to collected spectra, in characteristic vector analysis a priori comparison (characteristic) vectors are used to identify water constituents. This suggests an extensive laboratory or field test program to build up a catalog, cr library so to speak, of such comparison vectors.

However, once this is done, relative quantifications can be attempted without the need of extensive surface truth.

The procedures just developed are applied to the case of spatially-independent constituents A and C considered previously. Using equations (4-29) and (4-30), figure 18(a) shows the principal axes eigenvectors of figure 16(b) after a rotation of $\theta_1 = -27.9°$. As seen in figure 17(a), this brings the scalar multiple axis, Y_1, into alignment with the data distribution of constituent C. This is indicated by the equality of the v_1' (transformed) eigenvector with the characteristic vector v_C. It should be noted that v_2' (transformed) eigenvector is not equal to characteristic vector v_A. If now, the original principal axes are rotated through $\theta_2 = -63.9°$, figure 18(b) shows v_2'' conforms exactly to v_A, and in figure 17(a), the scalar multiples axis, Y_2, aligns in the direction of the data distribution of constituent A. With θ_1 and θ_2 known, the scalar multiples may be transformed into the oblique axes system (Y_1', Y_2'') by equations (4-33) and (4-34). Figure 19 shows the oblique axes space as defined relative to original scalar multiple space and after transformation into the oblique axes system. It is evident that one has lines of constant transformed scalar multiples. Equation (4-27), which may be written as

$$L_{ij} = \bar{L}_j + Y_{1i} v_{1j} + Y_{2i} v_{2j} \qquad (5\text{-}13)$$

is transformed into:

$$L_{ij} = \bar{L}_j + Y'_{1i} v_{Cj} + Y''_{2i} v_{Aj} \tag{5-14}$$

Equation (5-1) can be written as, for constituent A,

$$L_{ij} = B_j + M_{Aj} C_{Ai} \tag{5-15}$$

For the spectra of constituent A alone ($C_C = 0$), Y'_{1i} is a constant value from figure 19(b). Combining equations (5-14) and (5-15) and rearranging:

$$C_{Ai} = \frac{(\bar{L}_j - B_j - Y'_{1i} v_{Cj})}{M_{Aj}} + \frac{v_{Aj} Y''_{2i}}{M_{Aj}} \tag{5-16}$$

which has the form of:

$$C_{Ai} = a_j + b_j Y''_{2i} \tag{5-17}$$

Trial case calculations involving linear constituents show the functions a_j, b_j to be constants indicating constituent A concentrations are directly proportional to the transformed scalar multiples, Y''_{2i}. A similar line of derivation results in a linear expression relating C_{Ci} to Y'_{1i}.

For spatially-independent constituents A and B, a rotation of $\theta_1 = 61.7°$ produced $v_1' = v_A$ and aligned the Y_1 axis along the line of data for constituent A (fig. 15(a)). A second rotation of $\theta_2 = 25.7°$ showed $v_2'' = v_B$ with the Y_2 axis aligned along the constituent B line of data (fig. 15(a)).

A case was considered where all three line dumps in figure 13 were considered overflown in one flight line. Thirteen spectra (1-9, 27-30) for constituents A, B, and C were input to the characteristic vector analysis program. As expected, three eigenvectors were found to explain 100% of the observed data variance. The eigenvalues and percentage of variance explained by each eigenvector were:

Constituents A, B and C

$\lambda_1 = 1024.244$	$l_1 = 82.804\%$
$\lambda_2 = 212.035$	$l_2 = 17.142\%$
$\lambda_3 = 0.666$	$l_3 = 0.054\%$

From a principal axes viewpoint, the third eigenvector contributes little to explaining the data variance (99.946% explained by the first two eigenvectors). However, there is a danger here in concluding that two significant eigenvectors implies only two constituents originally formed the data set. In fact, three constituents are present, as evidenced by the small, but finite, third eigenvalue which must also be considered significant. If the scalar multiples corresponding to the three eigenvectors for this case are plotted in (Y_1, Y_2, Y_3) space,

the data distributions shown in figure 20(a) are obtained. Three lines of data, converged at the base water spectrum are obtained. Clearly, this is evidence of the three constituents comprising the data set. Equation (4-35) describes the reconstitution of the original spectra from these multiples, three eigenvectors, and a mean spectrum. As for the two-constituent examples, this three-constituent scalar multiple plot suggests an oblique axes system, whose axes are parallel to the lines of data shown. Under these conditions the calculated eigenvectors are transformed equal to the characteristic vectors for constituents A, B, and C. Chapter IV discussed the procedure of multiple, successive orthogonal transformations to determine the orientations angles $(\theta_{12},\theta_{13},\theta_{23})$ for each axis. The transformations are not considered here.

It is interesting to plot the scalar multiples projected on the various axes planes as shown in figures 20(b), 20(c) and 20(d). The three lines of multiples corresponding to the three constituents are evident, but are more clearly separated in some plots than others. Grew (1977b) used a characteristic vector analysis on flight data taken over four distinct acid-waste dump areas. While two eigenvectors accounted for 99.7% of the total data variance, a plot of scalar multiples for these first two "significant" eigenvectors showed four "linear cluster" features. The conclusion was to perform a characteristic vector analysis of each dump region separately to produce a different characteristic vector for each region. The analysis developed in this dissertation shows that the percentage of variance

explained by the first few significant eigenvectors is not necessarily an indication of the number of individual constituents determining the data set variation and, indeed, a full-dimensional plot of scalar multiples (or a full series of plots in two or three dimensions if working in hyperspace) may be necessary to isolate all of the linear data features.

Other cases of spatially-independent constituents were considered in the analysis. New constituents were formed by varying the phase difference λ_o in equations (5-2) and (5-3) over a range of values and also changing the range of concentrations used to calculate the spectra (e.g., equations (5-4) and (5-5)). Spectra for pairs of constituents (constituent A and a new constituent) were subjected to a characteristic vector analysis. Space does not permit a presentation of the individual results. Although individual case results varied in terms of characteristic vectors (for new constituents), principal axes eigenvectors, and scalar coefficients, the procedures and observations developed in Chapter IV and this section were consistent and applicable in all cases.

In summary, for spatially-independent ideal constituents, a characteristic vector analysis calculates principal axes eigenvectors equal in number to all spectrally different constituent families present. The high percentage of variance explained by the first few eigenvectors may give a false impression of the number of actual constituents producing the data set variation, especially if some of

these constituents are spectrally similar. Multiple orthogonal axes rotations can be used to isolate the characteristic vectors of the constituents with the rotation angles obtained used to perform an oblique transformation of scalar multiples, producing a parametric set of curves relating constituent concentrations to transformed scalar multiple values.

Mixtures of Constituents

A mixture occurs when two or more constituents coexist in the same water mass. In this section, constituent mixtures are formulated from exact, hypothetical, single-constituent data sets assuming (1) a linear variation of radiance with concentration for any constituent and (2) linear superposition of radiances (i.e., additive constituents) for mixtures of these constituents. The latter is based on the assumption that there are no physical, chemical, electrical, or other types of interactions or shadowing effects that preclude such superpositions. The objective of a characteristic vector analysis is to isolate the individual constituents in the mixture and quantify their concentrations on a relative basis.

Table 2 presented spectra for individual constituents A, B, and C analyzed for individual and spatially-independent cases. Also in table 2 are spectra for mixtures of constituents A + B (spectra 10-25) for the indicated concentrations. Tables 7 and 8 present mixture spectra for constituents A + C and A + B + C, respectively. Any of the spectra from these tables can be obtained from

$$L_i(\lambda) = 0.2 \sin\left[\frac{\pi}{600}(\lambda - 400)\right] C_{Ai}$$

$$+ 0.2 \sin\left[\frac{2\pi}{600}(\lambda - 400)\right] C_{Bi}$$

$$+ 0.2 \sin\left[\frac{\pi}{600}(\lambda - 450)\right] C_{Ci} \qquad (5\text{-}18)$$

by choosing a set of input concentrations (C_A, C_B, C_C) and the defining wavelengths (in these cases nine wavelengths between 500 and 900 nm).

For constituents A + B in mixtures, a characteristic vector analysis was performed on sets of 13, 17, 21 and 25 spectra (spectra numbers 1 through 13, 1 through 17, 1 through 21, 1 through 25, respectively in table 2). The input matrices of corresponding mixture concentrations (C_A, C_B) where $C_C = 0$ were:

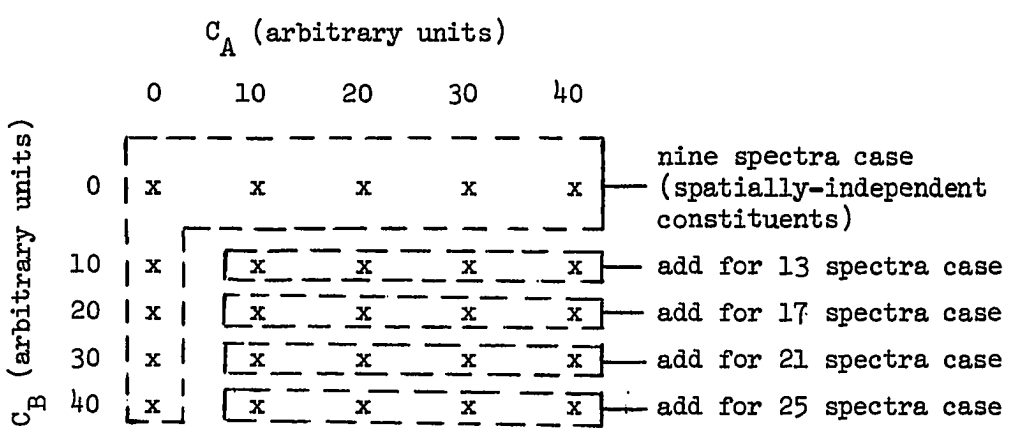

The added spectra for each succeeding case represents variable C_A with C_B held constant. A "complete" data matrix exists with 25 spectra with no "holes" (or missing spectra) in the matrix. For the 13-spectra case, two eigenvectors accounted for 100% of the total data variance with a breakdown of eigenvalues and percentages of variance explained by each eigenvector as:

Constituents A + B

(13-spectra)

$\lambda_1 = 845.866 \qquad l_1 = 76.745\%$

$\lambda_2 = 256.315 \qquad l_2 = 23.255\%$

Table 9 presents the mean vector and normalized principal axes eigenvectors. Characteristic vectors for constituents A and B are listed for comparison. As for the spatially-independent cases, for the mixture neither principal axis eigenvector equals either characteristic vector. Separate rotational transformations yield the results in table 9 where rotations through $\theta_1 = 48.0°$ gives $v_1' = v_A$ and $\theta_2 = 18.6°$ gives $v_2'' = v_B$. This demonstrates that the two constituents used to derive the data set spectra have been isolated. Figure 21(a) shows the scalar multiples before transformation with the rotation angles θ_1 and θ_2 labeled. Comparison of this figure with that for the 9-spectra set (fig. 15(a)) indicates the addition of a line of points corresponding to $C_B = 10$ units, $C_A = 10$, 20, 30, and 40 units. Transformation of the scalar multiples using equations (4-33) and (4-34) into the oblique axis system is shown as figure 21(b). The concentrations for

any mixture point (C_A, C_B) can be found from the intersection of scalar multiple lines representing lines of constant concentrations.

Similar results are obtained for the 17, 21, and 25 spectra cases. Two eigenvectors explain 100% of the data variance in each case. For brevity, figure 22 presents only the untransformed scalar multiples for these cases. It is evident that linear patterns of scalar multiples are added analogous to the manner by which the input concentrations matrices were formed. Rotation of the principal axes through the angles θ_1, θ_2 given in figure 22 isolated the characteristic vectors v_A and v_B in each instance.

For analysis of similar constituents A + C in mixtures, the same steps as for constituents A + B were followed with cases of 13, 17, 21, and 25 spectra analyzed as given by table 7. Figure 23 presents the untransformed scalar multiples for these cases. Once again there is a line-by-line buildup of scalar multiples as the concentration matrix is completed. The scalar multiple points are uniformly spaced analogous to the uniform spacing of the concentrations. Rotation of the principal axes through angles θ_1 and θ_2 given in figure 23 isolated characteristic vectors v_A and v_C in all cases.

Other cases were considered as for the spatially-independent constituents where constituent A was combined with new constituents formed by utilizing phase differences in the half-sine and full-sine waves. Changes in the ranges of constituents were also considered. Although individual cases varied in particular values of eigenvalues, eigenvectors and scalar multiples, the method of analysis remained

unchanged and two eigenvectors accounted for 100% of data variance for two-constituent mixtures. Rotation through two angles θ_1, θ_2 isolated the characteristic vectors for the constituents of the mixtures.

A single case of three constituents in a mixture was analyzed by characteristic vectors. Table 8 lists the input spectra used corresponding to three concentrations (C_A, C_B, C_C) of 0, 20, and 40 units in all possible combinations. The larger concentration increment was selected to limit the number of input spectra (27 spectra) for conciseness in reporting and clarity in display. Figure 24 shows the untransformed scalar multiplies for this data set in (Y_1, Y_2, Y_3) space. The pattern created is consistent with the pattern of constituent concentrations used to create the spectra.

A final test of the vector analysis procedures was to operate on a data set where the ranges of the two-constituent concentrations were different, the increments in concentrations varied, there were repeated spectra (caused by repeated concentration pairs) and missing spectra (caused by holes in the input concentrations matrix). A realistic example is depicted in figure 25 showing two line dumps, of constituents A and B crossing each other. The line dump for constituent B is symmetric about the midpoint but the line dump for constituent A is asymmetric about its highest concentration (as might be caused by wind shear). An aircraft makes two passes over the plumes using a line spectrometer collecting spectra at the points indicated between the on-off points for the spectrometer. A total of 30 spectra are collected, with the concentrations input matrix given by:

C_A (arbitrary units)

C_B (arbitrary units)	0	5	10	15	20	25
0	1,2,3,13, 14,15,16, 17,28,29,30	4	5,18		19	20
10	12,27			6	21	
20	11,26			22	7	
30	25		10,23			8
40		24			9	

The numbers refer to the spectra positions along the flight lines. It is evident that many base water spectra were collected (zero concentrations of A and B), with several other repeated concentration pairs and many missing pairs in the matrix. Table 10 lists the input spectra for this data set in the order of hypothetical collection. A characteristic vector analysis produced the scalar multiple plot of figure 26(a). The multiples have a much more random appearance. Repeated spectra appear as repeated scalar multiple points on the plot. The spectra numbers corresponding to points along the flight line are labeled. As with all previous cases discussed, the user has a choice of whether to obtain v_1' equal to v_A or v_B, and v_2'' equal to v_B or v_A through transformation. Two sets of applicable rotation angles (θ_1,θ_2) are possible. For this analysis, $v_1' \rightarrow v_A$ and $v_2'' \rightarrow v_B$

are desired. A rotation of $\theta_1 = 78.2^\circ$ produced a transformed first principal axis eigenvector, v_1', equal to the characteristic vector for constituent A. A second rotation of $\theta_2 = 238.9^\circ$ produced a transformed second principal axis eigenvector, v_2'', equal to the characteristic vector for constituent B. Transforming the original scalar multiples from (Y_{1i},Y_{2i}) to (Y_{1i}',Y_{2i}'') using equations (4-33) and (4-34), results in figure 26(b). In this system, lines of equal concentrations are parallel to either axis. For reference purposes, these lines of constant concentrations of C_A or C_B have been labeled on the figure although without surface truth they would not be known beforehand. Concentrations for any mixture point are the values of the intersecting constant concentration lines. Figure 27(a) shows the actual variation along the two flight lines of the concentrations of A and B with the spectra number a measure of distance along the flight path. With a base water present, the transformed scalar multiples (Y_{1i}',Y_{2i}'') were scaled by subtracting the scalar multiples corresponding to $C_A = 0$ or $C_C = 0$ and dividing by the range of each transformed scalar multiple set, a method discussed earlier in this chapter for producing scaled, scalar coefficients, (equation (5-10)). The results are plotted as figure 27(b). In a relative sense the variations of $h_i(Y_1')$ and $h_i(Y_2'')$ reproduce the variations in C_A and C_B exactly. This fact is a critical demonstration of the utility of characteristic vector analysis in not just isolating the constituents, but describing their concentrations and gradients along the flight path in a relative manner. In general, surface truth measurements are

needed to adjust the scales of $h_i(Y_1')$ and $h_i(Y_2'')$ to read in concentration units. Since a base water is present in this example, then only one more surface truth measurement of finite C_A and C_B is necessary to scale the coefficients to depict concentrations.

In summary, for mixtures of ideal constituents where linear superposition is assumed, a characteristic vector analysis calculates principal axes eigenvectors equal in number to the number of constituents comprising the mixtures. Multiple, orthogonal axes rotations are used to isolate the characteristic vectors of the constituents and the rotation angles used to perform an oblique transformation of the scalar multiples, producing transformed values directly related to the constituent concentrations.

This chapter has demonstrated how a vector analysis may be expected to operate under ideal conditions for hypothetical constituents. The succeeding chapters relax these ideal assumptions one-by-one to examine the sensitivities of the analysis to less-than-ideal conditions encountered in real world operations.

CHAPTER VI

NONLINEAR CONSTITUENTS

Up to this point it has been assumed that the radiance-concentration relationship for constituents in water is linear, i.e.,

$$L_i(\lambda) = B(\lambda) + M(\lambda)\, C_i \qquad (6\text{-}1)$$

where the base-water spectrum, $B(\lambda)$, could be, and has been subtracted out of the relationship for hypothetical constituent studies. The function $M(\lambda)$, as presented in previous hypothetical cases, clearly need not be a constant and may be any function of wavelength, λ. A first approximation to nonlinear behavior of the radiance-concentration relationship can be given as,

$$L_i(\lambda) = B(\lambda) + M(\lambda)\, C_i^p \qquad (6\text{-}2)$$

where p is any constant power, independent of wavelength. For such behavior, the terminology "simple nonlinear" will be applied to the constituents. Nonlinear behavior of a constituent is depicted in figure 28(a) which shows normalized radiance for Rhodamine WT dye mixed in varying concentrations in water at $\lambda = 660$ nm (Whitlock 1977a). Large radiance gradients at low concentrations and small radiance gradients at high concentrations are indicative of powers, $p < 1$. Whitlock (1977a) estimated $p = 0.2$ for Rhodamine WT dye at this wavelength. A reverse behavior, shown by figure 28(b), occurs when

$p > 1$. Figure 29(a) shows constituent A spectra for the linear case ($p = 1.0$) and for simple nonlinear behavior $p = 0.5$ and $p = 1.5$ in figures 29(b) and 29(c), respectively. Equation (5-4) was suitably modified by inclusion of a power term p to calculate these spectra.

A more sophisticated and general relation can be written as,

$$L_i(\lambda) = B(\lambda) + M(\lambda)\, C_i^{p(\lambda)} \qquad (6\text{-}3)$$

where the power, p, is wavelength dependent. Figure 29(d), for example, shows spectra for constituent A where $p(\lambda)$ varies linearly from 0.5 to 1.0 as λ increases from 500 to 900 nm. The spectra shape are changing as evidenced by the peak radiance shifting towards higher wavelengths for higher concentrations. Constituents whose radiance-concentration relationship follow equation (6-3) are referred to as "wavelength-dependent nonlinear constituents." In the models presented the base water superimposes linearly for all concentrations of the constituent. This need not be the case, and nonlinear superposition with a base water certainly can explain a constituent's apparent nonlinear behavior. The proposed models, however, lump all such nonlinear superposition behavior with base water into the concentration function. The term "nonlinear superposition" is reserved for instances involving mixtures of two or more variable constituents.

A study was conducted to examine how well the model functions (eqs. (6-1), (6-2), (6-3)) approximated real constituent spectral

families, and in the process determine the wavelength dependency, if any, of the power, p. Series of spectra for various constituents were obtained from previous tests conducted in the Marine Upwelled Spectral Signatures Laboratory at the NASA Langley Research Center. In this laboratory facility, constituents are mixed in a 3000-gallon water tank and illuminated by a Xenon lamp solar simulation light source. A spectrometer mounted above the water surface measures upwell radiance spectra in the 380 to 980 nm range. A filtering-deionization system assures a consistent base water for all tests and a circulation system maintains constituent materials in suspension. Some of the constituents tested in this facility along with the concentrations for which spectra were measured and the reference in which the data has been reported include:

Constituent	Concentrations Tested (ppm)	Reference
Primary sewage sludge	(0,4,17,34,69,80)	Usry et al 1977
Secondary sewage sludge	(0,10,39,78,155,180)	Witte et al 1977
Calvert soil	(0,4,17,34,69,86,129,173)	Whitlock et al 1977b
Ball soil	(4,17,34,69,86,129,173)	
Jordan soil	(0,4,17,34,69,86,129,173)	
Feldspar soil	(0,4,17,34,69,86,129)	
Bermuda Hundred sediments	(0,4,17,25,52,86,173)	Whitlock et al 1978
Bailey Bay sediments	(4,86,173)	
Shell Co. Industrial Biosolid sludge	(0,7,18,28,39,62,85,117)	Usry et al 1979
American Cyanamid waste	(0,7,10,17,23,26,28)	Witte et al 1979

Additional details of the test facility, individual experiments and the actual spectra data may be found in the references cited. The spectra were reported both in terms of radiances and normalized as reflectances. Reflectance values are used in this study. Although repetitive tests would ideally be needed to confirm the tested spectra, the following analysis conveys the general utility of the models proposed and estimates ranges of the powers $p(\lambda)$ for a variety of constituents.

A regression analysis was conducted, fitting the spectral data for each constituent to the general model

$$\rho(\lambda) = \rho_o(\lambda) + M(\lambda)\, C^{p(\lambda)} \tag{6-4a}$$

where reflectances are used and the base water reflectance, $\rho_o(\lambda)$, appears in all the spectra. The method involves choosing an initial value of p and redefining the concentrations by

$$\hat{C} = C^p \tag{6-4b}$$

At a fixed wavelength, linear regression was performed between the reflectance values, ρ, and redefined concentrations $\hat{C}$. The value of p was then incremented and the process repeated. The best regression fit, and best choice of power p, was the one which correctly matched the predicted base water reflectance, ρ_o, to the actual value. In the absence of an actual base water curve for comparison (Ball soil and

Bailey Bay constituents), the power p which gave the highest correlation coefficient r was accepted. This analysis was applied to all the spectral families previously listed on a wavelength-by-wavelength basis every 40 nm for 420 to 980 nm. The correlation coefficients (a measure of fit) obtained for the linear regression for all wavelengths and constituents ranged from 0.947 to 1.000 although most were 0.980 and higher. The lower correlation coefficients generally were in the wavelength range 780 to 980 nm where the Xenon lamp source characteristics led to difficulties in precisely obtaining reflectances. However, the overall high correlation coefficients suggest that the proposed model (in the general wavelength-dependent form) reproduces real world constituent spectral behavior well.

Figure 30 shows the powers $p(\lambda)$ obtained in this analysis for the various constituents. No constituents exhibit a strictly linear ($p = 1.0$) or simple nonlinear (p = constant not equal to 1.0) behavior but some constituents approximate this behavior better than others. For example, the primary and secondary sewage sludge, Jordan soil and Shell Company biosolid waste have only a weak wavelength dependency while other constituents such as Calvert soil, Bermuda Hundred and Bailey Bay sediments, and the American Cyanamid waste are notably wavelength-dependent in terms of the radiance-concentration relationship. The powers of most constituents, p, fall between 0.4 and 1.0, with the notable exception of the American Cyanamid waste ($p > 1.0$). The behavior of Feldspar between 740 to 860 nm is suspect and may be related to the Xenon lamp characteristics.

In summary, the study indicates that the models of nonlinear radiance (or reflectance)-concentration behavior proposed are a realistic approach to actual constituents and may be used to formulate hypothetical constituents for study by characteristic vector analysis.

Simple Nonlinear Constituents and Mixtures

The half-sine and full-sine wave test constituents A, B, C are modified to appear as simple nonlinear constituents by,

$$L_{Ai}(\lambda) = 0.2 \sin\left[\frac{\pi}{600}(\lambda - 400)\right] C_{Ai}^{p} \qquad (6\text{-}5)$$

$$L_{Bi}(\lambda) = 0.2 \sin\left[\frac{2\pi}{600}(\lambda - 400)\right] C_{Bi}^{p} \qquad (6\text{-}6)$$

$$L_{Ci}(\lambda) = 0.2 \sin\left[\frac{\pi}{600}(\lambda - 450)\right] C_{Ci}^{p} \qquad (6\text{-}7)$$

Mixtures are formed by a linear superposition of these simple nonlinear constituents. Characteristic vector analyses of individual constituents, spatially-independent constituents and mixtures of constituents were performed as in Chapter V except nonlinear powers $p = 0.5$ and 1.5 were used to formulate constituent spectra from equations (6-5) through (6-7). These powers were chosen as representative of those observed in the study on real constituents presented in figure 30.

For individual simple nonlinear constituents, table 11 presents the spectra for constituents A, B, and C using a power of $p = 0.5$ for concentrations 0, 10, 20, 30, 40 arbitrary units. Figure 29(b)

depicted such spectra for constituent A as an example. Characteristic vector analysis gives the mean vectors and normalized characteristic vectors presented in the table. A similar analysis using a power $p = 1.5$ is presented in table 12, with figure 29(c) as an example of constituent A. In all cases, a single eigenvector (hence, characteristic vector) continues to explain 100% of the total observed variance even though the constituents are simple nonlinear. Comparison with table 4, the linear case where $p = 1.0$, indicates a magnitude change in the mean vectors for the spectral families but, the normalized characteristic vectors for the constituents are unchanged. This indicates, geometrically, these unit vectors continue to point in the same characteristic directions in n-band space even when the constituents have become simple nonlinear. Table 13 shows the variation of the calculated scalar multiples (Y_A, Y_B, Y_C) versus the original input concentrations (C_A, C_B, C_C) for the individual constituents. Figure 31 shows these to be nonlinear relations. For arguments similar to those used to derive equation (5-7), but using the simple nonlinear constituent relation (6-2) substituted in place of the linear relation (5-1), one obtains for constituent A as an example,

$$Y_{Ai} = a + b\, C_{Ai}^{p} \qquad (6\text{-}8)$$

where a and b remain defined by equations (5-7) and are independent of wavelength. Consider a pair of scalar multiple values (Y_{A1}, Y_{A2})

and corresponding concentrations (C_{A1}, C_{A2}). From equation (6-8) differencing yields

$$\Delta Y_A = (Y_{A2} - Y_{A1}) = b\,(C_{A2}^p - C_{A1}^p) \tag{6-9}$$

The scalar multiple increment (as may be used in a contour mapping process) is no longer proportional to a concentration increment as for the linear case (eq. (5-8)) and relative quantification and interpretation is confused. However, equation (6-8) may be rewritten as

$$f(Y_{Ai}) = (Y_{Ai} - a)^{1/p} = b^{1/p}\, C_{Ai};\quad b > 0 \tag{6-10}$$

and

$$f(Y_{Ai}) = (a - Y_{Ai})^{1/p} = (-b)^{1/p}\, C_{Ai};\quad b < 0$$

and a differencing yields

$$(Y_{A2} - a)^{1/p} - (Y_{A1} - a)^{1/p} = b^{1/p}\,(C_{A2} - C_{A1});\quad b > 0 \tag{6-11}$$

and

$$(a - Y_{A2})^{1/p} - (a - Y_{A1})^{1/p} = (-b)^{1/p}\,(C_{A2} - C_{A1});\quad b < 0$$

These two equations suggest that the concentrations and concentration increments are proportional to scalar multiple functions. However, the value of a is unknown (the value of b is not required to prove

proportionality and p is presumed known from tank tests when the constituent is identified). A solution is to provide a surface truth point in the form of a base water where the constituent concentration is, by definition, zero. From equation (6-8) this yields for $C_A = 0$,

$$Y_A(C_A = 0) = a \tag{6-12}$$

which specifies the required value of a in equations (6-10) and (6-11). The transformation given by equations (6-10) and (6-12) was applied to the values in table 13 and then normalized by the range of the values as suggested in Chapter V. This is defined to be "simple nonlinear scaling." The transformation produces scalar multiple functions and increments proportional to the original concentrations as desired. For relative quantification contour mapping of simple nonlinear constituents the transformations using equations (6-10) through (6-12) are required. When a base water spectrum is not provided in the data set, no solution exists for single constituent relative quantification other than to provide two surface truth measurements to determine constants a and b in equations (6-10) and (6-11). This, however, is sufficient for absolute quantification provided the power, p, is known. In this regard, relative quantification is more restrictive for simple nonlinear constituents than in the linear case.

Characteristic vector analysis of spatially-independent constituents A and B was considered next (spectra formed using equation (6-5) with $C_A = 0, 10, 20, 30, 40$ plus spectra formed using equation (6-6)

with C_B = 10, 20, 30, 40). Powers of $p = 0.5$ and 1.5 were studied. In both instances, the calculated mean vectors and principal axes eigenvectors were different than those calculated for the linear case (fig. 14). However, 100% of the data variance continued to be explained by two eigenvectors. Figure 32(a) and (b) show the scalar multiples, Y_2 versus Y_1, corresponding to the simple nonlinear input spectra. The patterns formed by the scalar multiples are linear (and converged at the base water point) just as for the linear case in figure 15(a), even though the concentration variations are not. The nonlinearity, instead, shows up in the displacements of points along these scalar multiple lines with closer spacing towards the higher concentrations when $p = 0.5$ and the reverse true for $p = 1.5$. For $p = 0.5$, rotation angles $\theta_1 = 67.3°$ and $\theta_2 = 21.0°$ produce $v_1' = v_A$ and $v_2'' = v_B$, whereas for $p = 1.5$ these angles are $\theta_1 = 57.5°$ and $\theta_2 = 29.1°$. These angles are different than for the linear case since the principal axes eigenvectors were different in each case, but the chief interest here is the fact that the constituents were identified by the proper rotations θ_1, θ_2. The usual transformations into an oblique axes system (eqs. (4-33) and (4-34)) yield the transformed scalar multiples in figures 32(c) (for $p = 0.5$) and 32(d) (for $p = 1.5$). Finally, equations (6-10) and (6-12) were used to transform the scalar multiples into functions which are proportional to the original concentrations. The results are shown as figures 32(e) and 32(f).

Characteristic vector analysis of mixtures of constituents A + B was appraised. Spectra were formulated by linear superposition of

equations (6-5) and (6-6). The 13, 17, and 21 spectra cases originally considered in Chapter V are not discussed in the interest of brevity. Constituent concentrations for both A and B were 0, 10, 20, 30, 40 arbitrary units which in all possible combinations led to 25 calculated spectra (table 2, spectra numbers 1 through 25, shows the constituent concentration pair possibilities). Simple nonlinear powers $p = 0.5$ and $p = 1.5$ were again considered. As for the linear constituents example, all of the data set variance is explained by two eigenvectors. The rotation angles necessary to isolate the characteristic vectors for constituents A and B are $\theta_1 = 0°$ and $\theta_2 = 180°$ yielding $v_1' = v_A$ and $v_2'' = v_B$ for the cases of $p = 0.5$ and $p = 1.5$, the same as for the linear case. The patterns of the scalar multiples are the main interest and given as figure 33 for the two powers considered. Representative concentration pairs (C_A, C_B) are labeled. While the scalar multiples form straight lines, as in the linear case presented as figure 22(c), basic changes in the patterns are evident for lines of constant concentrations due to the variable displacements of individual points along the plot lines. Although the concentration increments were chosen equal, with a power of $p = 0.5$ the scalar multiple increments are larger at the low concentrations of A and B than at the high concentrations. For fixed amounts of noise for all spectra, the increased separation would suggest less interpretation error corresponding to these low concentration spectra. The situation is reversed in figure 33(b) for $p = 1.5$ where larger increments exist for the higher concentrations. No biasing is expected as $p \to 1.0$,

the linear case. This subject is investigated further in the noise analysis of Chapter VIII.

Clearly, it is possible to transform the scalar multiples using equations (4-33) and (4-34) where $\theta_1 = 0°$ and $\theta_2 = 180°$ and then calculate normalized functional forms using equations (6-10) and (6-12) as shown previously for the spatially-independent constituents. Further case studies involving constituents A + C and A + B show the same general features and are, for brevity, not presented here. However, to test the concepts developed for simple nonlinear constituents, the flight "experiment" developed in Chapter V (fig. 25) was utilized. The same constituent concentrations were used, however, the constituents were changed to simple nonlinear. Mixed powers were used in this example where $p = 0.2$ for constituent A and $p = 2.0$ for constituent B. Mixture spectra were formed from

$$L_{A+B}(\lambda) = 0.2 \sin\left[\frac{\pi}{600}(\lambda - 400)\right] C_A^{0.2} + 0.0002 \sin\left[\frac{2\pi}{600}(\lambda - 400)\right] C_B^{2.0} \qquad (6\text{-}13)$$

The constant, 0.0002, for constituent B was necessary to have spectra radiances for B of the same order of magnitude as for constituent A. Table 14 presents the resulting 30-spectra set. A characteristic vector analysis of this spectra set indicated two eigenvectors sufficient to explain all of the total data variance with 82.298% and 17.702% variances explained partitioned among the two principal axes eigenvectors.

Neither eigenvector equalled the characteristic vector of constituent A or B used to formulate this data set. Rotations of the principal axes, however, produced $v_1' = v_A$ for $\theta_1 = 29.4°$ and $v_2'' = v_B$ for $\theta_2 = 186.9°$. The scalar multiples for the principal axes system are depicted in figure 34(a). Spectra numbers refer each scalar multiple point to original spectra input of table 14. Comparison with figure 26(a), the linear case, shows significant differences in the relative positions of the plotted multiples. A significant clustering occurs in the first quadrant. Using equations (4-33) and (4-34) with the values of θ_1, θ_2 determined above, the scalar multiples transformed into an oblique axes system are depicted in figure 34(b). Lines of constant constituent concentrations have been added for reference purposes although they are not known beforehand in an actual situation. The clustering observed in the first quadrant of the previous figure now appears in the fourth quadrant of the transformed scalar multiples. It is clear that the cause of this clustering behavior is the nonlinearity of the two constituents both causing reduced relative spacing between scalar multiples in this quadrant.

With a base water present in this data set (both constituent concentrations zero), scalar multiple functions can be calculated according to the procedures developed in this chapter using equations (6-10) and (6-12). Since the particular constituents have been "identified" by rotations of the principal axes, the particular simple nonlinear powers associated with these constituents ($p = 0.2$ for A and $p = 2.0$ for B) are presumed known. Computation of the functions $f(Y_1')$ and

$f(Y_2^{"})$ normalized by the range yields exactly the same values as for the linear case of figure 27(b) and, for this reason, the figure is not repeated.

In summary, a simple nonlinear constituent model represents a next step in reproducing radiance-concentration constituent behavior. The effect on a characteristic vector analysis is manifested as nonlinear distributions among the scalar multiples calculated. The feasibility of relative quantification is more restrictive, requiring not only the presence of base water in the spectral data but also, after constituent identification, simple nonlinear powers p available to form scalar multiple functions. Prior laboratory experiments with individual constituents are useful for this purpose.

Wavelength-Dependent Nonlinear Constituents and Mixtures

The most sophisticated relation between upwell radiance and constituent concentrations considered allows for the possibility of a wavelength dependency in the concentration variable. As demonstrated in figure 29(d), this causes the actual spectral shape to vary with concentration. This raises the question as to whether this still represents an analytically determinate situation for characteristic vectors. The model is presented as equation (6-3). The wavelength dependency of power p for test cases was taken to be the linear functions:

$$p(\lambda) = \frac{0.5\lambda}{400} - 0.125 \qquad (6\text{-}14)$$

and

$$p(\lambda) = -\frac{0.5\lambda}{400} + 2.125 \qquad (6\text{-}15)$$

where λ is in nm. Basically, the first relation is designed to give $p(500\ nm) = 0.5$ and $p(900\ nm) = 1.0$ at the lowest and highest input wavelengths. This variation is similar to the observed power variations shown in figure 30. The second relation explores wavelength-dependent powers greater than 1.0 with $p(500\ nm) = 1.5$ and $p(900\ nm) = 1.0$. Individual hypothetical constituents were formulated by using equations (6-5) → (6-7) (base water subtracted out) and the wavelength-dependent powers $p(\lambda)$ in place of the simple nonlinear powers previously considered. These new constituents were termed A, B, and C. Concentrations, in arbitrary units of 0, 10, 20, 30, and 40 were used with wavelengths taken every 50 nm from 500 to 900 nm as before. Figure 29(d) presented constituent A and figure 35 constituents B and C for wavelength-dependent powers less than 1.0 (eq. (6-14)). The locus of maximums indeed shows a shift in the spectral shape for these constituents. It is evident A and B are spectrally significantly different while A and C are very similar. Tables 15 and 16 present the input spectra and mean vectors for these constituents and also for the cases where the wavelength-dependent powers are greater than 1.0 (eq. (6-15)).

Characteristic vector analysis of these individual constituent spectra reveal the inability of the technique to explain the total data variance using a single eigenvector, as was the case for linear and

simple nonlinear ideal constituents. Indeed, more than two principal axes eigenvectors are necessary, although two are sufficient to explain most of the data variance as the following table shows:

$0.5 \leq p(\lambda) \leq 1.0$

Constituent A	Constituent B	Constituent C
$l_1 = 99.650\%$	$l_1 = 99.681\%$	$l_1 = 99.736\%$
$l_2 = 0.349\%$	$l_2 = 0.318\%$	$l_2 = 0.264\%$
$l_1 + l_2 = 99.999\%$	$l_1 + l_2 = 99.999\%$	$l_1 + l_2 = 100.000\%$

$1.0 \leq p(\lambda) \leq 1.5$

Constituent A	Constituent B	Constituent C
$l_1 = 99.875\%$	$l_1 = 99.887\%$	$l_1 = 99.852\%$
$l_2 = 0.125\%$	$l_2 = 0.112\%$	$l_2 = 0.148\%$
$l_1 + l_2 = 100.000\%$	$l_1 + l_2 = 99.999\%$	$l_1 + l_2 = 100.000\%$

The nonlinearity for the constituents is revealed also by the correlation matrices for the wavelength bands. As noted in table 3 for ideal linear constituents (and also true for simple nonlinear constituents), there are perfect interband correlations for all bands ($r_{ij} = \pm 1.000$), but in table 17 the wavelength-dependent nonlinear constituents exhibit less than perfect correlations. Adjacent bands exhibit near perfect correlations, whereas widely-separated bands have poorer correlations indicative of the nonlinearity. Figure 8(b) suggests that ideal linear (and simple nonlinear) constituents have a data distribution in a

single direction in n-band space requiring only one eigenvector to "characterize" this direction. The wavelength-dependent nonlinear curve of data distribution in n-band space requires more than one eigenvector to totally characterize the finite curvature from point to point. However, for the hypothetical constituents tested, one vector does give a preferred or average direction for the data distribution explaining the data variance to a high degree. Figure 36 depicts the first principal axes eigenvectors for each of the hypothetical constituents which are taken to be the average characteristic vectors for these constituents.

To ascertain how input concentrations of these constituents are related to the scalar coefficients computed, equation (6-3) for the general wavelength-dependent nonlinear spectra model must equal equation (4-23), the spectra reconstituted from the eigenvectors:

$$L_i(\lambda) = B(\lambda) + M(\lambda)\, C_i^{p(\lambda)} = \bar{L}(\lambda) + \sum_{k=1}^{p} Y_{ki}\, v_k(\lambda) \qquad (6\text{-}16)$$

which is exact. It is assumed, however, that a single characteristic vector and associated scalar coefficients should continue to identify and quantify the constituent as:

$$B(\lambda) + M(\lambda)\, C_i^{p(\lambda)} = \bar{L}(\lambda) + Y_{1i}\, v_1(\lambda) + \varepsilon_i(\lambda) \qquad (6\text{-}17)$$

where $\varepsilon_i(\lambda)$ are the errors in truncating the remaining eigenvectors and scalar coefficients. Solving for Y_{1i},

$$Y_{1i} = [a(\lambda) + b(\lambda)\, C_i + e_i(\lambda)]^{1/p(\lambda)} \qquad (6\text{-}18)$$

where:

$$a(\lambda) = \frac{B(\lambda) - \overline{L}(\lambda)}{v_1(\lambda)}$$

$$b(\lambda) = M(\lambda)/v_1(\lambda)$$

$$e(\lambda) = -\varepsilon_i(\lambda)/v_1(\lambda)$$

For the linear and simple nonlinear constituent models, a and b were independent of wavelength, but for the wavelength-dependent situations, the power $p(\lambda)$ couples the system such that these coefficients $a(\lambda)$, $b(\lambda)$ are wavelength-dependent. In addition, an error term exists which is both wavelength and concentration dependent. Thus, the scalar coefficients are related to the concentrations in a complex, wavelength-dependent manner.

Harris (1975) discusses the problems of nonlinear relationships in multivariate statistics. Possible solutions to nonlinearity include (a) choosing ranges (of spectra) over which linearity is known to apply (may be impossible to define in cases of mixtures of constituents) or (b) using appropriate transformations of nonlinear relationships

into linear models (as was done for the simple nonlinear constituents). The above possible solutions, however, were "not meant to imply that all situations involving nonlinearity where the precise nature of the relevant functions can be spelled out on a priori grounds (e.g., eq. (6-3)) can be reduced by appropriate transformations to linear form." In such cases "little can be done beyond taking the linear formulas as approximations ... on grounds either of convenience or of the ease of interpreting linear combinations recognizing that measures of reliability (percent variation accounted for by principal components) may be lower" (Harris 1975).

The analysis for wavelength-dependent nonlinearity may be taken as

$$Y_{1i} \approx [a(\lambda) + b(\lambda)\ C_i]^{1/p(\lambda)} \qquad (6\text{-}19)$$

and considering the nature of the nonlinearity, one can proceed to assume $a(\lambda)$, $b(\lambda)$ and $p(\lambda)$ are constants as approximations. A linear approximation would let $p(\lambda) = 1.0$ whereas a simple nonlinear approximation can let $p(\lambda) = p_{avg}$ where p_{avg} is an average power over the wavelength interval considered.

These approximations were applied to the scalar multiples of hypothetical constituents. Table 18 shows the constituent concentrations used as input and the values when normalized by the range. Listed in order are the scalar multiplies for the constituents associated with each of the characteristic vectors of figure 36, the same multiplies after a linear

scaling approximation ($p(\lambda) = 1.0$ and equation (5-10)) and after a simple nonlinear scaling approximation (eqs. (6-10) and (6-12)) using average powers ($p_{avg} = 0.75$ for $0.5 \leq p(\lambda) \leq 1.0$ and $p_{avg} = 1.25$ for $1.0 \leq p(\lambda) \leq 1.5$). In four of the six cases, simple nonlinear scaling of the scalar multiples produced results closer to the actual scaled concentrations than by using a linear scaling. The data in table 18 is depicted as figure 37 where the 45° lines indicate perfect agreement between the scaled scalar multiples functions and the scaled concentrations. It is evident that for $0.5 \leq p(\lambda) \leq 1.0$, the simple nonlinear scaling approximation tends to overcorrect the linear scaling approximation, whereas for $1.0 \leq p(\lambda) \leq 1.5$, it produces considerably better results.

It was decided to examine how well a characteristic vector analysis operated on the constituents tested in Langley Research Center's Spectral Signatures Laboratory. Figure 30 depicted the power functions $p(\lambda)$ derived for these constituent tests by another analysis. The spectra for these tests (concentrations cited earlier in this chapter) were input to a characteristic vector analysis program every 40 nm for 420 to 980 nm. It was found that, in all cases, a single eigenvector was sufficient to explain a very high percentage of the data variance even for constituents, which by figure 30, were significantly wavelength-dependent nonlinear and had experimental error present. Two eigenvectors explained nearly all the data variance as:

Constituent	Percentage variance explained l_1	l_2	$l_1 + l_2$
Primary sewage sludge	99.839%	.069%	99.908%
Secondary sewage sludge	99.859%	.091%	99.950%
Calvert soil	98.898%	.897%	99.795%
Ball soil	99.562%	.360%	99.922%
Jordan soil	99.384%	.312%	99.696%
Feldspar soil	99.109%	.596%	99.705%
Bermuda Hundred sediments	99.635%	.278%	99.913%
Bailey Bay sediments	99.789%	.211%	100.000%
Shell Company Industrial Biosolid sludge	99.602%	.255%	99.857%
American Cyanamid waste	99.757%	.097%	99.854%

It is significant that constituents such as the primary and secondary sewage sludge, which demonstrate a rather weak power wavelength-dependency exhibited the highest percentage variance explained by a single eigenvector whereas Calvert soil and Feldspar soil, with stronger wavelength-dependent powers $p(\lambda)$ exhibited the smallest such values. Figure 38 depicts the first principal axes eigenvectors, taken to be the characteristic vectors for these constituents. The scalar multiples associated with these wavelength-dependent constituents were scaled approximately using linear scaling, equation (5-10) and simple nonlinear scaling, equations (6-10) and (6-12). For the simple

nonlinear scaling an average power for each constituent was calculated from figure 30 to be:

Constituent	Average power (420 - 980 nm)	Standard deviation σ	σ/p_{avg}
Primary sludge	.66	.07	.11
Secondary sludge	.77	.03	.04
Calvert soil	.69	.14	.20
*Ball soil	.81	.12	.15
Jordan soil	.82	.06	.07
Feldspar soil	.91	.22	.24
Bermuda Hundred sediments	.61	.14	.23
*Bailey Bay sediments	.80	.12	.15
Shell Company Industrial Biosolid waste	.58	.09	.16
American Cyanamid waste	1.40	.18	.13

*Ball soil and Bailey Bay sediments dropped from the final analysis because of a lack of suitable base water spectra.

The ratio of the standard deviation to the average power value is indicative of how strongly wavelength dependent each constituent appears.

Figure 39 presents the linear (crosses) and simple nonlinear (circles) scaling approximations for the calculated scalar multiples versus the actual scaled concentrations. In all cases there is a significant improvement by using the simple nonlinear scaling approximation (with the average powers previously listed). Also, the

agreement between the simple nonlinear scaled scalar multiples and the scaled actual concentrations is, in most cases, excellent meaning excellent relative quantification information. This analysis suggests, that where constituent model power information is available from previous testing (such as fig. 30), a simple nonlinear scaling of the scalar multiples is preferred for wavelength-dependent nonlinear constituents. Where no such information exists, a linear scaling approximation can be used, but with degraded results in the relative quantification.

The next stage of the analysis involved spatially-independent constituents. The spectra for the hypothetical wavelength-dependent nonlinear constituents (tables 15 and 16) were combined as for the linear and simple nonlinear cases as 9-spectra sets of constituents A + B and A + C for both linear power variations, $p(\lambda)$. A characteristic vector analysis of the sets showed the inability of the technique to explain the total data variances using just two principal axes eigenvectors, as was the case for linear and simple nonlinear spatially-independent constituents. Two eigenvectors did, however, explain most of the variance:

Spatially-Independent Constituents

(9-spectra)

$0.5 \leq p(\lambda) \leq 1.0$

Constituents A + B	Constituents A + C
$l_1 = 96.366\%$	$l_1 = 97.361\%$
$l_2 = 3.575\%$	$l_2 = 2.623\%$
$l_1 + l_2 = 99.941\%$	$l_1 + l_2 = 99.984\%$
$\theta_1 = 66.0°$	$\theta_1 = 36.6°$
$\theta_2 = 207.2°$	$\theta_2 = 258.0°$

$1.0 \leq p(\lambda) \leq 1.5$

Constituents A + B	Constituents A + C
$l_1 = 67.333\%$	$l_1 = 96.775\%$
$l_2 = 32.609\%$	$l_2 = 3.209\%$
$l_1 + l_2 = 99.942\%$	$l_1 + l_2 = 99.775\%$
$\theta_1 = 44.6°$	$\theta_1 = 342.3°$
$\theta_2 = 256.5°$	$\theta_2 = 311.6°$

Rotations of the principal axes through angles θ_1, θ_2 were used to achieve a best fit between transformed principal axes eigenvectors and the characteristic vectors shown in figure 36 in the search for the underlying structure. For θ_1, $v_1' \rightarrow v_A$ and for θ_2, $v_2'' \rightarrow v_B$ or v_C. The transformed eigenvectors depict average n-band space directions along which the distribution of constituent data are best described.

Untransformed scalar multiplies associated with the principal axes eigenvectors for the four examples are shown in figure 40. Several important trends are evident -- (1) the lines of scalar multiplies for the constituents are curved, indicative of their curvature in n-band space caused by the wavelength-dependency. This is opposed to the always straight lines found for the linear and simple nonlinear constituents, and (2) the degree of curvature in the scalar multiple lines is more pronounced for spectrally similar constituents A + C than for the dissimilar constituents A + B due to the scaling effect of the eigenvalues in calculating scalar multiples.

The scalar multiples were transformed into oblique axes systems using angles θ_1, θ_2 and equations (4-33) and (4-34) to yield figure 41. Dissimilar constituents A + B continue to give results similar to the linear and simple nonlinear constituents, with relatively small curvatures present. On the other hand, the curvatures are amplified in the transformed multiples for constituents A + C. Relative quantifications of scalar multiples along the transformed axes directions are degraded as a result.

Considered next were full mixtures of constituents A + B and A + C (25-spectra). Linear superposition of equations (6-5) and (6-6) or (6-5) and (6-7) plus the power variables given by equations (6-14) and (6-15) were used in the formulation. Constituent concentrations of the mixtures follow the same pattern given in table 2 for A + B and table 7 for A + C. With a characteristic vector analysis, it was determined that more than two principal axes

eigenvectors were needed to explain the total data set variances, although two were sufficient to explain most of it:

Mixtures - 25 spectra

$0.5 \leq p(\lambda) \leq 1.0$

Constituents A + B	Constituents A + C
$l_1 = 86.085\%$	$l_1 = 99.104\%$
$l_2 = 13.770\%$	$l_2 = 0.884\%$
$l_1 + l_2 = 99.855\%$	$l_1 + l_2 = 99.988\%$
$\theta_1 = 50.4°$	$\theta_1 = 43.2°$
$\theta_2 = 230.8°$	$\theta_2 = 234.5°$

$1.0 \leq p(\lambda) \leq 1.5$

Constituents A + B	Constituents A + C
$l_1 = 86.226\%$	$l_1 = 98.723\%$
$l_2 = 13.722\%$	$l_2 = 1.259\%$
$l_1 + l_2 = 99.948\%$	$l_1 + l_2 = 99.982\%$
$\theta_1 = 50.5°$	$\theta_1 = 322.2°$
$\theta_2 = 230.6°$	$\theta_2 = 319.4°$

Figure 42 depicts the scalar multiple patterns for these 25-spectra mixtures and associated with the first two principal axes eigenvectors. Lines of constant concentrations or "mesh lines" for the constituents are curved for all cases. The calculated patterns for mixtures A + B are not greatly different than those given for the simple nonlinear constituent mixtures in figure 33. For mixtures of similar wavelength-

dependent nonlinear constituents A + C, however, significant mesh line curvatures are evident. For $0.5 \leq p(\lambda) \leq 1.0$ especially, the curvatures lead to a region of overlap. By bringing the scalar multiples for a third principal axis eigenvector, Y_3, into the analysis, a three-dimensional curved surface can be defined by the mesh lines. The orientation of the surface is such that projection onto the $Y_1 - Y_2$ plane results in the overlap. To maintain a generality in the analysis, it has been assumed that one constituent is depicted in n-band space by one characteristic vector, mixtures of two constituents explained entirely by the plane passing through two characteristics vectors and so on. It is shown that wavelength-dependent nonlinear constituents do not exactly conform to this assumption and as such present a limitation in the characteristic vector analysis. In these instances, however, the planes formed by the first two principal axes eigenvectors (or rotated eigenvectors) are the best approximate explanation of mixture variance for two constituents. Figure 43 shows the scalar multiples transformed into oblique axes systems.

A test of the concepts developed for wavelength-dependent nonlinear constituents involved the flight "experiment" considered in previous analyses (fig. 25). Mixture spectra were formed from:

$$L_{A+B}(\lambda) = 0.2 \sin\left[\frac{\pi}{600}(\lambda - 400)\right] C_A^{\frac{(0.5\lambda - 0.125)}{400}} + 0.02 \sin\left[\frac{2\pi}{600}(\lambda - 400)\right] C_B^{\frac{(-0.5\lambda + 2.125)}{400}} \quad (6\text{-}20)$$

The constant, 0.02, for constituent B was necessary to keep constituent spectra for A and B of the same order of magnitude. Otherwise, the total variance would be dominated by a single constituent which is not the objective of this demonstration. Table 19 presents the resulting 30-spectra set. With a characteristic vector analysis, 68.498% and 31.420% of the total variance were explained by the first two principal axes eigenvectors for a total of 99.918% leaving 0.082% unexplained. A search for the characteristic vectors of the individual constituents used to formulate the spectra set was initiated. Mixed power variables were used in this spectra set. Thus, v_A is given in figure 36(a), whereas, v_B is given in figure 36(b). For $\theta_1 = 54.0°$, $v_1' \rightarrow v_A$ and for $\theta_2 = 212.2°$, $v_2'' \rightarrow v_B$. The scalar multiples associated with the first two principal axes eigenvectors are depicted in figure 44(a) with spectra numbers labeled, whereas the scalar multiples transformed into an oblique axes system (based on θ_1, θ_2) are given in figure 44(b). Lines of constant concentrations are provided for reference purposes. The curvature is indicative of the wavelength-dependent nature of the constituents.

With a base water present in the data set, one may proceed to attempt a relative quantification using the transformed scalar multiples. The constituents A and B have been "identified" by coordinate rotations. Presuming previous laboratory testing of the individual constituents reveals average power values ($p_{avg} = 0.75$ for A and $p_{avg} = 1.25$ for B), simple nonlinear scaling approximations were used to calculate $f(Y_1')$ and $f(Y_2'')$ normalized by the range. Figure 45(a)

shows these values for each constituent along the flight lines and figure 45(b) as compared to the constituent concentrations scaled by the range. A reasonable, but inexact relative quantification is achieved in the presence of mixed wavelength-dependent nonlinear constituents.

In summary, wavelength-dependent nonlinear constituent spectra can no longer be described exactly by single characteristic vectors and associated scalar multiples. For two spatially-independent constituents and two-constituent mixtures, scalar multiple lines display varying degrees of curvature dependent on the spectral similarity of the tested constituents. Relative quantifications are still possible using linear or simple nonlinear scaling approximations of the scalar multiples, with degradation of results dependent on constituent spectral similarity. These results demonstrate limitations to the use of characteristic vectors for these classes of constituents.

CHAPTER VII

NONLINEAR SUPERPOSITION

Up to this point, in the hypothetical data sets, the principle of additive constituents or linear superposition has been assumed, i.e., that the sum of the upwell radiances (or reflectances) of the individual constituents equals the observed radiance (or reflectance) of the mixture of constituents for the same concentrations. For an N-constituent mixture,

$$L_{\Sigma N}(\lambda) = L_1(\lambda) + L_2(\lambda) + \ldots + L_N(\lambda) \qquad (7\text{-}1)$$

or for a two-constituent mixture of A and B,

$$L_{A+B}(\lambda) = L_A(\lambda) + L_B(\lambda) \qquad (7\text{-}2)$$

In real constituents, however, there is no guarantee this will occur, due to possible various physical, chemical, and electromagnetic interactions when the constituents are combined. These effects include flocculation and formation of precipitates, absorption of dyes onto particulates and particulates into water, shadowing effects, electrostatic adhesions, and so forth. Also, these effects may have a time-dependent nature, such as when precipitates are formed when iron-acid waste is dumped into ocean water (Lewis and Collins 1977). The scattering and absorption of light in a mixture may behave differently than observed in individual tests, especially when the constituents themselves have a

nonlinear relation between radiance and concentration. In any such case, equation (7-2), for a two-constituent mixture, can be modified to read,

$$L_{A+B}(\lambda) = L_A(\lambda) + L_B(\lambda) + g(\lambda) \qquad (7\text{-}3)$$

where $g(\lambda)$ represents the measure of the deviation from linear superposition. The function $g(\lambda)$ may be positive or negative (mixture radiances greater than or less than the sum of the components, respectively) or zero - the instance of linear superposition. For any set of experimental mixture data, these function values can be calculated provided individual constituent test spectra are also available for the same concentrations of constituents in the mixture.

It is useful to employ a model for $g(\lambda)$ which would describe, at least in an approximate manner, the values observed in particular tests and also be used to predict spectra for superimposed constituents at concentrations not tested in mixtures. It is felt that the true relationship may be very complex and involve not only physical, but chemical and electrical properties of the constituents as variables. The relation may also vary with the type and number of constituents tested. It is beyond the scope of this presentation to investigate the exact form of such a relationship. To investigate the effects of nonlinear superposition on characteristic vector analysis, a simple intuitive model of interaction is proposed which will be seen to fit some experimental data fairly well. For two constituents one has

$$L_{A+B}(\lambda) = L_A(\lambda) + L_B(\lambda) + K(\lambda)\, L_A(\lambda)\, L_B(\lambda) \qquad (7\text{-}4)$$

where the equation is still "additive" in form except for the multiplicative term representing the joint effect or "interaction" of underlying properties determining $L_A(\lambda)$ and $L_B(\lambda)$. For three constituents, four multiplicative terms are needed to represent all interaction effects,

$$\begin{aligned} L_{A+B+C}(\lambda) = {} & L_A(\lambda) + L_B(\lambda) + L_C(\lambda) + K_1\, L_A(\lambda)\, L_B(\lambda) \\ & + K_2\, L_A(\lambda)\, L_C(\lambda) + K_3\, L_B(\lambda)\, L_C(\lambda) \\ & + K_4\, L_A(\lambda)\, L_B(\lambda)\, L_C(\lambda) \end{aligned} \qquad (7\text{-}5)$$

For four constituents, 11 interaction terms would be necessary. To limit the scope of the investigation, only two-constituent mixtures are considered. From equation (7-4) one has

$$g(\lambda) = K(\lambda)\, L_A(\lambda)\, L_B(\lambda) \qquad (7\text{-}6)$$

as the interaction term. In Chapter VI, models of radiance-concentration relations were proposed which may be used to replace $L_A(\lambda)$ and $L_B(\lambda)$. Using the general relation given by equation (6-3), equation (7-6) may be written as

$$g(\lambda) = k(\lambda)\, C_A^{q(\lambda)}\, C_B^{r(\lambda)} \qquad (7\text{-}7)$$

where $k(\lambda)$ now is some general wavelength term. The sign of $k(\lambda)$ would indicate whether the interaction increased or decreased the mixture upwell radiance, while the powers $q(\lambda)$ and $r(\lambda)$ represent the nonlinearity of effect of constituent A or B on $g(\lambda)$. The model function has the desired property that as either constituent presence disappears (C_A or $C_B \rightarrow 0$) the function also goes to zero. The other property the model function is presumed to model is that the nonlinear superposition either increases or decreases the mixture radiances in a power-law relation. The cases where increasing radiance of either or both constituents cause the function to first increase then decrease in some complicated fashion represents a more sophisticated effect not addressed here. Thus, the model function will reach maximum or minimum values at the largest values of radiances of each of the constituents.

To study the effects the function $g(\lambda)$, i.e., nonlinear superposition, has on characteristic vector analysis, the hypothetical constituents of half-sine and full-sine waves were employed. Recall from Chapter VI that the constituents themselves may have a linear, simple nonlinear, or wavelength-dependent nonlinearity in the radiance-concentration relationship. The same may hold true for the interaction function $g(\lambda)$ where $q(\lambda)$, $r(\lambda)$ are one, some other constants, or wavelength-dependent. There are evidently many different combinations

of model relationships that could be tested. Also, it is useful to examine instances where $g(\lambda)$ is large or small with respect to the linear combination and for positive and negative values. However, it is not necessary to examine all such combinations to obtain a general inference of the effect of nonlinear superposition on characteristic vector analysis.

There is one type of nonlinear superposition that may be handled in the assumed manner by characteristic vector analysis, i.e., for a two-constituent mixture, only two eigenvectors are necessary to perfectly describe the total data set variance. In this type of nonlinear superposition, mixture spectra are increased or decreased in a proportional manner from the linear superposition mixture spectra. Henceforth, this is referred to as "proportional nonlinear superposition." For constituents A and B, for example, using equation (7-7) this may be modeled by letting

$$k(\lambda) = k_p[M_A(\lambda) + M_B(\lambda)] \tag{7-8}$$

where $M_A(\lambda)$ and $M_B(\lambda)$ are the shaping functions associated with the general power-law equation (6-3) and k_p is some constant defining a maximum change in the nonlinear superposition process. The equation for proportional nonlinear superposition becomes, for constituents A and B, by combining equations (6-3), (7-3) and (7-8)

$$L_{A+B}(\lambda) = B(\lambda) + M_A(\lambda)\, C_A^{p_1(\lambda)} + M_B(\lambda)\, C_B^{p_2(\lambda)} + k_p[M_A(\lambda) + M_B(\lambda)]\, C_A^{q(\lambda)}\, C_B^{r(\lambda)} \tag{7-9}$$

The form of such an equation applies to any two constituents where the shaping functions are added in the interaction term. Specifically, the shaping functions for hypothetical constituents A and B are given by equations (5-2) and (5-3).

In this chapter, the effects of nonlinear superposition on characteristic vector analysis are studied by utilizing the full-mixture matrix of 25-spectra formed from two hypothetical constituents considered in previous chapters, where constituent concentrations in water are chosen as (0, 10, 20, 30, 40) arbitrary units. In equation (7-9), the base-water spectrum $B(\lambda)$ is assumed to be subtracted out of all spectra under the model assumptions that it affects only the mean spectrum, but not calculated eigenvectors or scalar multiples. Thus, $L_{A+B}(\lambda)$ calculated are base-water corrected spectra. With the shaping functions and concentrations defined, this leaves the choice of powers $p_1(\lambda)$ and $p_2(\lambda)$ for the constituents, and the powers $q(\lambda)$, $r(\lambda)$ plus the constant k_p in the interaction term. In the forthcoming sensitivity analysis, these values are varied over a range of possible conditions. The main interest is to examine changes in scalar multiple

patterns, to see if some general conclusions about nonlinear superposition effects are possible.

For the first cases examined, all powers in equation (7-9) are considered constant and equal to one, i.e., $p_1(\lambda) = p_2(\lambda) = q(\lambda) = r(\lambda) = 1.0$, with the constant k_p adjusted to yield a $\mp 10\%$, $\mp 25\%$ and $\mp 50\%$ maximum increase or decrease in spectra radiance values observed in a linear superposition case (see table 2). Recall, based on the model assumptions, that this maximum effect of the interaction term occurs for the maximum spectrum where $C_A = C_B = 40$ arbitrary units and decreases to zero (in a power-law variation--in this case linearly) as either constituent presence disappears. Six 25-spectra sets were formulated for constituents A + B. Tables 20 and 21 are the sets for a $\mp 25\%$ maximum interaction term effect, for example, which may be easily verified by comparison with table 2. A characteristic vector analysis of all the spectra sets was conducted. Since the constituents A and B are assumed linear in the radiance-concentration relationship, the characteristic vectors given in figure 12(b) were used as comparison vectors during rotational transformations of the principal-axes eigenvectors.

In general, two principal-axes eigenvectors were sufficient to explain 100% of the total data set variance for all spectra sets. Rotations of the principal axes through angles θ_1 and θ_2, matching transformed eigenvectors to characteristic vectors v_A and v_B, defined an oblique axes system. Equations (4-33) and (4-34), as usual, transformed the principal axes scalar multiples into the oblique

systems. Figure 46 presents the transformed scalar multiples for the six cases considered (∓10%, ∓25% and ∓50% maximum interaction term effect). Each plot has representative "corner point" concentrations labeled, and the rotation angles (θ_1,θ_2) necessary to transform the principal-axes system into the oblique-axes system are noted. As previously, the mesh lines represent lines of constant concentrations.

The main effects of the interaction term for the linear powers case is a convergence of the mesh lines for higher concentrations for a negative interaction term (radiances of mixture spectra reduced from the linear superposition case) and a divergence of the mesh lines for higher concentrations for a positive interaction term (radiances of mixture spectra increased from the linear superposition case). Figure 22(c) can be used as a comparison as the case where the interaction term is zero (linear superposition). The mesh lines for all cases remain linear. For divergent line cases (positive interaction term), the scalar multiples are more easily interpreted than for convergent line cases, e.g., the -50% case of figure 46(e) where the scalar multiples for high concentrations are close together.

In the next stage of the analysis, the constituent and interaction term powers, $p_1(\lambda)$, $p_2(\lambda)$, $q(\lambda)$, and $r(\lambda)$ were further varied. The constant k_p was chosen in all cases to give a ∓25% maximum interaction term effect. Cases included:

Case Number	Maximum Interaction	$p_1(\lambda)$	$p_2(\lambda)$	$q(\lambda)$	$r(\lambda)$
7,8	∓25%	0.5	0.5	0.5	0.5
9,10	∓25%	1.5	1.5	1.5	1.5
11,12	∓25%	0.5	1.5	0.5	1.5
13,14	∓25%	1.0	1.0	0.5	0.5
15,16	∓25%	1.0	1.0	1.5	1.5
17,18	∓25%	eq. (6-14)	eq. (6-15)	eq. (6-14)	eq. (6-15)

For cases 7 through 12, the powers in the interaction terms are the same as for the individual constituents, but for cases 13 through 16 the interaction term powers differ from those of the constituents. For cases 17 through 18, wavelength-dependent powers are used.

In general, except for the wavelength-dependent powers cases, two eigenvectors are sufficient to explain 100% of the total data set variance. Characteristic vectors for constituents A and B, used in comparisons for rotational transformations, depend on the constituent powers $p_1(\lambda)$, $p_2(\lambda)$ used and may be found in tables 11 and 12 and figure 36. Figure 47 presents the transformed scalar multiples (in the oblique axes system based on angles θ_1,θ_2) for cases 7 through 10 where the interaction term and constituent powers are all one value (all equal 0.5 or 1.5 respectively). These plots may be compared to figure 33 where the interaction terms are zero. The patterns of convergence and divergence of the mesh (constant concentration) lines is as observed in figure 46, but the displacements of scalar multiples

along the mesh lines are nonlinear and consistent with the powers used. Note especially, in figure 47(a), that the combination of simple nonlinear powers 0.5 and a negative interaction term both contribute to a clustering of scalar multiples in the first quadrant, while in figure 47(d), the simple nonlinear powers 1.5 and positive interaction term causes significant spreading of the scalar multiples in the first quadrant. All mesh lines remain linear.

Figure 48 shows the transformed scalar multiples for the mixed powers cases 11 and 12, but where the same powers are used for the interaction term concentrations as for the individual constituents (i.e., $p_1(\lambda) = q(\lambda)$ and $p_2(\lambda) = r(\lambda)$). The effect is to change the quadrant where clustering or spacing of the transformed scalar multiples occur.

Figure 49 presents the transformed scalar multiples for cases 13 through 16, where the interaction term powers are definitely different than those of the individual constituents. The mesh lines are no longer linear, but have a curved appearance except for the pure constituent lines where the interaction term is zero. The basic pattern established of a convergence of mesh lines for a negative interaction term and divergence for a positive interaction term continues as for all previous cases.

For cases 17 and 18 using wavelength-dependent powers, a characteristic vector analysis requires more than two eigenvectors to completely describe the data set variance for mixtures of two constituents. This is similar to the results observed when wavelength-dependent powers

were introduced in the chapter on nonlinear constituents. As then, two eigenvectors are sufficient to explain most of the variance (98.935% for the -25% interaction term and 99.799% for the +25% interaction term). Figure 50 shows the transformed scalar multiples for these cases. Convergence and divergence of the mesh lines as caused by the interaction term is evident, as is the curvatures caused by using wavelength-dependent powers (note that the pure constituent mesh lines are curved as well).

The analysis discussed in figures 46 through 50 (cases 1 through 18) was repeated for constituents A and C (slightly displaced half-sine waves). Equation (7-9) was suitably modified using constituent C in place of constituent B. A characteristic vector analysis demonstrated the transformed scalar multiple plots were basically the same as for constituents A and B except for the wavelength-dependent powers case (corresponding to cases 17 and 18 for constituents A + B). Figure 51 shows the transformed scalar multiples for these mixed wavelength-dependent powers. The curvatures are different than those for figure 50, consistent with the variable curvature results observed in the chapter on nonlinear constituents. Less than 100% of the total data variance was explained by two eigenvectors (99.936% for the negative interaction term and 99.978% for the positive interaction term).

The foregoing discussion examined nonlinear superposition in a proportional mode--a type which required, in most cases, only two eigenvectors for a two-constituent mixture. Relaxing this assumption, the function $k(\lambda)$ in equation (7-7) is free to take on an infinite

variety of forms. This dissertation cannot attempt to explore all the possibilities where $k(\lambda)$ assumes a nonproportional form, and as stated previously the particular constituents under study will dictate the ultimate form this model expression assumes. The function may be dependent or independent of the shaping functions of the individual constituents.

One case of this nonproportional type of nonlinear superposition was considered, however, to illustrate an important concept applicable to such nonproportional nonlinear superposition cases. Consider the case of constituents A and C (two similar but displaced half-sine waves). The function $k(\lambda)$ might exist as a product of the shaping functions:

$$k = k_p \, M_A(\lambda) \, M_C(\lambda) \tag{7-10}$$

Unit powers are used for the individual constituents and interaction term. Equation (7-9) may be rewritten (substituting eq. (7-10) in place of eq. (7-8) and calculating base-water corrected spectra only) as,

$$L_{A+C}(\lambda) = M_A(\lambda) \, C_A + M_C(\lambda) \, C_C + k_p \, M_A(\lambda) \, M_C(\lambda) \, C_A \, C_C \tag{7-11}$$

The constant k_p was adjusted to give an average maximum interaction term effect of $\mp 25\%$. The usual 25-spectra sets were calculated from equation (7-11). In model form, these new cases appear very similar

to those that resulted in figures 46(c) and 46(d), except for the differences in the interaction function, $k(\lambda)$. A characteristic vector analysis, however, shows three eigenvectors needed to explain 100% of the total data set variance. Two eigenvectors explain 99.805% and 99.979% of the data set variance for the negative and positive interaction terms, respectively. Figures 52(a) and 52(b) show the transformed scalar multiples for these cases and may be compared to figures 46(c) and 46(d) for the cases calculated in a proportional mode of nonlinear superposition. Indeed, they look quite similar, with convergence and divergence of linear mesh lines. What is not shown, however, is the fact that while all scalar-multiple points in figure 46(c) and 46(d) fall within the principal axes (or transformed oblique axes) plane, in figures 52(a) and 52(b) there is a finite displacement out of these planes for the mixture points (as confirmed by the finite scalar multiples required by the third principal-axes eigenvector). A geometric interpretation of these results is useful.

A Geometric Interpretation

In Chapter IV, a geometric interpretation of principal components analysis operating on a linear, additive mixture of two constituents was presented. Figure 9(b) demonstrated that all radiance data plotted in three-band space (for example) for the pure constituents and mixture points, lie in a plane defined by the characteristic vectors. These vectors assumed the directions of the pure constituent's line of data. The first two principal axes (Y_1, Y_2) also lie in this plane

and the corresponding eigenvectors and scalar multiples explained 100% of the observed data variance. For such cases, the third principal axis (and in n-band space, the third through nth principal axes) were superfluous. Figure 53(a) shows how a 25-spectra case for two constituents would appear under similar conditions where now the mesh lines indicate constant concentrations.

Based on the results obtained in this chapter, figure 53(b) shows the appearance of a two-constituent mixture with proportional nonlinear superposition and a negative interaction term. While the mesh lines collapse inward towards the origin (convergence at higher concentrations) and point D moves to E, all mixture points continue to lie in the plane formed by the characteristic vectors. The plane formed by the first two principal axes coincides with this plane with the result that two principal axes eigenvectors and associated scalar multiples continue to completely describe the observed data variance. Higher-order principal axes are superfluous.

Figure 53(c), however, presents the case of nonproportional, nonlinear superposition, as considered, for example, for the case shown in figure 52. When plotted in wavelength space, the mixture spectra points fall out of the plane defined by the characteristic vectors (lying along the pure constituent directions). The vertex point E moves out of the plane defined by ABC to point F. All mixture points now lie out of plane ABC. Because of this, the mesh lines define a warped surface. The plane formed by the first two principal axes will orientate such as to provide a best description of this surface, but additional

principal axes eigenvectors are required to complete the description. For more general nonlinear superposition cases, the surface may warp in a complex manner. When the constituents are wavelength-dependent as well, the lines of data representing the pure constituents are curved and added curvatures are present in the warped surface of the mixture points. These arguments may be extended into n-band hyperspace. In such cases, a principal components analysis, in calculating the first two principal axes, provides the best approximate description of the hyperspace surface.

Summarizing nonlinear superposition, and the observations from the previous test cases, the total radiance upwelled from a mixture of two constituents in water may be less than, equal to, or greater than the sum of the upwell radiances from the individual constituents tested alone in water (with proper corrections for the base waters). When they are equal, one has the usual assumed case of linear superposition. When they are not, one has nonlinear superposition. The actual relation to explain such nonlinear superposition behavior may be a complicated function of physical, chemical, and electrical properties of the particular individual constituents. However, a simple model of interaction is proposed which may relate to some cases of nonlinear superposition. The interaction function is further modeled by a power-law equation. Proportional and nonproportional modes of nonlinear superposition are considered.

A sensitivity analysis, varying constituent and interaction term powers plus the degree of the interaction term effect, demonstrated that

nonlinear superposition results in either a convergence (for mixture radiance decrements) or a divergence (for mixture radiance increments) of the transformed scalar multiple mesh lines for the sample cases. For a proportional mode of nonlinear superposition two eigenvectors explain the total data set variance for a two-constituent mixture except for cases of wavelength-dependent constituents and interaction term. Mesh lines for mixtures could be linear or curved. For wavelength-dependent constituents one has curvature in the mesh lines for the pure constituents as well. In a nonproportional mode of nonlinear superposition, the mesh lines may warp in a complex manner, requiring more than two eigenvectors (for a two-constituent mixture) to complete the data variance description. The first two principal axes, however, provide the best approximate description to these two-constituent cases. The next section examines a real world experiment case involving two wavelength-dependent nonlinear constituents that exhibit a nonlinear superposition in mixture formations.

Application to Mixture Experiment

To examine the concepts developed in this and previous chapters for a real data case, characteristic vector analysis of a set of mixture data obtained in the Langley Research Center's Marine Upwelled Spectral Signatures Laboratory was undertaken. The data set included measured reflectance spectra for (1) bottom sediments from the Bailey Bay and Bermuda Hundred areas on the James River near Hopewell, Virginia, mixed in filtered, deionized water for varying concentrations, and (2) a

mixture of Bermuda Hundred bottom sediments (at 25 ppm) with varying concentrations of Bailey Bay bottom sediments mixed in filtered, deionized water. Whitlock et al (1978) describe the particular experiment in detail. The concentrations matrix of available spectral reflectance data includes:

Bermuda Hundred bottom sediment concentrations in water, ppm

Bailey Bay bottom sediment concentrations in water, ppm	0	4	17	25	52	86	173
0	x	x	x	x	x	x	x
4	x			x			
17				x			
34				x			
86	x			x			
129				x			
173	x			x			

Figures 54, 55, and 56 (after Whitlock et al 1978) show, respectively, the measured reflectance spectra for the sediment samples individually, and in a mixture. Noted on the figures is the range of wavelengths used in this analysis. The Xenon lamp used as a radiance source for these experiments demonstrated operating characteristics in the collected spectra above 750 nm. This required data fairing and it was decided to avoid possible data problems at these higher wavelengths. Table 22 presents the actual reflectance data from figures 54 through 56 for the

wavelengths considered (every 40 nm for the range 460 to 780 nm). A previous analysis of individual constituents in Chapter VI classified Bermuda Hundred and Bailey Bay sediments as a wavelength-dependent nonlinear in terms of the radiance-concentration relationship (see fig. 30). To determine the form of superposition for these constituents, reflectance spectra for a linear superposition were calculated by adding the reflectance spectra for 25 ppm of Bermuda Hundred sediments to the reflectance spectra of 4, 86, and 173 ppm of Bailey Bay sediments. A base-water spectrum, given by spectra number 1 in table 22 was subtracted out--otherwise, the base water would be figured in twice, once for each constituent. This assumes that the base water was the same for both individual constituent experiments. The results are presented in Table 23. Next, the differences between the actual mixture reflectance spectra (see table 22) and the linear superposition reflectances were formed. These differences are the interaction terms, $g(\lambda)$, defined in equation (7-3), and are presented in table 23. The fact that $g(\lambda)$ is nonzero indicates that the mixing of Bermuda Hundred and Bailey Bay sediments involves a nonlinear superposition process. In general, except for one value at the highest wavelength, the interaction terms are negative. For some of the wavelengths, a power-law model for $g(\lambda)$ given by equation (7-7) would work well, but for the wavelength, range 500 to 620 nm, the interaction term first increases, then decreases at the highest concentration. A more sophisticated model for the interaction term is suggested, but is not explored further here. The main arguments have been demonstrated--that the constituents are

wavelength-dependent nonlinear, and they superimpose nonlinearly resulting in negative interaction terms, $g(\lambda)$.

Characteristic vectors were first calculated for each class of sediments using the individual constituent's reflectance data from table 22 input to a characteristic vector analysis program. The first principal axes eigenvectors in each case, taken to be characteristic vectors, explained 99.399% and 99.763% of the data variance for the Bermuda Hundred and Bailey Bay sediments, respectively. These values are somewhat different than those given in Chapter VI because of the reduced wavelength range used in the present analysis. Figure 57(a) shows the calculated characteristic vectors. They appear much the same as given originally in figure 38 except for an increased magnitude. This also is a consequence of using a reduced wavelength range. Appendix D demonstrates how characteristic vectors calculated for n-band spectral data can be used to derive those for m-band data directly. This concept is important if characteristic vectors (and scalar multiples) derived from one spectrometer system's data are compared to another spectrometer system's data where the systems differ in the number and values of wavelengths used. In general, there is a significant difference in the characteristic vectors for the two classes of bottom sediments, with the vector for Bailey Bay sediments having a much flatter response.

Next, the entire set of spectral curves given by table 22 was input to the characteristic vector analysis program. It was found that 99.474% of the total data variance was explained by the first two

principal axes eigenvectors. These eigenvectors are presented in figure 57(b). Comparison with the characteristic vectors in figure 57(a) demonstrate obvious major differences. Figure 58 shows the associated scalar multiple pattern for the first two principal axes eigenvectors. The points corresponding to the different constituents and mixture fall along different lines. To interpret these results properly, a search for simple structure was initiated, using rotational transformations, to transform these multiples into an oblique axes system.

A coordinate rotation through angle $\theta_1 = 319.1°$ revealed $v_1' \rightarrow v_{B100}$, i.e., the rotated first principal axis eigenvector approximated the characteristic vector for Bermuda Hundred sediments. Figure 59(a) shows these results. After a coordinate rotation of $\theta_2 = 292.1°$, the second principal axis eigenvector approximated (in optimal fashion) the characteristic vector for Bailey Bay sediments, i.e., $v_2'' \rightarrow v_{BB}$. This comparison is shown in figure 59(b). Using the angles θ_1, θ_2 the scalar multiples from figure 58 were transformed into an oblique axes system, Y_1', Y_2'', using equations (4-33) and (4-34). The results are presented in figure 60.

In general, the Y_1' axis aligns along the direction of increasing transformed scalar multiple values of Bermuda Hundred sediments, whereas the Y_2'' axis is along an average direction of increasing transformed scalar multiple values for Bailey Bay sediments. Note that the scalar multiple mesh lines for the individual constituents are not straight. As seen in the test cases in this chapter and Chapter VI,

this occurs when the constituents themselves are wavelength-dependent nonlinear, a fact shown for these constituents in Chapter VI.

Next, note that the mixture mesh line (resulting from addition of varying concentrations of Bailey Bay sediments to a fixed 25 ppm of Bermuda Hundred sediments) and the Bailey Bay pure constituent mesh line converge towards the higher concentrations. As seen in earlier test cases, this requires the existence of nonlinear superposition with a negative interaction term, a fact confirmed by the computations given in table 23.

There is some evidence of noise in this data set. The Bermuda Hundred scalar multiple mesh line is not smooth, for example. Also, spectra points 4 and 11 represent the same supposed condition of 25 ppm of Bermuda Hundred sediments in filtered, deionized water. These points were derived from different experiment runs. Hypothetically, they should match, but as seen in figure 60 and table 22, there is a slight spectral mismatch. Possible error sources include a small change in the filtered, deionized base water for the different experiment runs, a difference in the actual sediment amounts mixed into the base water, and spectrometer system noise. All arguments considered, the results still appear quite good, and the general observations of these past two chapters appear confirmed by this data example.

The question arises: how well do the transformed scalar multiples describe the constituent and mixture concentrations? As described in Chapter VI, wavelength-dependent nonlinear constituents impose a limitation in the use of characteristic vector analysis and a degradation

of relative quantification results is expected. In addition to this is the degradation caused by nonlinear superposition of the mixture. Still, the transformed scalar multiples were subjected to a linear and simple nonlinear scaling to examine the technique performance under adverse conditions.

The transformed scalar multiples for the individual sediment classes and mixture were plotted separately as a function of the known input concentrations. These results are given as figure 61. A smooth trend line was passed through each data distribution. Nonlinearities are evident. Recall, that a nonlinearity itself is not a limitation to characteristic vector analysis if it is a simple nonlinearity. This only causes shifts in the relative displacements of scalar multiple values along a mesh line. It is the wavelength-dependent nonlinearity, as seen in figure 60, that ultimately degrades the quantification results.

Transformed scalar multiples for this data set were subjected to linear and simple-nonlinear scaling, and the results plotted as a function of scaled concentrations (see previous examples in Chapter VI). For the simple nonlinear scaling, average powers, p_{avg} = 0.64 and
B100

p_{avg} = 0.76 were used based on the wavelength range considered (see
BB

fig. 30). The average power for Bailey Bay was also applied to the mixture transformed scalar multiples, regardless of the acknowledged nonlinear superposition. Figure 62 presents the final relative

quantification results. For the Bermuda Hundred sediment class, the results are very good, particularly after simple nonlinear scaling. For the Bailey Bay sediment class, the results are inconclusive. Additional spectral curve data at other concentrations may have better defined these results. There is little question, however, that simple nonlinear scaling worsens the relative quantification results for mixture spectra over those obtained by linear scaling. The combination of wavelength-dependency and nonlinear superposition may well contribute to these results. All in all, however, the relative quantification results may be considered fair to good under adverse conditions.

The discussion of this and previous chapters has demonstrated the use of characteristic vector analysis for exact, hypothetical data sets. As this last example has suggested, however, real world data may be subject to varying degrees of error and noise. The fact that input radiance or reflectance data may be inexact to begin with is examined in the next chapter.

CHAPTER VIII

NOISE

In actual laboratory or remote-sensing operations, spectral radiance data will contain certain degrees of error and noise. Most operational instruments contain onboard calibration systems to minimize radiance error. Noise, however, is more difficult to evaluate because of the many contributions from both the real world and from instrument system elements. Systematic noise may be highly structured in form, such as the repeatable undulations observed in some multispectral scanner data (LeCroy 1979). Knowledge of such structure can be used to devise spatial filtering techniques to correct the final data. Many other types of noise, however, are random in nature. For example, at the water surface, surface waves within a resolution element introduce a random reflectivity and hence, source noise. Within the atmosphere, high frequency variations in particulate densities and distributions introduce a propagation noise, and at the remote-sensor, thermal noise is added by the sensor and amplifying equipment.

Since random noise is common to all remote-sensing systems, this chapter will evaluate the effects of this type of noise on the usefulness of characteristic vector analysis as an identification and quantification technique. Specifically, the study addresses the questions of how characteristic vectors for constituents change with the addition of varying degrees of noise, at what noise levels does one encounter unacceptable levels of quantification misinterpretation, and how do

the nature of constituents, in terms of the radiance-concentration relationships, affect the quantification interpretations.

Theoretical Random Noise Effects

The noise added to ideal spectral radiance data is assumed to be random, uncorrelated with a zero mean. The noise covariance matrix, S_η, is then given by:

$$S_\eta = \begin{bmatrix} \sigma_1^2 & 0 & \cdot & \cdot & \cdot & 0 \\ 0 & \sigma_2^2 & & & & \cdot \\ \cdot & \cdot & & & & \cdot \\ \cdot & \cdot & & & & \cdot \\ 0 & 0 & \cdot & \cdot & \cdot & \sigma_n^2 \end{bmatrix} \qquad (8\text{-}1)$$

where:

n = total number of wavelengths or bands

In reality, the random noise observed in a system is device-dependent and σ_n^2, the noise variance, may vary from wavelength to wavelength. Whitlock et al (1979) present data for the standard deviation of data noise, σ_n, as a function of wavelength for several remote-sensing instruments and field experiment situations which demonstrate a variability in $\sigma_n(\lambda)$ among the instruments and field experiments. Even with the same instrument, $\sigma_n(\lambda)$ may vary from day-to-day (Jobson 1980). Considering the specific nature of $\sigma_n(\lambda)$, a general model was assumed whereby σ_n was constant at all wavelengths.

Under such conditions of identically distributed uncorrelated random noise, equation (8-1) is written as

$$S_\eta = \sigma_n^2 I \tag{8-2}$$

where I is the $n \times n$ identity matrix. Recall from Chapter IV that a principal components analysis involves calculating the eigenvalues and eigenvectors of the variance-covariance matrix, S_X (although in practice the $(P'P)_X$ matrix is used in place of S_X). For the noiseless case

$$v_k S_X = \lambda_k v_k \tag{8-3}$$

where:

v_k = kth eigenvector

λ_k = eigenvalue of the kth eigenvector

$k = 1,2,\ldots,p \qquad p \leq n$

With random noise added, however, the total covariance matrix is

$$S_T = S_X + S_\eta \tag{8-4}$$

and one is instead solving

$$\tilde{v}_k S_T = \tilde{\lambda}_k \tilde{v}_k \tag{8-5}$$

where the tilde (~) indicates eigenvectors and eigenvalues under the influence of noise.

Substitution os equations (8-2) and (8-4) into equation (8-5) yields

$$\tilde{v}_k \, (S_X + \sigma_n^2 \, I) = \tilde{\lambda}_k \, \tilde{v}_k \tag{8-6}$$

With rearrangement one obtains

$$\tilde{v}_k \, S_X = (\tilde{\lambda}_k - \sigma_n^2) \, \tilde{v}_k \tag{8-7}$$

Comparison of equations (8-3) and (8-7) leads to the conclusion that (Ready and Wintz 1973)

$$\tilde{v}_k = v_k \tag{8-8}$$

and

$$\tilde{\lambda}_k = \lambda_k + \sigma_n^2 \tag{8-9}$$

These results are most important because, in theory, equation (8-8) describes the insensitivity of calculated eigenvectors to additive, random noise, while equation (8-9) indicates the eigenvalues are uniformly increased by the noise variance, σ_n^2.

The fact that characteristic vectors for a constituent derived from noisy multispectral radiance data should be the same as for the noisefree data suggests that identification of constituents by a characteristic vector analysis remains unaffected by random noise. The total system variance for noisy linear (or simple nonlinear) constituents is given by

$$\text{tr } S_T = \lambda_1 + n\sigma_n^2 \tag{8-10}$$

where λ_1 is the largest eigenvalue derived from the noiseless case. Reall that $\lambda_2, \lambda_3, \ldots, \lambda_n$ would ideally be zero for single constituents under noisefree conditions. The variance explained by the first principal axis eigenvector in a noisy environment is therefore given by:

$$l_1 = \frac{(\lambda_1 + \sigma_n^2)}{(\lambda_1 + n\sigma_n^2)} \times 100 \tag{8-11}$$

while for the second to nth eigenvectors (nonzero now because of the presence of noise),

$$l_2 = l_3 = \ldots = l_n = \frac{\sigma_n^2}{(\lambda_1 + n\sigma_n^2)} \times 100 \tag{8-12}$$

Under less-than-ideal constituent conditions (wavelength-dependent nonlinear constituents, noise sources that are not random, limited input

spectral data), this described distribution of variances explained will not be as precise. For correlated multispectral data, as many researchers have shown (see Chapter IV), the first few eigenvectors will account for most of the data variance. An estimate of noise, then, can be made by examination of the nth eigenvalue,

$$\tilde{\lambda}_n \sim \sigma_n^2 \tag{8-13}$$

The scalar coefficients, which the present study has shown can be related to constituent concentrations, are also affected by additive, random noise. Recall from equation (4-25a) that the scalar coefficients in the absolute system (called System II) are given by

$$(Y_{ki})_{II} = \sum_{j=1}^{n} (v_{kj})_{II} P_{ij} \tag{8-14}$$

With the eigenvectors $(v_{kj})_{II}$ unaffected, in theory, by random noise,

$$(\tilde{Y}_{ki})_{II} = \sum_{j=1}^{n} (v_{kj})_{II} \tilde{P}_{ij} \tag{8-15}$$

for the noisy situation. The mean-corrected data are given by

$$\tilde{P}_{ij} = \tilde{L}_{ij} - \overline{L}_j \tag{8-16}$$

where the mean spectrum, $\bar{L}_j$, remains unchanged by random noise assumed to have a zero mean. Equation (8-16) may be rewritten as

$$\tilde{P}_{ij} = (L_{ij} + \eta_{ij}) - \bar{L}_j \tag{8-17}$$

where η_{ij} are the noise elements for the data set. Therefore

$$\tilde{P}_{ij} = P_{ij} + \eta_{ij} \tag{8-18}$$

or

$$(\tilde{Y}_{ki})_{II} = \sum_{j=1}^{n} (v_{kj})_{II}[P_{ij} + \eta_{ij}] \tag{8-19}$$

which reduces to

$$(\tilde{Y}_{ki})_{II} = (Y_{ki})_{II} + \sum_{j=1}^{n} (v_{kj})_{II}\, \eta_{ij} \tag{8-20}$$

which says that the noisy scalar coefficients are the noisefree scalar coefficients plus a weighted increment due to random noise. For ideal linear or simple nonlinear constituents, $(Y_{ki})_{II}$ are zero for $k > 1$ such that $(\tilde{Y}_{ki})_{II}$ for $k > 1$ are noise-related. The scalar coefficients in the relative system (System I), the scalar multiples, are related to the coefficients in System II by equation (4-26). Using this relation in equation (8-20) results in

$$(\tilde{Y}_{ki})_I = \sqrt{\frac{\lambda_k}{\tilde{\lambda}_k}}\,(Y_{ki})_I + \sum_{j=1}^{n} \frac{(v_{kj})_{II}}{\sqrt{\tilde{\lambda}_k}}\,\eta_{ij} \qquad (8\text{-}21)$$

This expression shows that the scalar multiples in a noisy situation are related to those under a noisefree environment plus the weighted noise increment. It is important to note that the noise is scaled by the square root of the corresponding eigenvalue. One can expect, therefore, that circular error distributions in the absolute scalar coefficient system will appear as elliptical in the scalar multiple system depending on the values of $\tilde{\lambda}_k$ for $k \geq 1$. The next section provides a practical demonstration of random noise effects for hypothetical constituents.

Model Random Noise

In the ensuing sensitivity analysis, random noise at several predetermined levels is parametrically added to original exact spectra of previously-introduced hypothetical constituents to produce noisy spectral data. These data are then used as input for characteristic vector analysis studies. Consider the ranges of spectral radiance values (in arbitrary units) for linear constituents A, B, and C given in table 2. In all cases the maximum range for the individual constituents is eight units. Noise was arbitrarily chosen such that σ_n was 1%, 2.5%, 5%, 10%, and 25% of the range, i.e.,

Noise (% of range)	σ_n (arbitrary units)
0	0
1%	0.08
2.5%	0.20
5%	0.40
10%	0.80
25%	2.00

These values of σ_n apply equally well to constituents A, B, or C. For simple-nonlinear constituents ($p = 0.5, 1.5$) or wavelength-dependent nonlinear constituents ($p(\lambda) < 1$, $p(\lambda) > 1$) considered in previous chapters, the noise standard deviations were scaled accordingly to give the same relative percentage of random noise with respect to the constituent's range of spectral radiances. These noise levels, determined for the individual constituents, were subsequently used in all studies involving single constituents, spatially-independent constituents, or mixtures of constituents. For convenience, the noise levels are referred to by the percentages, e.g., a 10% noise represents a noise standard deviation of 10% of a constituent's maximum range of radiance values.

To generate noisy spectra, a random number generator was used such that the noisy radiances are given by

$$\tilde{L}_{ij} = L_{ij} + R_n \sigma_n \qquad (8\text{-}22)$$

where R_n are computer-generated random numbers with a normal (Gaussian) distribution with zero mean and unit variance. Figure 63 shows the effects of random noise so generated on linear (p = 1.0) constituent A originally presented in figure 10. A progressive deterioration of the exact spectra is evident. With the 10% noise level, spectral overlap occurs at some wavelengths, and by the 25% noise level, the spectra are poorly defined with respect to the exact signals.

LeCroy (1979) evaluated the quality of remote-sensing data by the use of the signal-to-noise (S/N) ratio given by

$$S/N = \frac{\sigma_x}{\sigma_n} \tag{8-23}$$

where σ_x is the standard deviation of a spectral data set at any wavelength. While σ_n has been assumed independent of wavelength, σ_x and S/N are wavelength-dependent. One hundred sets of the five spectra for linear constituent A (see table 2), for a total of five hundred spectra, at five different noise levels were used to estimate the signal-to-noise ratios for the constituent in a noisy environment. The results as a function of wavelength were:

Wavelength (nm)	σ_x/σ_n at noise levels 1%	2.5%	5%	10%	25%
500	19.75	7.95	4.08	2.25	1.34
550	28.00	11.30	5.75	3.08	1.64
600	34.25	13.75	6.95	3.63	1.79
650	38.13	15.30	7.70	3.96	1.87
700	39.50	15.85	8.00	4.11	1.94
750	38.25	15.35	7.75	4.08	1.94
800	34.13	13.65	6.88	3.54	1.73
850	27.88	11.20	5.68	2.98	1.57
900	19.88	8.00	4.13	2.28	1.37

Whitlock and Kuo (1979) cite a rule-of-thumb, called the Daniel's criterion,

$$S/N = \frac{\sigma_x}{\sigma_n} \geq 3.16 \qquad (8\text{-}24)$$

that should be satisfied for all wavelengths if a multiple-regression analysis of a data set is to be meaningful. For the previously listed signal-to-noise ratios, the criteria is satisfied at noise levels 1%, 2.5%, and 5%, is satisfied only at some wavelengths for the 10% noise level, and is obviously not satisfied for the 25% noise level. The criteria appears to be a reasonable statement of the observations from figure 63 regarding signal interpretability. The 1%, 2.5%, and 5% noise levels may be referred to as "low," the 10% noise level as

"marginal" and the 25% noise level as "high." In this context, the remote-sensing data may be qualitatively referred to as "good," "marginal," and "poor," respectively. Similar signal-to-noise ratios are obtained for constituents B and C and for other powers, p, used. The ratios, however, shift with wavelength depending on the constituent chosen.

Because of the nature of random number generation, the smaller the number of spectra used, the less likely a true random noise (normal distribution, zero mean, unit variance) is achieved for the data set. Equation (8-8) states that eigenvectors should be unaffected by the presence of random noise assuming large enough numbers of input spectra are used. A study was conducted to examine how many sets of the original five spectra for linear constituent A, subject to a 10% independent random noise for each set, are needed as input to a characteristic vector analysis, such that equation (8-8) is satisfied. The number of spectra sets used were 1, 5, 10, 25, 50, and 100 corresponding to 5, 25, 50, 125, 250, and 500 total input spectra, respectively. Characteristic vector analysis calculated in each case a first principal axis eigenvector, assumed to be the characteristic vector for the constituent. These vectors were compared with the exact characteristic vector for linear constituent A (see table 4) by a sum of the squares difference between the exact and noise-influenced vectors:

Wavelength (nm)	Noisefree v_A	$\tilde{v}_A$ with 10% random noise for specific numbers of spectra sets 1	5	10	25	50	100
500	0.206	0.218	0.210	0.206	0.204	0.205	0.205
550	.292	.297	.288	.284	.297	.297	.298
600	.358	.337	.354	.354	.357	.362	.360
650	.399	.394	.408	.404	.403	.401	.396
700	.413	.413	.418	.418	.419	.416	.413
750	.399	.427	.403	.404	.398	.400	.403
800	.358	.375	.358	.358	.354	.349	.351
850	.292	.276	.289	.287	.285	.283	.288
900	.206	.158	.182	.203	.198	.207	.207
$\sum_{j=1}^{n} (v_{Aj} - \tilde{v}_{Aj})^2 =$		.0043	.0008	.0002	.0002	.0002	.0001

Clearly, even with one five-spectra set input with random noise, the vector calculated is not greatly different from the noisefree vector, but marked improvement is possible by utilizing greater numbers of spectra sets (up to 10 sets). Beyond 10 sets of spectra, the noise approaches a true random character and small improvement in the characteristic vector comparisons (sum of squares of differences) is noted. This study has two implications; first, to reduce random noise effects in remote-sensing data, larger numbers of input spectra for a characteristic vector analysis are preferred, and second, in laboratory

testing of constituents to derive comparison characteristic vectors, repeat testing at fixed constituent levels or increased spectra measurements at smaller concentration increments help reduce random noise effects.

Equations (8-11) and (8-12) describe the distribution of variance explained among the ordered eigenvectors and eigenvalues. Consider again 100 sets of linear constituent A spectra subject to noise levels 0%, 1%, 2.5%, 5%, 10%, and 25%. For the usual nine wavelengths used to define the spectra, up to nine eigenvalues and eigenvectors can be calculated from a characteristic vector analysis. The following distributions of variances explained were found:

Eigenvalue number	l_k, percentage variance explained for noise levels					
k	0%	1%	2.5%	5%	10%	25%
1	100%	99.890%	99.315%	97.321%	90.166%	61.001%
2	0	.016	.102	.398	1.461	5.792
3	0	.015	.092	.358	1.316	5.220
4	0	.014	.090	.352	1.293	5.129
5	0	.014	.087	.340	1.246	4.942
6	0	.014	.084	.328	1.205	4.778
7	0	.013	.080	.313	1.150	4.557
8	0	.012	.077	.301	1.104	4.378
9	0	.012	.074	.289	1.060	4.202

Using equations (8-11) and (8-12), the noisefree first eigenvalue $\lambda_1 = 46.93$, and the noise standard deviations $\sigma_n = .08, .2, .4, .8, 2.0$, one obtains for true random noise, by comparison,

Eigenvalue number	1_k, percentage variance explained for noise levels					
k	0%	1%	2.5%	5%	10%	25%
1	100%	99.891%	99.323%	97.354%	90.283%	61.413%
2 → 9 (each)	0%	.014	.085	.331	1.215	4.823

For the ideal spectral case, all the variance is explained with the use of one eigenvector, whereas, for the noise spectra cases, most of the variance is explained by the first eigenvector with remaining variance distributed more or less equally among the remaining eigenvalues which are noise-related.

The preceding analyses have demonstrated that 100 spectra sets will produce noise very nearly random and uncorrelated. In the forthcoming analyses this fact is used to allow the calculation of statistical distributions of scalar coefficient values about a mean to demonstrate at what noise levels and for what types of constituents is one likely to encounter quantification misinterpretation.

Single Constituents

Considered in this noise analysis were hypothetical constituents A, B, and C formulated using linear ($p = 1.0$), simple nonlinear ($p = 0.5, 1.5$) and wavelength-dependent powers ($p(\lambda) \lesssim 1$). Figure 63 exemplified

the appearance of a set five spectra of linear constituent A for several levels of random noise. One hundred sets of these spectra were subjected to a characteristic vector analysis at each noise level. Figure 64(a) is a plot of the calculated scalar multiples versus constituent concentrations for zero random noise (based on 500 spectra). When random noise was added, the calculated scalar multiples scattered about the true values in a Gaussian manner. The scatter increased in magnitude as the noise level increased. A statistical measure of this scatter is the standard deviation of the scalar multiples, σ_Y, about their mean. The standard deviations, σ_Y, were calculated at five concentration levels (0, 10, 20, 30, 40 units) and for all noise levels (1%, 2.5%, 5%, 10%, 25% random noise).

The value $3\sigma_Y$ was chosen to represent the noise bounds since 99.783% of all calculated scalar multiples should fall within the range $\pm 3\sigma_Y$. Noted on figure 64(a) are typical values of $\pm 3\sigma_Y$ for the higher noise levels studied (5%, 10%, 25%). They are all noted on this one figure only for convenience. In reality, the $\pm 3\sigma_Y$ bounds at 10% random noise applies equally at all concentrations, for example.

Since the relationship between the scalar multiples and concentrations is given by the curve (linear in this case), concentration increments or "errors" associated with the scatter bounds $\pm 3\sigma_Y$ can be found such that

$$(\tilde{C})_{\substack{max \\ min}} = (C)_{true} \pm (\Delta C)_{max} \qquad (8\text{-}25)$$

For the linear constituent cases, $\pm(\Delta C)_{max}$ are independent of concentration but depend on the level of random noise chosen as demonstrated in figure 64(b). Note that for $-(\Delta C)_{max}$, a cutoff is indicated beyond which negative concentrations are predicted.

Consider one wishes to group calculated scalar multiples for constituent A according to several concentration intervals, say (0 ± 5), (10 ± 5), (20 ± 5), (30 ± 5), (40 ± 5) arbitrary units. Figure 64(b) clearly shows that, with random noise not much above 10%, $(\Delta C)_{max}$ begins to exceed ±5 units. This says that scalar multiples will begin to mix between adjoining intervals, resulting in a misinterpretation. Reducing the interval spacing to ±2.5 units requires a reduction in the level of acceptable noise to just above 5%, and so on.

Consider next simple nonlinear constituents A for two powers, $p = 0.5$ and 1.5. Figure 65(a) shows the calculated scalar multiples versus constituent concentrations (no noise, 500 spectra). The nonlinear effects, originally shown in figure 31, are clearly evident. Depicted on these figures are the $\pm 3\sigma_y$ bounds corresponding to 10% random noise. For brevity, bounds for other noise levels are not presented. Whereas, in the linear case equal values of concentration increments $(+(\Delta C)_{max} = -(\Delta C)_{max})$ independent of concentration resulted, the nonlinearity in scalar multiples produces a vastly different picture. Figures 65(b) and 65(c) depict these results for all the noise levels considered.

For nonlinear power $p = 0.5$ the concentration errors increase with increasing concentration in a nonlinear manner. For example, if

one sets concentration error limits of $\pm(\Delta C)_{max} = 5$ units, at low concentrations acceptable noise levels range up to 25%, whereas at the highest concentrations 5% random noise is approaching an unacceptable level. Figure 29(b) demonstrates why this occurs. At low concentrations the spectra are widely separated in terms of radiance but become more closely spaced as concentrations increase. The closely-spaced spectra at high concentrations will intermingle and become confused at lower random noise levels than for the lower concentrations. These facts are reflected in the scalar multiple values in a characteristic vector analysis, hence in the predicted concentration errors.

For constituent powers $p = 1.5$, the results are reversed as figure 65(c) shows. For low concentrations, random noise must be kept small if the concentration errors are to be acceptable. Thus, if $(\Delta C)_{max} = \pm 5$ units, less than 5% random noise is allowable at the lower concentrations. For the higher concentrations, the requirements are reduced, as somewhat more than 10% random noise is acceptable. Note that the "cutoffs" for $-(\Delta C)_{max}$ reflect both negative concentration predictions and the fact that the hypothetical constituents are not defined for concentrations less than zero. Figure 29(c) demonstrates, for $p = 1.5$, the close spacing of the spectra at low concentrations. For additive random noise, these spectra will become confused before those at higher constituent concentrations. This explains the results in figure 65(c).

Wavelength-dependent powers were also considered in this analysis with $p(\lambda) \gtrless 1$ given by equations (6-14) and (6-15). Figures 66(a), 66(b), and 66(c) present the results. Considering the average powers for these two cases fall between $0.5 \leq p_{avg} \leq 1.0$ and $1.0 \leq p_{avg} \leq 1.5$, respectively, it is not surprising to find scalar multiple and concentration error plots intermediate between those presented in figures 64 and 65.

For constituents B and C, the analysis results were basically the same as for constituent A. While the concentration errors found for constituents B and C were slightly larger than for constituent A, the general curve shapes followed those presented in figures 64, 65, and 66. Because of these great similarities in results, for brevity, they are not reported here.

Spatially-Independent and Mixtures of Constituents

Many of the examples involving spatially-independent and mixtures of constituents A, B, and C originally studied in a noisefree environment in Chapters V, VI, and VII were subjected to a random noise analysis. One hundred sets of spectra for each example were analyzed using the technique of characteristic vectors at each of five levels of random noise (1%, 2.5%, 5%, 10%, 25%). For example, for 25-spectra mixture cases, 2500 noisy spectra were generated as input for the analysis. From the examples studied, a few representative cases were chosen for presentation of basic results. These results are figurative in nature to demonstrate noise levels and constituent types

wherein a misinterpretation of scalar coefficients, hence, constituent concentrations, occurs.

In Chapter IV it was demonstrated how the scalar coefficients associated with principal axes eigenvectors, and related to the constituent concentrations, could be presented in an absolute principal components system (II) or a relative scalar multiples system (I). Also, it was shown how, by rotational transformations, the scalar multiples could be transformed into an oblique axis system whereby each axis direction corresponds, presumably, to variations of particular constituent concentrations. In the following examples, it is shown how the error distributions due to random noise are transformed in the process, aiding in the interpretation of these diagrams.

Consider a simple case of spatially-independent linear constituents A + B. Scalar coefficients for 9-spectra input cases were presented in the principal components and scalar multiples systems in figure 15(b) and 15(a), respectively. Note the angle between the vectors for constituents A and B is 90° in figure 15(b) indicating greatly dissimilar constituents. Figure 67 shows the scalar coefficients in this system (II) as random noise levels are increased (1% noise levels not shown). The scatter in scalar coefficients is Gaussian and appears as circular distributions of radius $3\sigma_Y$. The circular distributions are uniform along the lines of constituents since linear constituents were assumed. For the 10% noise level, the distributions begin to overlap indicating quantification errors of ±5 units as the original spectra

were associated with concentration increments of 10 units (0, 10, 20, 30, 40 arbitrary units). For 25% random noise, there is obvious large scatter in the scalar coefficients about their true values. At low concentrations there is also a problem in identifying to which constituent a scalar coefficient point belongs as overlap occurs between constituents. Because the two constituents are spectrally different, however, at higher concentrations one can assign a scalar coefficient point (hence spectra) to a particular constituent even if the quantification of that point is subject to large error.

Figure 68 displays the same case scalar coefficients in the scalar multiples system (I). Because of scaling by the square root of the corresponding eigenvalues, the noise distributions are also scaled (see eq. (8-21)) and they appear as ellipses rather than circles. However, the same trends and comments apply as for figure 67.

Figure 69 shows the scalar multiples of figure 68 transferred into an oblique axes system by rotational transformations. The noise distributions are again circular since the vector lines of constituents A and B are again perpendicular as they were in figure 67. For this oblique axes system, displacements along either axis are proportional to the constituent concentrations. The same observations concerning the noise in figures 67 and 68 prevail here as well.

The last example has shown random noise effects on constituents spectrally very dissimilar. Scalar coefficients could be represented in several systems. Consider next the case of two linear constituents, A + C, which are spectrally very similar. Figures 17(b) and 17(a)

showed, respectively, the noisefree scalar coefficients (principal components and scalar multiples systems) from a characteristic vector analysis of 9 spectra for spatially-independent constituents. A very small angle (11.08°) existed between the first characteristic vectors of the two constituents representative of their spectral similarity. In figure 70, the effects of random noise on these scalar coefficients (System II) are presented. Even at 2-1/2% random noise, there is a question as to constituent separability for coefficients corresponding to 10 units concentration as the circular scatter distributions (radius $3\sigma_Y$) overlap. The separability worsens for higher noise levels. For 10% random noise, the circular distributions begin to overlap along individual constituent directions corresponding to maximum concentration errors of ±5 units. However, the problem of determining to which constituent to assign a particular scalar coefficient point (representing a spectra) is a more significant problem. At 25% random noise, there is marked confusion. There is a high probability of misinterpreting constituents even at the highest concentrations, in marked contrast to the same noise level for the dissimilar constituents in figure 67.

Figure 71 depicts the scalar multiplies system for the scalar coefficients. The same basic comments about constituent separability apply here as well. Note, however, the scaling effect of the eigenvalues is to produce pronounced elongated scatter distributions. This is due to the small value of the eigenvalue of the second principal axes eigenvector relative to the first eigenvalue. The 25% noise case is not presented.

In figure 72, the scalar multiples have been transferred into an oblique axes system. In contrast to the spectrally dissimilar constituents which returned to circular noise distribtuions in the oblique axes system, the noise distributions here are greatly elongated. It is evident that care must be exercised in interpreting scalar coefficient distributions for spectrally similar constituents in this system. Advantages obtained in visual discrimination by spreading the axes directions are tempered by the larger degree of scatter from random noise. However, the same basic comments concerning constituent separability are unchanged.

The effects of changing constituents from linear to simple-non-linear are examined in figures 73 and 74. For spatially-independent simple nonlinear constituents A + B, oblique axes scalar multiplies for random noise of 10% are depicted in figure 73. For power $p = 0.5$, the constituents are separable in terms of concentrations and constituents for low concentrations, whereas for high concentrations the noise distributions overlap significantly indicating large concentration errors, an effect already discussed in the single constituent case (see fig. 65(b)). For power $p = 1.5$, the overlap occurs at low concentrations. The additional problem of constituent separability occurs as well.

In figure 74, the same simple nonlinear powers were used but the constituents, A + C, are spectrally very similar. This results in oblique axes scalar multiple noise distributions (2.5% noise) very elongated in appearance. Otherwise, the same basic comments as for

constituents A + B apply. Constituent separability is a greater problem even at these low noise levels.

True mixtures were considered for basic 25-spectra cases of linear and simple-nonlinear constituents A + B and A + C subject to spectral random noise. Figure 75(a) represents 10% random noise superimposed on the exact case of linear constituents A + B depicted in figure 22(c). The oblique-axes scalar multiples are scattered symmetrically about the uniform pattern of the true values and at 10% noise just begin to overlap. For linear constituents A + C, figure 75(b) depicts the scatter of oblique axes scalar multiples for 2.5% noise. Constituent separability again is a major problem as the scatter is elongated. For example, one may have a point in an area of overlap which corresponds to concentrations (10,0) or (0,10), i.e., there is a question of whether the spectra point corresponds to constituent A or constituent C.

Simple nonlinear constituents in mixtures are depicted in figures 76 and 77. In figure 76, the oblique axes scalar multiples are for power $p = 0.5$ for constituents A + B and A + C at 10% and 2.5% noise levels, respectively. The clustering effect of scalar multiples in the first quadrant presents a significant problem in constituent quantification (large concentration errors indicated) in both cases. However, constituent separability is degraded for constituents A + C even for the lower noise level. Figure 77 shows similar cases but with simple nonlinear power $p = 1.5$ used. Clustering and overlap of oblique axes coefficients is greatest at

low concentrations with concentration errors and constituent separability problems greatest in the third quadrant of the diagrams.

Random noise imposes a scatter distribution independent of the original true patterns of scalar coefficients. For areas of clustering of these scalar coefficients, one observes greater problems in constituent identification and quantification. Some instances of nonlinear superposition enhance these problems. Consider a case of nonlinear superposition presented originally under noisefree conditions as figure 47(a) for simple nonlinear ($p = 0.5$) constituents. Clustering is greatest at the larger concentrations. A 10% random noise analysis produced the oblique axes scalar multiple distributions depicted in figure 78. Significant problems exist in attempts to quantify the transformed scalar multiples in the first quadrant. For example, a scalar multiples point within the error bounds of the true (30,30) concentration point, might also be assignable to concentration levels (30,40), (40,40) or (40,30).

It is clear from the preceding discussion that the nature of individual constituents, in terms of the radiance-concentration relation, and similarity of constituents, in a spectral sense, are significant parameters that effect accurate quantification and identification in the presence of random noise. These concepts are further examined in a real-world test of mixtures of sediments in water.

Application to Laboratory Test Case

Whitlock (1977a) described early two-constituent tests performed in Langley Research Center's Marine Upwell Spectral Signatures Laboratory. Test constituents included Ball Clay and feldspar sediments mixed individually and together in water for various concentrations. Figures 79(a) and 79(b) depict the measured normalized upwell radiance spectra for the individual sediments in water. Spectra corresponding to a number of mixture cases were also collected (not presented here). The available concentrations matrix of collected spectra included:

Feldspar concentration, ppm

Ball Clay Concentration ppm	0	4	9	17	35	52	69	86	129	173
0		10	11	12	13	14	15	16	17	18
4	1									
9	2			19	20		21			
17	3			22	23		24			
35	4									
52	5			25	26		27			28
69	6									
186	7									
129	8			29						30
173	9			31	32	33				34

Spectra numbers are for identification purposes. While not a complete matrix, a good sampling range was obtained. A total of 34 spectra were collected. In the present investigations, spectra were defined using ten wavelengths, every 40 nm between 420 to 780 nm (see fig. 79).

To test for linearity of constituents, the spectra of individual constituents were regression-fitted, wavelength-by-wavelength, with the power-law model of equation (6-3). Figure 80(a) shows the spectral powers obtained. The constituents, based on these tests and power-law model, are considered to be wavelength-dependent nonlinear, although Ball Clay shows a weaker wavelength-dependency than does feldspar. Note that the powers for Ball Clay are less-than-one whereas for feldspar they are generally greater-than-one. Results for Ball Clay in this test are consistent with those of a later test presented in figure 30, but for feldspar, these early test results differ from those presented for another test involving feldspar in figure 30. This demonstrates the advisability of repetitive testing to confirm specific optical physics relationships for constituents.

A characteristic vector analysis of the individual spectra sets was conducted. Figure 80(b) presents the normalized first principal axis eigenvectors for Ball Clay and feldspar. The eigenvectors appear quite consistent with those presented in figure 38 for later laboratory tests. Figure 81 shows the associated scalar multiples for these individual eigenvectors as a function of concentration. The curves

defined are consistent with the powers less than or greater than one from figure 80(a) (see also fig. 66).

The next stage of the analysis was to compute eigenvectors and scalar multiples for all 34 normalized radiance spectra corresponding to the listed concentrations matrix. Variances explained by the first two eigenvectors were 99.759% and 0.190%, respectively. The fact that so much variance could be explained by the first principal axis direction suggests constituents which are spectrally very similar. Indeed, the smallest interband correlation r_{ij} for this data set was 0.990.

Figure 82 shows the associated scalar multiples pairs corresponding to all 34 spectra. For clarity, the individual constituent and mixture points have been symbol coded, numbered according to the reference numbers of the listed concentrations matrix, and individual constituent points connected in order of increasing concentrations. Some general trends are present. For example, lower concentrations of constituents are in the second quadrant whereas highest concentrations fall mainly in the first and fourth quadrants. However, it is not possible to demonstrate a more quantitative pattern.

There are several problems associated with this data set. First, individual constituent and mixture tests required the laboratory water tank be emptied and refilled for each test series. Although filtering-deionization equipment were used to produce a consistent base water, small base water differences nevertheless existed. Also, in these early

tests, spectral fluctuations were present, which may be noted by the curve irregularities observed in figure 79. Indeed, Whitlock (1977a) estimates the standard error of the laboratory data to be 5.7% of the range of measurement values.

For a better understanding of this data set, the spectra were processed in the following manner. The power-law regression solutions that resulted in the powers presented in figure 80 were used to calculate power-fitted spectral curves corresponding to the individual constituent spectra in figure 79. The effect was to remove random fluctuations observed in figure 79. Base water spectra (predicted normalized radiance for zero concentration of constituents) were subtracted from the spectra in each constituent case to alleviate the problem of unequal base waters for the constituents. For mixture spectra corresponding to the mixtures of constituent concentrations indicated in the input matrix, linear superposition of the base water-corrected power-fitted spectra was performed.

The 34 processed spectra were analyzed by the characteristic vectors technique. Variances explained by the first two eigenvectors were found to be 99.760% and 0.215%, respectively. The scalar multiples associated with these eigenvectors are given in figure 83 and may be compared with those of the data set presented in figure 82. Consider the scalar multiple pattern for the individual Ball Clay constituent. The sweeping curve of the power-fit case has replaced some of the irregular patterns observed in figure 82 especially with regards to spectra numbers 4 and 5. The wavelength-dependent nonlinearity

of the constituent is amplified in the Y_2 direction by the scaling effect from the small second principal axis eigenvalue. This same effect was observed in figure 40 for spectrally similar constituents. For feldspar, a curved plot is also in evidence. The marked clustering of scalar multiples at lower concentrations has been demonstrated by previous test cases to be related to powers $p(\lambda)$ of the radiance-concentration relation greater than one. Some of the randomness, especially in the Y_2 direction, has been removed for the power-fitted spectra. Note at the higher concentrations, just as for the Ball Clay curve, a more consistent characteristic direction is assumed by the patterns of scalar multiples.

Some of the scalar multiples of the mixture spectra simulated by a linear superposition are rather consistent with those for the original data, but some are not. Consider point 34 corresponding to constituent concentrations (173,173). The differences in scalar multiples are not large in the Y_1 direction as compared to the Y_2 direction. In many cases, much larger scatters in the Y_2 direction are observed. While some of the differences may be attributed to possible nonlinear superposition processes, it is also suspected that random noise in the raw data also plays a major role. To test this hypothesis, a random noise analysis of the processed power-fitted spectra was conducted. Fifty sets of 34 noisy spectra were generated (1700 total spectra) and subjected to a characteristic vector analysis. Noise levels of σ_n = 1%, 2.5%, and 5% of the maximum range of Ball Clay normalized radiances were investigated. From this analysis, $\pm 3\sigma_{Y_1}$ and $\pm 3\sigma_{Y_2}$ values of

scalar multiple scatter were calculated. Figure 83 depicts the typical observed scatter bounds for the 1% and 2.5% noise cases. Clearly, the scatter for the Y_2 axes direction is much larger than that of the Y_1 direction and may explain some of the differences between figures 82 and 83.

It is concluded that great care must be exercised in interpreting scalar multiple patterns for spectrally-similar constituents as random noise plays a significant role for these cases. The scatter distributions of scalar multiples for feldspar and Ball Clay will overlap considerably even at low noise levels making constituent separability a very real problem. The wavelength-dependent nonlinear nature of the constituents also tend to compound the interpretations.

Random noise has been shown to have variable effects on the use of a characteristic vector analysis. While constituent identification in general, in isolating characteristic vectors of a data set are not affected, in theory, by the presence of random noise, the scalar coefficients associated with individual spectra are subject to errors in constituent identification (separability) and quantification. Spectral similarity and the nature of radiance-concentration relations of individual constituents affect the degree of these errors.

The final problem area to be addressed does not deal directly with the nature of the constituents involved or the exactness of the measurement technique but rather with the changes in spectral signals that occur with a radiative transfer to the altitude of the remote

sensor. The prime consideration is with the nature of the intervening atmosphere.

CHAPTER IX

ATMOSPHERICS

Under laboratory conditions, researchers are free to make measurements of emergent upwell radiance from a water surface without the need to account for atmospheric effects. In the real world, remote sensing measurements are made at such distances that the intervening atmosphere, as shown in figure 1, modifies the upwell radiance spectra in its upward transfer to the altitude of the remote sensor. Characteristic vector analysis must operate on these modified signals. This chapter examines the effects these atmospheric modifications have on the identification, in terms of characteristic vectors, and quantification, in terms of the scalar coefficients, of constituents, both individually and in mixtures.

The Radiative Transfer Equation

The apparent radiance of a water surface, viewed at an altitude Z consists of several components given by (see Austin 1974):

$$L_Z = T_a (L + L_{sky} + L_{sun}) + L^* \qquad (9\text{-}1)$$

where:

L_Z = apparent upwell radiance at altitude Z

T_a = atmospheric transmittance

L = emergent upwell radiance from water surface

L_{sky} = upwell radiance from the reflection of diffuse skylight off the water surface

L_{sun} = upwell radiance from the specular reflection of sunlight (sunglitter) off the water surface

L^* = path radiance (sunlight and skylight scattered within atmosphere and towards the remote sensor)

As Turner et al (1971, 1973, 1977) and Austin (1974) note, the modification terms have the following functional dependencies:

$$T_a = T_a(\lambda, Z, \Phi, \text{atmospheric type})$$

$$L_{sky} = L_{sky}(\lambda, Z, H, \psi, \Phi, \text{atmospheric type, W, background surface reflectances})$$

$$L_{sun} = L_{sun}(\lambda, H, \psi, \Phi, W)$$

$$L^* = L^*(\lambda, Z, H, \psi, \Phi, \text{atmospheric type, background surface reflectances})$$

where:

λ = wavelength

Z = altitude of remote sensor

H = solar altitude

ψ = solar azimuth

Φ = remote-sensor off-nadir scan angle

W = windspeed

The atmospheric type depends on such variables as ozone, carbon dioxide, water vapor, and aerosols including their size distributions and vertical and/or horizontal gradients. Background surface reflectances may vary depending on ground cover, surface films on water and proportions of land/water coverage.

In a general sense, the remote-sensing description is complex, but with proper mission planning and certain assumptions, a relatively simple model is possible. Consider the use of a spectrometer which measures only along a nadir line of flight (Φ = constant). The mission is flown at a fixed altitude (Z = constant) along a fixed flight line over a short enough time period that the solar geometry does not change appreciably (H, ψ fixed). Also, the mission is executed when the solar altitude and/or windspeeds are low enough such that sunglitter is not a factor ($L_{sun} = 0$). Assume a relatively constant background reflectance and no bottom reflectances. Under these assumptions equation (9-1) becomes

$$L_Z(\lambda) = T_a(\lambda)[L(\lambda) + L_{sky}(\lambda)] + L^*(\lambda) \qquad (9\text{-}2)$$

where it is understood that T_a, L_{sky} and L^* also depend on the atmospheric type. Many remote-sensing missions are planned to fix many of the influential variables as just outlined.

Austin (1974) estimates $L_{sky}(\lambda)$ by replacement with

$$L_{sky}(\lambda) = .021\ L^*(\lambda) \qquad (9\text{-}3)$$

where the factor .021 represents the Fresnel reflectance for a smooth surface for a nadir-looking sensor. Utilizing equations (9-2) and (9-3) to calculate the apparent radiance at altitude requires knowledge of the transmittance and path radiance as a function of wavelength and atmospheric type.

Model Atmospheres

The transmittance represents the attenuation effect of the atmosphere on the upwell radiance signal. Austin (1974) presents model results and experimental evidence of the spectral distribution of vertical transmittance through the entire air mass (i.e., satellite altitudes) for various atmosphere types. Two model curves were selected for use in this analysis as shown in figure 84(a). The upper curve represents transmittance for a clear sky (no aerosols) where the scattering is of the Rayleigh type. Attenuation is strongest in the blue (low) spectral range. The lower curve in figure 84(a) represents the results for a Mie scattering type of atmosphere containing aerosols. The transmittance is reduced over that of the Rayleigh type, but the general curve shapes are similar. The two curves have been extrapolated for the 700 to 1000 nm wavelength range based on transmittance spectral variation model studies by Turner (1973).

Path radiance is due to sunlight and skylight scattered into the path of sight between the water surface and remote sensor. At satellite altitudes, this component even on clear days may exceed the emergent upwell signal from the water by a factor of four or five. The spectral variation of path radiance is presented in figure 84(b) for the Rayleigh and Mie scattering atmosphere types based on model information presented by Austin (1974) and measurements of sky radiance (which has a similar spectral variation to path radiance) by Klemas et al (1978a). The data has been arbitrarily normalized to one at 700 nm and plotted on a log scale. The actual magnitude depends on the path distance between the remote sensor and water surface.

Consider next the spectra originally formulated for linear constituent A, given in figure 10, and specifically the spectrum for 40 arbitrary units concentration. The normalized path radiance curves in figure 84(b) were scaled arbitrarily such that the "Rayleigh" type path radiance exceeded the transmitted peak value of modified upwell radiance $(T_a(L + L_{sky}))$ by a factor of two, whereas for the "Mie" type atmosphere, the path radiance factor was taken to be five. Equations (9-2) and (9-3) were then used to calculate total radiance spectra for the altitude of the remote sensor for all upwell spectra given by figure 10. Figure 85 shows a typical example for the different atmosphere types, plotted on a semi-log scale. The original upwell spectrum is for 40 units concentration of constituent A. The transmitted curves $(T_a(L + L_{sky}))$ are somewhat changed in shape

from the original upwell spectrum. The path radiances, L*, are the largest single factors of the total spectra. Spectra-wise, the total signal received at the remote sensor looks little like what originally emerged from the water surface.

Henceforth, the "Rayleigh" atmosphere type is termed the "weak" atmosphere, whereas the "Mie" atmosphere is termed the "strong" atmosphere. The spectral transmittance (fig. 84(a)) and absolute magnitude path radiance spectra (fig. 85) for these two atmosphere types were utilized to modify all upwell spectra considered in the subsequent analyses.

In this analysis, a restrictive form of the general radiative transfer equation is utilized and the particular transmittance and path radiance functions used correspond to nadir-looking remote-sensing flight at satellite or high altitudes. These restrictions and conditions, however, do not diminish the goal of evaluating any basic changes in the characteristic vector analysis technique. In earlier chapters, characteristic vector analysis was shown to apply in an exact manner (total variance explained for each constituent present using a single characteristic vector for each constituent) for linear and simple nonlinear individual, spatially-independent, and mixtures of constituents as well as for the 30-spectra "flight cases" formulated utilizing these constituent forms. The following analysis restricts itself to a study of such exact cases with the reasoning that any basic changes in characteristic vector analysis will apply as well to the instances

of wavelength-dependent constituents or nonlinear superposition of constituents.

Linear and Simple Nonlinear Constituents

Spectra of linear constituents A, B, and C (see table 2) and simple nonlinear constituents A, B, and C with powers $p = 0.5$ (see table 11) and $p = 1.5$ (see table 12) were modified using equations (9-2) and (9-3) based on the weak and strong atmospheric parameters presented in the previous section. Path radiances were suitably adjusted for the simple nonlinear powers to maintain the same relative magnitudes with respect to the constituent spectra. Table 24 lists the modified spectra obtained for constituent A for power-law powers $p = 0.5$, 1.0, and 1.5 for both weak and strong atmospheres. These spectra may be compared to the unmodified spectra given in tables 2, 11, and 12. Similar modified results were obtained for constituents B and C but, for brevity, are not presented here. All of the modified spectra sets for the three constituents were subjected to a characteristic vector analysis.

The mean spectral radiances for the modified constituent spectral sets all exhibited a large increase over those for the unmodified spectra, not an unexpected result because of the additive nature of the sky and path radiances. Also, the correlation matrices R for all constituent cases remained equal to unity indicating total interband correlations, as for the atmosphere-free constituents (e.g., table 3 for the linear constituent cases). This result indicated, in previous

previous work, that a single eigenvector should define an n-band space direction that accounts for 100% of the total data variance (i.e., distribution) along that direction. Indeed, this was the case for all constituent spectra sets, whether linear or simple nonlinear powers were used. Most importantly, however, these characteristic vectors were not the same as derived for the atmosphere-free constituents as the comparison table 25 shows. With the intervening atmosphere modifying the spectral characteristics of the upwell spectra (changing characteristic vectors), a potential problem exists in constituent identification if, for example, the characteristic vectors from laboratory tests or derived under different atmospheric conditions are used for comparison in the rotational transformation search for structure described in previous chapters. The scalar multiples, on the other hand, for the atmosphere-modified spectra sets, remained identical to those of the atmosphere-free cases (see tables 5 and 13). This indicates that relative quantification, without surface truth, or absolute quantification, with minimal surface truth, is unaffected by the added atmosphere. It is precisely this result that allows for a multiple-regression correlation of spectral radiances with surface-truth data even in the presence of a horizontally-homogeneous atmosphere (Whitlock 1977a).

A question arises as to the causal factor for the characteristic vector changes. It is suspected that since $T_a L_{sky}$ and L^* are simply additive constant terms for all spectra (i.e., a horizontally-

homogeneous atmosphere), the changes are related to the atmospheric transmittance, specifically, its spectral variation. To test this supposition, the strong atmosphere constituent cases (linear and simple nonlinear powers) were reexamined using a constant, average value of atmospheric transmittance, $T_a = 0.782$, as a substitute for the wavelength-dependent curve presented in figure 84(a). It was found that characteristic vectors derived for these data sets were equal to the original vectors calculated for the atmosphere-free spectra. This confirmed that it is the wavelength-dependent character of the transmittance, $T_a(\lambda)$, alone which results in a wavelength shift of the spectra sets, resulting in a characteristic vector shift. In the examples considered, for the weak and strong atmospheres, the changes in vector components ranged up to 11.9% and 16.5%, respectively. How important might these spectral shifts be under other atmospheric conditions? Turner (1973) presents model results, for 1 km altitude, for wavelength-dependent transmittance at several values of horizontal visual range, a parameter that gives a practical description of atmospheric types for remote-sensing applications. Figure 86 reproduces these data for the wavelength ranges of interest for this study. A visual range of infinity (transmittance equals one) is the case of no atmosphere. For visual ranges 336 km and 23 km one has a very clear and moderately clear atmosphere whereas for 8 km and 2 km one has a moderately hazy and dense haze atmosphere, respectively. Constituent A spectra were modified by using these transmittance curves. The strong atmosphere sky and path radiances were left unchanged as they do not, for a

horizontally homogeneous atmosphere, cause any changes in the characteristic vectors as previously demonstrated. The characteristic vector components, v_{Aj}, derived for the transmittance functions given in figure 86 were:

Wavelength (nm)	v_{Aj} at specific visual ranges (km)				
	∞	336	23	8	2
500	0.206	0.204	0.200	0.185	0.143
550	.292	.290	.286	.271	.225
600	.358	.357	.353	.344	.309
650	.399	.399	.398	.394	.378
700	.413	.413	.415	.417	.417
750	.399	.399	.402	.407	.425
800	.358	.358	.361	.371	.401
850	.292	.293	.296	.306	.338
900	.206	.207	.210	.219	.248

The characteristic vectors do change with each transmittance function, but percentagewise the changes are not as large as for the transmittance and remain rather small until hazy atmospheric conditions are reached (visual ranges 8 and 2 km).

In the previous examples, the spectra within a set were modified equally by the particular atmosphere used, either strong or weak. This was referred to as a horizontally-homogeneous atmosphere since, if the spectra were considered to be collected along a flight path, the atmosphere appeared the same at all collection points along that flight

path. For the next simulations, however, the atmosphere was allowed to vary along the flight path for which upwell spectra were collected. This represents a horizontally-variable atmosphere. Specifically, the spectra were considered collected in order of increasing constituent concentrations, i.e., 0, 10, 20, 30, 40 arbitrary units as flight line distance increased. The atmospheric modification terms of transmittance, $T_a(\lambda)$, and path radiance, $L^*(\lambda)$, were linearly varied from weak to strong along the flight path. Thus, at the limits, at zero constituent concentration at one end of the flight path, the upwell spectra were modified using weak atmospheric terms, whereas, at the other end of the flight line, at 40 units constituent concentration, strong atmospheric modification terms were used. Intermediate concentrations were modified with atmospheric terms intermediate between weak and strong. This represents a realistic situation, for example, of an aircraft collecting upwell spectra corresponding to rising sediment concentrations in the ocean as a shoreline is approached. The atmosphere may be changing as well from clear conditions over the ocean to hazy conditions near land. Henceforth, this is referred to as the "weak-to-strong" atmosphere modification. The opposite situation was also considered, whereby the atmosphere varied instead from strong-to-weak along the hypothetical flight line. If the concentrations of constituents in water were random along the flight line, this flip-flop of atmospheric variation would be immaterial. But with a directional preference shown by the constituent concentrations, the order of atmospheric variation is important.

All constituent spectra sets previously considered were modified using a weak-to-strong and strong-to-weak linear atmospheric variation along the flight path. A characteristic vector analysis of the modified spectra sets revealed interesting and important variations from the horizontally-homogeneous atmosphere and no atmosphere results. For all cases considered, the correlation matrices for the radiance spectra had terms less than one present indicating less than perfect interband correlations. Indeed, the percentages of variance explained using the first principal axes eigenvector ranged from 98.412% to 99.999% depending on the constituent (A, B, or C) and power ($p = 0.5, 1.0, 1.5$) used. This same less-than-perfect behavior was exhibited for the atmosphere-free constituent spectra sets when they were wavelength-dependent nonlinear. In the present situation, it is the variable atmospheric modification terms that have added a wavelength-dependent nonlinearity. The first eigenvectors, taken to be characteristic vectors, showed marked deviations from either the atmosphere-free or horizontally-homogeneous atmosphere derived characteristic vectors. Additionally, the scalar multiples associated with these vectors changed from case to case, the first such changes for atmosphere-modified constituent spectra. In the interest of brevity, only constituent A results are presented for powers $p = 0.5$, 1.0, and 1.5 in table 26. Comparison with table 25 shows the obvious changes in characteristic vector component values. The scalar multiples may be compared with tables 5 and 13. One may conclude that for a variable atmosphere, there is a distinct problem in constituent identification using

characteristic vectors. It is more complex than for the horizontally-homogeneous atmosphere cases, with the vectors changing not only with constituents but also with particular powers of the radiance-concentration relationship for a constituent. Added to this is the problem of variation in scalar multiple values which have been, in this dissertation, linked to the constituent concentrations. The variable results suggest a problem in constituent quantification with a variable atmosphere. To examine the degree of problem or limitation that exists, linear and simple nonlinear scaling of the scalar multiples were performed using the techniques developed in Chapters V and VI. The results are plotted as figure 87 for the linear and simple nonlinear powers for constituent A for both the weak-to-strong and strong-to-weak atmospheric variations. It is evident that less-than-perfect quantification results now exist for variable-atmosphere cases. The seemingly close fit for the linear case ($p = 1.0$) is deceptive as a linear atmospheric variation is superimposed on a linear concentration variation along the flight path. A more general atmospheric variation would likely degrade these results as well.

In summary, it has been shown that a horizontally-homogeneous atmospheric presence will modify constituent characteristic vectors but not the associated scalar multiples while for a variable atmosphere, both the vectors and scalar multiples vary as the measured upwell spectra assume a wavelength-dependent nonlinearity.

Spatially-Independent and Mixtures of Constituents

Nine and 25-spectra sets of constituents A + B and A + C for linear ($p = 1.0$) and simple-nonlinear ($p = 0.5, 1.5$) radiance-concentration relationships, originally studied in Chapters V and VI, were modified by the horizontally-homogeneous weak and strong atmospheres. These modified spectra sets were subjected to characteristic vector analysis. For the usual transfer, by axes rotations, of calculated scalar multiples into an oblique axis system, comparison characteristic vectors were required for constituent identification. For this study, table 25 provides the choice of using atmosphere-influenced characteristic vectors (weak or strong) or the original vectors derived without the presence of atmospheric effects. Axes rotations using both possibilities were investigated.

Analysis results demonstrated that even under the influence of a horizontally-homogeneous atmosphere, the first two principal axes eigenvectors calculated, in all cases, accounted for 100% of the total data variance. However, the distribution of the percentages of variance explained (l_1 and l_2) varied from those derived for the atmosphere-free cases (Chapters V and VI) as did the scalar multiple values in the original principal axes system. Plots of the scalar multiple points showed, however, the same relative distributions as for the atmosphere-free situations. Axes rotations were first executed using the atmosphere-influenced characteristic vectors (table 25) to identify constituents (recall eqs. (5-11), (5-12), (4-33), (4-34)). After transfer into

the oblique axis system, the transformed scalar multiples were the same, in all cases, as those derived in Chapters V and VI (see figs. 19, 32, and 33, for example). Assuming a base water presence, relative quantification using linear or simple-nonlinear scaling yielded exact results in all cases.

Axes rotations were also performed using the atmosphere-free characteristic vectors for constituent identification. Optimum rotation angles (satisfying eqs. (5-11) and (5-12)) were different from those for the atmosphere-free situations in Chapters V and VI or those found using the atmosphere-influenced constituent vectors just discussed. Transference of the calculated scalar multiples into the so-defined oblique axes systems resulted in values not the same as for the atmosphere-free conditions. Linear or simple-nonlinear scaling of these transformed scalar multiples resulted in inaccurate relative quantification information.

To illustrate some typical results of this study, consider the case of a strong atmosphere modified 25-spectra set representing a mixture of linear constituents A + C. No problems in constituent identification or relative quantification were encountered when the strong atmosphere-influenced characteristic vectors for A and C were used for comparison purposes. Problems were encountered, however, when the atmosphere-free characteristic vectors, v_A and v_C from table 25 were used in a rotational search for structure. Equations (5-11) and (5-12) were not satisfied exactly. Figure 88(a) presents the transformed scalar multiples in the optimized oblique axes system. Clearly, the

lines of constant concentrations of A and C do not align with the Y_1', Y_2'' axes as they should. Figure 88(b) shows the constant concentration mesh lines after application of linear scaling, knowing point O to have been base water. Point X lies along the mesh line for zero concentration of constituent C, but a negative concentration is indicated. Likewise, point Y should indicate a zero concentration of constituent A, but a positive concentration is implied. For mixture point Z, the implied concentration for constituent C is too low.

It is concluded that the presence of a horizontally-homogeneous atmosphere does not necessarily degrade the ability of a characteristic vector analysis to provide accurate relative quantification provided the comparison characteristic vectors used for identification also have been modified by the same type atmosphere. Use of any other comparison vectors results not only in an inability to identify the constituents present, but inaccurate relative quantification information as well. A technique that is very useful in estimating atmosphere-modified characteristic vectors is to find scene locations (training samples) consisting only of single constituents in base water. Use of the atmosphere-modified spectra from these areas define atmosphere-modified characteristic vectors that may be used in the rest of the scene, especially in mixture areas, provided the atmosphere is horizontally homogeneous. This training sample technique was used by Klemas et al (1978a, 1978b) for acid waste, sediment, sewage sludge, clouds and ice in background ocean water. First eigenvectors from these

constituent types demonstrated a day-to-day variability consistent with the atmospheric type changes that occurred.

As a final example of the influence of the atmopshere on characteristic vector analysis, the 30-spectra hypothetical remote-sensing mission depicted by figure 25 for linear constituents A + B was subjected to modification by: (1) strong and weak horizontally-homogeneous atmopsheres and (2) a variable atmosphere which linearly varied from strong-to-weak along the flight lines (strong for spectra numbers 1 or 30 to weak at spectra numbers 14 or 16--see fig. 25). The major purpose was to compare relative quantification results influenced by atmospherics to the exact results depicted by figure 27(b).

For the cases involving horizontally-homogeneous atmospheres, when the appropriate atmosphere-influenced comparison vectors were used (strong or weak, respectively--see table 25), constituent identifications were exact and relative quantification results equalled those of figure 27(b). When the atmosphere-free characteristic vectors were used, however, the identification of constituents A and B were only approximate and relative quantifications were less accurate. Depicted in figure 89(a) are the quantification results when a strong atmosphere was present, whereas, figure 89(b) shows the results when a weak atmosphere was present. Comparison with figure 27(b) reveals the same general distributions of relative quantifications of A and B, but differences up to 0.060 and 0.047 relative quantification units are noted for the strong and weak atmospheric cases, respectively.

More seriously degraded results were obtained when a variable atmosphere was present. It was found that two eigenvectors accounted for 99.651% of the total system variance, less than perfect suggesting wavelength-dependent nonlinearities present. Figure 90(a) shows the scalar multiples calculated for the principal axes system and may be compared with those for atmosphere-free conditions in figure 26(a) (the distribution for the horizontally-homogeneous atmosphere cases were the same as figure 26(a), except rotated to different angles). There are obvious large changes in the distribution of points for the variable-atmosphere condition. In particular, the base water points for the atmosphere-free (or even horizontally-homogeneous) conditions were the same (spectra numbers 1 to 3, 13 to 17, 28 to 30) corresponding to equal spectra. In the variable-atmosphere case the base waters at opposite ends of the flight line are spectrally very much different due to the changing atmospheric contributions. This shows up in the scalar multiple distribution as widely-separated base water points.

To initiate a search for underlying structure, comparison vectors were needed. The question is what ones to use--atmosphere-free, strong- or weak-influenced or some combination of the latter. To begin with, the atmosphere-free characteristic vectors for v_A and v_B were used. Even at best, the minimum results of equations (5-11) and (5-12) were significantly worse than that for the horizontally-homogeneous atmosphere situations. Regardless of these results, the

scalar multiples from figure 90(a) were transformed using the rotation angles θ_1, θ_2 suggested and the results scaled linearly as in previous cases. Clearly, the results, depicted in figure 90(b), are poor. Evidence of constituent B appears as the twin peaks of the distribution, but the relative values are considerably in error at many points (see fig. 27(b)). The curve for constituent A is worse, possessing a single peak not comparable at all to those shown in figure 27(b). Attempts were made to improve the quality of the results by using other sets of comparison vectors including strong atmosphere-influenced, weak atmosphere-influenced and an average of the latter characteristic vectors. No significant improvements in the results were noted.

These examples have demonstrated that a variable atmosphere may degrade identification and quantification results much more seriously than the presence of a horizontally-homogeneous atmosphere. The variable atmosphere situations chosen were extreme, representing satellite altitude conditions (i.e., viewing through the entire atmosphere) with clear and hazy conditions at opposite ends of a flight line. The implications here suggest collecting data at lower altitudes, along shorter flight lines and for clear conditions for a relatively horizontally-homogeneous atmosphere. These conditions are indeed sought after in remote-sensing missions to reduce atmospheric effects on signal variability. These study results have demonstrated the advisability of continuing to satisfy these mission criteria.

Atmospheric Correction Modeling

Although it is advisable to fly remote-sensing missions under conditions that minimize atmospheric effects on upwell spectral signals, such criteria may in turn severely limit the frequency and spatial coverage of remote sensing, restricting its operational usefulness. Having the capability to correct for atmospheric effects under less-than-ideal conditions assumes a major importance.

In the examples studied, the functional dependencies noted for the terms in equation (9-1) were suppressed by restrictions and assumptions. However, replacing a nadir-viewing spectrometer with an off-nadir scanner instrument allows for side-to-side scene capability along the flight line, but also introduces the off-nadir scan angle dependency into the atmospheric terms. Collection of data at different times of the day introduces sun angle effects (not to mention the possibility of changing atmosphere types). It would be very useful to have a theoretical model that would account for these, and other functional dependencies, and allow an atmospheric correction for every resolution element (pixel) in the scene. An example of an atmospheric radiative transfer model that possesses such capabilities was developed by Turner et al (1971, 1973, 1977). The model calculates total downwelling radiance, transmittance and path radiance for a plane-parallel, horizontally-homogeneous atmosphere as a function of altitude (Coney and Salzman 1979). The model is applicable for haze levels ranging from near fog conditions to near total clarity for the entire range of wavelengths used by the remote-sensing instruments in table 1. The

model does require certain input (beyond the usual geographical and sun-remote sensor geometry information). These input, some of which may be estimated if not measured, include atmospheric properties such as spectral optical thicknesses, haze type, aerosol refractive index, background albedo among others. Such additional measurements may require greater mission complexity and surface truth stations to fulfill the goal of increased identification-quantification accuracies of constituents. A recent study (Coney and Salzman 1979) compared measured remote-sensing data to that calculated from the model. The conclusions were that the model performed adequately in a nadir-looking direction, but not as well for off-nadir scan angles. Further research may be necessary to determine if increased model sophistication is needed to improve off-nadir capabilities.

A somewhat different approach to an atmospheric-correction algorithm was devised by Gordon (1978) and is being applied to correct Coastal Zone Color Scanner (CZCS) satellite data. Rather than work a large radiative-transfer model, the approach is semiempirical utilizing the remote-sensing data itself to estimate atmospheric effects. The basic premise is that ocean water (or any low turbidity water area) is nearly opaque to near-infrared radiation (e.g., 750 nm) and the total radiance measured at these wavelengths is due entirely to atmospheric (Rayleigh and aerosol backscatter) and surface reflection effects. Also assumed is the proportionality of atmospheric and surface reflection effects at any wavelength to the measurements made in the near-infrared region.

The wavelength-dependent proportionality factors are determined either by in-situ measurements or estimated from comparison of clear water radiance observations with a priori information made at similar solar elevation angles. The true water radiances (after removal of atmospheric and surface effects) at each pixel and wavelength then become the total measured radiances reduced by the proportionality factor times the total measured radiance.

The correction algorithm has been shown to work well in some test cases (Gordon 1980). In the Gulf of Mexico, for example, corrected images revealed an impressive series of eddy-like structures indistinguishable from atmospheric effects in the original images. It should be noted, however, that the multiplicative transmittance term, T_a, given in equation (9-1) is not measured and that at least one clear water area is required in the image to determine the atmospheric and surface radiances in the near-infrared region. A horizontally-homogeneous atmosphere is implied in the analysis, although the technique has been applied to images where the haze levels were not constant.

The analyses of this chapter have demonstrated the advisability of correcting for atmospheric and surface effects before a characteristic vector analysis is conducted. Although present atmospheric correction models and techniques are in a state of research and development, consideration should be given to their utilization in a research mode. The final test of their applicability would, of course, be the accuracy of identification and quantification results of characteristic vector analysis of corrected input spectra.

CHAPTER X

RECOMMENDATIONS, SUMMARY, AND CONCLUSIONS

In this investigation the use of characteristic vector analysis in the study of water quality has been examined. Specifically, the investigation has focused on how the technique resolves total radiance signals into eigenvectors and associated scalar coefficients and their relationships to the identification and quantification of water constituents. To realize this objective, technique operation was checked on a progression of hypothetical test cases and a limited number of laboratory data sets. As a result of this investigation, an improved understanding of technique usage and limitations has been obtained in the areas of optical physics, in terms of constituent-water interactions, and environmental effects, in terms of measurement noise and atmospherics. Final technique evaluation requires a combination of controlled laboratory experiments in conjunction with field flight experiments which are beyond the scope of this present investigation. As discussed earlier, use of characteristic vector analysis on actual remote-sensing data has been conducted by several investigators (Mueller 1973, 1976; Grew 1977a, 1977b; Klemas et al 1978a, 1978b; Philpot and Klemas 1979) with varying degrees of success. Some of the observations from those flight experiments may now be more readily understood in light of the results of this present investigation.

Under ideal conditions, characteristic vector analysis has the potential of identifying individual constituents in water and performing

a relative quantification of such constituents, even when in mixtures, with a minimum of surface truth calibration. However, poor results may arise with the indiscriminate use of the technique in actual field experiments where the modifications to ideal conditions are not recognized or understood. Hypothetical constituent test cases were used to determine what constitutes ideal conditions. The technique of characteristic vectors was found to identify and quantify exactly when (1) the constituents under study had a radiance-concentration relationship that was linear, (2) the linear constituents superimposed linearly (were additive) in mixtures with no optical, physical, chemical, or electromagnetic interactions, and (3) the radiance data were free of measurement noise and atmospheric effects. While these constitute the major conditions for exact operation of the technique, a number of implied conditions must be fulfilled in any laboratory or field use. These include (1) the water scene under consideration contains varying concentrations of only the constituents under study--other constituents may be present in the scene only in the sense that they remain constant in concentration and do not interact with the study constituents, (2) the vertical concentration gradients and particle-size distributions of the constituents are spatially uniform in the field and correspond to the same conditions studied in laboratory experiments, (3) study constituents are spectrally different in upwell radiance, and (4) previous laboratory testing of constituents of interest in remote sensing has been accomplished to derive the comparison characteristic vectors needed to identify constituents in the field mixture experiments. In

the latter instance, it is useful, but not required, to have a prior knowledge concerning the number and type of constituents involved in a scene of data. This information can greatly reduce the scope of rotational transformational procedures utilized by characteristic vector analysis in identifying the variable constituents in the water.

The major conditions outlined above result in what were termed ideal, additive, linear constituents. From hypothetical test case results it is concluded that for single constituents, the characteristic vector technique defines one eigenvector and associated scalar coefficients sufficient to describe the entire observed data set variance. This eigenvector direction in wavelength hyperspace along which the scalar coefficients, representing individual spectra, are distributed is the characteristic vector for the constituent. For linear constituents, the scalar coefficients are directly proportional to the constituent concentrations. Presuming the minimum scalar coefficient value represents zero constituent concentration, or base water, linear scaling between the extremes of the scalar coefficients results in an accurate relative quantification of the constituent data set. Absolute quantification requires an additional surface truth sample.

For spatially-independent constituents (two or more constituents, not mixed, in the same data scene) and mixtures of constituents, constituent identification using the technique requires comparison vectors. These comparison vectors are the characteristic vectors derived a priori for the individual constituents under study. Principal

axes eigenvectors defined by analysis of the data set spectra are transformed by axes rotation until they equal the comparison vectors. It is concluded that the corresponding transformed scalar coefficients are directly proportional to the constituent concentrations and can be used to quantify in a relative sense exactly as for single constituents. The investigation focused on two-constituent mixtures. However, the results are applicable to any number of constituents provided ideal, additive, linear conditions apply to all constituents. Analytically, it is recognized that the rotational search for structure increases markedly in complexity with each additional constituent. This may limit the practical use of the technique to two or three constituent mixtures.

The scalar coefficients may be displayed in plots as principal component values or scaled by the eigenvalues as scalar multiples. The former system depicts true wavelength space relationships between characteristic vectors of constituents whereas the latter produces visually clearer displays especially for spectrally similar constituents. Transfer into an oblique axes system aligns the distributions of scalar multiples orthogonally according to constituents for ease in quantification. For this reason, this system is recommended.

The remaining analyses in this investigation progressively relaxed the ideal, additive, linear assumptions one-by-one to examine the sensitivities of the technique to less-than-ideal conditions expected in real world operations.

A power-law model may be used to describe nonlinear radiance-concentration behavior for many constituents. The model was regression-fitted to laboratory spectra sets of several sediments, sewage sludges and industrial wastes. It is concluded that no constituent exhibited a strictly linear radiance-concentration behavior. For some constituents the power exponents were nearly independent of wavelength. For complete wavelength independency, these constituents were termed simple nonlinear. For other constituents, the power exponents were strong functions of wavelength and were termed wavelength-dependent nonlinear constituents.

From hypothetical test cases using exact simple nonlinear constituents, singly, spatially-independent and in mixtures, it is concluded that each constituent could be identified exactly by a single characteristic vector as for linear constituents, but that the scalar coefficients are nonlinearly distributed, according to concentration, along the vector directions. For mixtures, these nonlinear distributions may result in clustering of scalar coefficient points represented on plots. Such clustering may be misinterpreted as representing very similar constituent concentrations. For accurate relative quantification, in lieu of surface truth, knowledge of the power exponent is essential to convert the scalar coefficients, by a nonlinear scaling, into relative concentrations. This latter fact strongly suggests the advisability of laboratory testing of constituents to determine the nature of the radiance-concentration relationships. From hypothetical

test cases using exact wavelength-dependent nonlinear constituents, singly, spatially-independent and in mixtures, it is concluded that constituent spectra sets can no longer be described exactly by single characteristic vectors and associated scalar coefficients. Attempts to quantify the scalar coefficients in a relative manner by linear or simple-nonlinear scaling produce degraded results. Plots of scalar coefficients for spatially-independent constituents and mixtures assume curved patterns indicative of their wavelength-dependent nature. Such curvatures become pronounced for scalar multiples of spectrally similar constituents in an oblique axes system. It is concluded that wavelength-dependent nonlinear constituents demonstrate a limitation in the proper use of characteristic vector analysis. In practice, it may be possible to avoid such limitations for some wavelength-dependent nonlinear constituents by choosing ranges of concentration over which the radiance-concentration relationship appears linear or simple nonlinear. This again suggests knowledge of constituent behavior best obtained by carefully controlled laboratory testing.

Nonlinear superposition of mixture constituents results when interactions occur which cause measured upwell radiances for the mixture to differ from a simple sum of radiances for the individual constituents at the same concentrations. This nonlinear superposition behavior may be a complex function of physical, chemical and electromagnetic properties of the individual constituents. The number of possible interactions increase dramatically with each new constituent present in a mixture. A simple interaction model for two-constituent

mixtures was used to formulate hypothetical test cases for testing of characteristic vector analysis in nonlinear superposition cases. Effects on scalar coefficient patterns, related to the constituent concentrations, were evaluated.

It was observed for negative constituent interaction (mixture radiance decrements from additive conditions) that scalar coefficient patterns converged for the mixture spectra. Clustering effects from this convergence become especially pronounced when the constituents have nonlinear radiance-concentration relationships. For positive constituent interactions (mixture radiance increments to additive conditions), the scalar coefficient patterns show a divergence for the mixture spectra. Wavelength-dependent nonlinear constituents add curvature, hence complexity, to these plots.

It is concluded that nonlinear superposition imposes an additional limitation on the use of characteristic vector analysis in quantifying constituents in mixtures. Without prior knowledge of the action of study constituents in a nonlinear superposition process, the convergence and divergence of scalar coefficients could be misinterpreted as constituent concentrations less than or greater than that which actually exists. Laboratory testing of constituents of prime interest in remote sensing in various mixtures over ranges of concentration is recommended to investigate and estimate the degree of such nonlinear superposition behavior.

Noise is an expected consequence of any real world measurements whether in a laboratory or in the field. Random noise is commonly

found in remote-sensor systems. It is concluded from hypothetical test cases that the effects of random noise on identification and quantification of constituents by a characteristic vector analysis depends on three major factors: (1) the degree of random noise, (2) the form of the radiance-concentration relationships of individual constituents and constituent interactions and (3) the spectral similarity of constituents in mixtures. Ideally, random noise does not affect the characteristic vectors of constituents or their identification in mixtures by rotational transformations of principal axes eigenvectors. This requires that the noise have a true random character which is possible when a sufficiently large number of input spectra are available for analysis. This requirement leads to the recommendation that, for laboratory testing of constituents either singly or in mixture tests, repetitive testing be performed using small concentration increments where possible to maximize the number of collected spectra. Confirmation of constituent optical relationships and more precise definition of comparison characteristic vectors are a desired result.

For linear constituents it is concluded that random noise present in spectra induces a scatter in corresponding calculated scalar coefficients which is independent of the constituent concentrations. The concentration errors implied by this scatter in scalar coefficients depend only on the level of random noise present. For simple or wavelength-dependent nonlinear constituents, the implied concentration errors caused by random noise depend both on the degree of random noise

and the magnitude of the nonlinearity. For power exponents less than one, concentration errors are largest for large concentrations and decrease nonlinearly with decreasing constituent concentrations for any level of random noise. The opposite effect is true for nonlinear constituents with power exponents greater than one.

For spatially-independent and mixtures of constituents, it is concluded that in addition to the degree of random noise, nature of individual constituents, and constituent interactions, the degree of spectral similarity is of major concern. For spatially-independent spectrally dissimilar constituents, even in the presence of a large degree of random noise and large implied concentration errors, the individual constituents will be identifiable at the larger concentrations. For spectrally similar constituents, however, the problem of constituent identification for individual spectra may be more serious than the implied concentration errors. Even at low levels of random noise, individual spectra may not be classified with a reasonable certainty as representative of a particular constituent.

For mixtures of constituents, all of the aforementioned factors concerning degrees of noise, types of constituents and interactions, and similarity of constituent spectra are influential. From hypothetical test cases, it is concluded that for spectrally similar constituents, unacceptable errors in identification and quantification using scalar coefficients will be achieved at lower levels of random noise than for constituents which are spectrally dissimilar. The form of the radiance-concentration relationships of the individual constituents

will also influence the concentrations at which such errors are the largest. Nonlinear superposition may further compound any interpretation of scalar coefficients by causing clustering in tight patterns which are easily confused by the presence of random noise.

A characteristic vector analysis of a laboratory experiment involving spectral measurements of two soil types individually and in mixtures was conducted. The soil types had wavelength-dependent non-linearities and were spectrally similar. It was demonstrated that the addition of even low levels of random noise were sufficient to explain observed differences between scalar coefficients calculated from raw data and those obtained from processed data.

The intervening atmosphere between a remote sensor and the water surface acts to modify measured upwell radiance spectra. An exact description of the radiative transfer is complex, depending on many variables of remote-sensor-solar geometry, altitude, wavelength, atmosphere type and conditions. Proper mission planning can fix many of these influential variables and thus prevent uncontrolled data variability. A relatively simple radiative transfer model involving only atmospheric transmittance, sky, and path radiance components results. It is concluded for hypothetical test cases using this model and model atmospheres that for horizontally-homogeneous atmospheres, characteristic vectors of constituents will be changed in a spectral sense. This change was attributed entirely to the wavelength-dependency of the transmittance function. It is further concluded that relative quantification by characteristic vector analysis is unaffected by

a horizontally-homogeneous atmosphere provided comparison characteristic vectors are used which have been properly modified by the atmosphere. Use of any other comparison vectors results not only in an inability to properly identify constituents present, but inaccurate relative quantification as well.

From hypothetical test cases using model atmospheres, it is concluded that a horizontally-variable atmosphere may degrade identification and quantification results obtained by characteristic vector analysis to a serious and unacceptable degree. Variable atmospheric conditions are more likely to exist for data collection along long flight lines, where both spatial and temporal changes may occur, and for high altitudes. Because of the serious problems with a variable atmosphere and functional dependencies that exist in a general radiative transfer solution, it is advisable to correct remote-sensing data for atmospheric and surface effects before a characteristic vector analysis is conducted. A number of theoretical and semiempirical correction models and algorithms are presently in use. Their ability, however, to provide accurate atmospheric corrections under a variety of solar-remote sensor geometry and atmospheric conditions has not been demonstrated. In view of this, it is recommended that collection procedures for spectral data during remote-sensing missions continue to satisfy mission criteria which reduce to a minimum atmospheric effects on signal variability.

It is recognized that the hypothetical test cases and limited laboratory data analyzed in this study have provided only a limited

insight in the use of characteristic vector analysis. Concept validation requires the combined use of controlled laboratory and field experiments. Based on the results of this study, however, it is believed that the analysis technique has promising future applications. Since the technique can, under favorable conditions, identify and relatively quantify constituents with little or no surface truth, it is particularly attractive for use in remote areas where surface truth may be difficult or expensive to obtain. Reliance, instead, is placed on information concerning constituents obtained a priori under controlled laboratory experiments. The technique can successfully handle situations where constituents demonstrate a simple nonlinearity in the radiance-concentration relationship, where random noise is present, and for horizontally-homogeneous atmospheric conditions where spectral data have been obtained under controlled mission criteria.

The most serious problems and limitations on technique usage relate to the wavelength-dependent nonlinear nature of constituents, nonlinear superposition interactions between constituents, random noise effects on spectrally similar constituents and horizontally variable atmospheres. It is recommended that for the characteristic vector analysis technique to be of value, extensive laboratory testing of constituents of foremost interest to remote sensing be conducted to determine which constituents are most likely to be analyzed successfully using the technique, and which ones possess possible limiting factors in terms of wavelength-dependencies, strong interactions with other constituents or close spectral similarities with other

constituents. In flight experiments, minimal atmospheric measurements of parameters such as optical depth or visual range would isolate regions of variable atmospheres.

REFERENCES

Abotteen, R. A. "Principal Component Greenness Transformation in Multitemporal Agricultural Landsat Data." Proceedings of the Twelfth International Symposium on Remote Sensing of Environment. Ann Arbor, Michigan: n.p., April 1978.

Algazi, V. R. "Multispectral Combination and Display of ERTS-1 Data." Proceedings of Third Earth Resources Technology Satellite-1 Symposium. Washington, DC: n.p., December 1973.

Austin, R. W. "The Remote Sensing of Spectral Radiance from below the Ocean Surface." Optical Aspects of Oceanography. (Jerlov, N. G. and Nielsen, E. S., editors). New York: Academic Press, Inc., 1974.

Boland, D. H. P. Trophic Classification of Lakes Using LANDSAT-1 (ERTS-1) Multispectral Scanner Data. EPA-600/3-76-037. Springfield, Virginia: National Technical Information Service, April 1976.

Condit, H. R., and Grum, F. "Spectral Energy Distribution of Daylight." J. Optical Society of America 54 (July 1964): 937-944.

Condit, H. R. "The Spectral Reflectance of American Soils." Photogrammetric Engineering 36 (September 1970): 955-966.

Condit, H. R. "Application of Characteristic Vector Analysis to the Spectral Energy Distribution of Daylight and the Spectral Reflectance of American Soils." Applied Optics 11 (January 1972): 74-86.

Coney, T. A., and Salzman, J. A. "A Comparison of Measured and Calculated Upwelling Radiance over Water as a Function of Sensor Altitude." Proceedings of the Thirteenth International Symposium on Remote Sensing of Environment. Ann Arbor, Michigan: n.p., April 1979.

Cooley, W. W., and Lohnes, P. R. Multivariate Procedures for the Behavioral Sciences. New York: John Wiley and Sons, 1967.

Duntley, S. Q.; Austin, R. W.; Wilson, W. H.; Edgerton, C. F.; and Moran, S. E. Ocean Color Analysis. Scripps Institution of Oceanography Ref. 74-10. San Diego, California: n.p., April 1974.

Friederichs, G. A., and Scarpace, F. L. "A Method of Determining Spectral Dye Densities in Color Films." Proceedings of the American Society of Photogrammetry. Washington, DC: n.p., March 1977.

Fontanel, A.; Blanchet, C.; and Lallemand, C. "Enhancement of LANDSAT Imagery by Combination of Multispectral Classification and Principal Component Analysis." Proceedings of the NASA Earth Resources Survey Symposium. Houston, Texas: n.p., June 1975.

Gordon, H. "Removal of Atmospheric Effects from Satellite Imagery of the Oceans." Applied Optics 17 (May 1978): 1631-1635.

Gordon, H. "Phytoplankton Pigments from the Nimbus-7 Coastal Zone Color Scanner: Comparisons with Surface Measurements." Science 210 (October 3, 1980): 63-65.

Grew, G. W. "Characteristic Vector Analysis as a Technique for Signature Extraction of Remote Ocean Color Data." Proceedings of the Sixth Annual Remote Sensing of Earth Resources Conference. Tullahoma, Tennessee: n.p., March 1977.

Grew, G. W. "Signature Extraction of Ocean Pollutants by Eigenvector Transformation of Remote Spectra." Proceedings of the Fourth Joint Conference on Sensing of Environmental Pollutants. Washington, DC: n.p., November 1977.

Hardy, D. M., and Walton, J. J. "Principal Components Analysis of Vector Wind Measurements." J. of Applied Meteorology 17 (August 1978): 1153-1162.

Harman, H. H. Modern Factor Analysis. Chicago: The University of Chicago Press, 1967.

Harris, R. J. A Primer of Multivariate Statistics. New York: Academic Press, 1975.

Hayden, B. P.; Felder, W. N.; Fisher, J. S.; Resio, D. T.; Vincent, C. L.; and Dolan, R. Systematic Variations in Inshore Bathymetry. AD/A-006 393. Springfield, Virginia: National Technical Information Service, January 1975.

James, W., and Burgess, F. J. "Ocean Outfall Dispersion." Photogrammetric Engineering 36 (December 1970): 1241-1250.

Jenson, S. K., and Waltz, F. A. "Principal Components Analysis and Canonical Analysis in Remote Sensing." Proceedings of the American Society of Photogrammetry. Washington, DC: n.p., March 1979.

Jerlov, N. G. Marine Optics. New York: Elservier Publishing Company, 1968.

Jobson, Daniel. National Aeronautics and Space Administration, Langley Research Center, Hampton, Virginia. Interview. 7 April 1980.

Johnson, R. W., and Bahn, G. S. Quantitative Analysis of Aircraft Multispectral-Scanner Data and Mapping of Water Quality Parameters in the James River in Virginia. NASA TP-1021. Springfield, Virginia: National Technical Information Service, December 1977.

Kitchen, J. C. Particle Size Distributions and the Vertical Distribution of Suspended Matter in the Upwelling Region Off Oregon. NASA CR-156668. Springfield, Virginia, National Technical Information Service, January 1975.

Klemas, V.; Philpot, W.; and Davis, G. Determination of Spectral Signatures of Substances in Natural Waters. NASA CR-156998. Springfield, Virginia: National Technical Information Service, March 1978.

Klemas, V.; Bartlett, D.; and Philpot, W. "Remote Sensing of Coastal Environment and Resources." Proceedings Coastal Mapping Symposium. Rockville, Maryland: n.p., August 1978.

Klooster, S. A., and Scherz, J. P. "Water Quality by Photographic Analysis." Photogrammetric Engineering 40 (August 1974): 927-935.

Kuo, C. Y., and Cheng, R. Y. K. Laboratory Requirements for In-situ and Remote Sensing of Suspended Material. Technical Report 76-C2. Norfolk, Virginia. Old Dominion University, 1976.

LeCroy, S. R. Signal and Noise Data from Recent Multispectral Scanner Experiments and Their Effects on Multiple Regression Analysis. Vought Hampton Memorandum V-19100/9LTR-038, Hampton, Virginia: n.p., January 1979.

Lewis, B. W., and Collins, V. G. Remotely Sensed and Laboratory Spectral Signatures of An Ocean-Dumped Acid Waste. NASA TN D-8467, Springfield, Virginia: National Technical Information Service, July 1977.

Lodwick, G. D. "Measuring Ecological Changes in Multitemporal LANDSAT Data Using Principal Components." Proceedings of the Thirteenth International Symposium on Remote Sensing of Environment. Ann Arbor, Michigan: n.p., April 1979.

Morris, R. H., and Morrissey, J. H. "An Objective Method for Determining of Equivalent Neutral Densities of Color Film Images. II. Determination of Primary Equivalent Neutral Densities." J. Optical Society of America 44 (July 1954): 530-534.

Mueller, J. L. "The Influence of Phytoplankton on Ocean Color Spectra." Ph.D. dissertation. Oregon State University, 1973.

Mueller, J. L. "Ocean Color Spectra Measured off the Oregon Coast: Characteristic Vectors." Applied Optics 15 (February 1976): 394-402.

Murai, S. Water Environment Evaluation for Inland Sea by Principal Component Analysis. NASA CR-149565. Springfield, Virginia: National Technical Information Service, December 1976.

Nie, N. H.; Hull, C. H.; Jenkins, J. G.; Steinbrenner, K.; and Bent, D. H. Statistical Package for the Social Sciences. New York: McGraw-Hill Book Company, 1975.

Ohlhorst, C. W., and Bahn, G. S. "Mapping of Particulate Iron In An Ocean Dump." Photogrammetric Engineering and Remote Sensing 45 (August 1979): 1117-1122.

Philpot, W., and Klemas, V. Detection of Ocean Waste in the New York Bight. Final Report NASA Grant NSG 1398. Springfield, Virginia: National Technical Information Service, March 1979.

Podwysocki, M. H.; Gunther, F. J.; and Blodget, H. W. Discrimination of Rock and Soil Types by Digital Analysis of LANDSAT Data. NASA TM X-71290. Springfield, Virginia: National Technical Information Service, January 1977.

Ready, P. J., and Wintz, P. A. "Information Extraction, SNR Improvement, and Data Compression in Multispectral Imagery." IEEE Transactions on Communications COM 21 (October 1973): 1123-1131.

Santisteban, A., and Munoz, L. "Application of Image Principal Component Technique to the Geological Study of a Structural Basin in Central Spain." Symposium Proceedings Machine Processing of Remotely Sensed Data. West Lafayette, Indiana: n.p., June 1977.

Scholz, D.; Fuhs, N.; and Hixson, M. "An Evaluation of Several Different Classification Schemes: Their Parameters and Performance." Proceedings of the Thirteenth International Symposium on Remote Sensing of Environment. Ann Arbor, Michigan: n.p., April 1979.

Simonds, J. L. "Application of Characteristic Vector Analysis to Photographic and Optical Response Data." J. Optical Society of America 53 (August 1963): 968-974.

Strandberg, C. H. "Water Quality Analysis." Photogrammetric Engineering 32 (March 1966): 234-248.

Taylor, M. M. "Principal Components Colour Display of ERTS Imagery." Proceedings of Third Earth Resources Technology Satellite-1 Symposium. Washington, DC: n.p., December 1973.

Turner, R. E.; Malila, W. A.; and Nalepka, R. F. "Importance of Atmospheric Scattering in Remote Sensing, or Everything You've Always Wanted to Know About Atmospheric Scattering But Were Afraid to Ask." Proceedings of the Seventh International Symposium on Remote Sensing of Environment. Ann Arbor, Michigan: n.p., May 1971.

Turner, R. E. "Atmospheric Effects in Remote Sensing." Proceedings of Earth Resources Observation and Information Analysis Systems Conference. Tullahoma, Tennessee: n.p., March 1973.

Turner, R. E. Atmospheric Transformation of Multispectral Remote Sensor Data. NASA CR-135338. Springfield, Virginia. National Technical Information Service, November 1977.

Usry, J. W.; Witte, W. G.; Whitlock, C. H.; and Gurganus, E. A. Laboratory Measurements of Radiance and Reflectance Spectra of Dilute Primary-Treated Sewage Sludge. NASA TP-1038. Springfield, Virginia: National Technical Information Service, November 1977.

Usry, J. W.; Witte, W. G.; Whitlock, C. H.; and Gurganus, E. A. Laboratory Measurements of Radiance and Reflectance Spectra of a Dilute Biosolid Industrial Waste Product. NASA TP-1401. Springfield, Virginia: National Technical Information Service, February 1979.

Whitlock, C. H. "Fundamental Analysis of the Linear Multiple Regression Technique for Quantification of Water Quality Parameters From Remote Sensing Data." Ph.D. dissertation. Old Dominion University, 1977.

Whitlock, C. H.; Usry, J. W.; Witte, W. G.; and Gurganus, E. A. Laboratory Measurements of Upwelled Radiance and Reflectance Spectra of Calvert, Ball, Jordan, and Feldspar Soil Sediments. NASA TP-1039. Springfield, Virginia: National Technical Information Service, December 1977.

Whitlock, C. H.; Witte, W. G.; Gurganus, E. A.; and Usry, J. W. Laboratory and Field Measurements of Upwelled Radiance and Reflectance Spectra of Suspended James River Sediments Near Hopewell, Virginia. NASA TP-1292. Springfield, Virginia: National Technical Information Service, October 1978.

Whitlock, C. H., and Kuo, C. Y. "A Regression Technique for Evaluation and Quantification for Water Quality Parameters from Remote Sensing Data." Proceedings of the Thirteenth International Symposium on Remote Sensing of the Environment. Ann Arbor, Michigan: n.p., April 1979.

Williams, D. L., and Borden, F. Y. A Reduction in Ag/Residential Signature Conflict Using Principal Components Analysis of LANDSAT Temporal Data. NASA TM X-71387. Springfield, Virginia: National Technical Information Service, July 1977.

Witte, W. G.; Usry, J. W.; Whitlock, C. H.; and Gurganus, E. A. Laboratory Measurements of Radiance and Reflectance Spectra of Dilute Secondary-Treated Sewage Sludge. NASA TP-1089. Springfield, Virginia: National Technical Information Service, December 1977.

Witte, W. G.; Usry, J. W.; Whitlock, C. H.; and Gurganus, E. A. Spectral Measurements of Ocean-Dumped Wastes Tested in the Marine Upwelled Spectral Signature Laboratory. NASA TP-1480. Springfield, Virginia: National Technical Information Service, September 1979.

Yost, E. F., and Wenderoth, S. "Multispectral Color Aerial Photography." Photogrammetric Engineering 33 (September 1967): 1020-1033.

APPENDIX A

LIST OF SYMBOLS

a = intercept coefficient in scalar coefficient-concentration relationship given by equation (5-7)

B = base water upwell radiance

b = slope coefficient in scalar coefficient-concentration relationship given by equation (5-7)

C = constituent concentration in water

$\hat{C}$ = transformed linear concentrations defined by equation (6-4b)

e = error function defined in equation (6-18)

f = simple-nonlinear scaling function defined by equations (6-10) and (6-12)

g = interaction function in nonlinear superposition

H = solar altitude

h = linear scaling function defined by equation (5-10)

I = identity matrix

J = constant defined by equation (D-3)

K = general interaction coefficients in nonlinear superposition

k = interaction coefficients in power-law model of nonlinear superposition

k_p = constant interaction coefficients

L = upwell spectral radiance from water

$\bar{L}$ = mean spectral radiance of collected spectra

L_{sun} = spectral radiance from reflected sunlight

L_{sky} = spectral radiance from reflected diffuse skylight

L^* = spectral path radiance

L_Z = total spectral radiance at altitude of remote sensor

l = percentage of total variance explained by an eigenvector

M = proportionality (shaping) function for radiance-concentration relationship

P = matrix of mean-corrected spectra

P' = transpose of matrix of mean-corrected spectra

p'p = elements of matrix formed by product of P' and P

R = correlation matrix

r = elements of correlation matrix

S_X = variance-covariance matrix for original wavelength axes system

S_η = variance-covariance matrix for noise

S_T = total variance-covariance matrix defined by equation (8-4)

S/N = signal-to-noise ratio defined by equation (8-23)

s = elements of S_X

T = rotation transformation matrix

T_a = atmospheric transmittance

t = elements of T

U = spectral data sample

u = eigenvector for alternate spectrometer system

V = vectors for iterations on variance-covariance matrix

v = eigenvector or characteristic vector

W = windspeed

X = wavelength or band in original measurement system

Y = scalar coefficients

y = scalar coefficients for alternate spectrometer system

Z = altitude of remote sensor

α = intercept coefficient in regression equation

β = slope coefficient in regression equation

Δ = increment change in variable

ε = error in estimation of variable

θ = angle of rotation of principal axes from original position

λ = wavelength

λ_k = eigenvalues

λ_o = phase difference

ρ = upwell reflectance from water

ρ_o = base-water upwell reflectance

σ = standard deviation

σ_n = noise standard deviation

σ_X = standard deviation of spectral radiance data

σ_Y = standard deviation of scalar coefficients

ϕ = angle between oblique axes defined by equation (4-32)

Φ = off-nadir scan angle of remote sensor

ψ = solar azimuth

Subscripts:

A,B,C = refers to hypothetical constituents A, B, C

avg = average

BB = Bailey Bay sediments

B_{100} = Bermuda Hundred sediments

I, II = systems of calculating eigenvectors and scalar coefficients

i = index of spectra or sample point numbers

j = index of wavelength or band numbers

k = index of retained eigenvectors

m = total number of spectra (or sample points)

N = number of constituents

n = total number of wavelengths or bands

p = total number of retained eigenvectors

u = upwell

X = reference to original wavelength system

Y = reference to principal axes system

Superscripts:

d = degree of polynomial in regression equation (3-2)

p = power in nonlinear constituent model

q,r = powers used in power-law model of interaction term for nonlinear superposition

',","' = transformed variables after first, second, and third axes rotations

Special:

$\sim$ = denotes variables with noise present

APPENDIX B

CALCULATION PROCEDURE FOR EIGENVALUES AND EIGENVECTORS

The variance-covariance matrix of spectral data, S, is related to the product of the transpose of the mean-corrected data matrix, P', and P itself by

$$S = \frac{1}{(m - 1)} (P' P) \qquad (C\text{-}1)$$

Eigenvalues and eigenvectors of (P' P) can be calculated directly from

$$v_k(P' P) = \lambda_k v_k \qquad (C\text{-}2)$$

A simple iterative method of converging on a sequence of eigenvectors and eigenvalues is described by Simonds (1962). These steps, with slight modification, include:

(1) premultiply (P' P), an $n \times n$ matrix, by an arbitrary $(1 \times n)$ row vector, V_o. Although the choice of V_o is arbitrary, a row vector of ones is customary,

(2) normalize the resulting product, $V_o(P' P)$, a $(1 \times n)$ row vector, by dividing by its largest element and denote the result by V_1,

(3) premultiply (P' P) by V_1 and normalize again by the largest element, denoting the result by V_2,

(4) continue the iterations until $V_M \rightarrow V_{M-1}$ to a preset level of accuracy.

(5) The largest element of V_M is the first eigenvalue. Normalize V_M by one of two methods,

(a) in System I (Simonds 1962), such that the sum of the squares of the elements of V_M equals the largest element, or eigenvalue λ_1, or

(b) in System II (Mueller 1973), such that the sum of the squares of the elements of V_M equals unity.

(6) Denote the normalized vector V_M by v_1, the eigenvector corresponding to the largest eigenvalue.

(7) Compute the residual matrix $(P' P - v_1' v_1)$, return to step (1) and repeat the sequence to obtain the second largest eigenvalue, λ_2, and corresponding eigenvector, v_2.

(8) Continue the procedure for as many eigenvalues and eigenvectors ($k_{max} = n$) as needed to fully account for the original data variance or such that an acceptable high percentage is explained.

Convergence in the above procedure is rapid, requiring only a few iterations in most cases considered. The results of the computations are a hierarchal sequence of eigenvalues and corresponding eigenvectors.

APPENDIX C

CONVERSION OF EIGENVECTORS AND SCALAR MULTIPLES FOR DIFFERENT SPECTRA MEASUREMENT SYSTEMS

A question arises as to how the number and placement of wavelengths or bands used to define input spectra to a characteristic vector analysis affects the calculated normalized eigenvectors (or characteristic vectors) and associated scalar multiples. One might foresee the situations of, for example, detailed spectrometer measurements made in the laboratory or from an aircraft at n-wavelengths, compared to measurements made from a different spectrometer utilizing m wavelengths where $m < n$. Conversion of normalized eigenvectors and scalar multiples from one system to another is considered in the following discussion.

Exact Conversion Formulation

By definition, for an n-band normalized eigenvector, the sum of the squares of all the components is one;

$$\sum_{j=1}^{n} (v_{kj})^2 = 1 \qquad \text{(D-1)}$$

which is true for any of k eigenvectors. For the case of a scene of data measured by an m-band spectrometer, the normalized eigenvectors have the property,

$$\sum_{j=1}^{m} (u_{kj})^2 = 1 \qquad \text{(D-2)}$$

where $m < n$.

Assume that the wavelengths or bands specified in equation (D-2) are some subset of the wavelengths or bands specified in equation (D-1). Sum the squares of the elements of the eigenvectors v_{kj}, but only at the m wavelengths specified by the second spectrometer system. Equation (D-1) reduces to

$$\sum_{j=1}^{m} (v_{kj})^2 = J \tag{D-3}$$

where $J < 1$ since $m < n$.

Equation (D-3) may be rewritten as

$$\frac{1}{J} \sum_{j=1}^{m} (v_{kj})^2 = 1 \tag{D-4}$$

Equating equations (D-4) and (D-2)

$$\frac{1}{J} \sum_{j=1}^{m} (v_{kj})^2 = \sum_{j=1}^{m} (u_{kj})^2 \tag{D-5}$$

This change is proportional and applicable on a term-by-term basis as

$$u_{kj} = \sqrt{\frac{1}{J}}\, v_{kj} \tag{D-6}$$

where $j = 1,2,\ldots,m$.

The scalar multiples associated with each vector are Y_{ki} and y_{ki}, respectively. Since the products of the eigenvectors and scalar multiples are the same in both instances (to yield the same input spectra), it can be shown that

$$y_{ki} = \sqrt{J}\ Y_{ki} \tag{D-7}$$

Equations (D-3), (D-6) and (D-7) specify the conversion of eigenvectors and scalar multiples from one spectrometer system to another.

If the m wavelengths of the second spectrometer system do not correspond to wavelengths in the n-band spectrometer system, an approximate solution is possible in equation (D-3) by interpolation of the values v_{kj} at the m wavelengths of the second spectrometer system. However, for any of the m wavelengths falling outside of the n-wavelength range of the first spectrometer system, an extrapolation is necessary which is considerably more presumptive in nature. Also, if the first spectrometer system, for which the eigenvectors and scalar multiples are known, has considerably less defining wavelengths or bands than the second system into which the eigenvectors and scalar multiples are to be converted, considerable interpolation and assumption of spectral variations between wavelengths is necessary, and the expression becomes more speculative.

Consider the case where the eigenvectors, v_{kj}, are constant with wavelength. By equation (D-1)

$$n\, v_{ki}^2 = 1 \tag{D-8}$$

and by equation (D-3)

$$m\, v_{ki}^2 = J \tag{D-9}$$

A ratio of equations (D-9) and (D-8) becomes

$$J = \frac{m}{n} \tag{D-10}$$

and equations (D-6) and (D-7) become

$$u_{kj} = \sqrt{\frac{n}{m}}\; v_{kj} \tag{D-11}$$

and

$$u_{ki} = \sqrt{\frac{m}{n}}\; Y_{ki} \tag{D-12}$$

which are the equations cited by Mueller (1973). These equations become approximate when the eigenvectors are not constant (see fig. 38 for example). Under these circumstances, accuracies are considerably reduced when m and n are small.

Figures 38 and 57(a) demonstrate the change in characteristic vectors for Bermuda Hundred and Bailey Bay sediments in water as the

numbers of wavelengths is reduced from 15 (every 40 nm from 420 to 960 nm) to 9 (every 40 nm from 460 to 780 nm). The characteristic vectors in figure 57(a) can be directly calculated from the vectors presented in figure 38, using equations (D-3) and (D-6).

APPENDIX D

TABLES

TABLE 1.- MEASUREMENT CHARACTERISTICS OF TYPICAL AIRCRAFT AND SATELLITE MULTISPECTRAL SCANNERS

Sensor	Ocean Color Sensor (OCS)	Bendix Modular Multispectral Scanner (M_2S)	Multichannel Ocean Color Sensor (MOCS)	Test Bed Aircraft Multispectral Scanner (TBAMS)	Nimbus 7 Coastal Zone Color Scanner (CZCS)	LANDSATS 1,2,3	LANDSAT D
Wavelength Ranges (nm)	423 - 443 461 - 481 499 - 519 537 - 557 573 - 593 610 - 630 652 - 672 688 - 708 723 - 743 762 - 782	380 - 440 440 - 490 495 - 535 540 - 580 580 - 620 620 - 660 660 - 700 700 - 740 760 - 860 970 - 1060 + Thermal	400 ↑ 20 Channels 15 nm Bandwidth Each ↓ 700	460 - 480 502 - 522 548 - 568 590 - 610 630 - 650 670 - 690 703 - 723 + Thermal	433 - 453 510 - 530 540 - 560 660 - 680 700 - 800 + Thermal	500 - 600 600 - 700 700 - 800 800 - 1100 + *Thermal *LANDSAT 3 only	450 - 520 520 - 600 630 - 690 760 - 900 1550 - 1750 + Thermal
Surface Swath Width (km)	25	6.8	1.6	3.8	1500	185	185
Surface Resolution (m) for Characteristic Altitude (km)	75 at 19.8 km	7 at 2.4 km	10.5 × 21.4 at 5.3 km	7 at 3.3 km	800 at 925 km	70 at 900 km	30 at 705 km

TABLE 2.- CONCENTRATION AND RADIANCE VALUES FOR HYPOTHETICAL IDEAL, LINEAR CONSTITUENTS A, B, C - SINGLE CONSTITUENTS AND MIXTURES WITH CONSTANT BASE WATER SPECTRUM REMOVED

Spectra Number	Constituent Concentrations			Radiances (arbitrary units) at specific wavelengths (nm)								
	C_A	C_B	C_C	500	550	600	650	700	750	800	850	900
1	0	0	0	0.000	0.000	0.000	0.000	0.000	0.000	0.000	0.000	0.000
2	0	10	0	1.732	2.000	1.732	1.000	.000	-1.000	-1.732	-2.000	-1.732
3	0	20	0	3.464	4.000	3.474	2.000	.000	-2.000	-3.464	-4.000	-3.464
4	0	30	0	5.196	6.000	5.196	3.000	.000	-3.000	-5.196	-6.000	-5.196
5	0	40	0	6.928	8.000	6.928	4.000	.000	-4.000	-6.928	-8.000	-6.928
6	10	0	0	1.000	1.414	1.732	1.932	2.000	1.932	1.732	1.414	1.000
7	20	0	0	2.000	2.828	3.464	3.864	4.000	3.864	3.464	2.828	2.000
8	30	0	0	3.000	4.243	5.196	5.796	6.000	5.796	5.196	4.243	3.000
9	40	0	0	4.000	5.657	6.928	7.727	8.000	7.727	6.928	5.647	4.000
10	10	10	0	2.732	3.414	3.464	2.932	2.000	.932	.000	-.586	-.732
11	20	10	0	3.732	4.828	5.196	4.864	4.000	2.864	1.732	.828	.268
12	30	10	0	4.732	6.243	6.928	6.796	6.000	4.796	3.464	2.243	1.268

TABLE 2.- CONTINUED

Spectra Number	Constituent Concentrations			Radiances (arbitrary units) at specific wavelengths (nm)								
	C_A	C_B	C_C	500	550	600	650	700	750	800	850	900
13	40	10	0	5.732	7.657	8.660	8.727	8.000	6.727	5.196	3.657	2.268
14	10	20	0	4.464	5.414	5.196	3.932	2.000	-.068	-1.732	-2.586	-2.464
15	20	20	0	5.464	6.828	6.928	5.864	4.000	1.868	.000	-1.172	-1.464
16	30	20	0	6.464	8.243	8.660	7.796	6.000	3.796	1.732	.243	-.464
17	40	20	0	7.464	9.657	10.392	9.727	8.000	5.727	3.464	1.657	.536
18	10	30	0	6.196	7.414	6.928	4.932	2.000	-1.068	-3.464	-4.586	-4.196
19	20	30	0	7.196	8.828	8.660	6.864	4.000	.864	-1.732	-3.172	-3.196
20	30	30	0	8.196	10.243	10.392	8.796	6.000	2.796	.000	-1.758	-2.196
21	40	30	0	9.196	11.657	12.124	10.727	8.000	4.727	1.732	-.343	-1.196
22	10	40	0	7.928	9.414	8.660	5.932	2.000	-2.068	-5.196	-6.586	-5.928
23	20	40	0	8.928	10.828	10.392	7.864	4.000	-.136	-3.464	-5.172	-4.928
24	30	40	0	9.928	12.243	12.124	9.796	6.000	1.796	-1.732	-3.757	-3.928
25	40	40	0	10.928	13.657	13.856	11.727	8.000	3.727	.000	-2.343	-2.928
26	0	0	0	0.000	0.000	0.000	0.000	0.000	0.000	0.000	0.000	0.000

TABLE 2.- CONCLUDED

Spectra Number	Constituent Concentrations			Radiances (arbitrary units) at specific wavelengths (nm)								
	C_A	C_B	C_C	500	550	600	650	700	750	800	850	900
27	0	0	10	.518	1.000	1.414	1.732	1.932	2.000	1.932	1.732	1.414
28	0	0	20	1.035	2.000	2.828	3.464	3.864	4.000	3.864	3.464	2.828
29	0	0	30	1.553	3.000	4.243	5.196	5.796	6.000	5.796	5.196	4.243
30	0	0	40	2.071	4.000	5.657	6.928	7.727	8.000	7.727	6.928	5.657

TABLE 3.- CORRELATION MATRICES FOR SINGLE-CONSTITUENT SPECTRA

OF IDEAL, LINEAR CONSTITUENTS A, B, C

Constituent A

Correlations at specific wavelengths (nm)

λ-nm	500	550	600	650	700	750	800	850	900
500	1.000	1.000	1.000	1.000	1.000	1.000	1.000	1.000	1.000
550	1.000	1.000	1.000	1.000	1.000	1.000	1.000	1.000	1.000
600	1.000	1.000	1.000	1.000	1.000	1.000	1.000	1.000	1.000
650	1.000	1.000	1.000	1.000	1.000	1.000	1.000	1.000	1.000
700	1.000	1.000	1.000	1.000	1.000	1.000	1.000	1.000	1.000
750	1.000	1.000	1.000	1.000	1.000	1.000	1.000	1.000	1.000
800	1.000	1.000	1.000	1.000	1.000	1.000	1.000	1.000	1.000
850	1.000	1.000	1.000	1.000	1.000	1.000	1.000	1.000	1.000
900	1.000	1.000	1.000	1.000	1.000	1.000	1.000	1.000	1.000

TABLE 3.- CONTINUED

Constituent B

Correlations at specific wavelengths (nm)

λ-nm	500	550	600	650	700	750	800	850	900
500	1.000	1.000	1.000	1.000	1.000	-1.000	-1.000	-1.000	-1.000
550	1.000	1.000	1.000	1.000	1.000	-1.000	-1.000	-1.000	-1.000
600	1.000	1.000	1.000	1.000	1.000	-1.000	-1.000	-1.000	-1.000
650	1.000	1.000	1.000	1.000	1.000	-1.000	-1.000	-1.000	-1.000
700	1.000	1.000	1.000	1.000	1.000	-1.000	-1.000	-1.000	-1.000
750	-1.000	-1.000	-1.000	-1.000	-1.000	1.000	1.000	1.000	1.000
800	-1.000	-1.000	-1.000	-1.000	-1.000	1.000	1.000	1.000	1.000
850	-1.000	-1.000	-1.000	-1.000	-1.000	1.000	1.000	1.000	1.000
900	-1.000	-1.000	-1.000	-1.000	-1.000	1.000	1.000	1.000	1.000

TABLE 3.- CONCLUDED

Constituent C

Correlations at specific wavelengths (nm)

λ-nm	500	550	600	650	700	750	800	850	900
500	1.000	1.000	1.000	1.000	1.000	1.000	1.000	1.000	1.000
550	1.000	1.000	1.000	1.000	1.000	1.000	1.000	1.000	1.000
600	1.000	1.000	1.000	1.000	1.000	1.000	1.000	1.000	1.000
650	1.000	1.000	1.000	1.000	1.000	1.000	1.000	1.000	1.000
700	1.000	1.000	1.000	1.000	1.000	1.000	1.000	1.000	1.000
750	1.000	1.000	1.000	1.000	1.000	1.000	1.000	1.000	1.000
800	1.000	1.000	1.000	1.000	1.000	1.000	1.000	1.000	1.000
850	1.000	1.000	1.000	1.000	1.000	1.000	1.000	1.000	1.000
900	1.000	1.000	1.000	1.000	1.000	1.000	1.000	1.000	1.000

TABLE 4.- MEAN RADIANCE AND CHARACTERISTIC VECTOR SPECTRA FOR HYPOTHETICAL, LINEAR CONSTITUENTS A, B, C

Mean radiance (arbitrary units)	λ, wavelength, nm 500	550	600	650	700	750	800	850	900
$\bar{L}_A$	2.000	2.828	3.464	3.864	4.000	3.864	3.464	2.828	2.000
$\bar{L}_B$	3.464	4.000	3.464	2.000	0.000	-2.000	-3.464	-4.000	-3.464
$\bar{L}_C$	1.035	2.000	2.828	3.464	3.864	4.000	3.864	3.464	2.828

Characteristic vectors normalized to eigenvalue (arbitrary units)	λ, wavelength, nm 500	550	600	650	700	750	800	850	900
v_A	3.162	4.472	5.477	6.109	6.325	6.109	5.477	4.472	3.162
v_B	5.477	6.325	5.477	3.162	0.000	-3.162	-5.477	-6.325	-5.477
v_C	1.637	3.162	4.472	5.477	6.109	6.325	6.109	5.477	4.472

Characteristic vectors normalized to unity (arbitrary units)	λ, wavelength, nm 500	550	600	650	700	750	800	850	900
v_A	0.206	0.292	0.358	0.399	0.413	0.399	0.358	0.292	0.206
v_B	0.369	0.426	0.369	0.213	0.000	-0.213	-0.369	-0.426	-0.369
v_C	0.109	0.210	0.297	0.363	0.405	0.420	0.405	0.363	0.297

TABLE 5.- SCALAR COEFFICIENTS FOR HYPOTHETICAL, LINEAR CONSTITUENTS A, B, C

	Spectra Number	Constituent Concentration	$(Y_{1i})^{*}_{I}$	$(Y_{1i})^{**}_{II}$
Constituent A	1	0	-0.632	-9.688
	6	10	-0.316	-4.844
	7	20	0.000	0.000
	8	30	0.316	4.844
	9	40	0.632	9.688
Constituent B	1	0	-0.632	-9.381
	2	10	-0.316	-4.690
	3	20	0.000	9.000
	4	30	0.316	4.690
	5	40	0.632	9.381
Constituent C	26	0	-0.632	-9.536
	27	10	-0.316	-4.768
	28	20	0.000	0.000
	29	30	0.316	4.768
	30	40	0.632	9.536

*scalar multiples (System I)

**principal component values (System II)

TABLE 6.- CORRELATION MATRICES FOR SPATIALLY-INDEPENDENT COMBINATIONS OF HYPOTHETICAL, IDEAL, LINEAR CONSTITUENTS A AND B, A AND C

Constituents A and B

Correlations at specific wavelengths (nm)

λ-nm	500	550	600	650	700	750	800	850	900
500	1.000	.986	.885	.504	-.013	-.318	-.466	-.541	-.581
550	.986	1.000	.948	.635	.145	-.164	-.319	-.401	-.444
600	.885	.948	1.000	.848	.454	.160	-.000	-.087	-.135
650	.504	.635	.848	1.000	.857	.658	.530	.454	.410
700	-.013	.145	.454	.857	1.000	.952	.891	.848	.822
750	-.318	-.164	.160	.658	.952	1.000	.987	.970	.956
800	-.466	-.319	-.000	.530	.891	.987	1.000	.996	.991
850	-.541	-.401	-.087	.454	.848	.970	.996	1.000	.999
900	-.581	-.444	-.135	.410	.822	.956	.991	.999	1.000

TABLE 6.- CONCLUDED

Constituents A and C

Correlations at specific wavelengths (nm)

λ-nm	500	550	600	650	700	750	800	850	900
500	1.000	.973	.935	.900	.866	.830	.787	.729	.635
550	.973	1.000	.992	.976	.958	.936	.908	.867	.796
600	.935	.992	1.000	.996	.987	.974	.955	.924	.867
650	.900	.976	.996	1.000	.997	.990	.977	.955	.908
700	.866	.958	.987	.997	1.000	.998	.990	.974	.936
750	.830	.936	.974	.990	.998	1.000	.997	.987	.958
800	.787	.908	.955	.977	.990	.997	1.000	.996	.976
850	.729	.867	.924	.955	.974	.987	.996	1.000	.992
900	.635	.796	.867	.908	.936	.958	.976	.992	1.000

TABLE 7.- CONCENTRATION AND RADIANCE VALUES FOR HYPOTHETICAL IDEAL, LINEAR CONSTITUENTS A + C: SINGLE CONSTITUENTS AND MIXTURES WITH CONSTANT BASE WATER SPECTRUM REMOVED

Spectra Number	Constituent Concentrations			Radiances (arbitrary units) at specific wavelengths (nm)								
	C_A	C_B	C_C	500	550	600	650	700	750	800	850	900
1	0	0	0	0.000	0.000	0.000	0.000	0.000	0.000	0.000	0.000	0.000
2	0	0	10	.518	1.000	1.414	1.732	1.932	2.000	1.932	1.732	1.414
3	0	0	20	1.035	2.000	2.828	3.464	3.864	4.000	3.864	3.464	2.828
4	0	0	30	1.553	3.000	4.243	5.196	5.796	6.000	5.796	5.196	4.243
5	0	0	40	2.071	4.000	5.657	6.928	7.727	8.000	7.727	6.928	5.657
6	10	0	0	1.000	1.414	1.732	1.932	2.000	1.932	1.732	1.414	1.000
7	20	0	0	2.000	2.828	3.464	3.864	4.000	3.864	3.464	2.828	2.000
8	30	0	0	3.000	4.243	5.196	5.796	6.000	5.796	5.196	4.243	3.000
9	40	0	0	4.000	5.647	6.928	7.727	8.000	7.727	6.928	5.657	4.000
10	10	0	10	1.518	2.414	3.146	3.664	3.932	3.932	3.664	3.146	2.414
11	20	0	10	2.518	3.828	4.878	5.596	5.932	5.864	5.396	4.560	3.414
12	30	0	10	3.518	5.243	6.610	7.528	7.932	7.796	7.128	5.975	4.414

TABLE 7.- CONCLUDED

Spectra Number	Constituent Concentrations			Radiances (arbitrary units) at specific wavelengths (nm)								
	C_A	C_B	C_C	500	550	600	650	700	750	800	850	900
13	40	0	10	4.518	6.657	8.342	9.459	9.932	9.727	8.860	7.389	5.414
14	10	0	20	2.035	3.414	4.560	5.396	5.864	5.932	5.596	4.878	3.828
15	20	0	20	3.035	4.828	6.293	7.328	7.864	7.864	7.328	6.293	4.828
16	30	0	20	4.035	6.243	8.025	9.260	9.864	9.796	9.060	7.707	5.828
17	40	0	20	5.035	7.657	9.757	11.192	11.864	11.727	10.792	9.121	6.828
18	10	0	30	2.553	4.414	5.975	7.128	7.796	7.932	7.528	6.610	5.243
19	20	0	30	3.553	5.828	7.707	9.060	9.796	9.864	9.260	8.025	6.243
20	30	0	30	4.553	7.243	9.439	10.992	11.796	11.796	10.992	9.439	7.243
21	40	0	30	5.553	8.657	11.171	12.924	13.796	13.727	12.724	10.853	8.243
22	10	0	40	3.071	5.414	7.389	8.860	9.727	9.932	9.459	8.342	6.657
23	20	0	40	4.071	6.828	9.121	10.792	11.727	11.864	11.192	9.757	7.657
24	30	0	40	5.071	8.243	10.853	12.724	13.727	13.796	12.924	11.171	8.657
25	40	0	40	6.071	9.657	12.585	14.656	15.727	15.727	14.656	12.585	9.657

TABLE 8.- CONCENTRATION AND RADIANCE VALUES FOR HYPOTHETICAL IDEAL, LINEAR CONSTITUENTS A + B + C: SINGLE CONSTITUENTS AND MIXTURES WITH CONSTANT BASE WATER SPECTRUM REMOVED

Spectra Number	Constituent Concentrations			Radiances (arbitrary units) at specific wavelengths (nm)								
	C_A	C_B	C_C	500	550	600	650	700	750	800	850	900
1	0	0	0	0.000	0.000	0.000	0.000	0.000	0.000	0.000	0.000	0.000
2	0	0	20	1.035	2.000	2.828	3.464	3.864	4.000	3.864	3.464	2.828
3	0	0	40	2.071	4.000	5.657	6.928	7.727	8.000	7.727	6.928	5.657
4	20	0	0	2.000	2.828	3.464	3.864	4.000	3.864	3.464	2.828	2.000
5	20	0	20	3.035	4.828	6.293	7.328	7.864	7.864	7.328	6.293	4.828
6	20	0	40	4.071	6.828	9.121	10.792	11.727	11.864	11.192	9.757	7.657
7	40	0	0	4.000	5.657	6.928	7.727	8.000	7.727	6.928	5.657	4.000
8	40	0	20	5.035	7.657	9.757	11.192	11.864	11.727	10.792	9.121	6.828
9	40	0	40	6.071	9.657	12.585	14.656	15.727	15.727	14.656	12.585	9.657
10	0	20	0	3.464	4.000	3.464	2.000	.000	-2.000	-3.464	-4.000	-3.464
11	0	20	20	4.499	6.000	6.293	5.464	3.864	2.000	.400	-.536	-.636
12	0	20	40	5.535	8.000	9.121	8.928	7.727	6.000	4.263	2.928	2.193

TABLE 8.- CONCLUDED

Spectra Number	Constituent Concentrations			Radiances (arbitrary units) at specific wavelengths (nm)								
	C_A	C_B	C_C	500	550	600	650	700	750	800	850	900
13	20	20	0	5.464	6.828	6.928	5.864	4.000	1.864	.000	-1.172	-1.464
14	20	20	20	6.499	8.828	9.757	9.328	7.864	5.864	3.864	2.293	1.364
15	20	20	40	7.535	10.828	12.585	12.792	11.727	9.864	7.727	5.757	4.193
16	40	20	0	7.464	9.657	10.392	9.727	8.000	5.727	3.464	1.657	.536
17	40	20	20	8.499	11.657	13.221	13.192	11.864	9.727	7.328	5.121	3.364
18	40	20	40	9.535	13.657	16.049	16.656	15.727	13.727	11.192	8.585	6.193
19	0	40	0	6.928	8.000	6.928	4.000	.000	-4.000	-6.928	-8.000	-6.928
20	0	40	20	7.963	10.000	9.757	7.464	3.864	.000	-3.064	-4.536	-4.100
21	0	40	40	8.999	12.000	12.585	10.928	7.727	4.000	.799	-1.072	-1.271
22	20	40	0	8.928	10.828	10.392	7.864	4.000	-.136	-3.464	-5.172	-4.928
23	20	40	20	9.963	12.828	13.221	11.328	7.864	3.864	.400	-1.707	-2.100
24	20	40	40	10.999	14.828	16.049	14.792	11.727	7.864	4.263	1.757	.729
25	40	40	0	10.928	13.657	13.856	11.727	8.000	3.727	.000	-2.343	-2.928
26	40	40	20	11.963	15.657	16.685	15.192	11.864	7.727	3.864	1.121	-.100
27	40	40	40	12.999	17.657	19.513	18.656	15.727	11.727	7.727	4.585	2.729

TABLE 9.- MEAN RADIANCE, PRINCIPAL AXES EIGENVECTORS, CHARACTERISTIC VECTORS AND TRANSFORMED EIGENVECTORS FOR THIRTEEN-SPECTRA CASE OF HYPOTHETICAL LINEAR CONSTITUENTS A AND B IN MIXTURES

	λ, wavelength, nm								
	500	550	600	650	700	750	800	850	900
Mean radiance (arbitrary units)									
L_{A+B}	3.404	4.330	4.530	4.049	3.077	1.895	0.799	0.022	-0.327
Principal axes eigenvectors (normalized to unity)									
v_1	-0.016	0.027	0.113	0.229	0.352	0.452	0.498	0.471	0.369
v_2	0.423	0.516	0.502	0.390	0.215	0.026	-0.129	-0.212	-0.208
Characteristic vectors for A and B (normalized to unity)									
v_A	0.206	0.292	0.358	0.399	0.413	0.399	0.358	0.292	0.206
v_B	0.369	0.426	0.369	0.213	0.000	-0.213	-0.369	-0.426	-0.369

TABLE 9.- CONCLUDED

	λ, wavelength - nm								
	500	550	600	650	700	750	800	850	900
Principal axes eigenvectors after rotation of $\theta_1 = 48.0°$									
$v_1' = v_A$	0.206	0.292	0.358	0.399	0.413	0.399	0.358	0.292	0.206
v_2'	0.202	0.205	0.122	-0.032	-0.220	-0.393	-0.503	-0.516	-0.422
Principal axes eigenvectors after rotation of $\theta_2 = 18.6°$									
v_1''	0.061	0.121	0.202	0.297	0.386	0.449	0.466	0.425	0.325
$v_2'' = v_B$	0.369	0.426	0.369	0.213	0.000	-0.213	-0.369	-0.426	-0.369

TABLE 10.- CONCENTRATION AND RADIANCE VALUES FROM HYPOTHETICAL FLIGHT EXPERIMENT OVER TWO MIXED LINE DUMPS OF CONSTITUENTS A + B. SPECTRA LISTED IN SAME ORDER OF COLLECTION SHOWN IN FIGURE 25.

Spectra Number	Constituent Concentrations			Radiances (arbitrary units) at specific wavelengths (nm)								
	C_A	C_B	C_C	500	550	600	650	700	750	800	850	900
1	0	0	0	0.000	0.000	0.000	0.000	0.000	0.000	0.000	0.000	0.000
2	0	0	0	0.000	0.000	0.000	0.000	0.000	0.000	0.000	0.000	0.000
3	0	0	0	0.000	0.000	0.000	0.000	0.000	0.000	0.000	0.000	0.000
4	5	0	0	.500	.707	.866	.966	1.000	.966	.866	.707	.500
5	10	0	0	1.000	1.414	1.732	1.932	2.000	1.932	1.732	1.414	1.000
6	15	10	0	3.232	4.121	4.330	3.898	3.000	1.898	.866	.121	-.232
7	20	20	0	5.464	6.828	6.928	5.865	4.000	1.864	.000	-1.172	-1.464
8	25	30	0	7.696	9.536	9.526	7.830	5.000	1.830	-.866	-2.464	-2.696
9	20	40	0	8.928	10.828	10.392	7.864	4.000	-.136	-3.464	-5.172	-4.928
10	10	30	0	6.196	7.414	6.928	4.932	2.000	-1.068	-3.464	-4.586	-4.196
11	0	20	0	3.464	4.000	3.464	2.000	.000	-2.000	-3.464	-4.000	-3.464
12	0	10	0	1.732	2.000	1.732	1.000	.000	-1.000	-1.732	-2.000	-1.732
13	0	0	0	0.000	0.000	0.000	0.000	0.000	0.000	0.000	0.000	0.000

TABLE 10.- CONTINUED

Spectra Number	Constituent Concentrations			Radiances (arbitrary units) at specific wavelengths (nm)								
	C_A	C_B	C_C	500	550	600	650	700	750	800	850	900
14	0	0	0	0.000	0.000	0.000	0.000	0.000	0.000	0.000	0.000	0.000
15	0	0	0	0.000	0.000	0.000	0.000	0.000	0.000	0.000	0.000	0.000
16	0	0	0	0.000	0.000	0.000	0.000	0.000	0.000	0.000	0.000	0.000
17	0	0	0	0.000	0.000	0.000	0.000	0.000	0.000	0.000	0.000	0.000
18	10	0	0	1.000	1.414	1.732	1.932	2.000	1.932	1.732	1.414	1.000
19	20	0	0	2.000	2.828	3.464	3.864	4.000	3.864	3.464	2.828	2.000
20	25	0	0	2.500	3.536	4.330	4.830	5.000	4.830	4.330	3.536	2.500
21	20	10	0	3.732	4.828	5.196	4.864	4.000	2.864	1.732	.828	.268
22	15	20	0	4.964	6.121	6.062	4.898	3.000	.896	-.866	-1.879	-1.964
23	10	30	0	6.196	7.414	6.928	4.932	2.000	-1.068	-3.464	-4.586	-4.196
24	5	40	0	7.428	8.707	7.794	4.966	1.000	-3.034	-6.062	-7.293	-6.428
25	0	30	0	5.196	6.000	5.196	3.000	.000	-3.000	-5.196	-6.000	-5.196
26	0	20	0	3.464	4.000	3.464	2.000	.000	-2.000	-3.464	-4.000	-3.464
27	0	10	0	1.732	2.000	1.732	1.000	.000	-1.000	-1.732	-2.000	-1.732

TABLE 10.- CONCLUDED

Spectra Number	Constituent Concentrations			Radiances (arbitrary units) at specific wavelengths (nm)								
	C_A	C_B	C_C	500	550	600	650	700	750	800	850	900
28	0	0	0	0.000	0.000	0.000	0.000	0.000	0.000	0.000	0.000	0.000
29	0	0	0	0.000	0.000	0.000	0.000	0.000	0.000	0.000	0.000	0.000
30	0	0	0	0.000	0.000	0.000	0.000	0.000	0.000	0.000	0.000	0.000

TABLE 11.- CONCENTRATIONS, RADIANCE VALUES, MEAN VALUES AND CHARACTERISTIC VECTORS FOR SIMPLE NONLINEAR HYPOTHETICAL CONSTITUENTS A, B, C. NONLINEAR POWER = 0.5.

Concentrations		Radiances (arbitrary units) at specific wavelengths (nm)								
	C_A	500	550	600	650	700	750	800	850	900
Constituent A	0	0.000	0.000	0.000	0.000	0.000	0.000	0.000	0.000	0.000
	10	.316	.447	.548	.611	.632	.611	.548	.447	.316
	20	.447	.632	.775	.864	.894	.864	.775	.632	.447
	30	.548	.775	.949	1.058	1.095	1.058	.949	.775	.548
	40	.632	.894	1.095	1.222	1.265	1.222	1.095	.894	.632
Mean vector, $\bar{L}_A$		.389	.550	.673	.751	.777	.751	.673	.550	.389
Characteristic vector, v_A		.206	.292	.358	.399	.413	.399	.358	.292	.206
	C_B									
Constituent B	0	0.000	0.000	0.000	0.000	0.000	0.000	0.000	0.000	0.000
	10	.548	.632	.548	.316	.000	-.316	-.548	-.632	-.548
	20	.775	.894	.775	.447	.000	-.447	-.775	-.894	-.775
	30	.949	1.095	.949	.548	.000	-.548	-.949	-1.095	-.949
	40	1.095	1.265	1.095	.632	.000	-.632	-1.095	-1.265	-1.095
Mean vector, $\bar{L}_B$		.673	.777	.673	.389	.000	-.389	-.673	-.777	-.673
Characteristic vector, v_B		.369	.426	.369	.213	.000	-.213	-.369	-.426	-.369

TABLE 11.- CONCLUDED

Concentrations		Radiances (arbitrary units) at specific wavelengths (nm)								
	C_C	500	550	600	650	700	750	800	850	900
Constituent C	0	0.000	0.000	0.000	0.000	0.000	0.000	0.000	0.000	0.000
	10	.164	.316	.447	.548	.611	.632	.611	.548	.447
	20	.231	.447	.632	.775	.864	.894	.864	.775	.632
	30	.284	.548	.775	.949	1.058	1.095	1.058	.949	.775
	40	.326	.632	.894	1.095	1.222	1.265	1.222	1.095	.894
Mean vector, $\bar{L}_C$		.201	.389	.550	.673	.751	.777	.751	.673	.550
Characteristic vector, v_C		.109	.210	.297	.363	.405	.420	.405	.363	.297

TABLE 12.- CONCENTRATIONS, RADIANCE VALUES, MEAN VALUES AND CHARACTERISTIC VECTORS FOR SIMPLE NONLINEAR HYPOTHETICAL CONSTITUENTS A, B, C. NONLINEAR POWER = 1.5.

Concentrations		Radiances (arbitrary units) at specific wavelengths (nm)								
	C_A	500	550	600	650	700	750	800	850	900
Constituent A	0	0.000	0.000	0.000	0.000	0.000	0.000	0.000	0.000	0.000
	10	3.162	4.472	5.477	6.109	6.325	6.109	5.477	4.472	3.162
	20	8.944	12.649	15.492	17.279	17.889	17.279	15.492	12.649	8.944
	30	16.432	23.238	28.460	31.744	32.863	31.744	28.461	23.238	16.432
	40	25.298	35.777	43.818	48.872	50.596	48.872	43.818	35.777	25.298
Mean vector, $\bar{L}_A$		10.767	15.226	18.649	20.801	21.535	20.801	18.650	15.226	10.767
Characteristic vector, v_A		.206	.292	.358	.399	.413	.399	.358	.292	.206
	C_B									
Constituent B	0	0.000	0.000	0.000	0.000	0.000	0.000	0.000	0.000	0.000
	10	5.477	6.325	5.477	3.162	.000	-3.162	-5.477	-6.325	-5.477
	20	15.492	17.889	15.492	8.944	.000	-8.944	-15.492	-17.889	-15.492
	30	28.460	32.863	28.461	16.432	.000	-16.432	-28.460	-32.863	-28.461
	40	43.818	50.596	43.818	25.298	.000	-25.298	-43.818	-50.596	-43.818
Mean vector, $\bar{L}_B$		18.649	21.535	18.650	10.767	.000	-10.767	-18.649	-21.535	-18.650
Characteristic vector, v_B		.369	.426	.369	.213	.000	-.213	-.369	-.426	-.369

TABLE 12.- CONCLUDED

Concentrations		Radiances (arbitrary units) at specific wavelengths (nm)								
	c_C	500	550	600	650	700	750	800	850	900
Constituent C	0	0.000	0.000	0.000	0.000	0.000	0.000	0.000	0.000	0.000
	10	1.637	3.162	4.472	5.477	6.109	6.325	6.109	5.477	4.472
	20	4.630	8.944	12.649	15.492	17.279	17.889	17.279	15.492	12.649
	30	8.506	16.432	23.238	28.460	31.744	32.863	31.744	28.461	23.238
	40	13.095	25.298	35.777	43.818	48.872	50.596	48.872	43.818	35.777
Mean vector, $\bar{L}_C$		5.574	10.767	15.226	18.649	20.801	21.535	20.801	18.650	15.227
Characteristic vector, v_C		.109	.210	.297	.363	.405	.420	.405	.363	.297

TABLE 13.- SCALAR MULTIPLES FOR SIMPLE NONLINEAR CONSTITUENTS

	Constituent Concentrations *C_A	Scalar Multiples *Y_A	Functional **$f(Y_A)$	$\frac{f(Y_A)}{\text{Range } f(Y_A)}$
Power p = 0.5	0	-.786	0.0	0.0
	10	-.147	.408	.25
	20	.118	.816	.50
	30	.322	1.228	.75
	40	.493	1.636	1.00
Power p = 1.5	0	-.525	0.0	0.0
	10	-.371	.287	.25
	20	-.089	.575	.50
	30	.276	.862	.75
	40	.709	1.150	1.00

*Identical values for constituents B and C

**$f(Y_{Ai}) = (Y_{Ai} - Y_A(C_A = 0))^{1/p}$

TABLE 14.- SPECTRA FROM HYPOTHETICAL FLIGHT EXPERIMENT OVER TWO MIXED LINE DUMPS OF SIMPLE NONLINEAR CONSTITUENTS A (p = 0.2) AND B (p = 2.0). SPECTRA LISTED IN SAME ORDER AS SHOWN IN FIGURE 25.

Spectra Number	Constituent Concentrations			Radiances (arbitrary units) at specific wavelengths (nm)								
	C_A	C_B	C_C	500	550	600	650	700	750	800	850	900
1	0	0	0	0.000	0.000	0.000	0.000	0.000	0.000	0.000	0.000	0.000
2	0	0	0	0.000	0.000	0.000	0.000	0.000	0.000	0.000	0.000	0.000
3	0	0	0	0.000	0.000	0.000	0.000	0.000	0.000	0.000	0.000	0.000
4	5	0	0	.138	.195	.239	.267	.276	.267	.239	.195	.138
5	10	0	0	.158	.224	.275	.306	.317	.306	.275	.224	.158
6	15	10	0	.189	.263	.315	.342	.344	.322	.280	.223	.155
7	20	20	0	.251	.337	.385	.392	.364	.312	.246	.177	.113
8	25	30	0	.346	.449	.486	.458	.381	.278	.174	.089	.034
9	20	40	0	.459	.577	.592	.512	.364	.192	.038	-.063	-.095
10	10	30	0	.314	.404	.430	.396	.317	.216	.119	.044	.003
11	0	20	0	.069	.080	.069	.040	.000	-.040	-.069	-.080	-.069
12	0	10	0	.017	.020	.017	.010	.000	-.010	-.017	-.020	-.017

TABLE 14.- CONTINUED

Spectra Number	Constituent Concentrations			Radiances (arbitrary units) at specific wavelengths (nm)								
	C_A	C_B	C_C	500	550	600	650	700	750	800	850	900
13	0	0	0	0.000	0.000	0.000	0.000	0.000	0.000	0.000	0.000	0.000
14	0	0	0	0.000	0.000	0.000	0.000	0.000	0.000	0.000	0.000	0.000
15	0	0	0	0.000	0.000	0.000	0.000	0.000	0.000	0.000	0.000	0.000
16	0	0	0	0.000	0.000	0.000	0.000	0.000	0.000	0.000	0.000	0.000
17	0	0	0	0.000	0.000	0.000	0.000	0.000	0.000	0.000	0.000	0.000
18	10	0	0	.158	.224	.275	.306	.317	.306	.275	.224	.158
19	20	0	0	.182	.257	.315	.352	.364	.352	.315	.257	.182
20	25	0	0	.190	.269	.330	.368	.381	.368	.330	.269	.190
21	20	10	0	.199	.277	.333	.362	.364	.342	.298	.236	.165
22	15	20	0	.241	.323	.367	.372	.344	.292	.228	.163	.103
23	10	30	0	.314	.404	.430	.396	.317	.216	.119	.044	.003
24	5	40	0	.415	.515	.516	.427	.276	.107	-.038	-.125	-.139
25	0	30	0	.156	.180	.156	.090	.000	-.090	-.156	-.180	-.156
26	0	20	0	.069	.080	.069	.040	.000	-.040	-.069	-.080	-.069

TABLE 14.- CONCLUDED

Spectra Number	Constituent Concentrations			Radiances (arbitrary units) at specific wavelengths (nm)								
	C_A	C_B	C_C	500	550	600	650	700	750	800	850	900
27	0	10	0	.017	.020	.017	.010	.000	-.010	-.017	-.020	-.017
28	0	0	0	0.000	0.000	0.000	0.000	0.000	0.000	0.000	0.000	0.000
29	0	0	0	0.000	0.000	0.000	0.000	0.000	0.000	0.000	0.000	0.000
30	0	0	0	0.000	0.000	0.000	0.000	0.000	0.000	0.000	0.000	0.000

TABLE 15.- CONCENTRATIONS, RADIANCE SPECTRA, AND MEAN VECTORS FOR WAVELENGTH-DEPENDENT NONLINEAR HYPOTHETICAL CONSTITUENTS A, B, C.

$0.5 \leq p(\lambda) \leq 1.0$

	Concentrations	Radiances (arbitrary units) at specific wavelengths (nm)								
	C_A	500	550	600	650	700	750	800	850	900
Constituent A	0	0.000	0.000	0.000	0.000	0.000	0.000	0.000	0.000	0.000
	10	.316	.516	.730	.941	1.125	1.255	1.299	1.225	1.000
	20	.447	.763	1.126	1.515	1.891	2.203	2.382	2.345	2.000
	30	.548	.958	1.451	2.002	2.546	3.063	3.397	3.430	3.000
	40	.632	1.126	1.737	2.440	3.181	3.869	4.369	4.492	4.000
	Mean Vector $\bar{L}_A$	.389	.673	1.009	1.380	1.752	2.078	2.289	2.298	2.000
	C_B									
Constituent B	0	0.000	0.000	0.000	0.000	0.000	0.000	0.000	0.000	0.000
	10	.548	.730	.730	.487	.000	-.649	-1.299	-1.732	-1.732
	20	.775	1.079	1.126	.784	.000	-1.140	-2.382	-3.317	-3.464
	30	.949	1.355	1.451	1.036	.000	-1.585	-3.397	-4.851	-5.196
	40	1.095	1.593	1.737	1.263	.000	-2.003	-4.369	-6.353	-6.928
	Mean Vector $\bar{L}_B$	.673	.951	1.009	.714	.000	-1.076	-2.289	-3.251	-3.464

TABLE 15.- CONCLUDED

	Concentrations	Radiances (arbitrary units) at specific wavelengths (nm)								
	C_C	500	550	600	650	700	750	800	850	900
Constituent C	0	0.000	0.000	0.000	0.000	0.000	0.000	0.000	0.000	0.000
	10	.164	.365	.596	.843	1.086	1.299	1.449	1.500	1.414
	20	.231	.539	.920	1.358	1.827	2.281	2.657	2.873	2.828
	30	.284	.677	1.185	1.795	2.476	3.171	3.788	4.201	4.243
	40	.326	.796	1.418	2.188	3.073	4.006	4.873	5.502	5.657
	Mean Vector $\bar{L}_C$	.201	.476	.824	1.236	1.692	2.151	2.553	2.815	2.828

TABLE 16.- CONCENTRATIONS, RADIANCE SPECTRA, AND MEAN VECTORS FOR WAVELENGTH-DEPENDENT NONLINEAR HYPOTHETICAL CONSTITUENTS A, B, C.

$1.0 \leq p(\lambda) \leq 1.5$

	Concentrations	Radiances (arbitrary units) at specific wavelengths (nm)								
	C_A	500	550	600	650	700	750	800	850	900
Constituent A	0	0.000	0.000	0.000	0.000	0.000	0.000	0.000	0.000	0.000
	10	3.162	3.873	4.107	3.967	3.557	2.975	2.310	1.633	1.000
	20	8.944	10.489	10.653	9.853	8.459	6.776	5.038	3.411	2.000
	30	16.432	18.788	18.604	16.776	14.042	10.966	7.949	5.248	3.000
	40	25.298	28.410	27.631	24.472	20.119	15.432	10.987	7.124	4.000
	Mean Vector $\bar{L}_A$	10.767	12.312	12.199	11.014	9.235	7.230	5.257	3.483	2.000
	C_B									
Constituent B	0	0.000	0.000	0.000	0.000	0.000	0.000	0.000	0.000	0.000
	10	5.477	5.477	4.107	2.054	.000	-1.540	-2.310	-2.310	-1.732
	20	15.492	14.834	10.653	5.100	.000	-3.507	-5.038	-4.824	-3.464
	30	28.460	26.570	18.604	8.684	.000	-5.676	-7.949	-7.421	-5.196
	40	43.818	40.178	27.631	12.668	.000	-7.988	-10.987	-10.074	-6.928
	Mean Vector $\bar{L}_B$	18.649	17.412	12.199	5.701	.000	-3.742	-5.257	-4.926	-3.464

TABLE 16.- CONCLUDED

Concentrations		Radiances (arbitrary units) at specific wavelengths (nm)								
	C_C	500	550	600	650	700	750	800	850	900
Constituent C	0	0.000	0.000	0.000	0.000	0.000	0.000	0.000	0.000	0.000
	10	1.637	2.738	3.354	3.557	3.435	3.080	2.576	2.000	1.414
	20	4.630	7.417	8.698	8.834	8.171	7.015	5.619	4.177	2.828
	30	8.506	13.285	15.190	15.041	13.564	11.353	8.866	6.427	4.243
	40	13.095	20.089	22.560	21.941	19.433	15.976	12.254	8.725	5.657
Mean Vector $\bar{L}_C$		5.574	8.706	9.960	9.875	8.921	7.485	5.863	4.266	2.828

TABLE 17.- CORRELATION MATRICES FOR WAVELENGTH-DEPENDENT HYPOTHETICAL NONLINEAR CONSTITUENTS*

$0.5 \leq p(\lambda) \leq 1.0$

Correlations at specific wavelengths (nm)

λ-nm	500	550	600	650	700	750	800	850	900
500	1.000	.999	.996	.991	.986	.979	.972	.965	.957
550	.999	1.000	.999	.996	.993	.988	.982	.976	.970
600	.996	.999	1.000	.999	.997	.994	.989	.985	.979
650	.991	.996	.999	1.000	.999	.997	.994	.991	.987
700	.986	.993	.997	.999	1.000	.999	.998	.995	.992
750	.979	.988	.994	.997	.999	1.000	.999	.998	.996
800	.972	.982	.989	.994	.998	.999	1.000	1.000	.998
850	.965	.976	.985	.991	.995	.998	1.000	1.000	1.000
900	.957	.970	.979	.987	.992	.996	.998	1.000	1.000

*Matrices same for constituents A, B, C except constituent B has sign reversals similar to that shown in Table 3.

TABLE 17.- CONCLUDED

$1.0 \leq p(\lambda) \leq 1.5$

Correlations at specific wavelengths (nm)

λ-nm	500	550	600	650	700	750	800	850	900
500	1.000	1.000	.999	.998	.997	.995	.993	.989	.985
550	1.000	1.000	1.000	.999	.998	.997	.995	.992	.988
600	.999	1.000	1.000	1.000	.999	.998	.996	.994	.991
650	.998	.999	1.000	1.000	1.000	.999	.998	.996	.993
700	.997	.998	.999	1.000	1.000	1.000	.999	.998	.995
750	.995	.997	.998	.999	1.000	1.000	1.000	.999	.997
800	.993	.995	.996	.998	.999	1.000	1.000	1.000	.999
850	.989	.992	.994	.996	.998	.999	1.000	1.000	1.000
900	.985	.988	.991	.993	.995	.997	.999	1.000	1.000

TABLE 18.- SCALAR MULTIPLES AND SCALED FUNCTIONS

FOR WAVELENGTH-DEPENDENT NONLINEAR CONSTITUENTS A, B, C

Concentration	0	10	20	30	40
Concentration/range	0	.250	.500	.750	1.000
		$0.5 \leq p(\lambda) \leq 1.0$			
Y_A	-.673	-.282	.031	.323	.602
Linear scaling	0.0	.307	.552	.781	1.000
Simple-nonlinear scaling	0.0	.207	.453	.719	1.000
Y_B	.655	.298	-.016	-.320	-.617
Linear scaling	0.0	.281	.528	.767	1.000
Simple-nonlinear scaling	0.0	.184	.399	.702	1.000
Y_C	-.664	-.291	.024	.321	.609
Linear scaling	0.0	.293	.540	.774	1.000
Simple-nonlinear scaling	0.0	.195	.440	.710	1.000

TABLE 18.- CONCLUDED

$1.0 \leq p(\lambda) \leq 1.5$

Y_A	-.552	-.361	-.067	.289	.691
Linear scaling	0.0	.154	.390	.677	1.000
Simple-nonlinear scaling	0.0	.224	.471	.732	1.000
Y_B	-.539	-.366	-.077	.283	.699
Linear scaling	0.0	.140	.373	.664	1.000
Simple-nonlinear scaling	0.0	.207	.454	.721	1.000
Y_C	-.561	-.357	.059	.293	.684
Linear scaling	0.0	.164	.403	.686	1.000
Simple-nonlinear scaling	0.0	.235	.483	.739	1.000

TABLE 19.- SPECTRA FROM HYPOTHETICAL FLIGHT EXPERIMENT OVER TWO MIXED LINE DUMPS OF WAVELENGTH-DEPENDENT NONLINEAR CONSTITUENTS. SPECTRA LISTED IN SAME ORDER AS SHOWN IN FIGURE 25.

Spectra Number	Constituent Concentrations			Radiances (arbitrary units) at specific wavelengths (nm)								
	C_A	C_B	C_C	500	550	600	650	700	750	800	850	900
1	0	0	0	0.000	0.000	0.000	0.000	0.000	0.000	0.000	0.000	0.000
2	0	0	0	0.000	0.000	0.000	0.000	0.000	0.000	0.000	0.000	0.000
3	0	0	0	0.000	0.000	0.000	0.000	0.000	0.000	0.000	0.000	0.000
4	5	0	0	.224	.350	.474	.584	.669	.714	.708	.639	.500
5	10	0	0	.316	.516	.730	.941	1.125	1.255	1.299	1.225	1.000
6	15	10	0	.935	1.196	1.352	1.449	1.524	1.590	1.621	1.560	1.326
7	20	20	0	1.996	2.246	2.192	2.025	1.891	1.853	1.878	1.863	1.654
8	25	30	0	3.346	3.522	3.155	2.635	2.236	2.074	2.101	2.149	1.980
9	20	40	0	4.829	4.781	3.890	2.782	1.891	1.404	1.283	1.338	1.307
10	10	30	0	3.162	3.173	2.591	1.809	1.125	.687	.504	.483	.480
11	0	20	0	1.549	1.483	1.065	.510	.000	-.351	-.504	-.482	-.346
12	0	10	0	.548	.548	.411	.205	.000	-.154	-.231	-.231	-.173
13	0	0	0	0.000	0.000	0.000	0.000	0.000	0.000	0.000	0.000	0.000

TABLE 19.- CONTINUED

Spectra Number	Constituent Concentrations			Radiances (arbitrary units) at specific wavelengths (nm)								
	C_A	C_B	C_C	500	550	600	650	700	750	800	850	900
14	0	0	0	0.000	0.000	0.000	0.000	0.000	0.000	0.000	0.000	0.000
15	0	0	0	0.000	0.000	0.000	0.000	0.000	0.000	0.000	0.000	0.000
16	0	0	0	0.000	0.000	0.000	0.000	0.000	0.000	0.000	0.000	0.000
17	0	0	0	0.000	0.000	0.000	0.000	0.000	0.000	0.000	0.000	0.000
18	10	0	0	.316	.516	.730	.941	1.125	1.255	1.299	1.225	1.000
19	20	0	0	.447	.763	1.126	1.515	1.891	2.203	2.382	2.345	2.000
20	25	0	0	.500	.865	1.295	1.766	2.236	2.641	2.896	2.891	2.500
21	20	10	0	.995	1.310	1.536	1.720	1.891	2.049	2.151	2.115	1.827
22	15	20	0	1.936	2.132	2.006	1.753	1.524	1.393	1.348	1.309	1.154
23	10	30	0	3.162	3.173	2.591	1.809	1.125	.687	.504	.483	.480
24	5	40	0	4.605	4.368	3.237	1.851	.669	-.085	-.390	-.368	-.193
25	0	30	0	2.846	2.657	1.860	.868	.000	-.568	-.795	-.742	-.520
26	0	20	0	1.549	1.483	1.065	.510	.000	-.351	-.504	-.482	-.346
27	0	10	0	.548	.548	.411	.205	.000	-.154	-.231	-.231	-.173

TABLE 19.- CONCLUDED

Spectra Number	Constituent Concentrations			Radiances (arbitrary units) at specific wavelengths (nm)								
	C_A	C_B	C_C	500	550	600	650	700	750	800	850	900
28	0	0	0	0.000	0.000	0.000	0.000	0.000	0.000	0.000	0.000	0.000
29	0	0	0	0.000	0.000	0.000	0.000	0.000	0.000	0.000	0.000	0.000
30	0	0	0	0.000	0.000	0.000	0.000	0.000	0.000	0.000	0.000	0.000

TABLE 20.- CONCENTRATIONS AND RADIANCE VALUES FOR HYPOTHETICAL LINEAR CONSTITUENTS A + B. MIXTURES FORMED BY PROPORTIONAL NONLINEAR SUPERPOSITION. MAXIMUM SPECTRUM DECREASED BY 25% FROM LINEAR SUPERPOSITION CASE.

Spectra Number	Constituent Concentrations			Radiances (arbitrary units) at specific wavelengths (nm)								
	C_A	C_B	C_C	500	550	600	650	700	750	800	850	900
1	0	0	0	0.000	0.000	0.000	0.000	0.000	0.000	0.000	0.000	0.000
2	0	10	0	1.732	2.000	1.732	1.000	.000	-1.000	-1.732	-2.000	-1.732
3	0	20	0	3.464	4.000	3.464	2.000	.000	-2.000	-3.464	-4.000	-3.464
4	0	30	0	5.196	6.000	5.196	3.000	.000	-3.000	-5.196	-6.000	-5.196
5	0	40	0	6.928	8.000	6.928	4.000	.000	-4.000	-6.928	-8.000	-6.928
6	10	0	0	1.000	1.414	1.732	1.932	2.000	1.932	1.732	1.414	1.000
7	20	0	0	2.000	2.828	3.464	3.864	4.000	3.864	3.464	2.828	2.000
8	30	0	0	3.000	4.243	5.196	5.796	6.000	5.796	5.196	4.243	3.000
9	40	0	0	4.000	5.657	6.928	7.727	8.000	7.727	6.928	5.657	4.000
10	10	10	0	2.561	3.201	3.248	2.749	1.875	.874	.000	-.549	-.686
11	20	10	0	3.391	4.402	4.763	4.497	3.750	2.747	1.732	.902	.359
12	30	10	0	4.220	5.602	6.279	6.246	5.625	4.621	3.464	2.352	1.405

TABLE 20.- CONCLUDED

Spectra Number	Constituent Concentrations			Radiances (arbitrary units) at specific wavelengths (nm)								
	C_A	C_B	C_C	500	550	600	650	700	750	800	850	900
13	40	10	0	5.049	6.803	7.794	7.994	7.500	6.494	5.196	3.803	2.451
14	10	20	0	4.123	4.987	4.763	3.565	1.750	-.185	-1.732	-2.513	-2.373
15	20	20	0	4.781	5.975	6.062	5.131	3.500	1.631	.000	-1.025	-1.281
16	30	20	0	5.440	6.962	7.361	6.696	5.250	3.446	1.732	.462	-.190
17	40	20	0	6.098	7.950	8.660	8.261	7.000	5.261	3.464	1.950	.902
18	10	30	0	5.684	6.774	6.279	4.382	1.625	-1.243	-3.464	-4.476	-4.059
19	20	30	0	6.172	7.548	7.361	5.764	3.250	.514	-1.732	-2.952	-2.922
20	30	30	0	6.659	8.322	8.444	7.146	4.875	2.271	.000	-1.428	-1.784
21	40	30	0	7.147	9.096	9.526	8.529	6.500	4.029	1.732	.096	-.647
22	10	40	0	7.245	8.561	7.794	5.199	1.500	-2.301	-5.196	-6.439	-5.745
23	20	40	0	7.562	9.121	8.660	6.398	3.000	-.602	-3.464	-4.879	-4.562
24	30	40	0	7.879	9.682	9.526	7.597	4.500	1.097	-1.732	-3.318	-3.379
25	40	40	0	8.196	10.243	10.392	8.796	6.000	2.796	.000	-1.757	-2.196

TABLE 21.- CONCENTRATIONS AND RADIANCE VALUES FOR HYPOTHETICAL LINEAR CONSTITUENTS A + B. MIXTURES FORMED BY PROPORTIONAL NONLINEAR SUPERPOSITION. MAXIMUM SPECTRUM INCREASED BY 25% OVER LINEAR SUPERPOSITION CASE.

Spectra Number	Constituent Concentrations			Radiances (arbitrary units) at specific wavelengths (nm)								
	C_A	C_B	C_C	500	550	600	650	700	750	800	850	900
1	0	0	0	0.000	0.000	0.000	0.000	0.000	0.000	0.000	0.000	0.000
2	0	10	0	1.732	2.000	1.732	1.000	.000	-1.000	-1.732	-2.000	-1.732
3	0	20	0	3.464	4.000	3.464	2.000	.000	-2.000	-3.464	-4.000	-3.464
4	0	30	0	5.196	6.000	5.196	3.000	.000	-3.000	-5.196	-6.000	-5.196
5	0	40	0	6.928	8.000	6.928	4.000	.000	-4.000	-6.928	-8.000	-6.928
6	10	0	0	1.000	1.414	1.732	1.932	2.000	1.932	1.732	1.414	1.000
7	20	0	0	2.000	2.828	3.464	3.864	4.000	3.864	3.464	2.828	2.000
8	30	0	0	3.000	4.243	5.196	5.796	6.000	5.796	5.196	4.243	3.000
9	40	0	0	4.000	5.657	6.928	7.727	8.000	7.727	6.928	5.657	4.000
10	10	10	0	2.903	3.628	3.681	3.115	2.125	.990	.000	-.622	-.778
11	20	10	0	4.074	5.255	5.629	5.230	4.250	2.980	1.732	.755	.176
12	30	10	0	5.244	6.883	7.578	7.345	6.375	4.970	3.464	2.133	1.131

TABLE 21.- CONCLUDED

Spectra Number	Constituent Concentrations			Radiances (arbitrary units) at specific wavelengths (nm)								
	C_A	C_B	C_C	500	550	600	650	700	750	800	850	900
13	40	10	0	6.415	8.510	9.526	9.460	8.500	6.960	5.196	3.510	2.085
14	10	20	0	4.806	5.841	5.629	4.298	2.250	.048	-1.732	-2.659	-2.556
15	20	20	0	6.147	7.682	7.794	6.597	4.500	2.097	.000	-1.318	-1.647
16	30	20	0	7.489	9.523	9.959	8.895	6.750	4.145	1.732	.023	-.739
17	40	20	0	8.830	11.364	12.124	11.193	9.000	6.193	3.464	1.364	.170
18	10	30	0	6.708	8.054	7.578	5.482	2.375	-.893	-3.464	-4.696	-4.333
19	20	30	0	8.221	10.109	9.959	7.963	4.750	1.213	-1.732	-3.391	-3.471
20	30	30	0	9.733	12.163	12.341	10.445	7.125	3.320	.000	-2.087	-2.608
21	40	30	0	11.245	14.218	14.722	12.926	9.500	5.426	1.732	-.782	-1.745
22	10	40	0	8.611	10.268	9.526	6.665	2.500	-1.835	-5.196	-6.732	-6.111
23	20	40	0	10.294	12.536	12.124	9.330	5.000	.330	-3.464	-5.464	-5.294
24	30	40	0	11.977	14.803	14.722	11.994	7.500	2.494	-1.732	-4.197	-4.477
25	40	40	0	13.660	17.071	17.321	14.659	10.000	4.659	.000	-2.929	-3.660

TABLE 22.- CONCENTRATIONS AND REFLECTANCE DATA (%) FOR BERMUDA HUNDRED (B_{100}), BAILEY BAY (BB), AND MIXTURES OF SAME SEDIMENTS IN DEIONIZED WATER.

Spectra Number	Sediment Concentrations (ppm)		Reflectances (%) at specific wavelengths (nm)								
	B_{100}	BB	460	500	540	580	620	660	700	740	780
1	0	N/A	.36	.34	.28	.25	.18	.08	.08	.10	.17
2	4	N/A	.68	.70	.71	.56	.47	.32	.21	.18	.25
3	17	N/A	.96	1.03	1.06	1.08	.93	.84	.67	.38	.42
4	25	N/A	1.12	1.23	1.30	1.26	1.21	1.05	.86	.52	.51
5	52	N/A	1.48	1.58	1.82	1.96	1.82	1.68	1.52	.88	.85
6	86	N/A	1.64	1.89	2.20	2.46	2.32	2.24	2.02	1.26	1.21
7	173	N/A	2.14	2.46	3.10	3.62	3.59	3.42	3.21	2.18	2.01
8	N/A	4	.72	.72	.64	.60	.48	.40	.37	.27	.35
9	N/A	86	1.80	1.88	1.92	1.90	1.84	1.68	1.60	1.24	1.20
10	N/A	173	2.60	2.64	2.80	2.78	2.72	2.69	2.56	2.24	2.14

TABLE 22.- CONCLUDED

Spectra Number	Sediment Concentrations (ppm) B_{100}	BB	Reflectances (%) at specific wavelengths (nm) 460	500	540	580	620	600	700	740	780
11	25	0	1.17	1.19	1.44	1.46	1.28	1.14	1.01	.59	.63
12	25	4	1.19	1.27	1.47	1.47	1.32	1.16	1.09	.68	.63
13	25	17	1.35	1.42	1.60	1.66	1.53	1.41	1.20	.81	.86
14	25	34	1.45	1.57	1.81	1.85	1.71	1.57	1.48	1.03	1.06
15	25	86	1.82	1.95	2.19	2.25	2.11	2.00	1.86	1.46	1.45
16	25	129	2.08	2.28	2.59	2.63	2.50	2.43	2.32	1.95	2.01
17	25	173	2.60	2.84	3.20	3.16	3.02	2.84	2.79	2.35	2.55

TABLE 23.- LINEAR SUPERPOSITION AND INTERACTION TERM REFLECTANCE (%) CALCULATIONS

FOR MIXTURES OF BERMUDA HUNDRED AND BAILEY BAY SEDIMENTS IN WATER

Sediment Concentrations (ppm)		Linear superposition reflectances (%) at specific wavelengths (nm)								
B_{100}	BB	460	500	540	580	620	660	700	740	780
25	4	1.48	1.61	1.66	1.61	1.51	1.37	1.15	.69	.69
25	86	2.56	2.77	2.94	2.91	2.87	2.65	2.38	1.66	1.54
25	173	3.36	3.53	3.82	3.79	3.75	3.66	3.34	2.66	2.48

Sediment Concentrations (ppm)		Interaction term g(λ) (%) at specific wavelengths (nm)								
B_{100}	BB	460	500	540	580	620	660	700	740	780
25	4	-.29	-.34	-.19	-.14	-.19	-.21	-.06	-.01	-.06
25	86	-.74	-.82	-.75	-.66	-.76	-.65	-.52	-.20	-.09
25	173	-.76	-.69	-.62	-.63	-.73	-.82	-.55	-.31	.07

TABLE 24.- RADIANCES FOR CONSTITUENT A AFTER MODIFICATION BY WEAK AND STRONG ATMOSPHERES

	Power-law exponent	C_A	Radiances (arbitrary units) at specific wavelengths (nm) 500	550	600	650	700	750	800	850	900
Weak Atmosphere	p = 0.5	0	11.533	7.906	5.413	3.754	2.602	1.776	1.255	.878	.602
		10	11.803	8.306	5.921	4.335	3.214	2.375	1.796	1.322	.917
		20	11.915	8.472	6.131	4.576	3.468	2.623	2.020	1.505	1.047
		30	12.000	8.599	6.293	4.761	3.662	2.814	2.192	1.646	1.147
		40	12.072	8.706	6.429	4.917	3.826	2.974	2.337	1.765	1.232
	p = 1.0	0	72.964	50.002	34.234	23.715	16.468	11.206	7.911	5.533	3.828
		10	73.817	51.268	35.839	25.554	18.404	13.101	9.620	6.936	4.823
		20	74.670	52.534	37.445	27.393	20.340	14.996	11.330	8.339	5.818
		30	75.523	53.800	39.051	29.232	22.276	16.892	13.039	9.742	6.813
		40	76.376	55.065	40.656	31.071	24.212	18.787	14.749	11.145	7.808
	p = 1.5	0	461.461	316.244	216.514	149.980	104.155	70.871	50.026	34.994	24.216
		10	464.158	320.246	221.592	155.795	110.277	76.864	55.432	39.430	27.362
		20	469.090	327.565	230.875	166.429	121.471	87.821	65.316	47.542	33.115
		30	475.477	337.042	242.897	180.199	135.967	102.011	78.116	58.046	40.565
		40	483.040	348.265	257.133	196.506	153.132	118.814	93.274	70.485	49.387

TABLE 24.- CONCLUDED

	Power-law exponent	C_A	Radiances (arbitrary units) at specific wavelengths (nm) 500	550	600	650	700	750	800	850	900
Strong Atmosphere	p = 0.5	0	10.578	9.045	7.751	6.566	5.623	4.770	4.089	3.470	2.961
		10	10.791	9.368	8.165	7.042	6.129	5.267	4.540	3.841	3.225
		20	10.880	9.502	8.336	7.241	6.338	5.472	4.727	3.995	3.335
		30	10.948	9.604	8.467	7.392	6.499	5.630	4.870	4.113	3.419
		40	11.005	9.691	8.578	7.520	6.635	5.763	4.991	4.213	3.490
	p = 1.0	0	68.895	57.204	49.005	41.550	35.526	30.187	25.849	21.946	18.713
		10	67.570	58.225	50.313	43.059	37.127	31.757	27.275	23.122	19.549
		20	68.245	59.247	51.620	44.568	38.727	33.328	28.700	24.297	20.385
		30	68.920	60.268	52.928	46.077	40.327	34.899	30.126	25.472	21.221
		40	69.595	61.289	54.236	47.586	41.927	36.469	31.551	26.647	22.057
	p = 1.5	0	423.073	361.794	309.927	262.790	224.692	190.915	163.488	138.801	118.352
		10	425.208	365.022	314.063	267.562	229.752	195.881	167.995	142.517	120.996
		20	429.111	370.926	321.624	276.285	239.003	204.963	176.236	149.312	125.829
		30	434.165	378.571	331.415	287.582	250.983	216.722	186.911	158.111	132.089
		40	440.150	387.625	343.010	300.960	265.170	230.648	199.550	168.531	139.501

TABLE 25.- COMPARISON OF ATMOSPHERE-FREE CHARACTERISTIC VECTORS WITH THOSE DERIVED FOR CONSTITUENTS A, B, AND C AFTER MODIFICATION BY WEAK AND STRONG ATMOSPHERES

	Characteristic vector components at specific wavelengths (nm)								
	500	550	600	650	700	750	800	850	900
Characteristic vectors for constituent A									
v_A (no atmosphere)	0.206	0.292	0.358	0.399	0.413	0.399	0.358	0.292	0.206
v_A (weak atmosphere)	0.184	0.273	0.346	0.397	0.417	0.409	0.369	0.303	0.214
v_A (strong atmosphere)	0.177	0.267	0.342	0.395	0.418	0.411	0.373	0.307	0.219
Characteristic vectors for constituent B									
v_B (no atmosphere)	0.369	0.426	0.369	0.213	0.000	-0.213	-0.369	-0.426	-0.369
v_B (weak atmosphere)	0.333	0.404	0.362	0.215	0.000	-0.221	-0.386	-0.447	-0.389
v_B (strong atmosphere)	0.320	0.396	0.358	0.214	0.000	-0.223	-0.391	-0.455	-0.397
Characteristic vectors for constituent C									
v_C (no atmosphere)	0.109	0.210	0.297	0.363	0.405	0.420	0.405	0.363	0.297
v_C (weak atmosphere)	0.096	0.194	0.284	0.357	0.405	0.425	0.413	0.372	0.305
v_C (strong atmosphere)	0.091	0.189	0.279	0.354	0.404	0.425	0.416	0.376	0.309

TABLE 26.- CHARACTERISTIC VECTORS AND SCALAR MULTIPLES FOR CONSTITUENT A SPECTRA MODIFIED BY ATMOSPHERES VARIABLE IN A WEAK-TO-STRONG AND STRONG-TO-WEAK PATTERN. CONSTITUENT POWERS = 0.5, 1.0, AND 1.5.

Atmospheric Variation	Power-Law Exponent	Characteristic vector components at specific wavelengths (nm)								
		500	550	600	650	700	750	800	850	900
Weak-to-strong	p = 0.5	-0.057	0.185	0.328	0.390	0.418	0.413	0.387	0.346	0.300
	p = 1.0	-0.055	0.185	0.327	0.391	0.417	0.414	0.387	0.346	0.298
	p = 1.5	-0.054	0.185	0.328	0.391	0.417	0.414	0.387	0.346	0.298
Strong-to-weak	p = 0.5	-0.300	0.080	0.284	0.354	0.385	0.384	0.374	0.362	0.363
	p = 1.0	-0.317	0.072	0.280	0.351	0.379	0.382	0.372	0.362	0.365
	p = 1.5	-0.313	0.074	0.281	0.352	0.380	0.383	0.373	0.362	0.364

Scalar Multiples

Weak-to-strong				Strong-to-weak			
C_A	p = 0.5	p = 1.0	p = 1.5	C_A	p = 0.5	p = 1.0	p = 1.5
0	-0.688	-0.641	-0.613	0	0.561	0.645	0.688
10	-0.266	-0.312	-0.330	10	0.375	0.310	0.282
20	0.040	0.008	-0.016	20	0.043	-0.013	-0.057
30	0.322	0.320	0.312	30	-0.309	-0.323	-0.341
40	0.592	0.624	0.647	40	-0.669	-0.619	-0.573

APPENDIX E

FIGURES

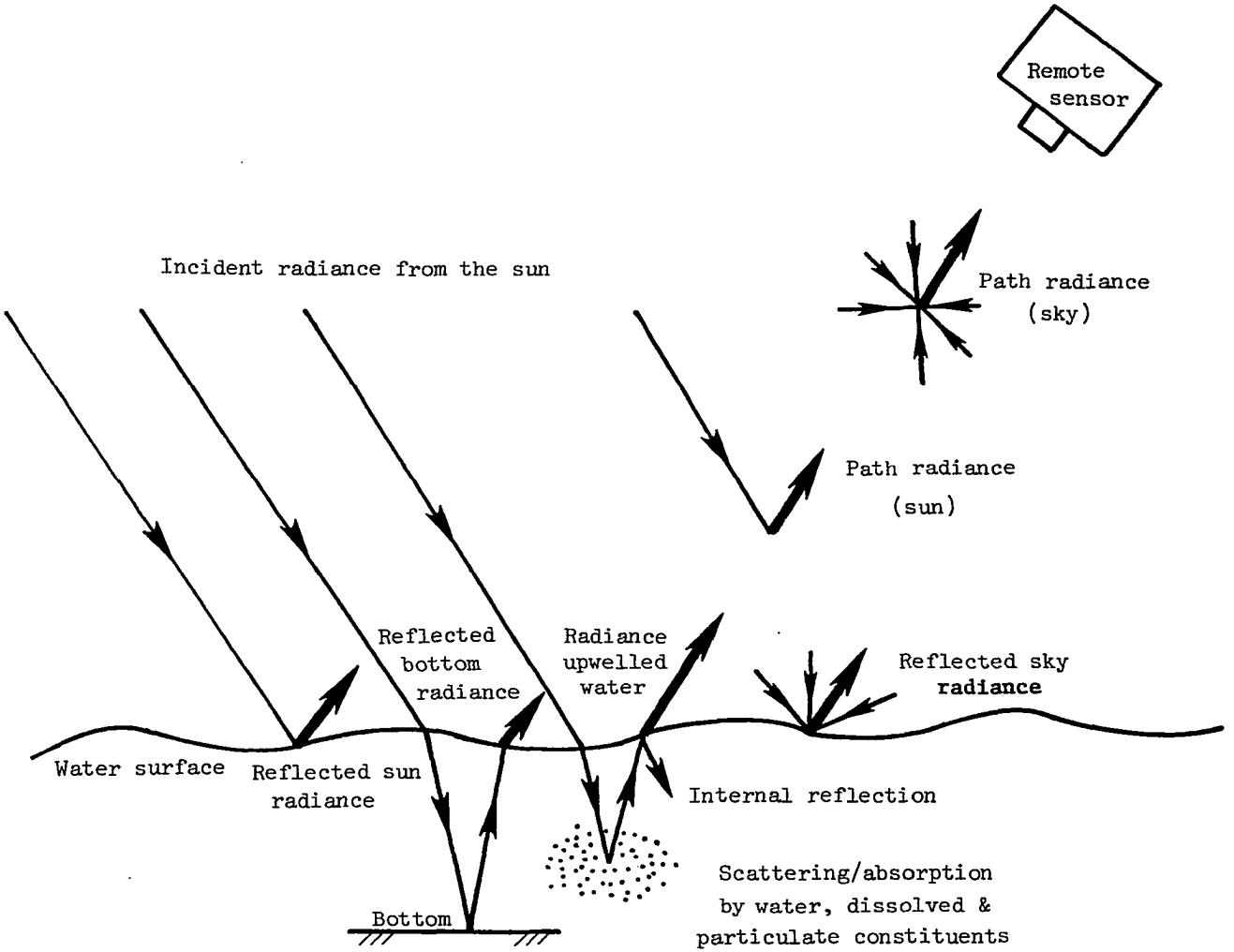

Figure 1.- Radiation components measured by remote sensors.

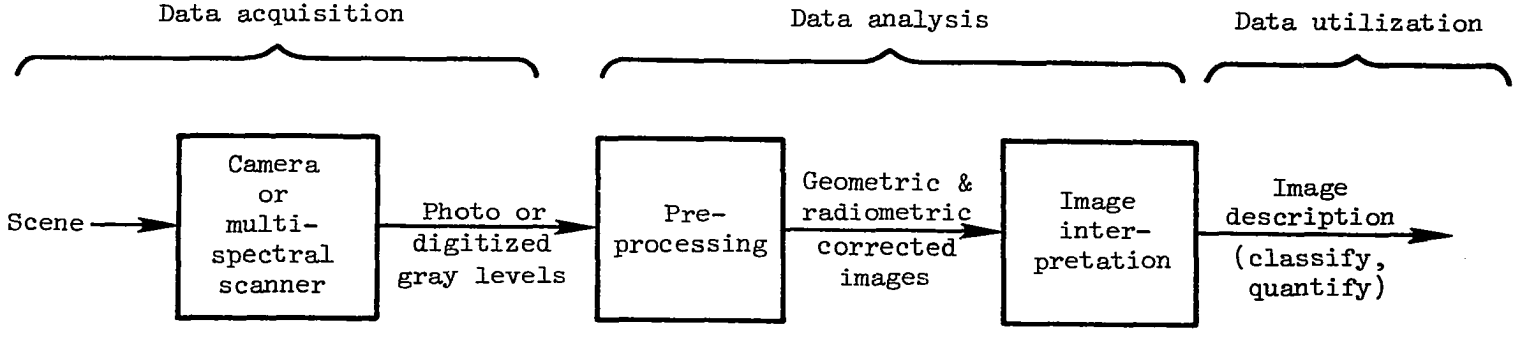

Figure 2.- Block diagram of remote-sensing image processing system.

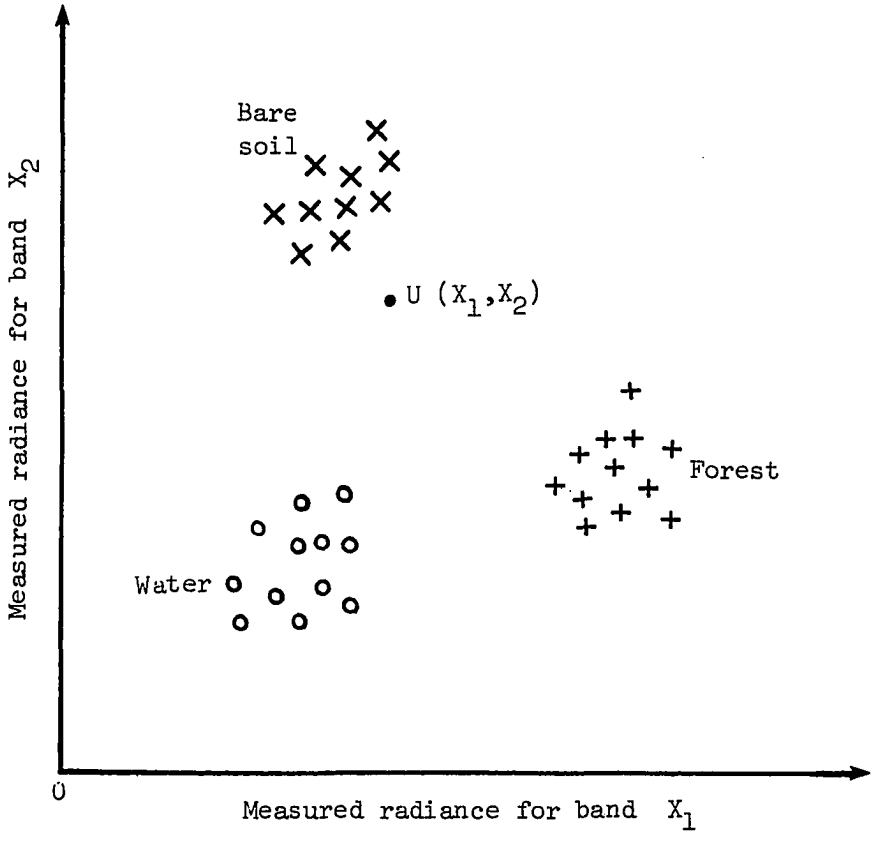

Figure 3.- Multispectral scanner returns for several categories or classes of surface features.

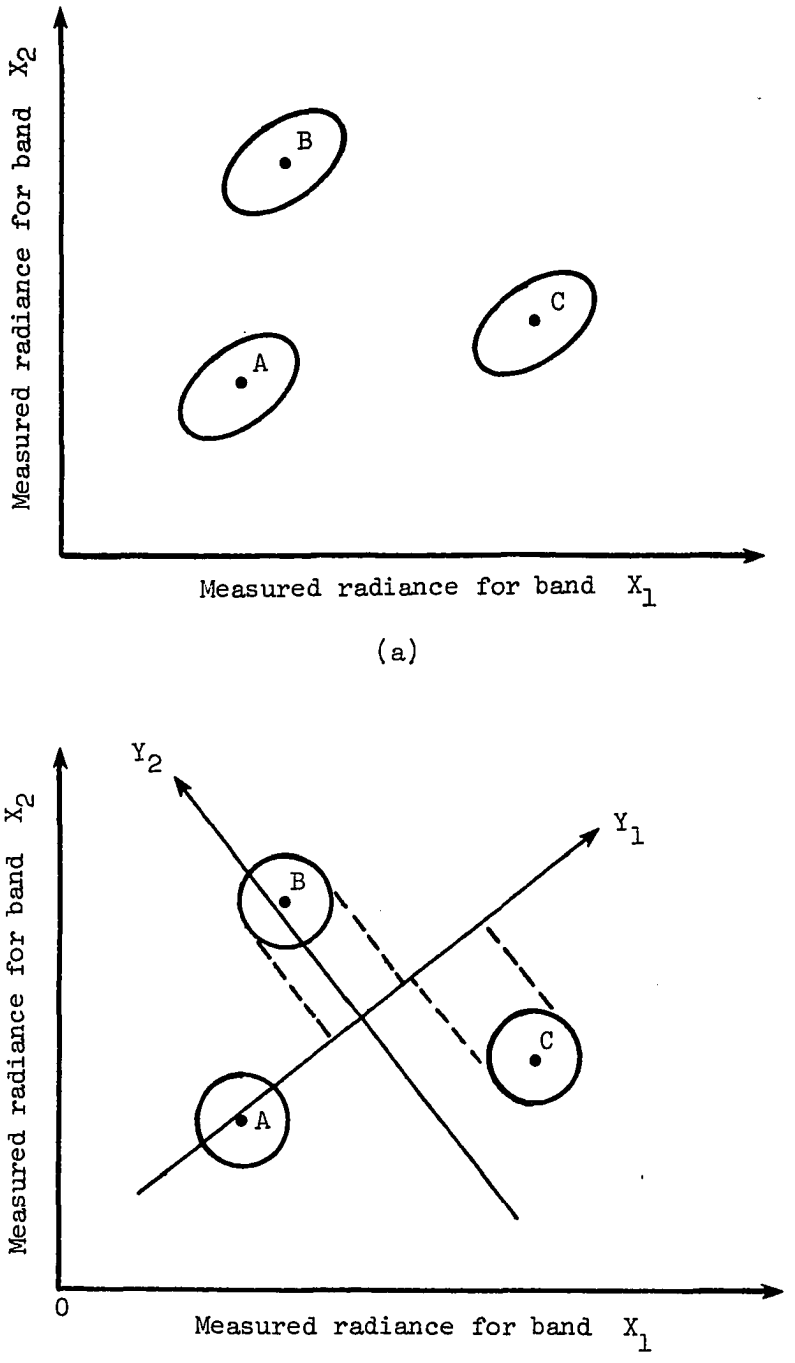

Figure 4.- (a) Mean values and density distributions for categories A, B, C in measured axes system (X_1,X_2). (b) Canonical axes (Y_1,Y_2) produced by rotation, translation and scaling. (After Podwysocki et al 1977).

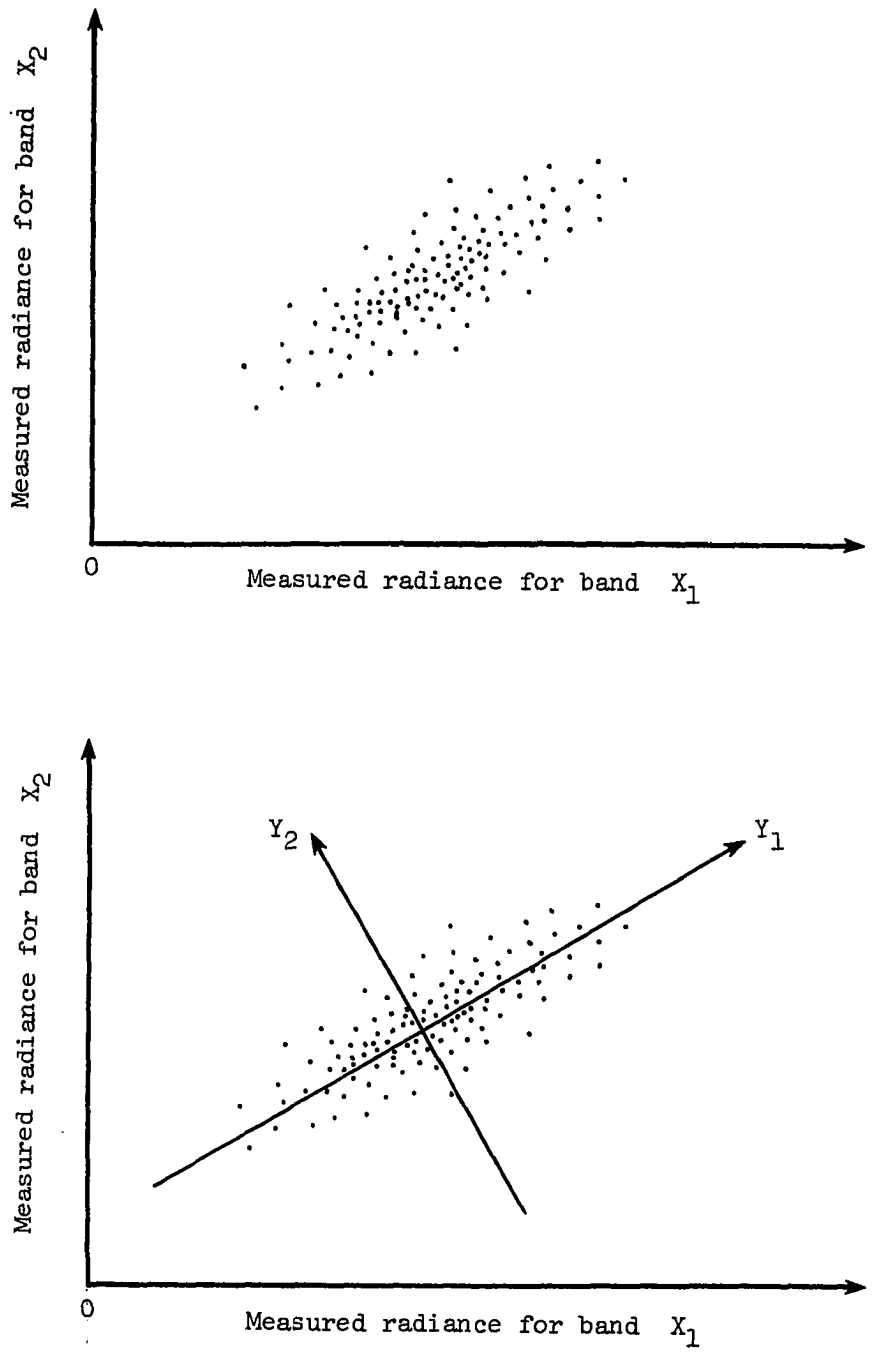

Figure 5.- Elliptical scatter pattern for hypothetical data set for multispectral scanner bands (X_1,X_2) and the principal components axes (Y_1,Y_2) that explain maximum data variance.

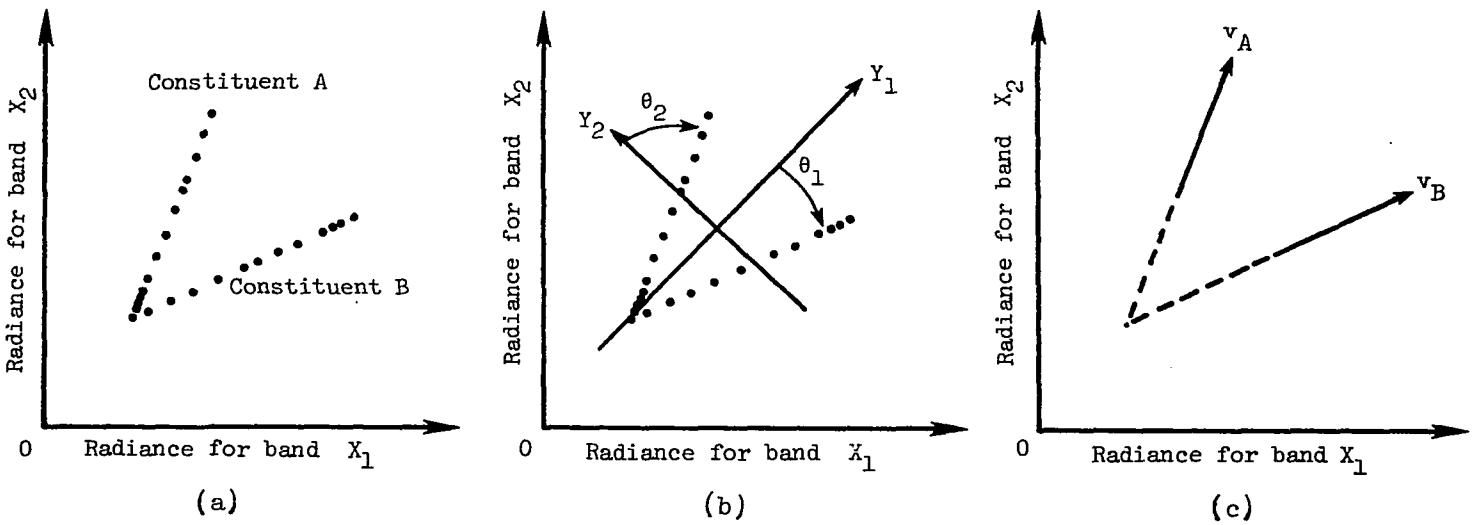

Figure 6.- (a) Two-band radiance data for two ideal, spatially-independent constituents in water. (b) Principal components axes for same data. (c) Characteristic vectors for the two constituents (vectors in directions of first principal axes of separate analyses of each data distribution).

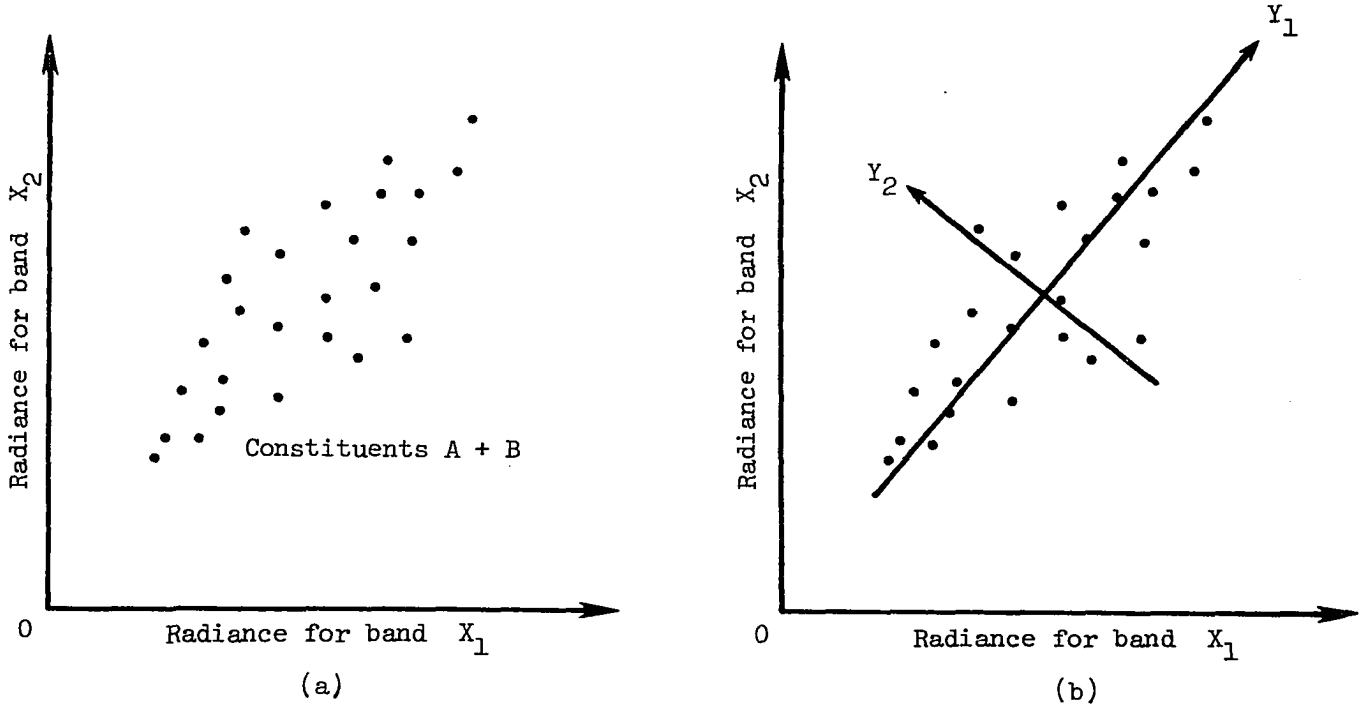

Figure 7.- (a) Two-band radiance data for mixture of two ideal constituents in water. (b) Principal components axes for same data.

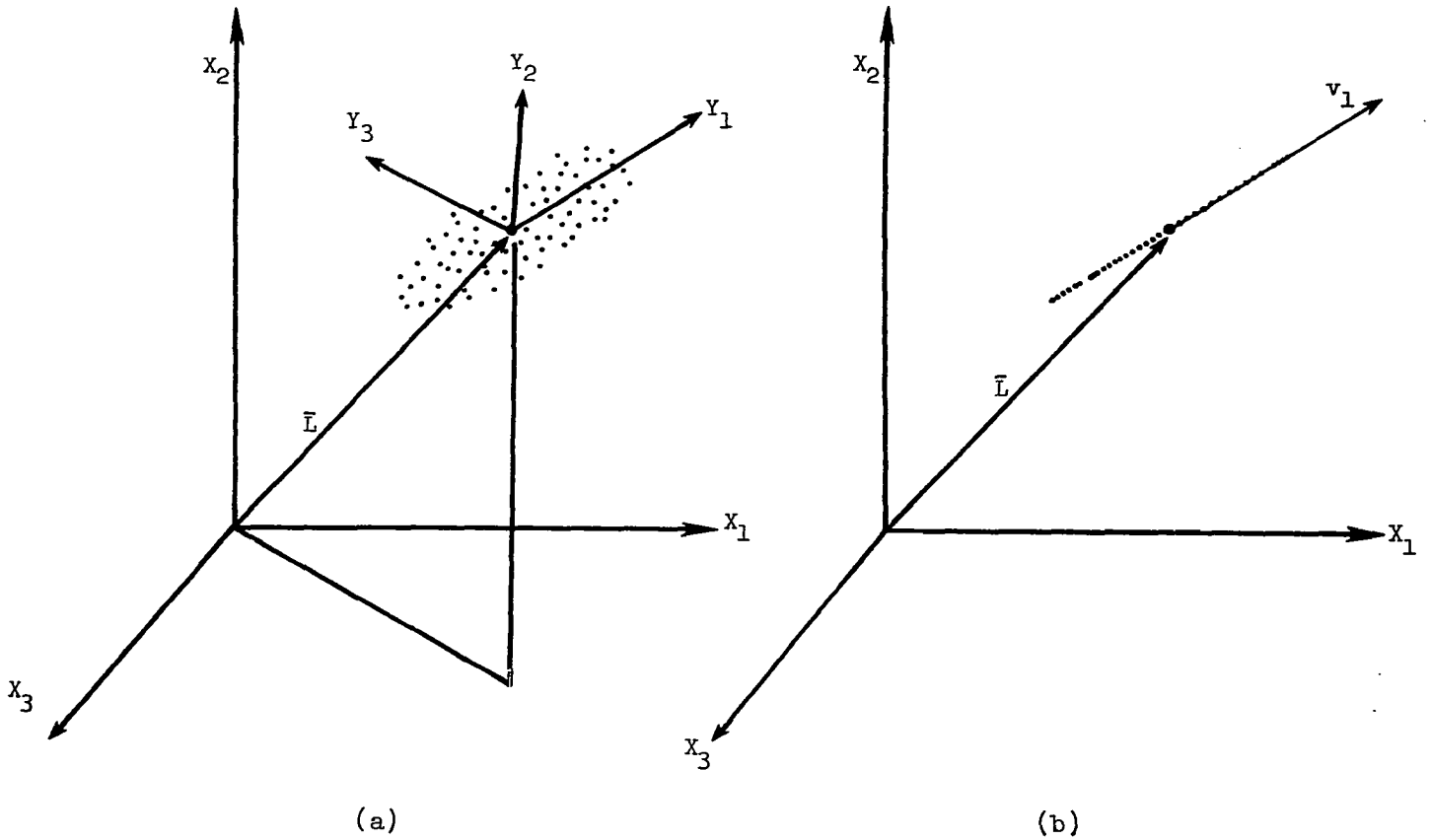

Figure 8.- (a) Three-band radiance data for single constituent in water. Principal components axes and mean spectrum vector shown. (b) Characteristic vector for ideal single constituent in water (vector in direction of first principal axis).

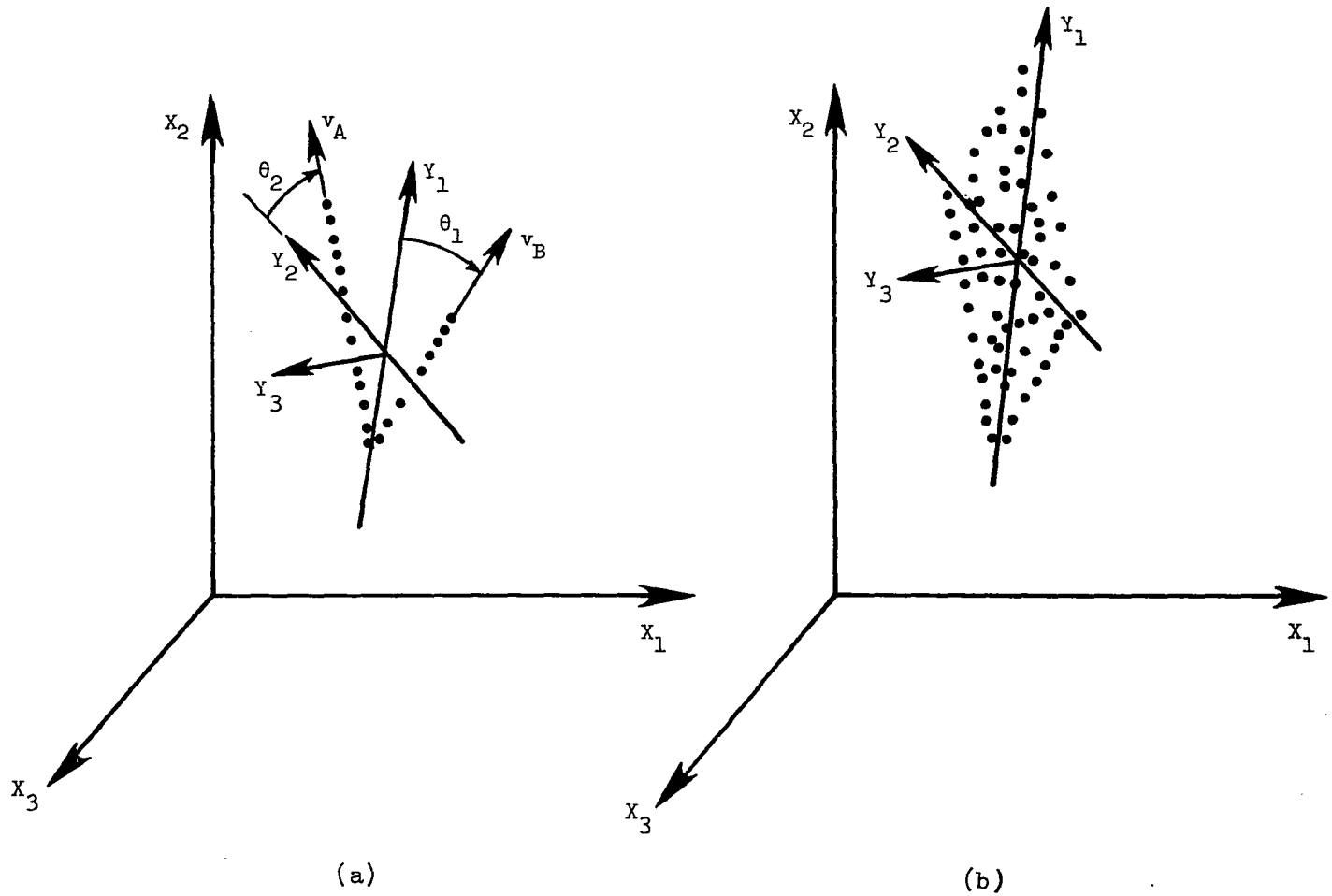

Figure 9.- (a) Three-band radiance data for two ideal, spatially independent constituents in water. Principal axes and characteristic vectors for the constituents are shown. (b) Three-band radiance data for mixtures of two ideal constituents in water. Principal axes are shown.

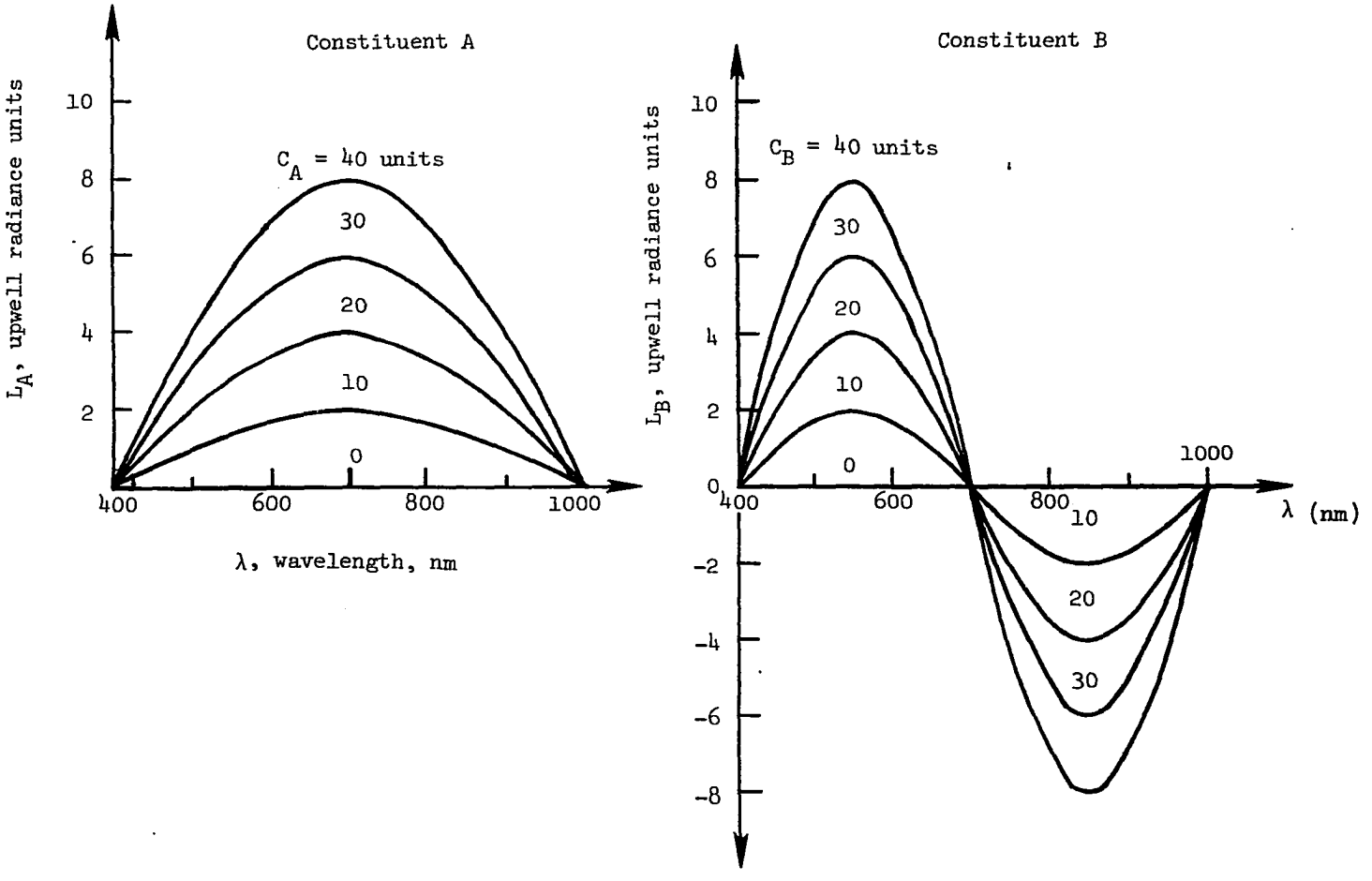

Figure 10.- Upwell radiance spectra for varying concentrations of hypothetical constituents A and B. Base water spectrum removed.

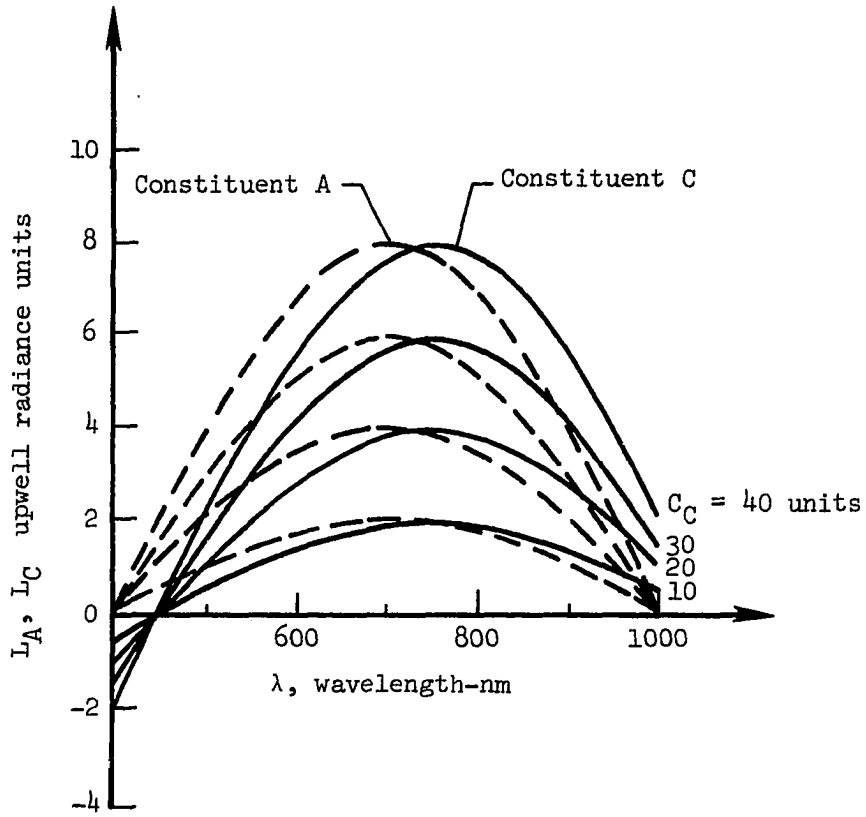

Figure 11.- Upwell radiance spectra for varying concentrations of hypothetical constituents A and C. Base water spectrum removed.

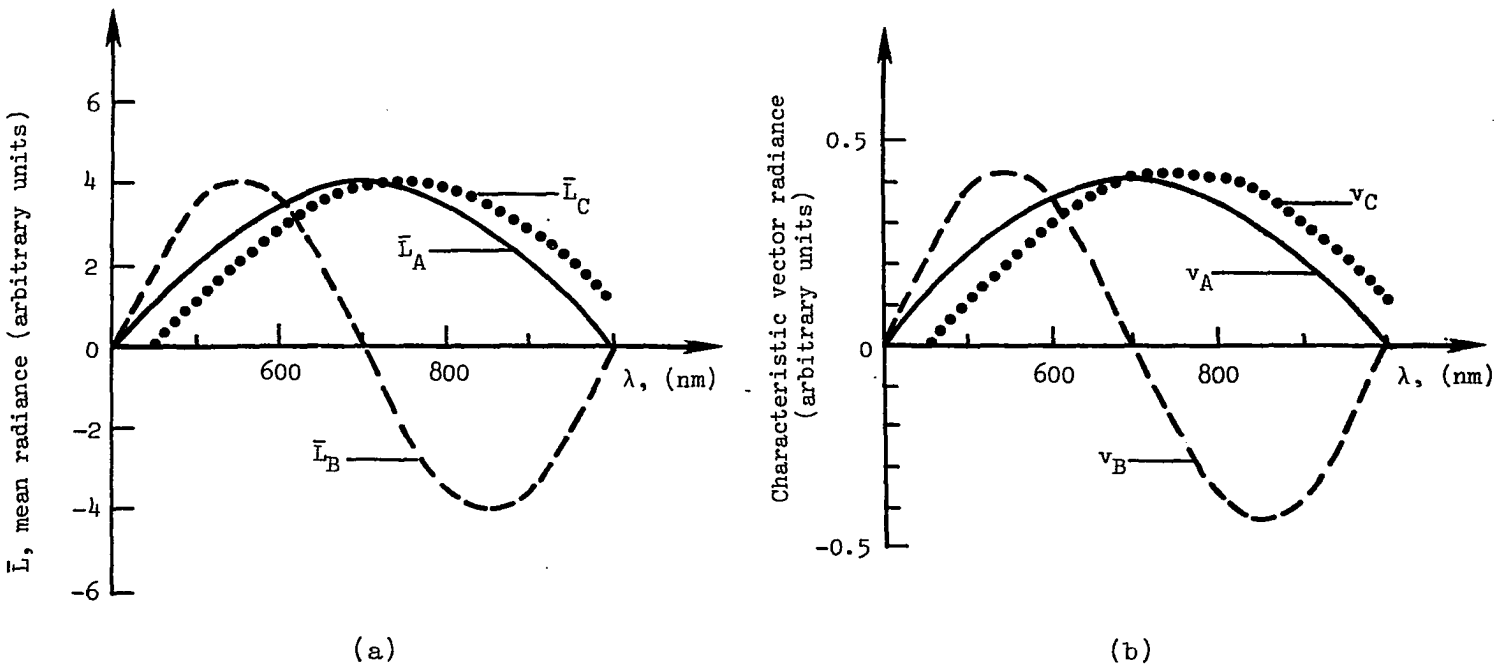

Figure 12.- (a) Mean radiance spectra for three hypothetical constituent families. Base water spectrum removed. (b) Characteristic vector spectra for three hypothetical constituent families. Vector magnitudes normalized to unity.

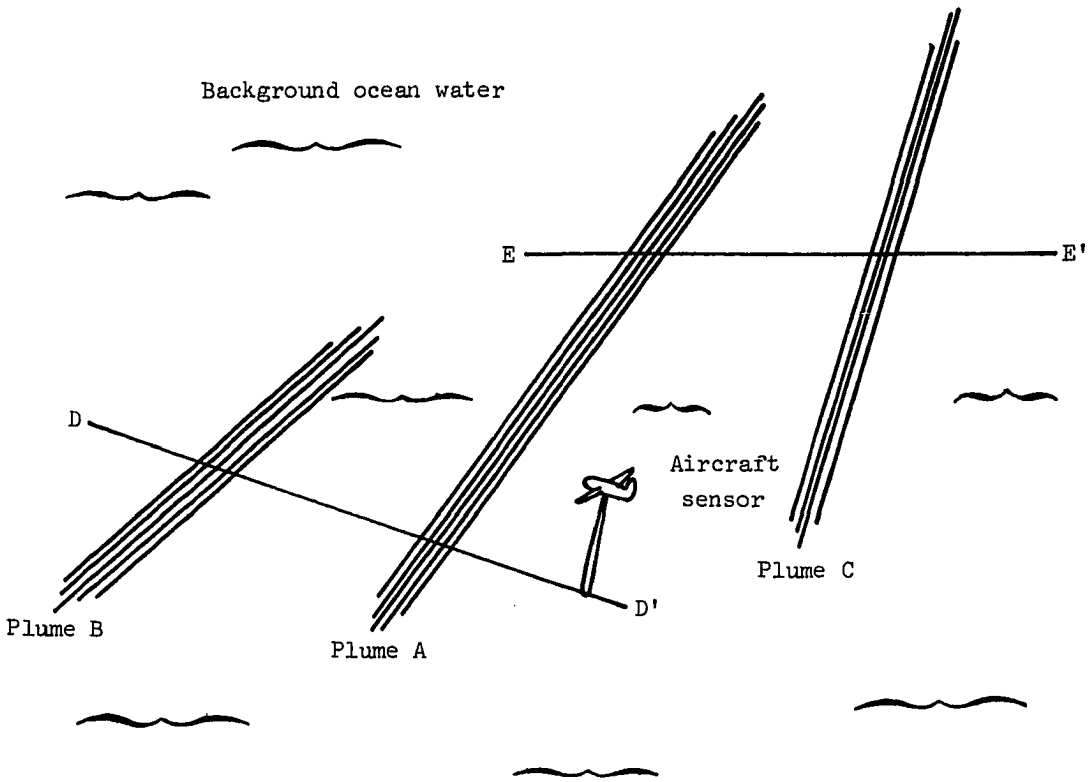

Figure 13.- Line dumps of hypothetical constituents A, B, C in background waters. Upwell radiance data collected along flight lines D - D' and E - E'.

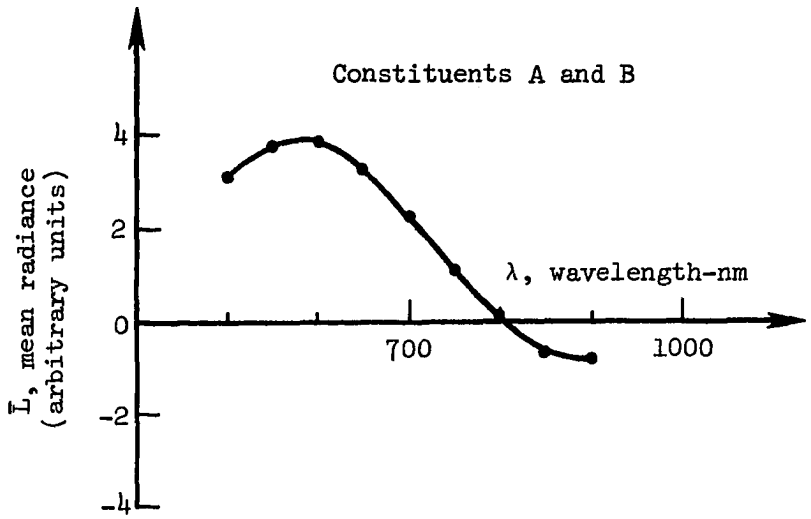

(a)

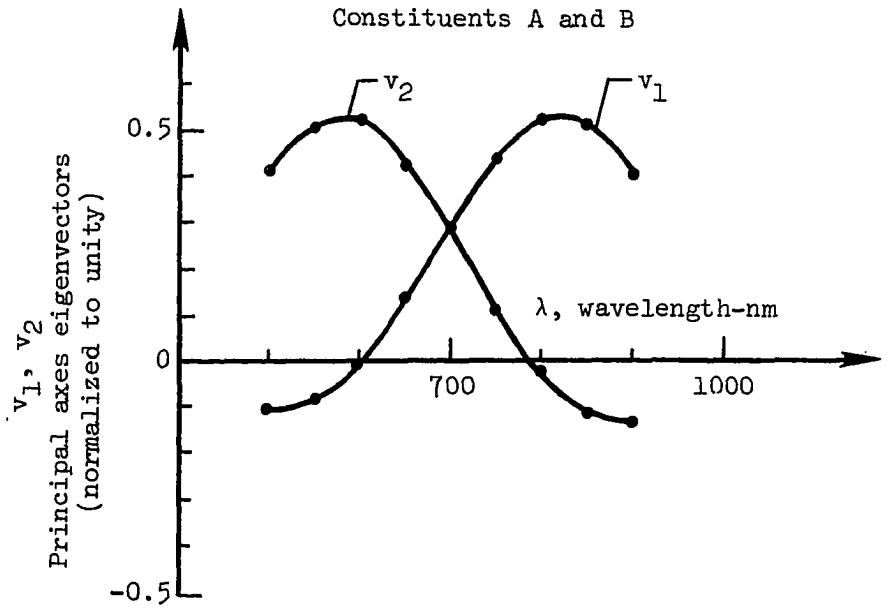

(b)

Figure 14.- (a) Mean vector and (b) two principal axes eigenvectors from spectral radiance set of spatially-independent hypothetical constituents A and B.

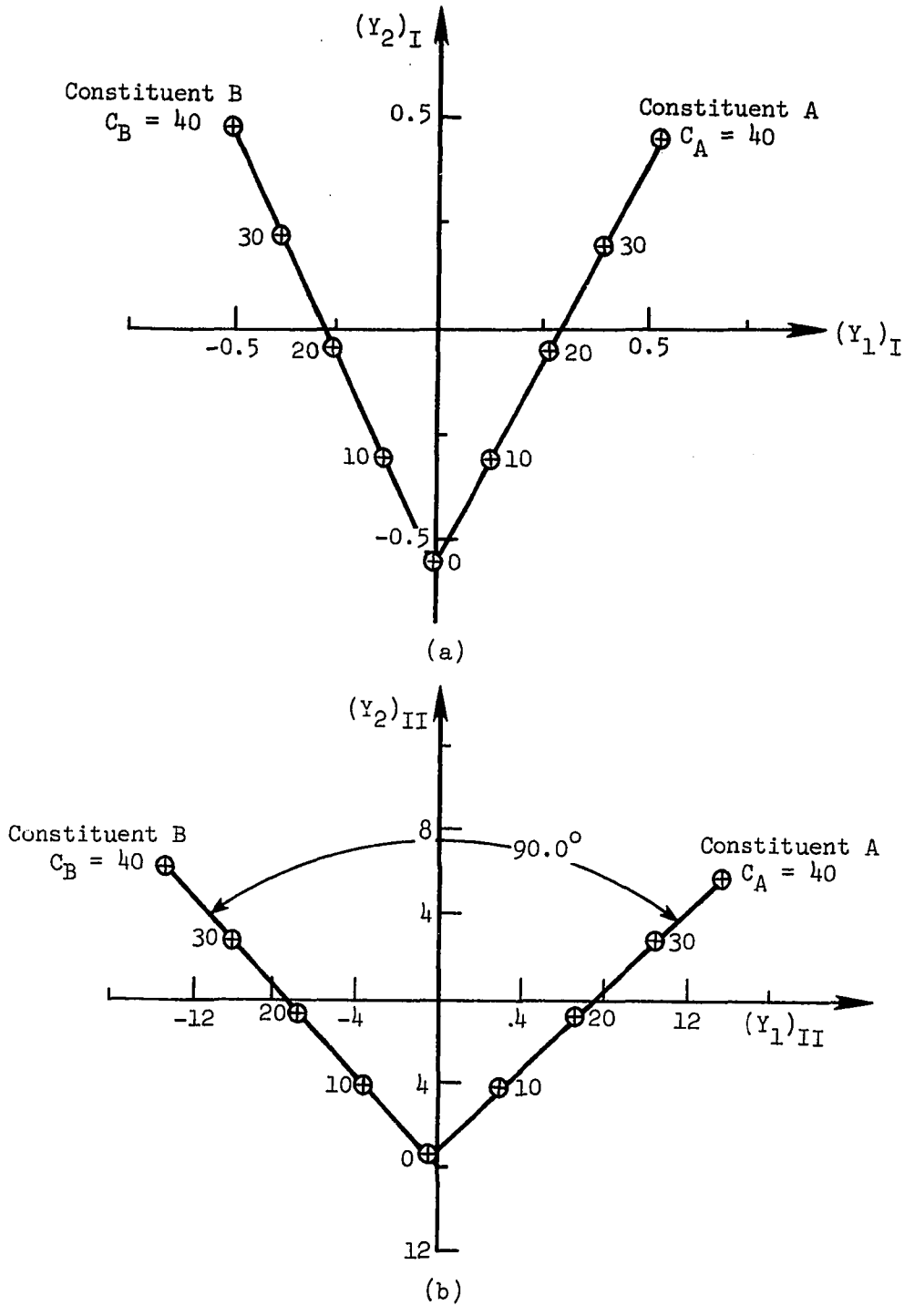

Figure 15.- (a) Scalar multiplies (System I) and (b) principal component values (System II) from spectral radiance set of spatially independent hypothetical constituents A and B.

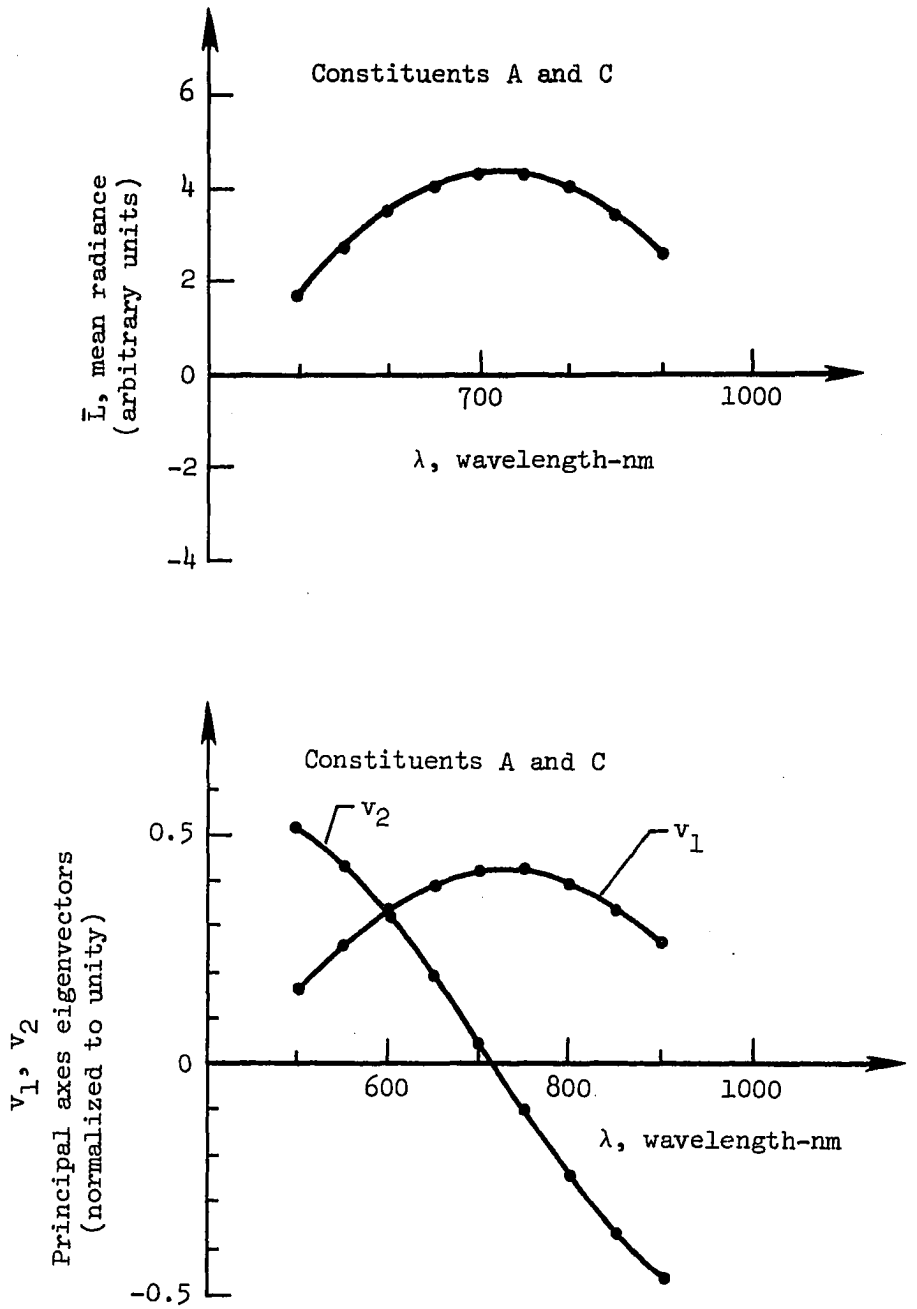

Figure 16.- (a) Mean vector and (b) two principal axes eigenvectors from spectral radiance set of spatially-independent hypothetical constituents A and C.

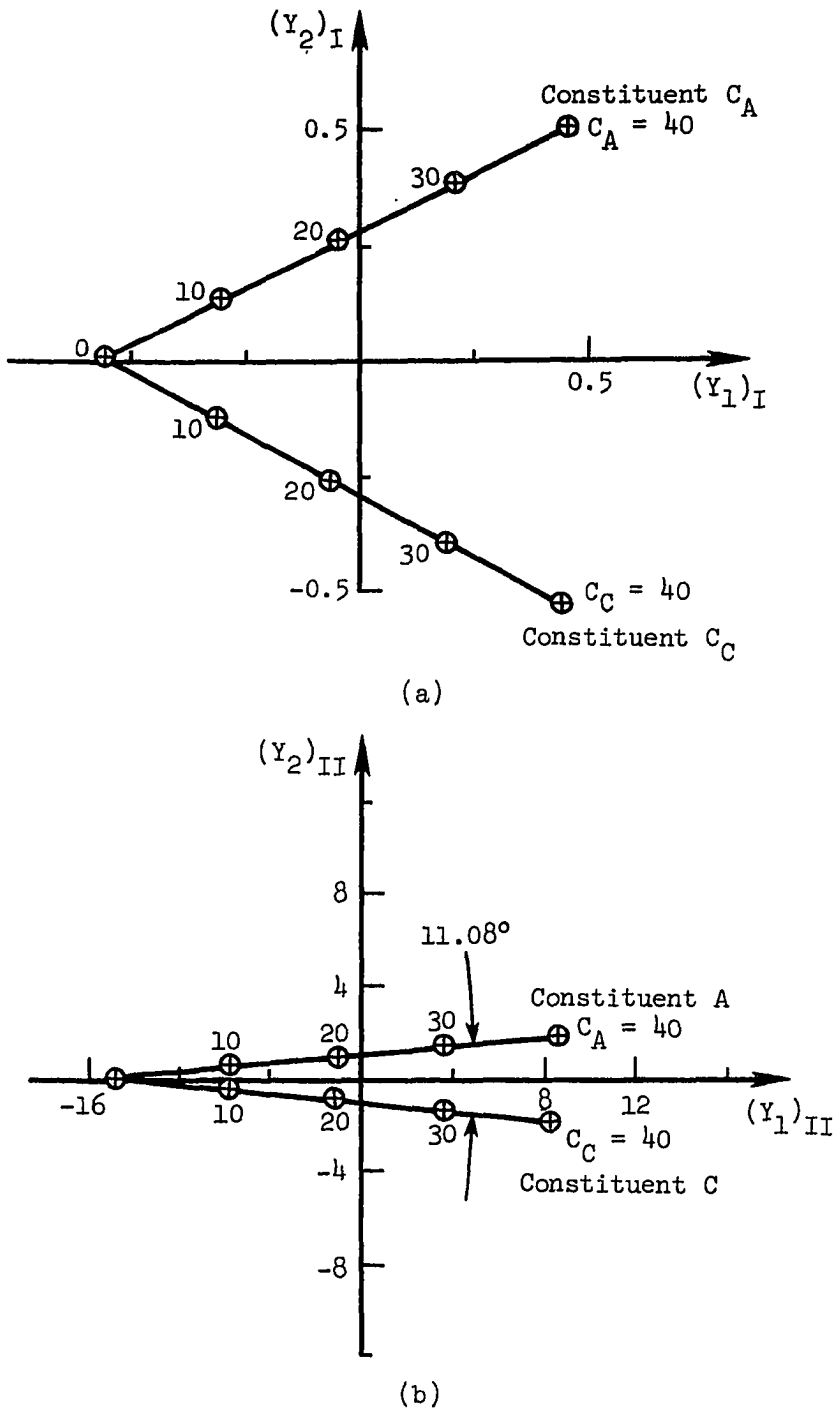

Figure 17.- (a) Scalar multiples (System I) and (b) principal component values (System II) from spectral radiance set of spatially independent hypothetical constituents A and C.

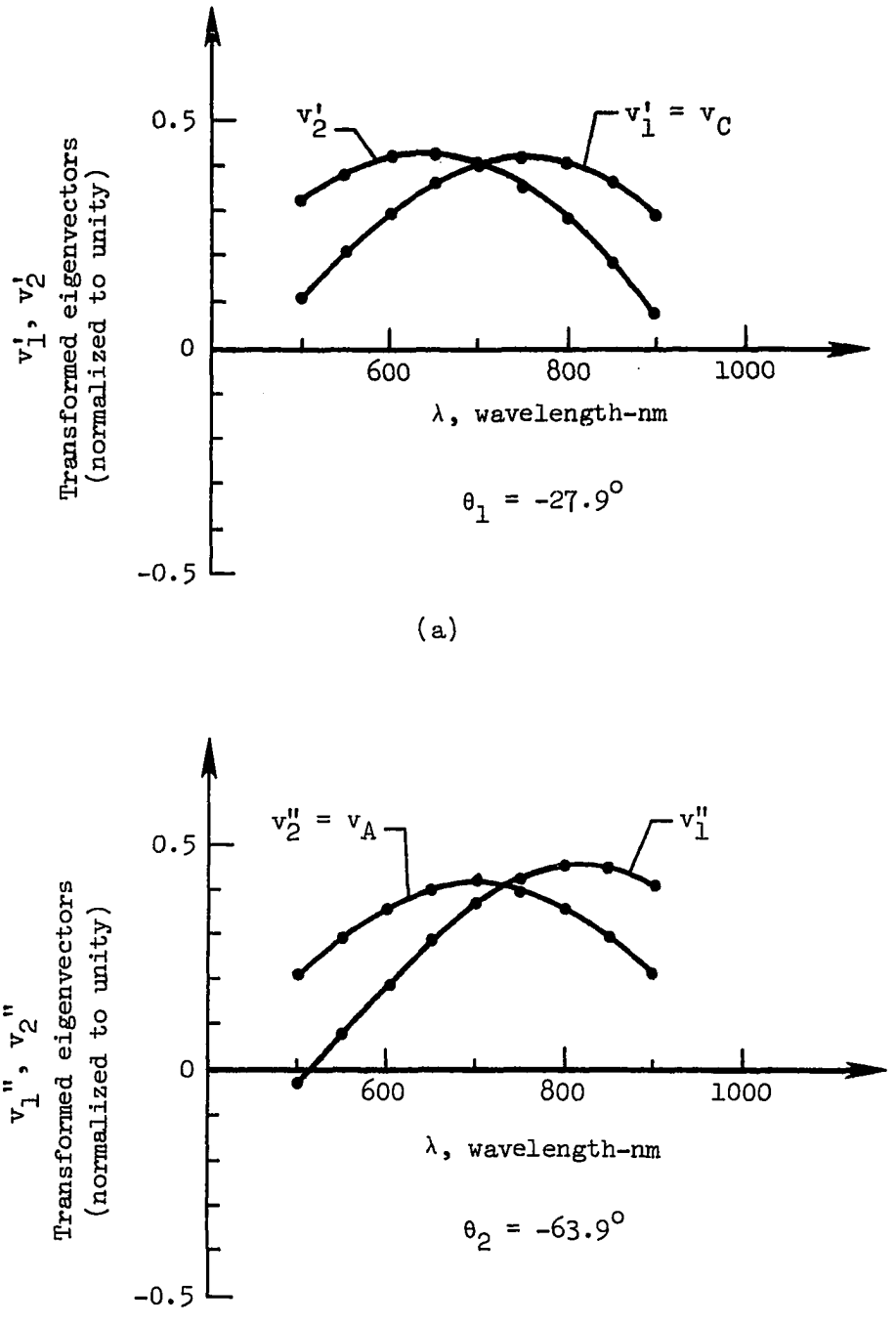

Figure 18.- Principal axes eigenvectors for spectra of spatially-independent constituents A and C after rotation transformations of (a) $\theta_1 = -27.9^\circ$ and (b) $\theta_2 = -63.9^\circ$.

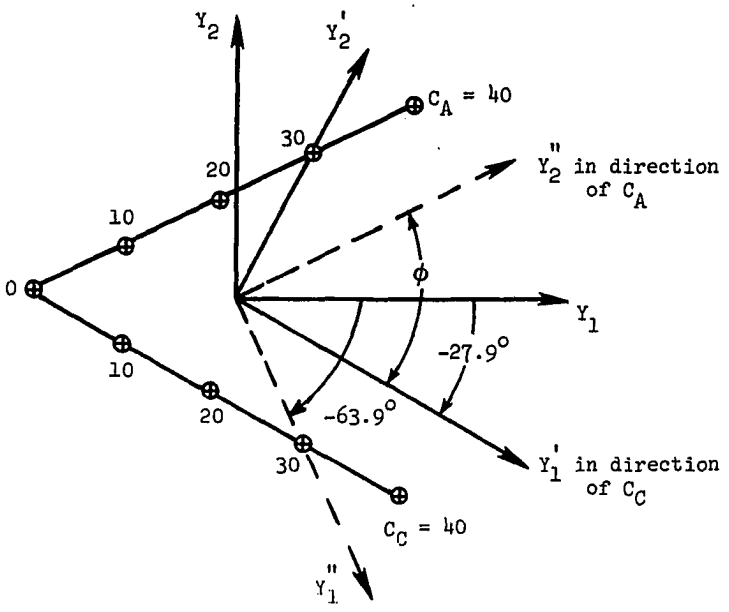

(a)

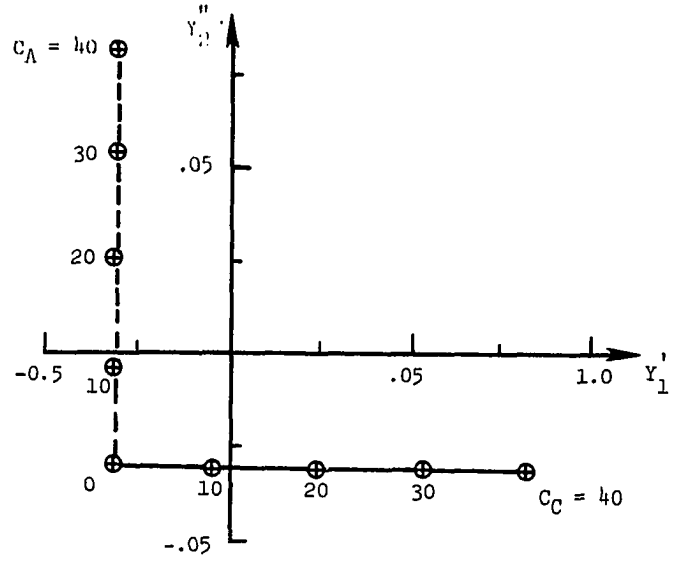

(b)

Figure 19.- Scalar multiples for spatially-independent constituents A and C where (a) shows multiple use of orthogonal transformations to define oblique axes Y_1',Y_2'' and (b) transformation into this Y_1',Y_2'' space.

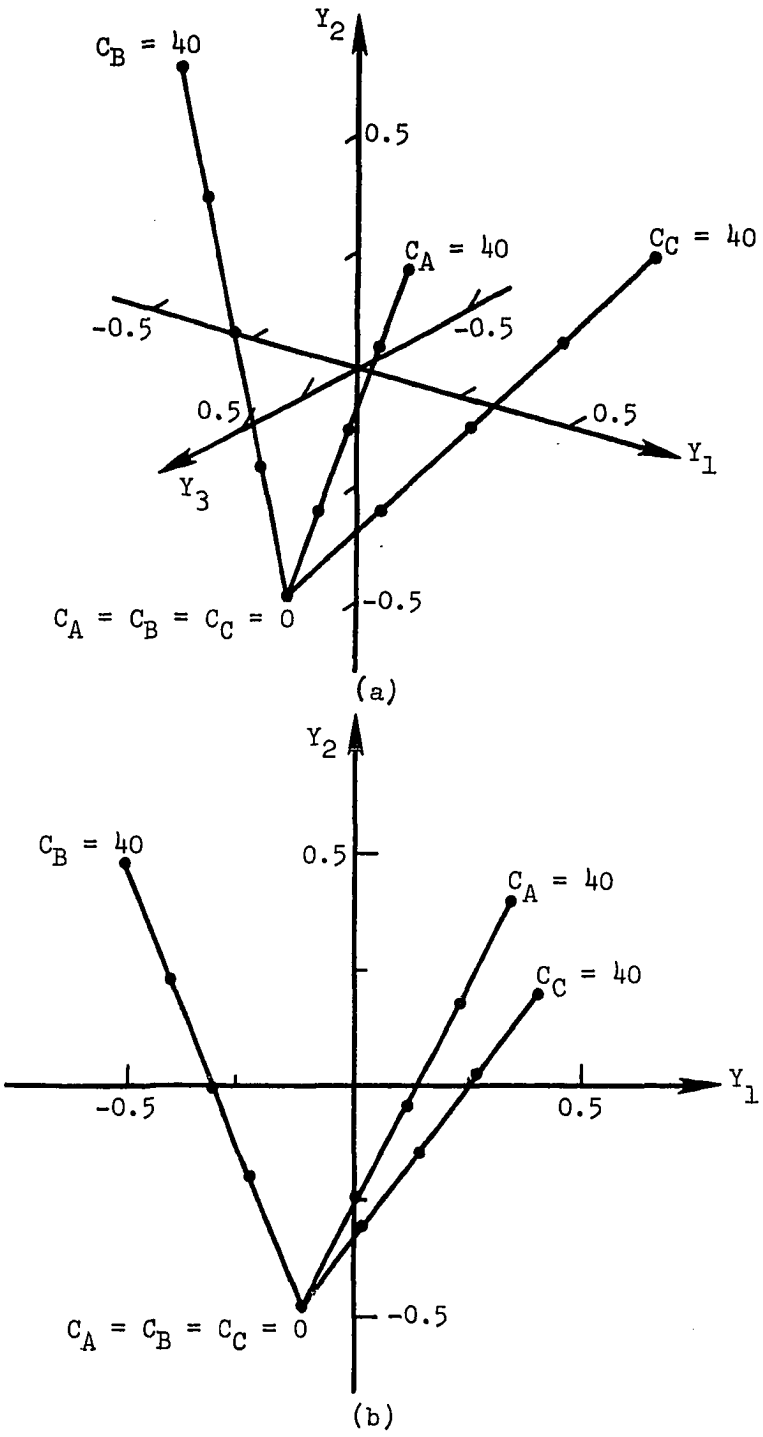

Figure 20.- (a) Scalar multiplies for spatially-independent constituents A, B, and C. (b) Projection of scalar multiplies onto Y_1 - Y_2 plane.

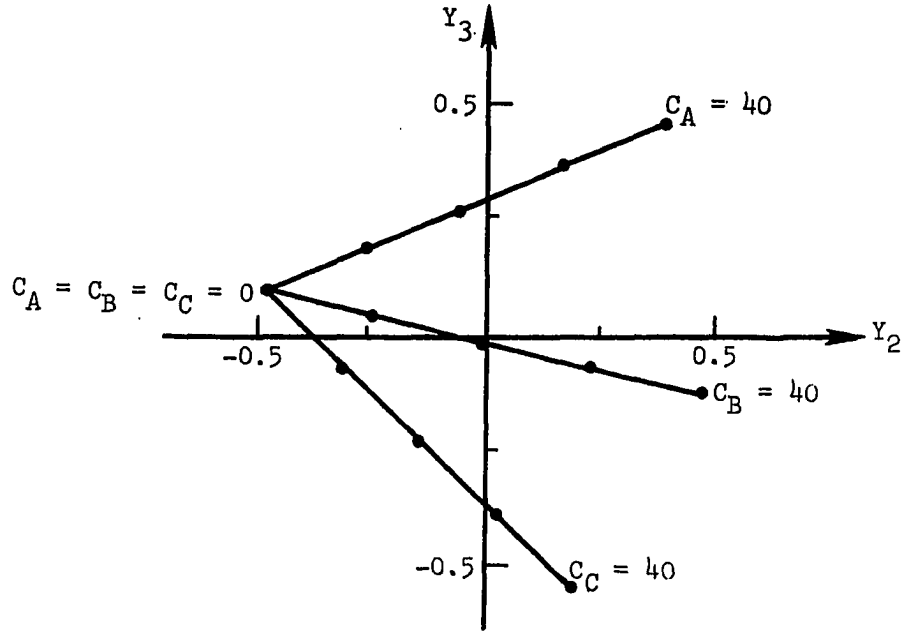

(c)

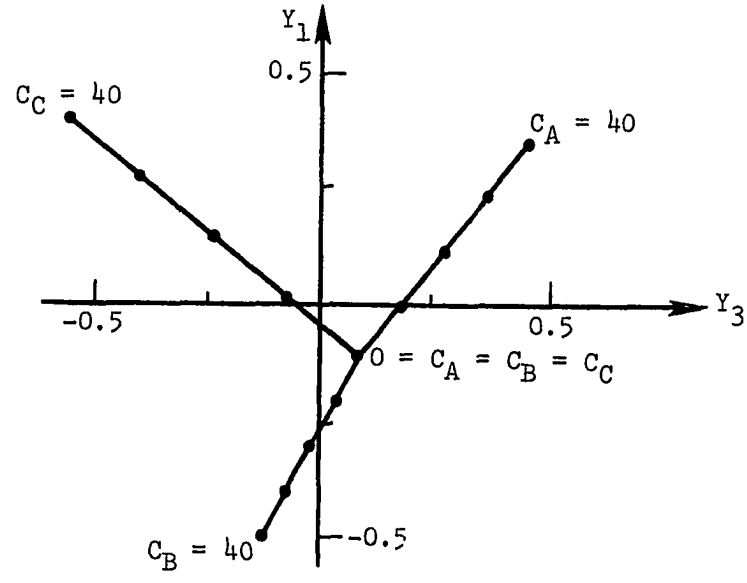

(d)

Figure 20.- Concluded. - (c) Projection of scalar multiples onto $Y_2 - Y_3$ plane. (d) Projection of scalar multiples onto $Y_3 - Y_1$ plane.

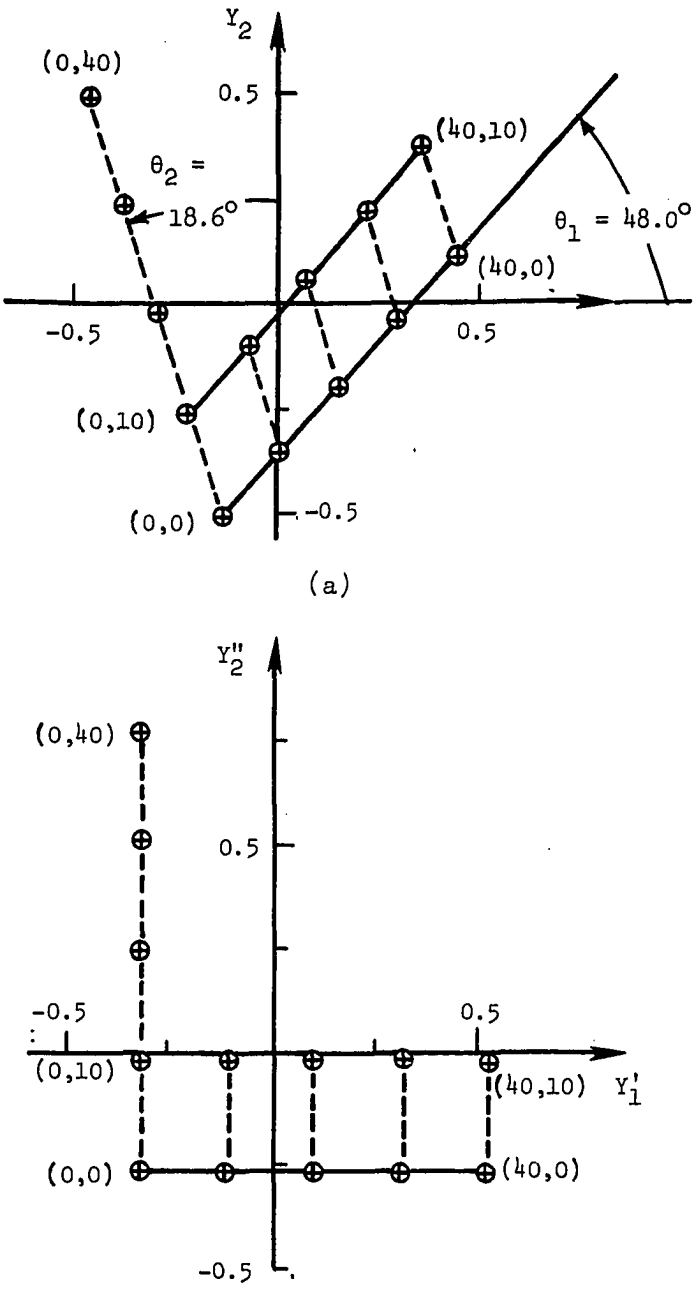

Figure 21.- Scalar multiples for 13- spectra case of mixtures of constituents A + B. (a) Original principal axes system. (b) Transformed oblique axes system using θ_1, θ_2. Representative concentration pairs (C_A, C_B) are labeled.

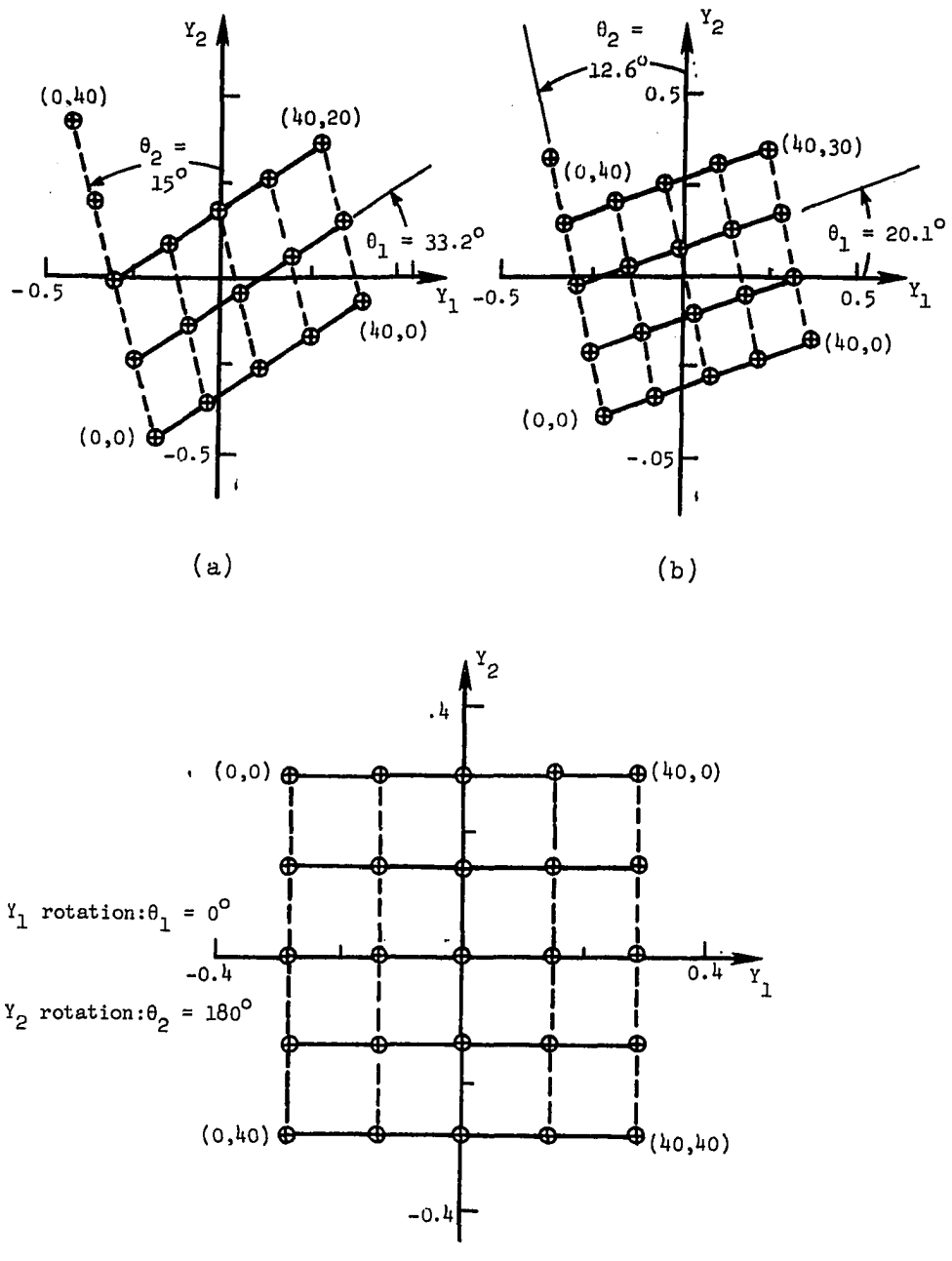

Figure 22.- Scalar multiples for mixtures of constituents A + B for (a) 17, (b) 21, and (c) 25-spectra cases. Representative concentration pairs (C_A, C_B) are labeled. Transformation into oblique axes system uses θ_1, θ_2.

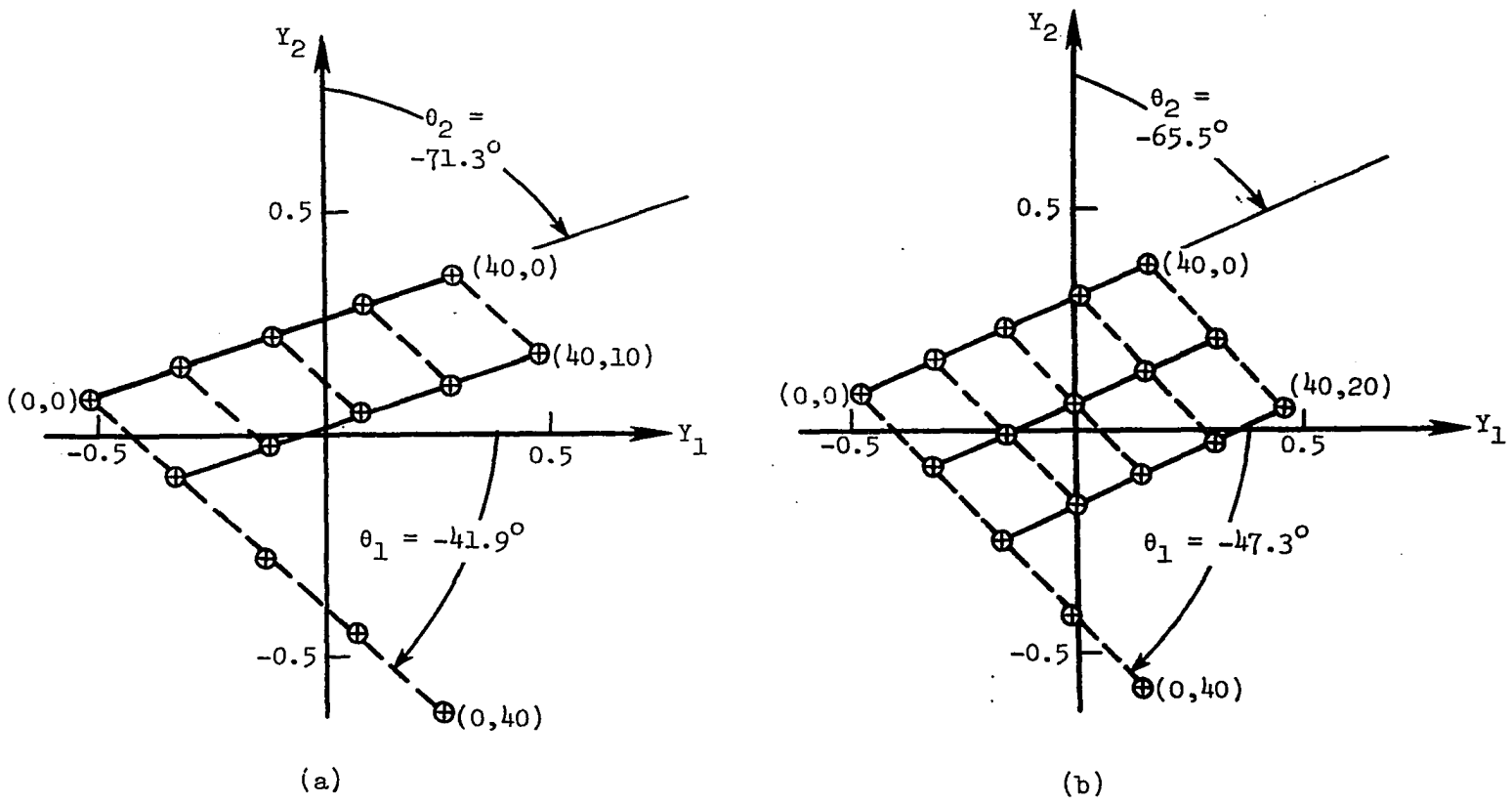

Figure 23.- Scalar multiples for mixtures of constituents A + C for (a) 13, (b) 17, (c) 21, and (d) 25-spectra cases. Representative concentration pairs (C_A, C_C) are labeled. Transformation into oblique axes system uses θ_1, θ_2.

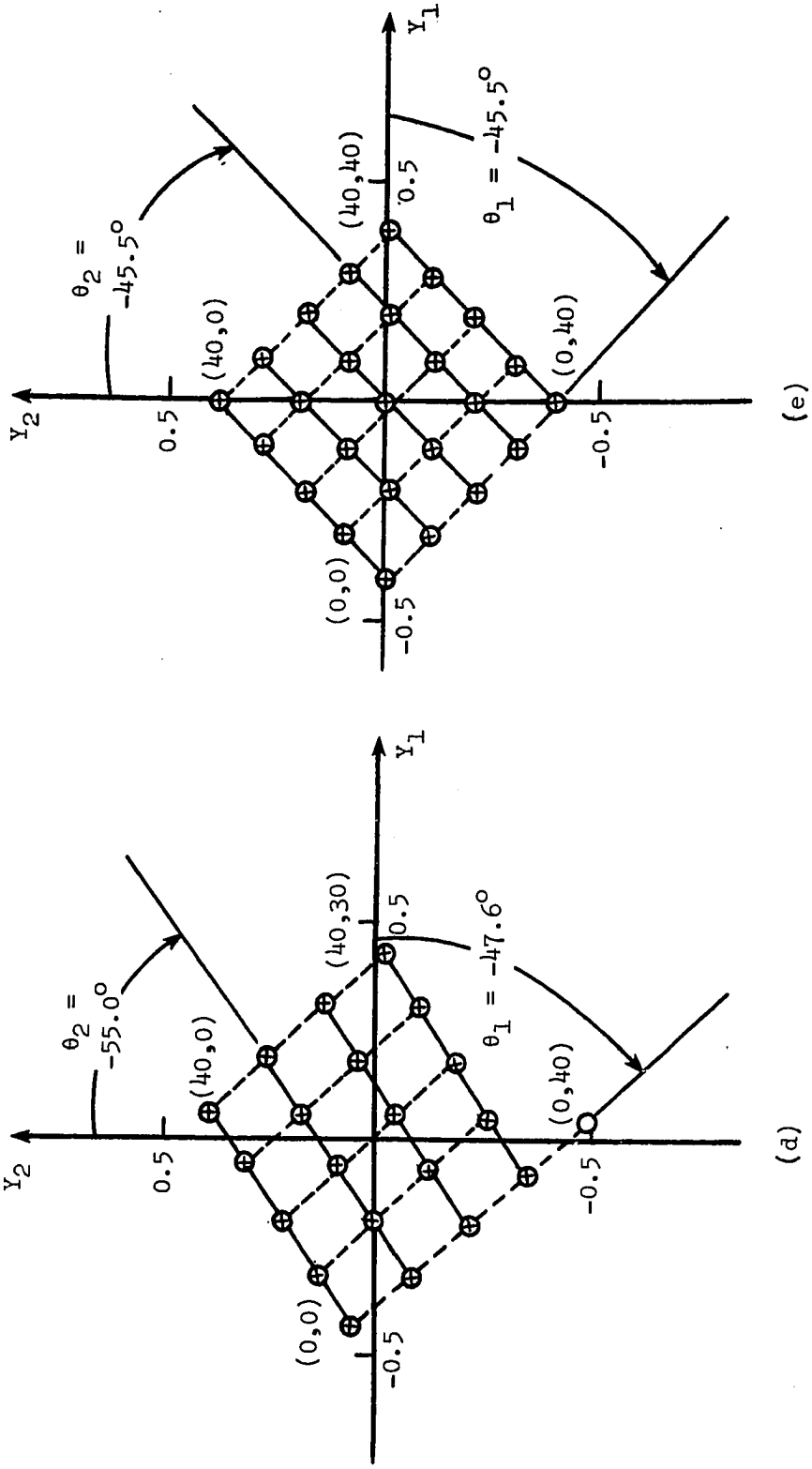

Figure 23.- Concluded.

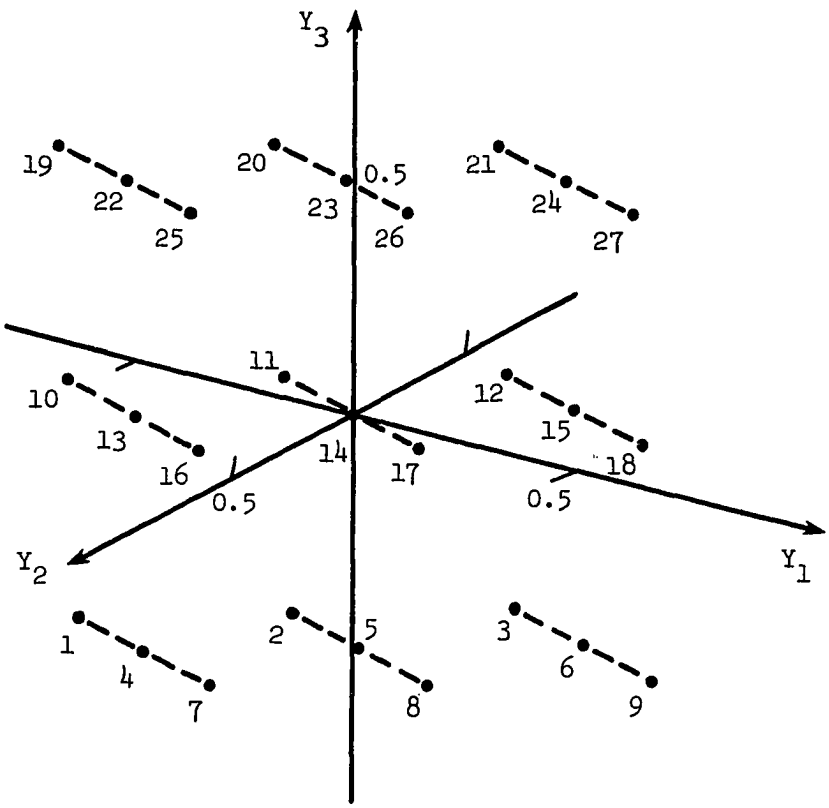

Figure 24.- Scalar multiples for three constituent mixtures of A + B + C. Spectra numbers refer to Table 8.

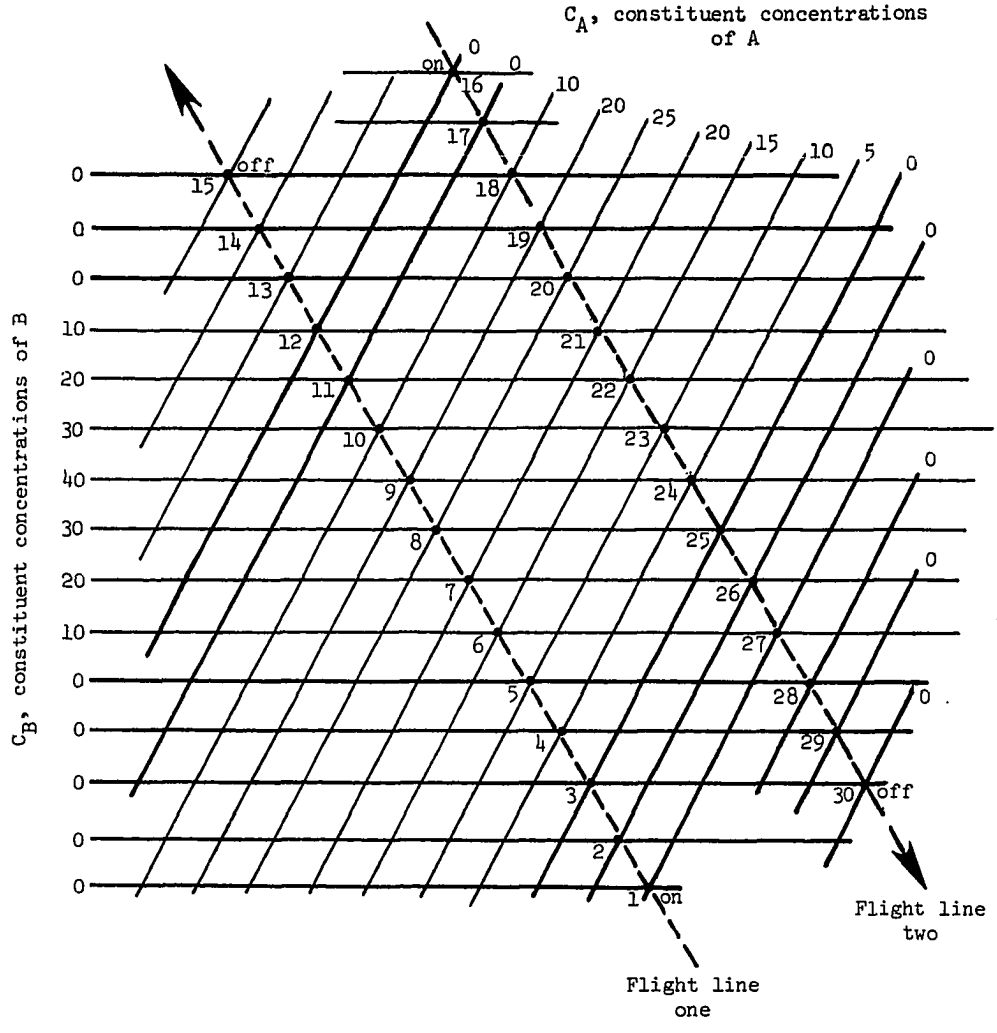

Figure 25.- Flight lines over mixtures of hypothetical constituents A + B at crossing of two line dumps. Spectra numbers in order of collection with concentrations (C_A, C_B) at intersections. On-off points for spectrometer noted.

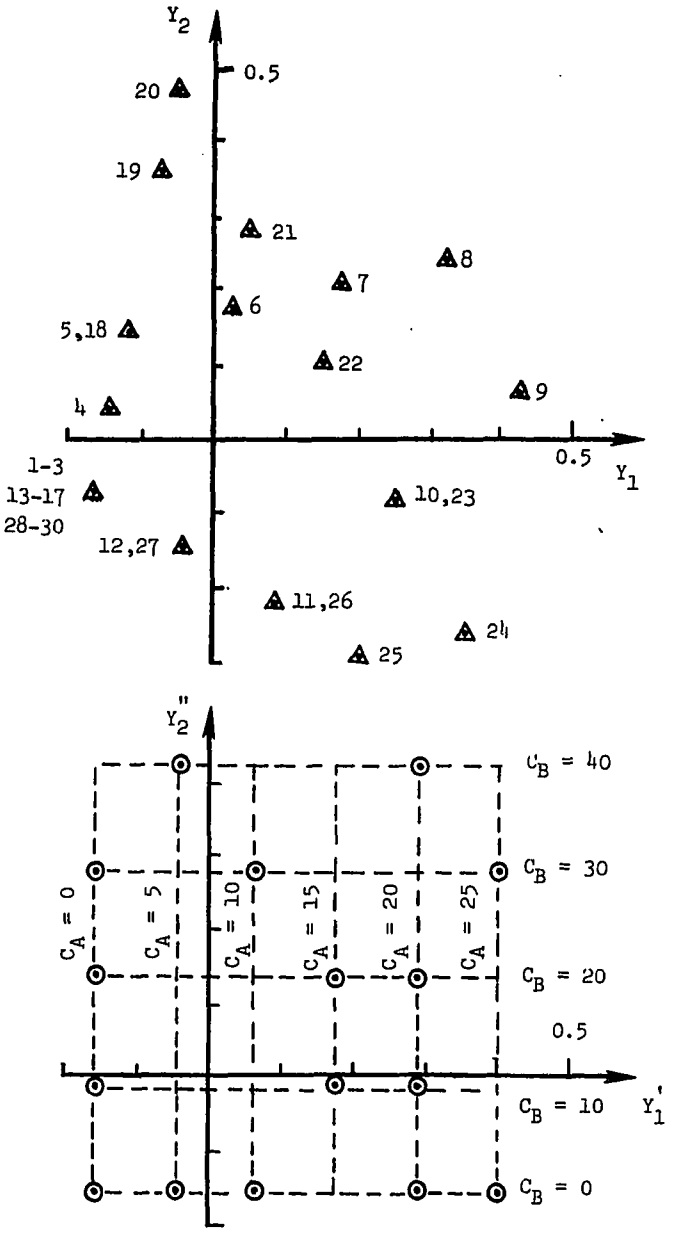

Figure 26.- Scalar multiples for flight lines over mixtures of line dumps A + B. (a) Original principal axes system - spectra numbers labeled. (b) Transformed oblique axes system - lines of constant concentrations labeled.

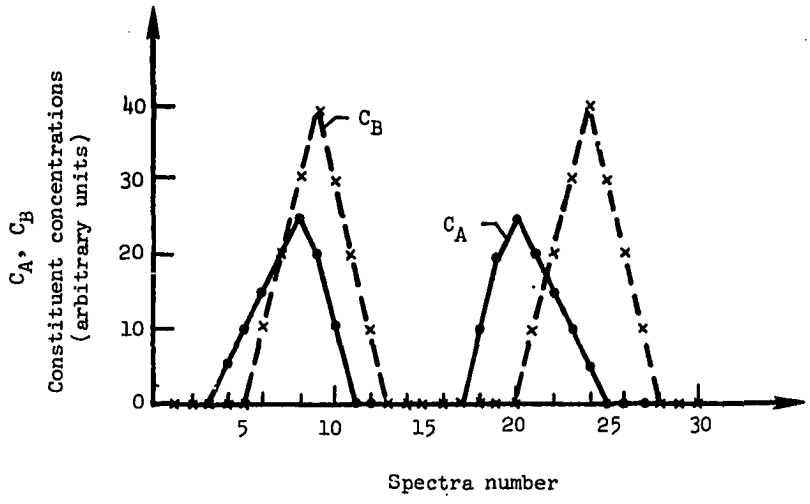

(a)

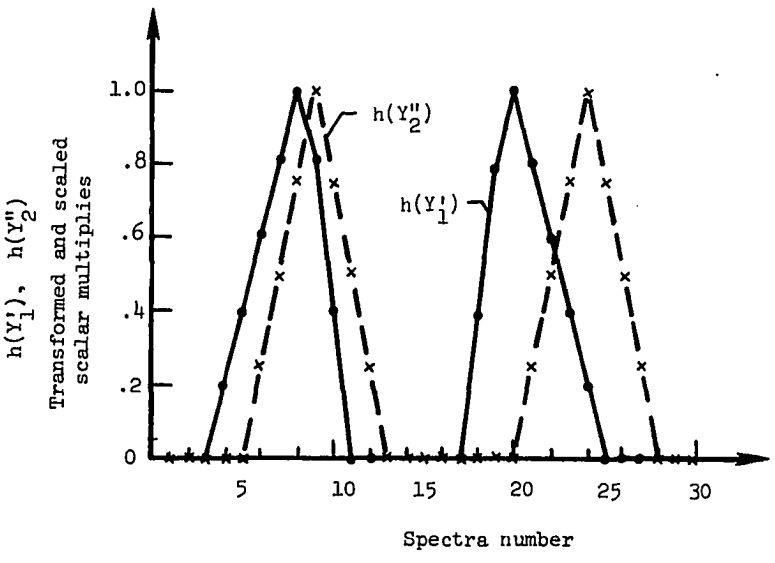

(b)

Figure 27.- (a) Constituent concentrations C_A, C_B in mixtures along hypothetical flight lines. (b) Transformed and scaled, scalar multiples along same flight lines.

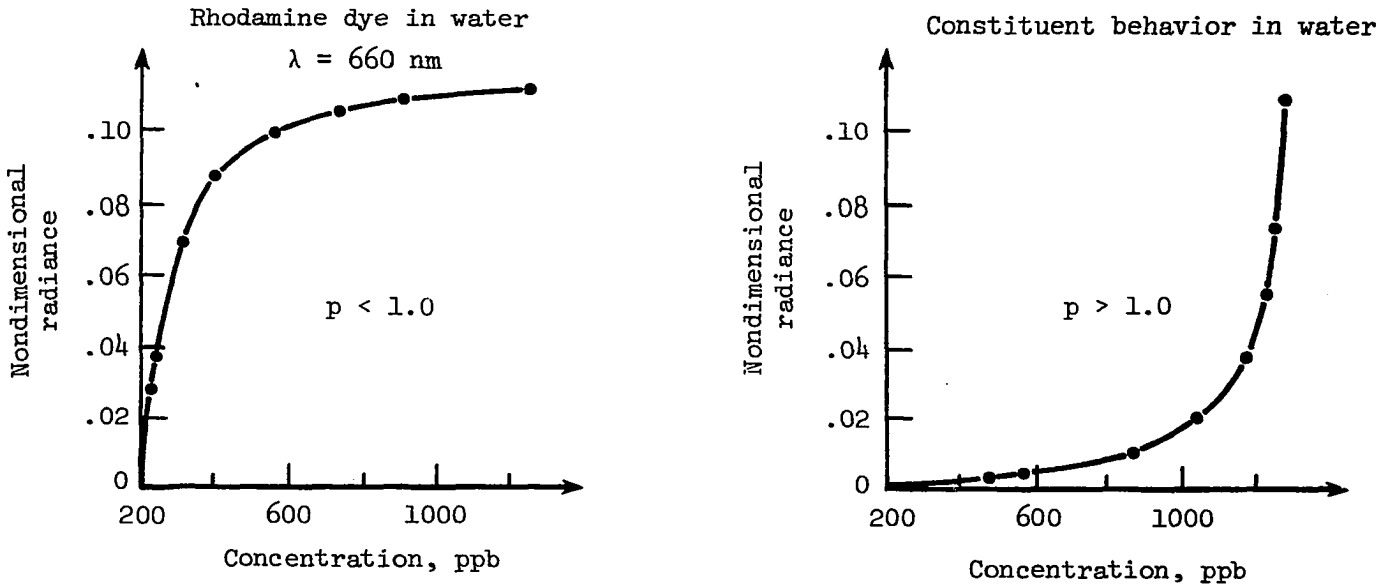

Figure 28.- Nonlinear radiance-concentration functions.

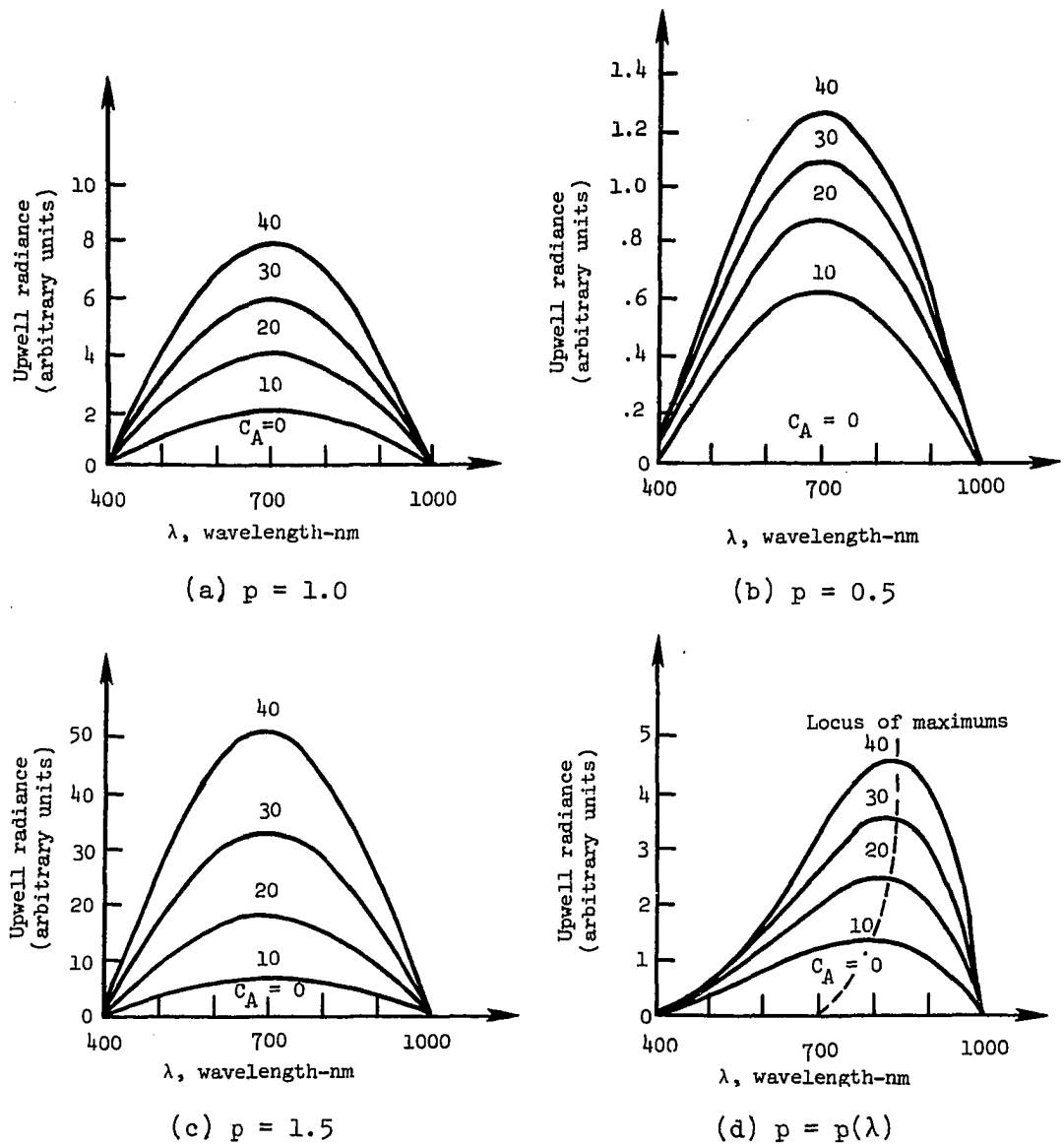

Figure 29.- Hypothetical constituent A with a (a) linear, (b), (c) simple nonlinear and (d) wavelength-dependent nonlinear radiance-concentration relationship.

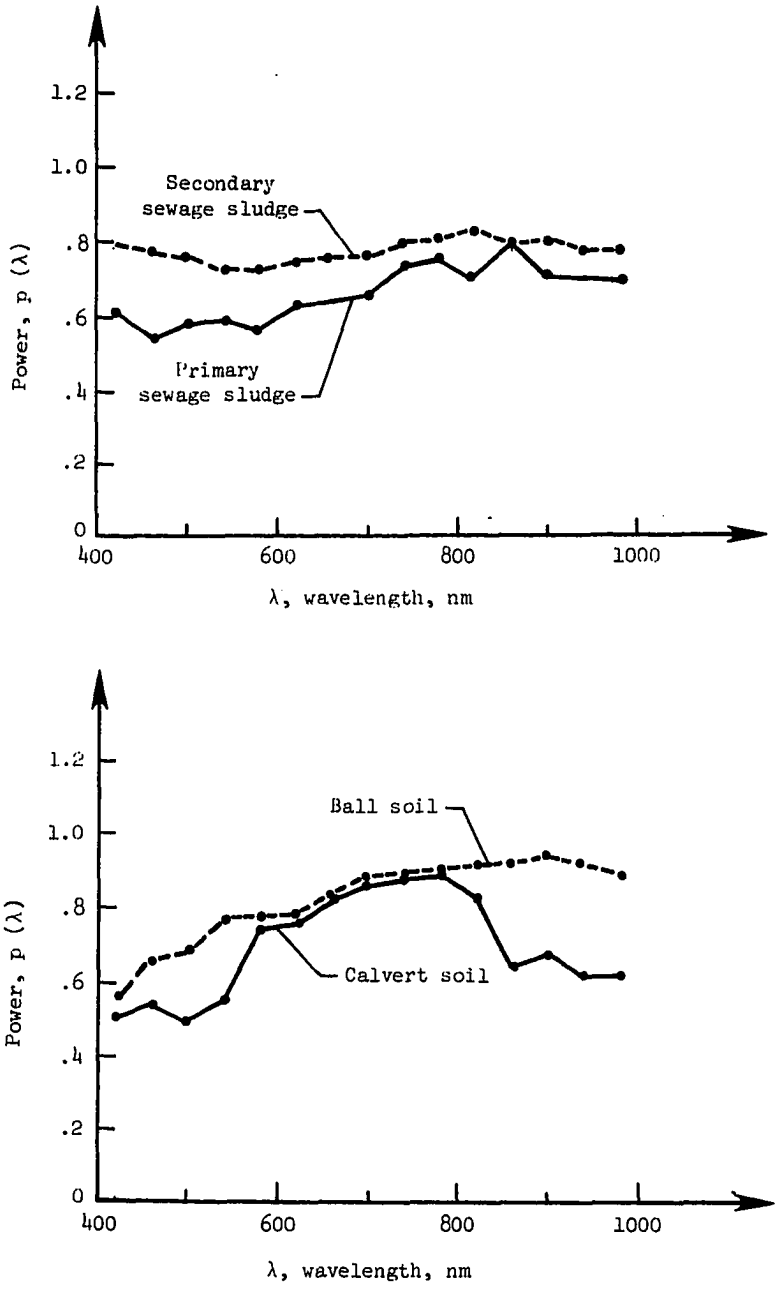

Figure 30.- Power functions for power-law regression fit to constituents tested in Marine Upwelled Spectral Signatures Laboratory.

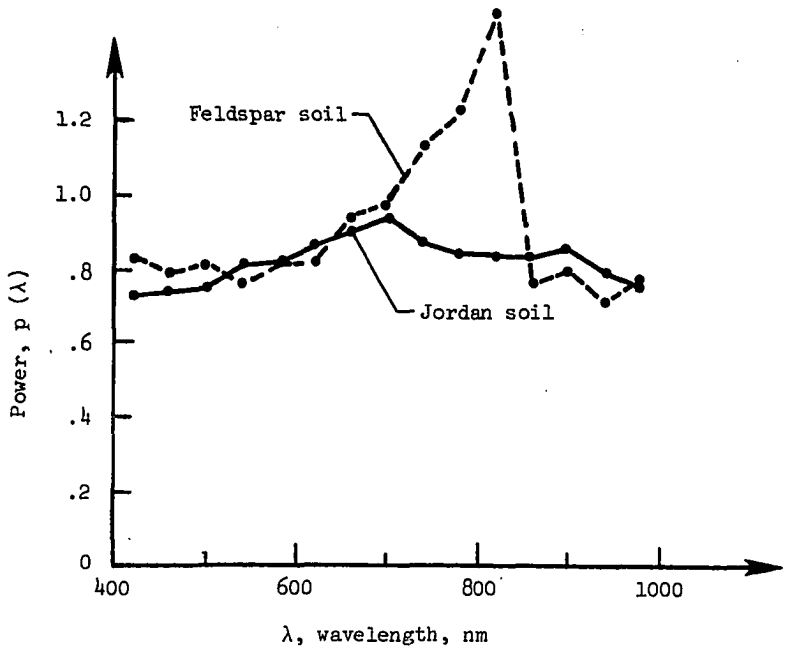

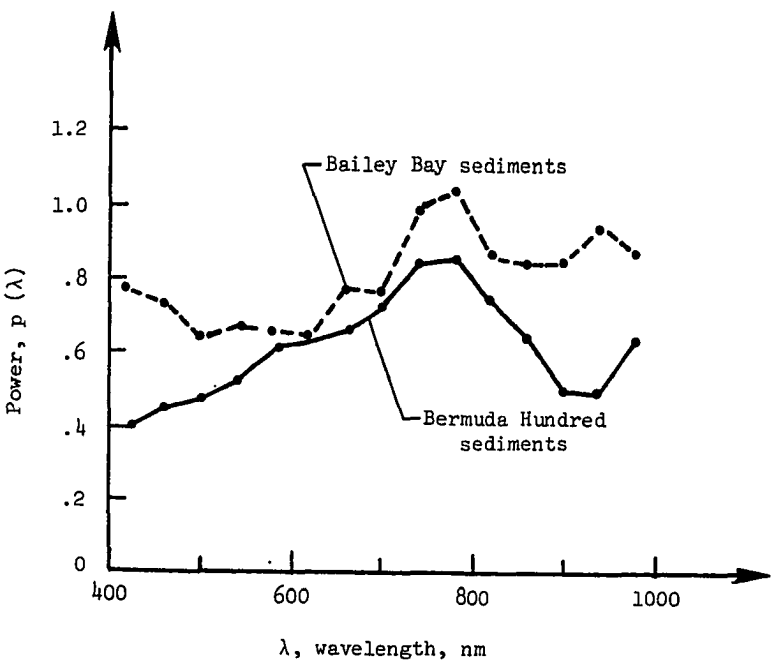

Figure 30.- Continued.

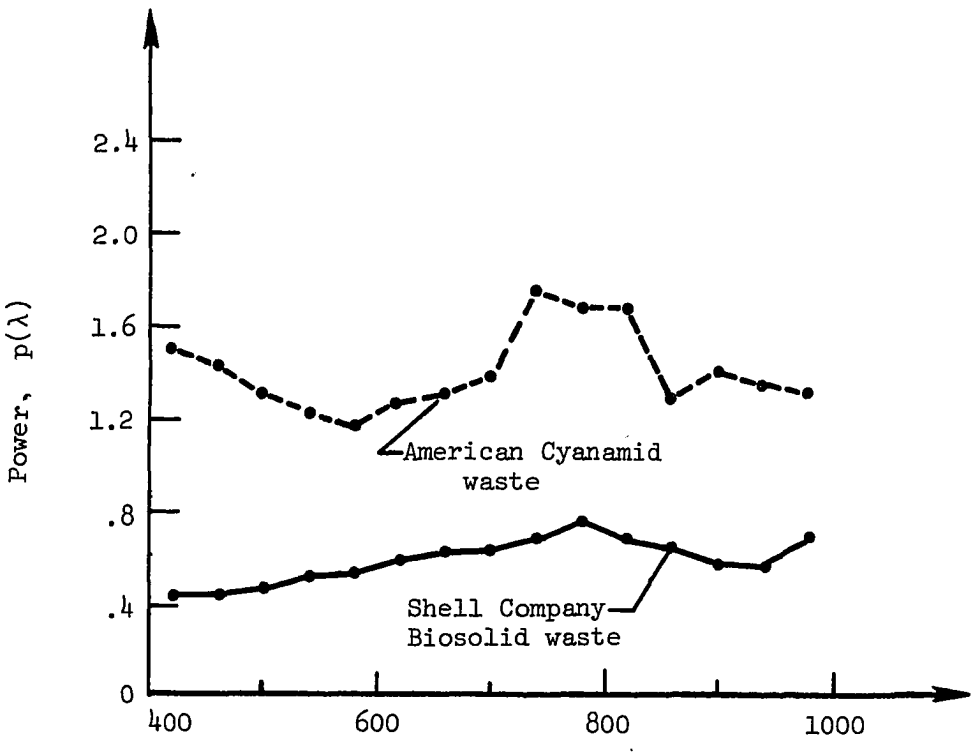

λ, wavelength - nm

Figure 30.- Concluded.

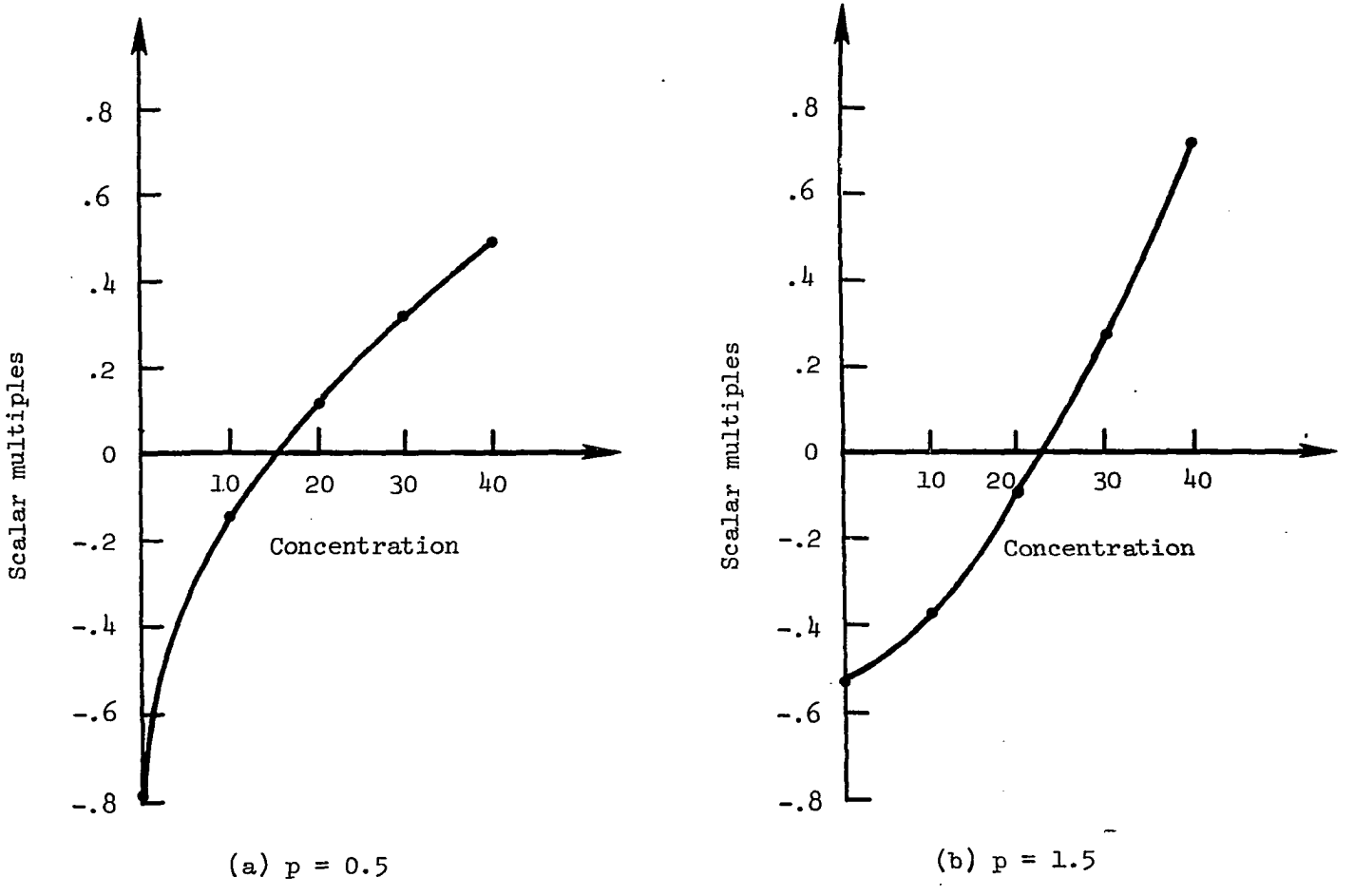

Figure 31.- Nonlinearity between scalar multiples and concentrations for simple nonlinear constituents A, B, C.

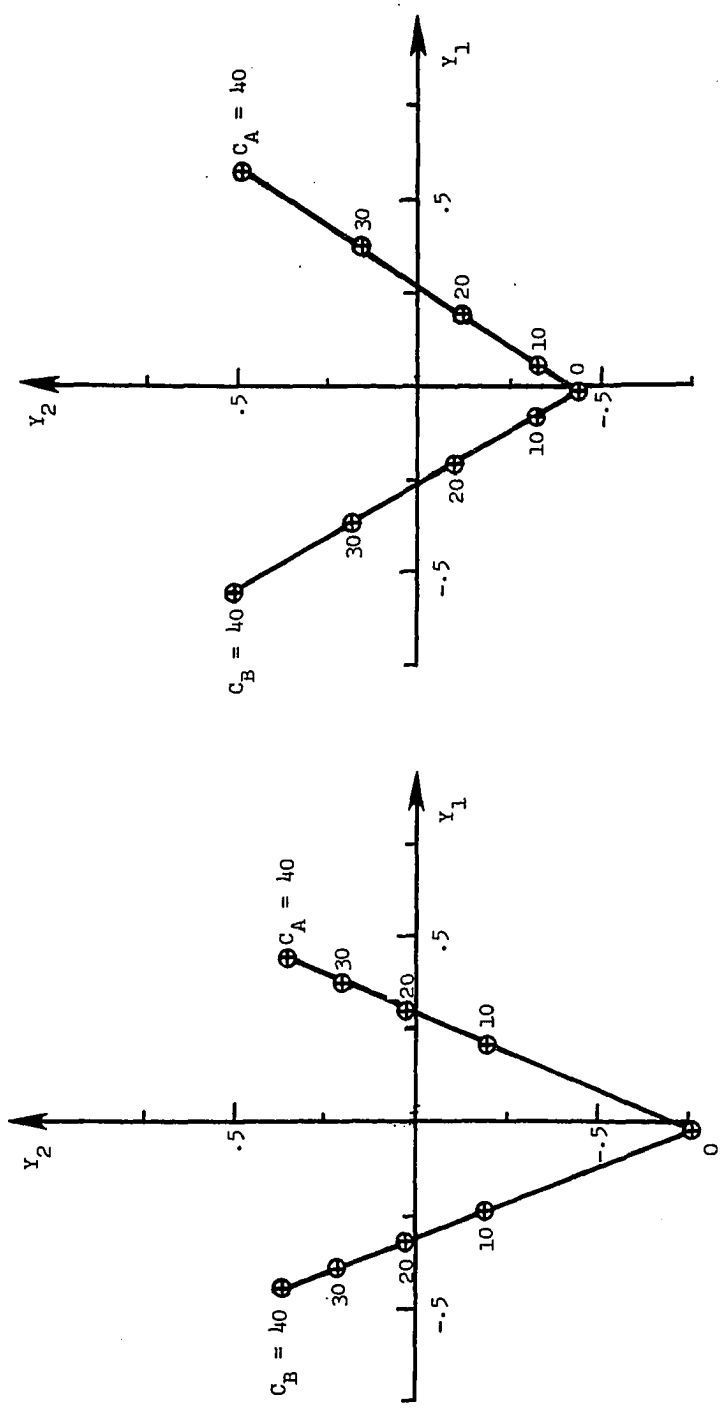

Figure 32.- Scalar multiples in principal axes system for spatially-independent simple nonlinear constituents A and B. (a) p = 0.5, (b) p = 1.5.

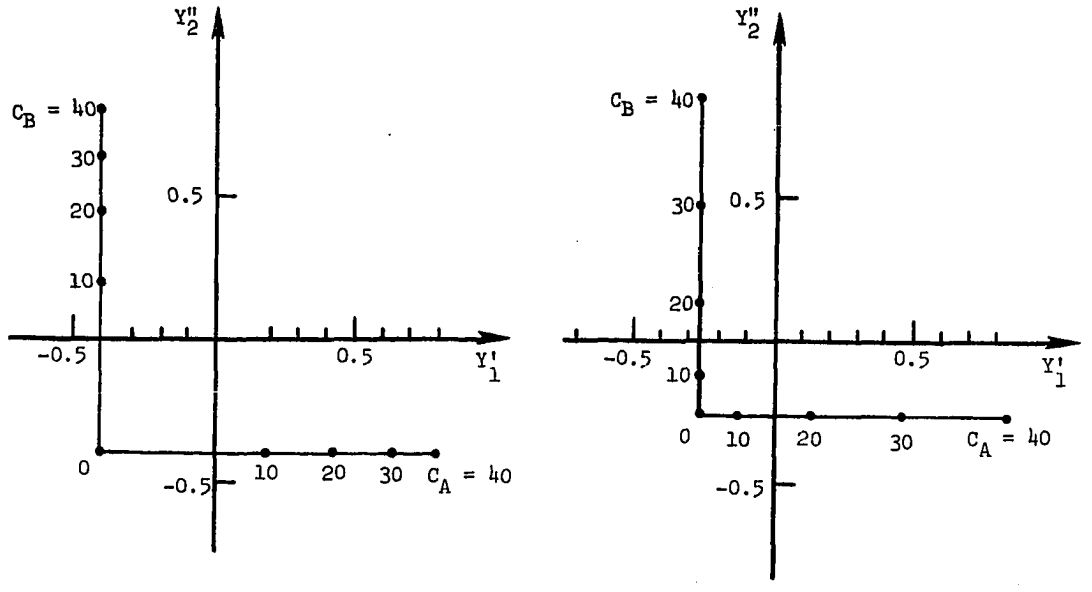

(c) p = 0.5

(d) p = 1.5

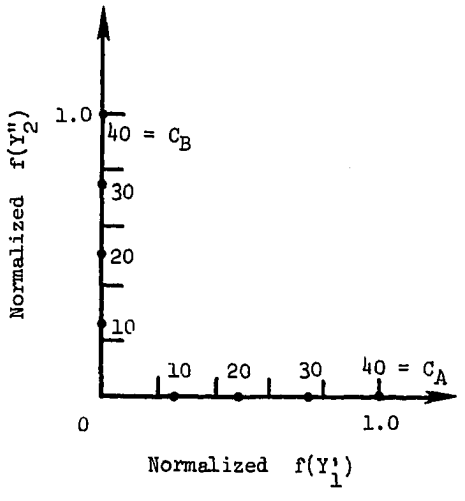

(e) p = 0.5

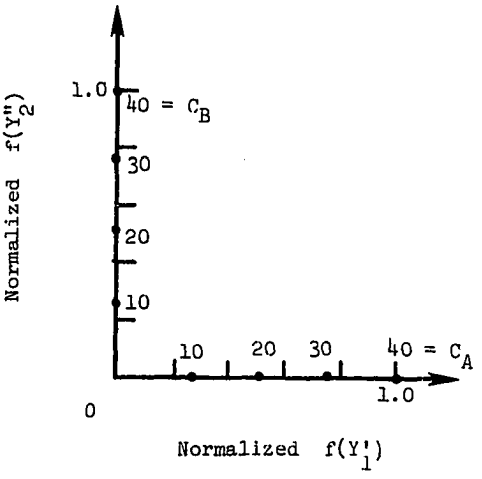

(f) p = 1.5

Figure 32.- (c), (d) Scalar multiples in transformed oblique axes system. (e), (f) Normalized functions of transformed scalar multiples.

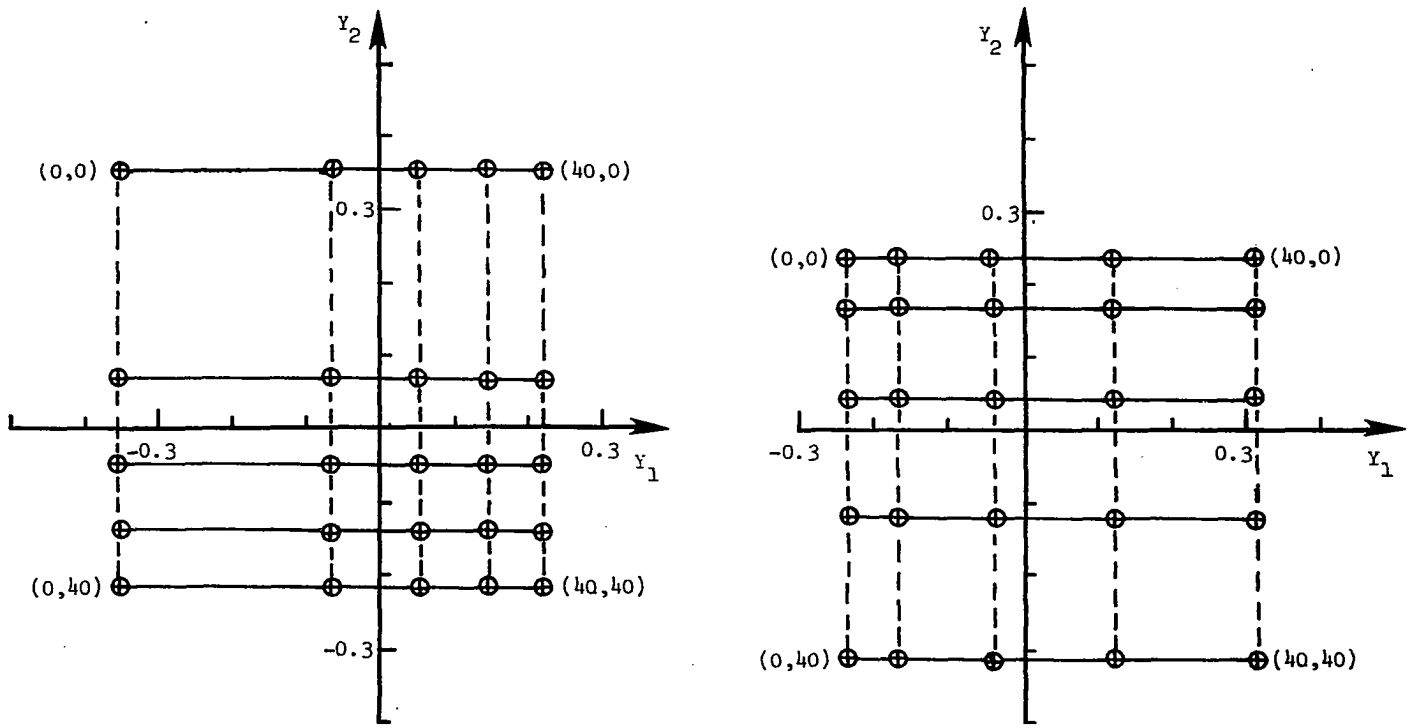

(a) p = 0.5 (b) p = 1.5

Figure 33.- Scalar multiples for mixtures of simple nonlinear constituents A + B. Model powers (a) p = 0.5 and (b) p = 1.5. Representative concentration pairs (C_A, C_B) are labeled.

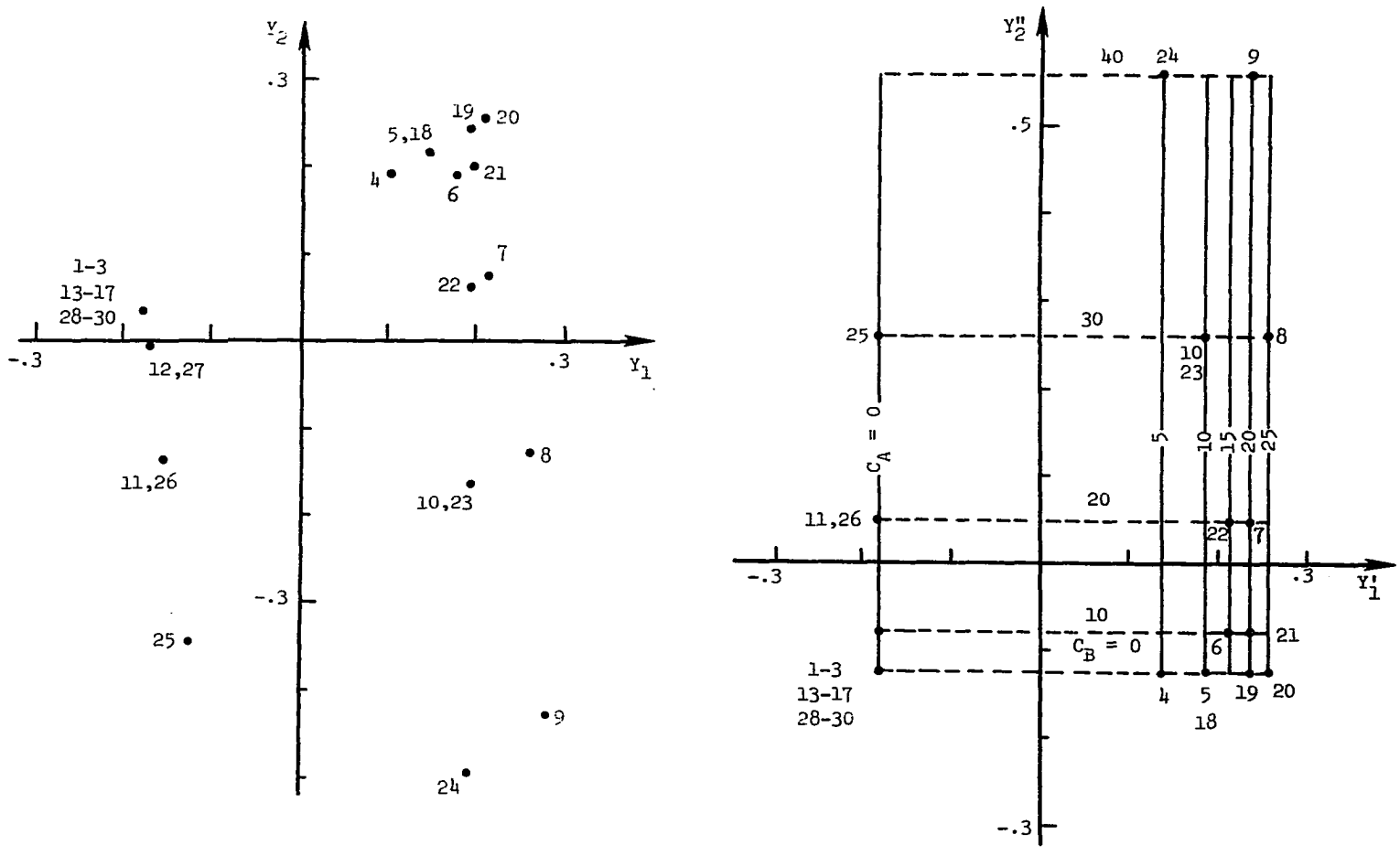

Figure 34.- (a) Scalar multiples in principal axes system and (b) transformed into oblique axes system for flight experiment involving hypothetical simple nonlinear constituents in mixtures.

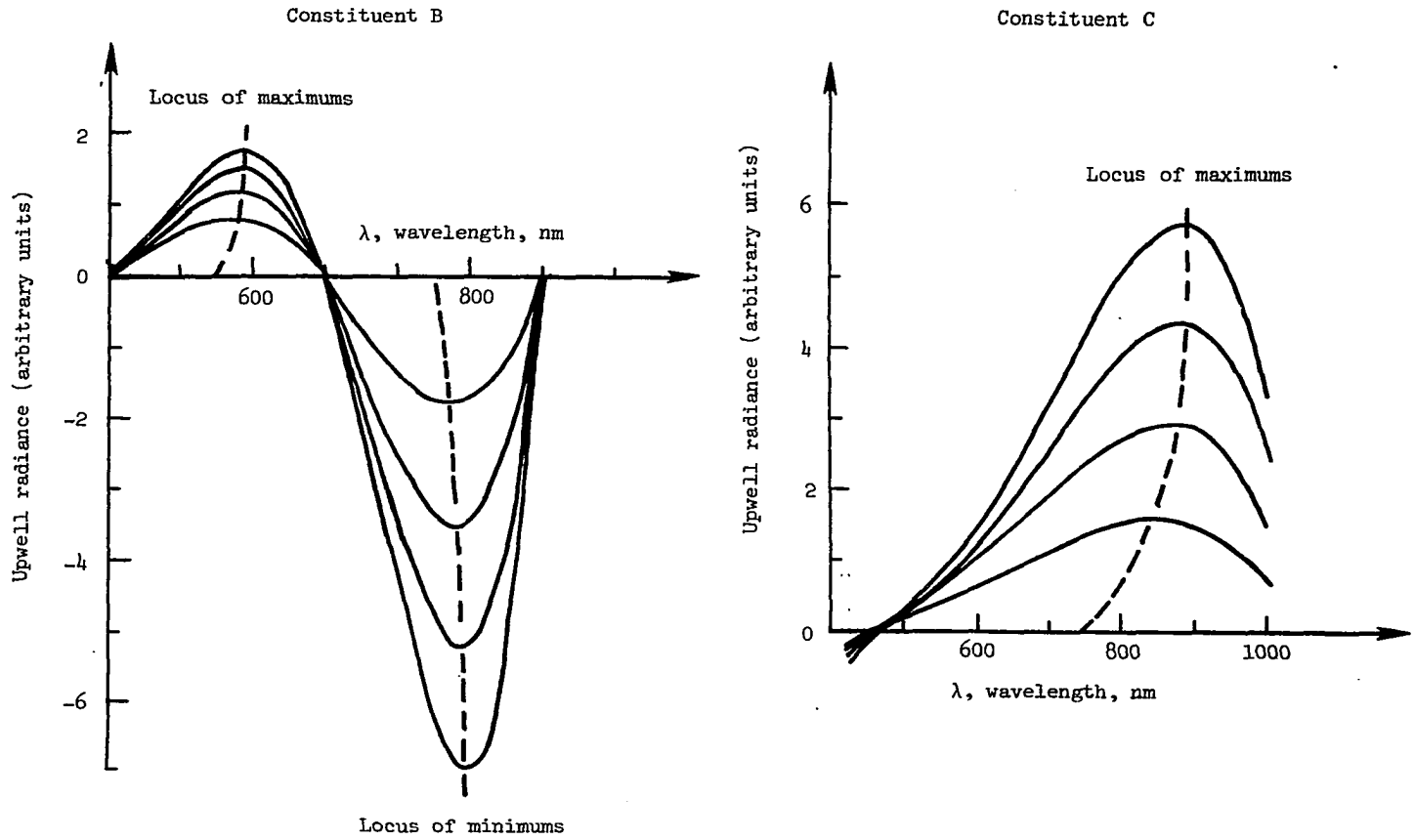

Figure 35.- Wavelength-dependent nonlinear constituents B and C.
Power range: $0.5 \leq p(\lambda) \leq 1.0$.

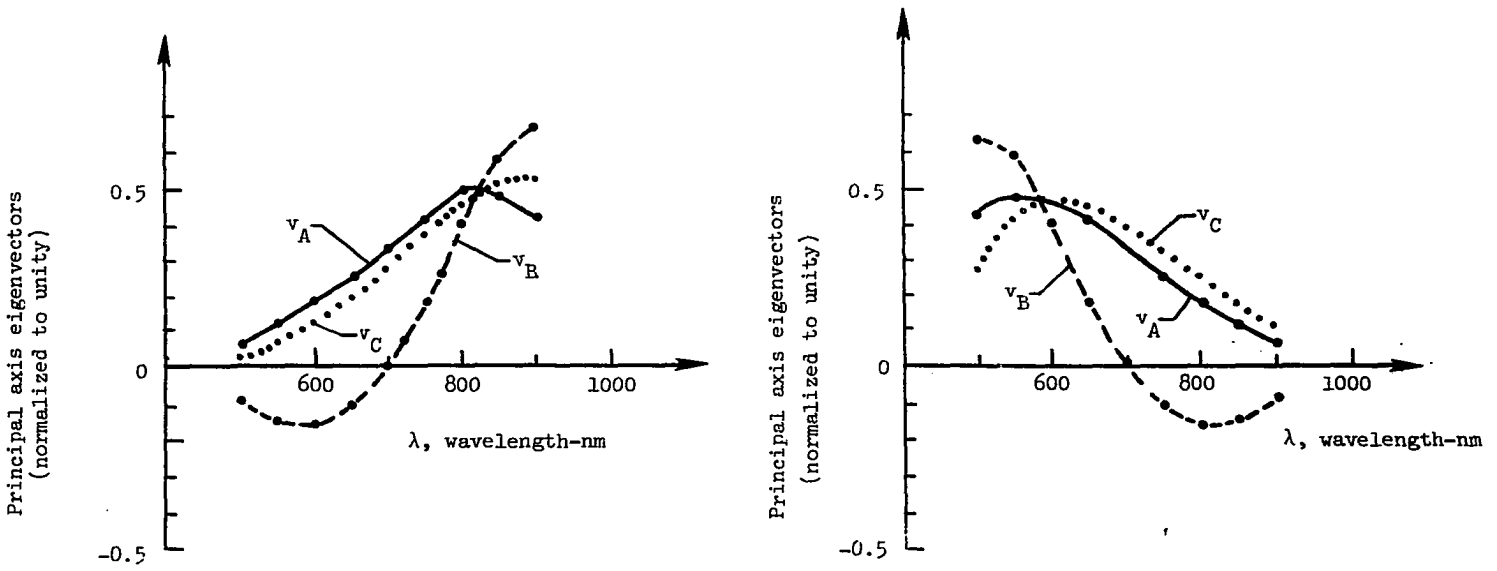

(a) $0.5 \leq p(\lambda) \leq 1.0$ (b) $1.0 \leq p(\lambda) \leq 1.5$

Figure 36.- First principal axis eigenvectors as characteristic vectors for wavelength-dependent nonlinear constituents.

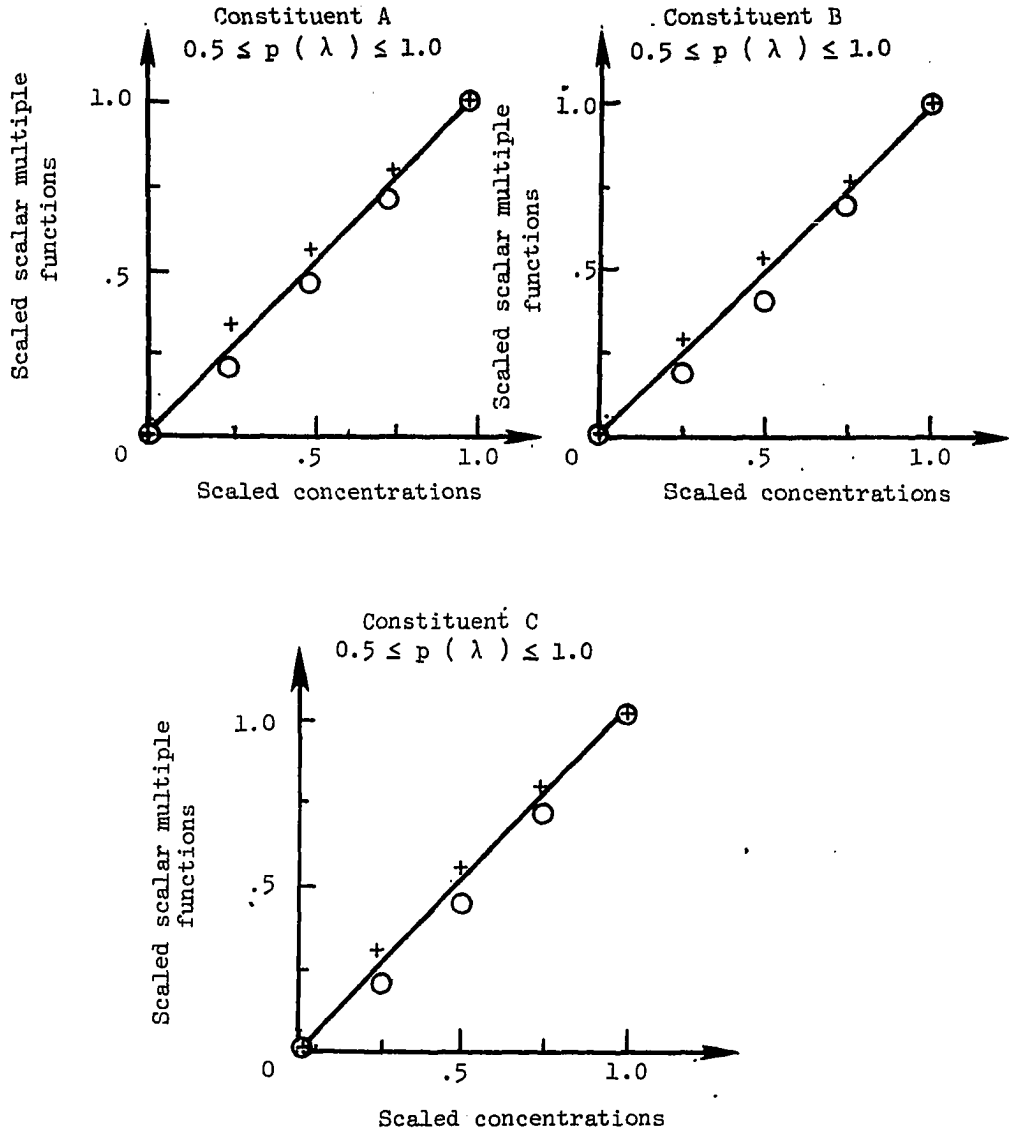

Figure 37.- Comparison between scaled scalar multiple functions and scaled concentrations for wavelength-dependent hypothetical constituents A, B and C. Crosses (+) are linear scaling approximations; circles (O) are simple nonlinear scaling approximations.

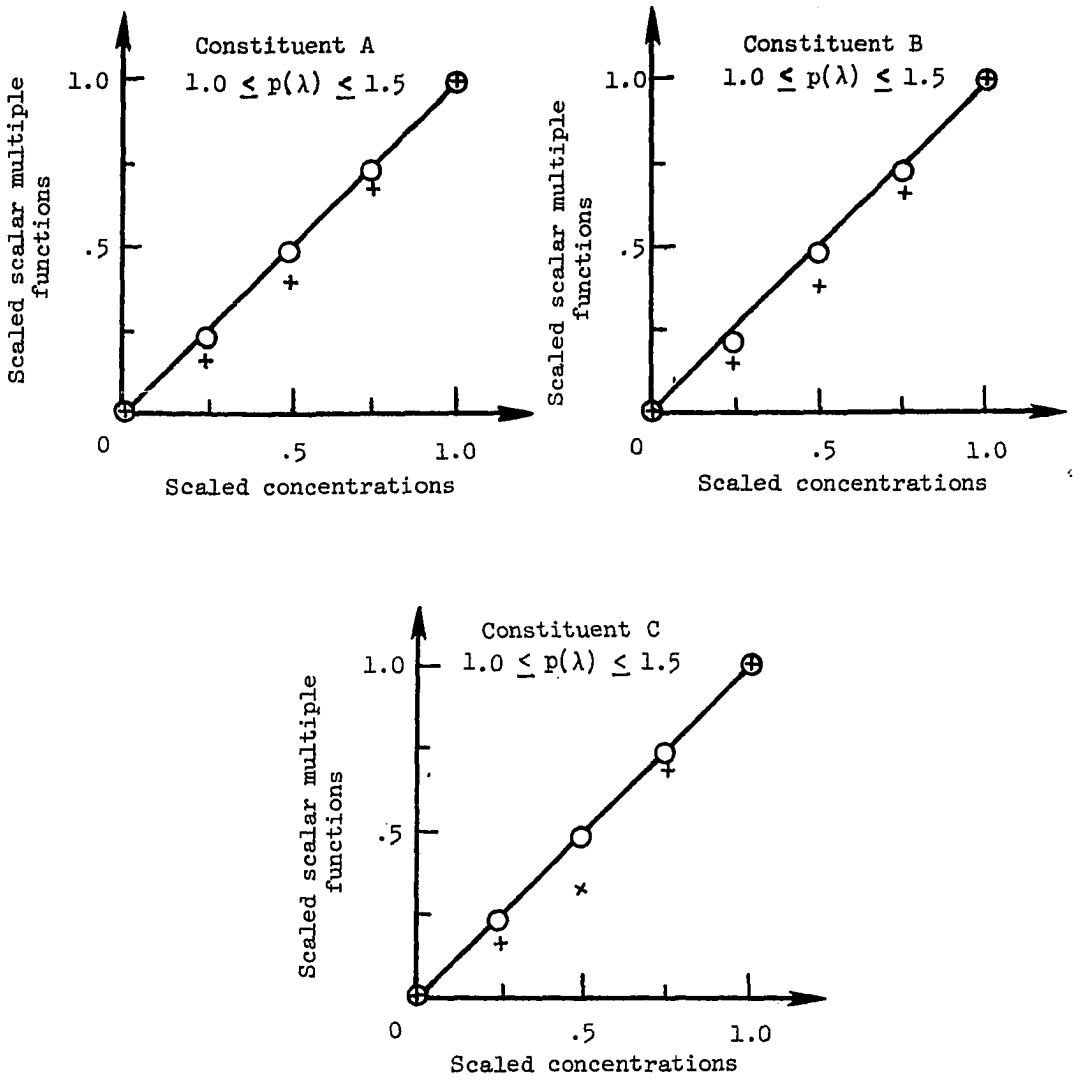

Figure 37.- Concluded.

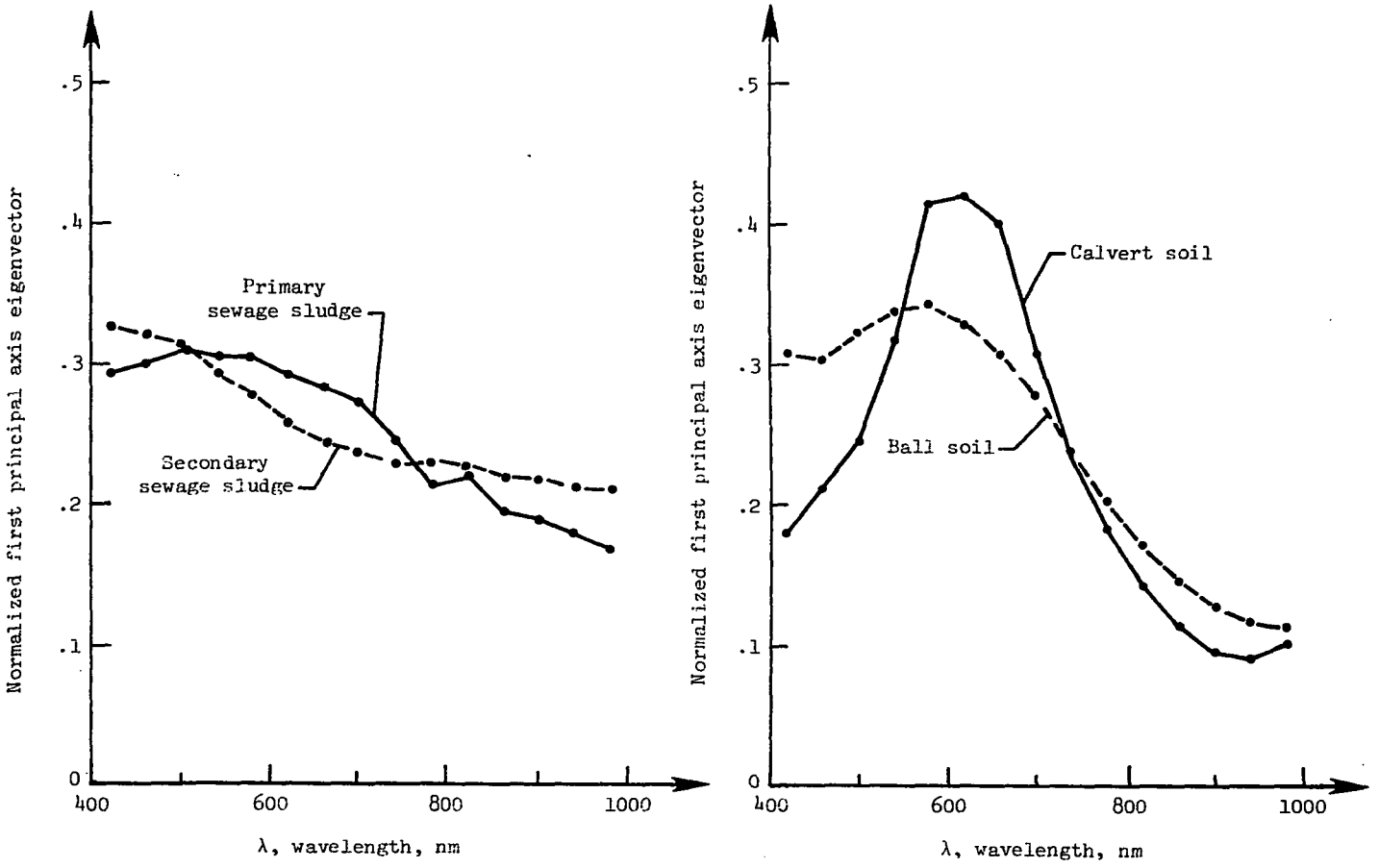

Figure 38.- First principal axis eigenvectors (normalized to unity) for constituents tested in the Marine Upwelled Spectral Signatures Laboratory.

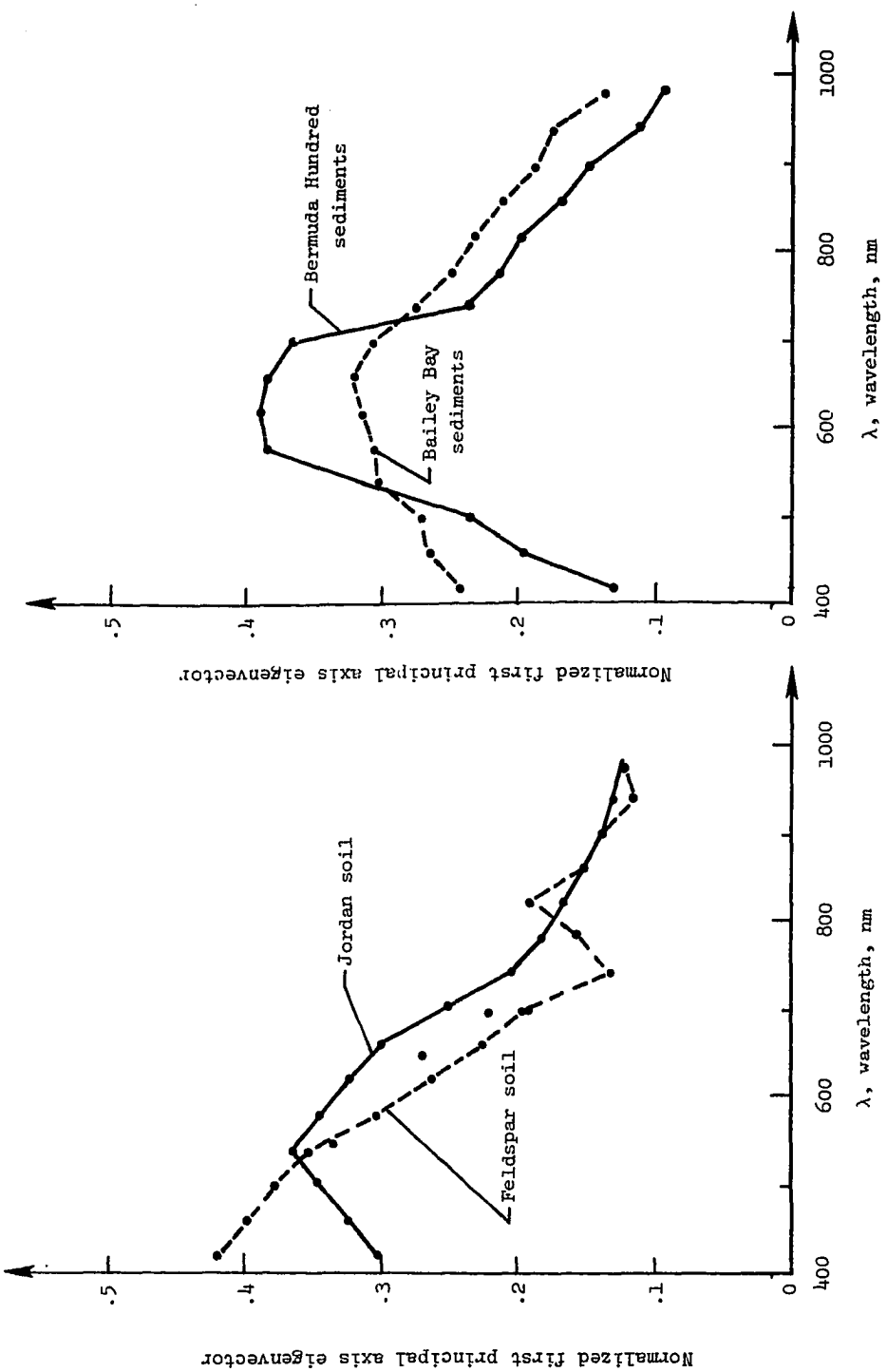

Figure 38.- Continued.

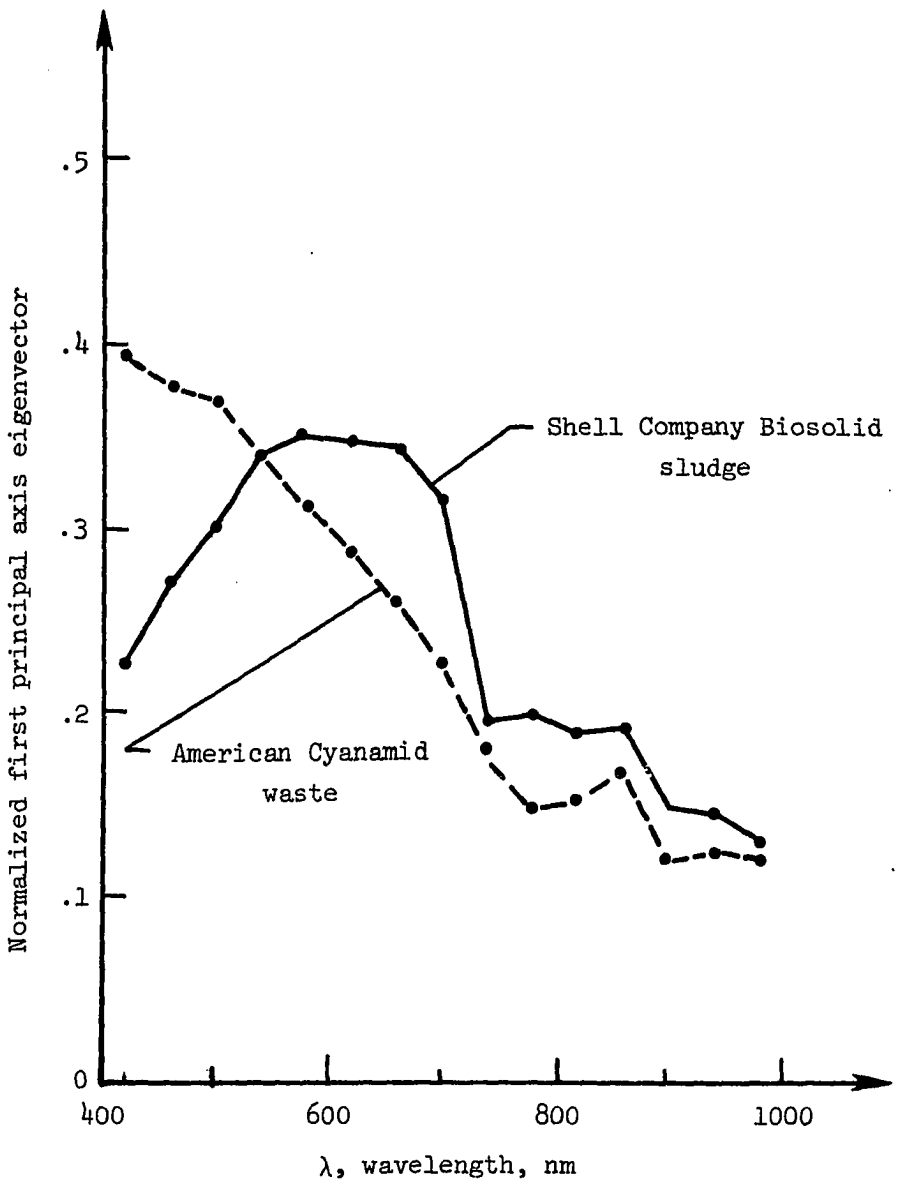

Figure 38.- Concluded.

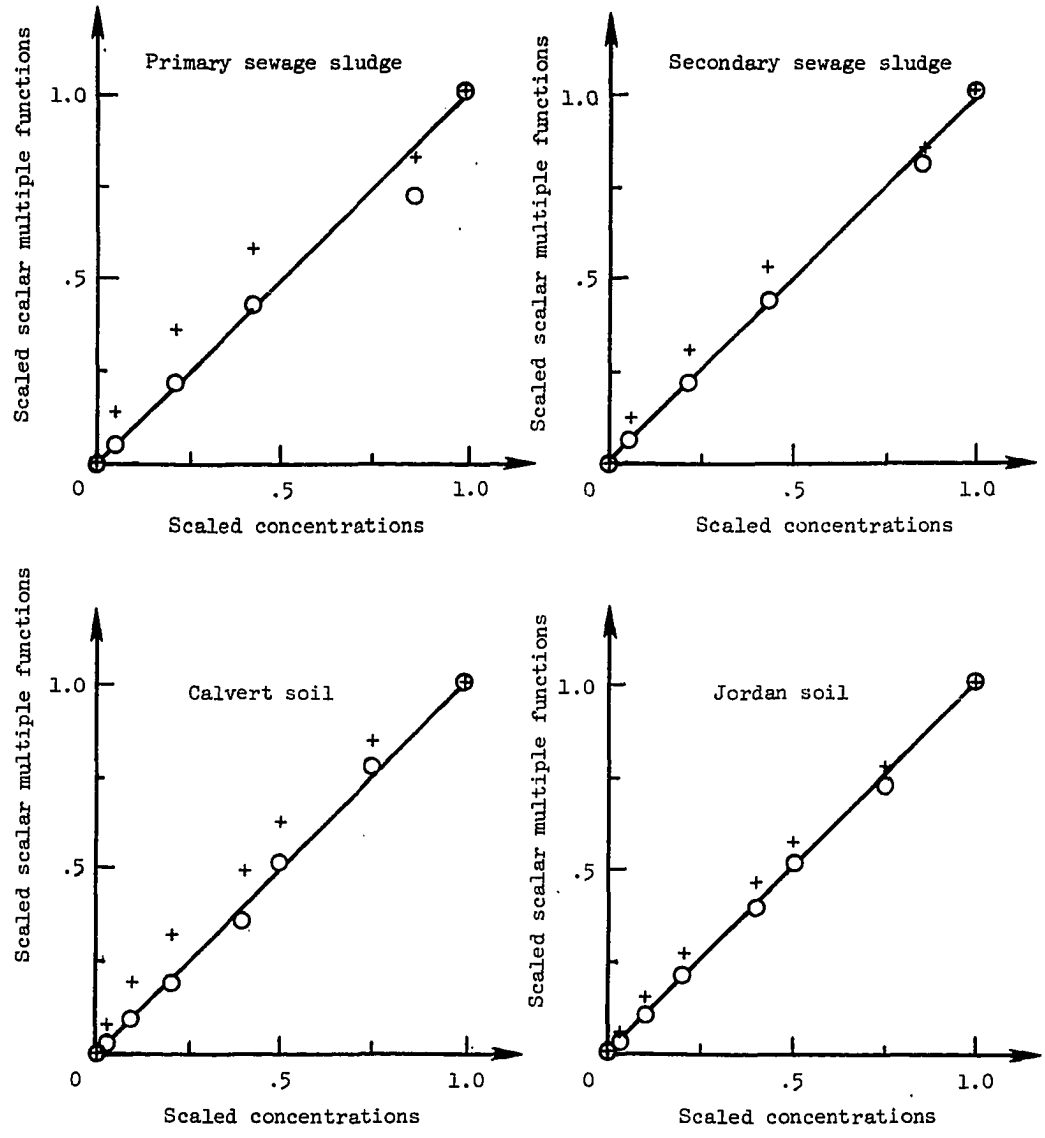

Figure 39.- Comparison between scaled scalar multiple functions and scaled concentrations for constituents tested in the Marine Upwelled Spectral Signatures Laboratory. Crosses (+) are linear scaling approximations; circles (O) are simple nonlinear scaling approximations.

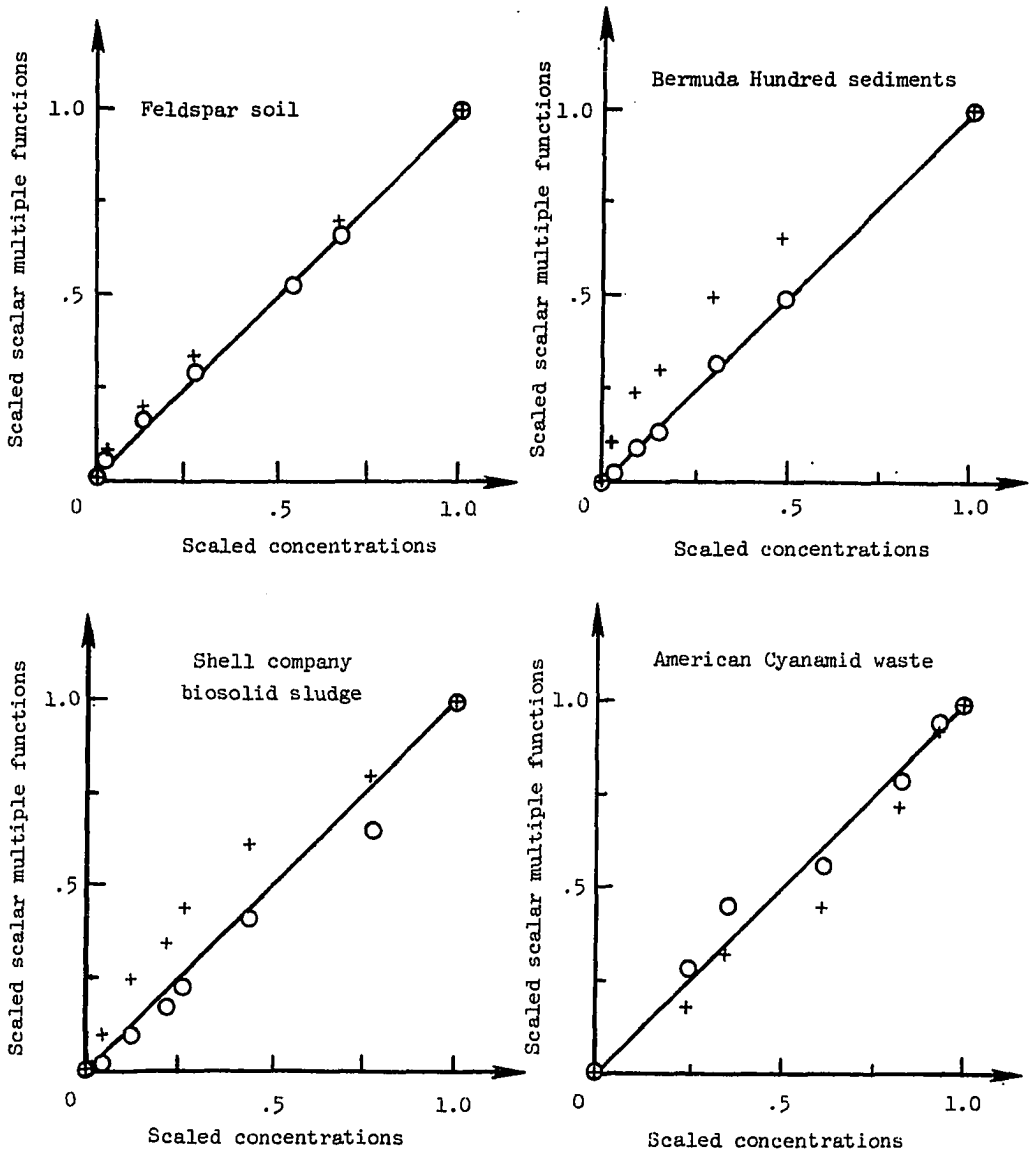

Figure 39.- Concluded.

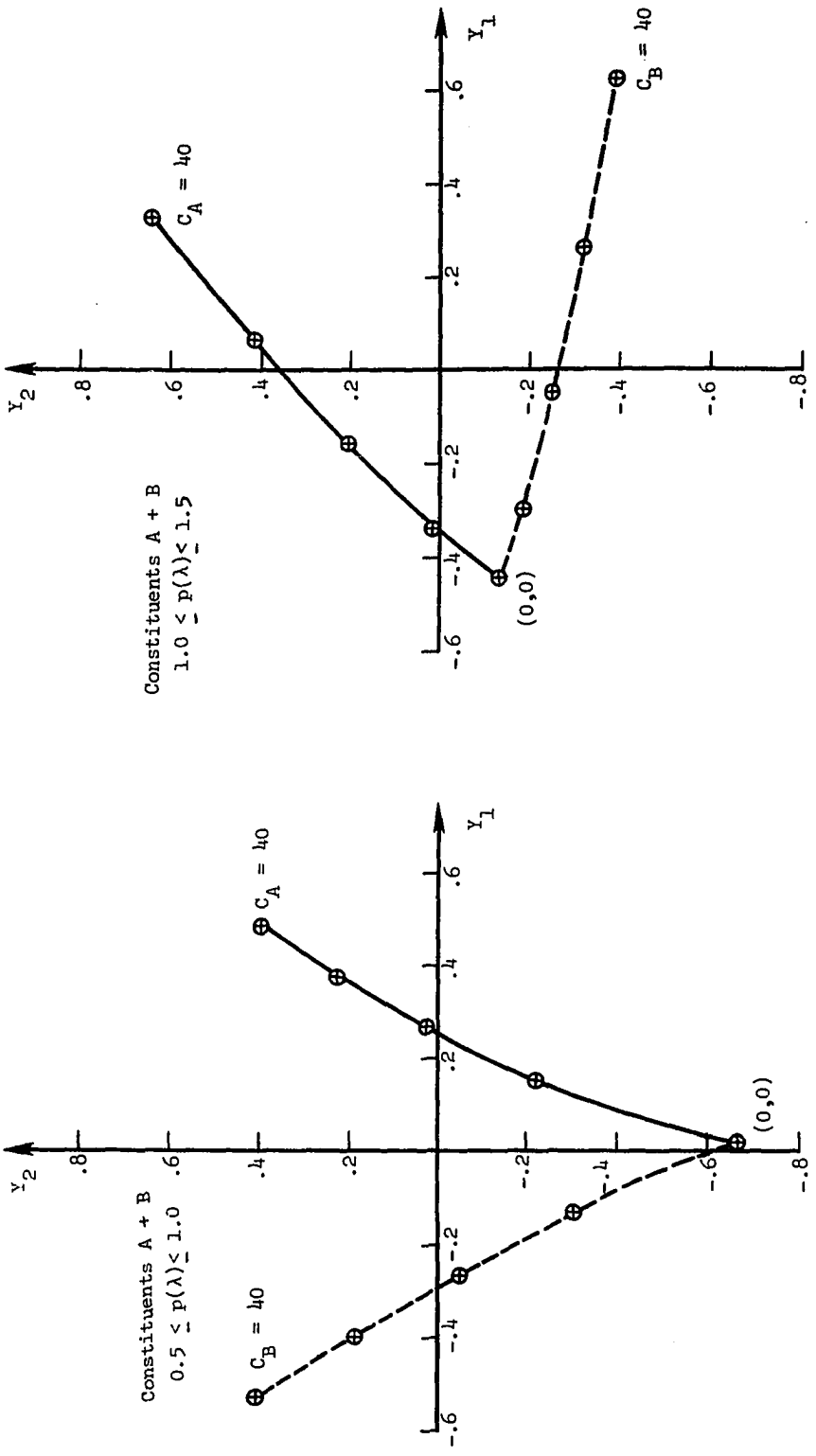

Figure 40.- Scalar multiples for spatially-independent wavelength-dependent nonlinear constituents A + B, A + C.

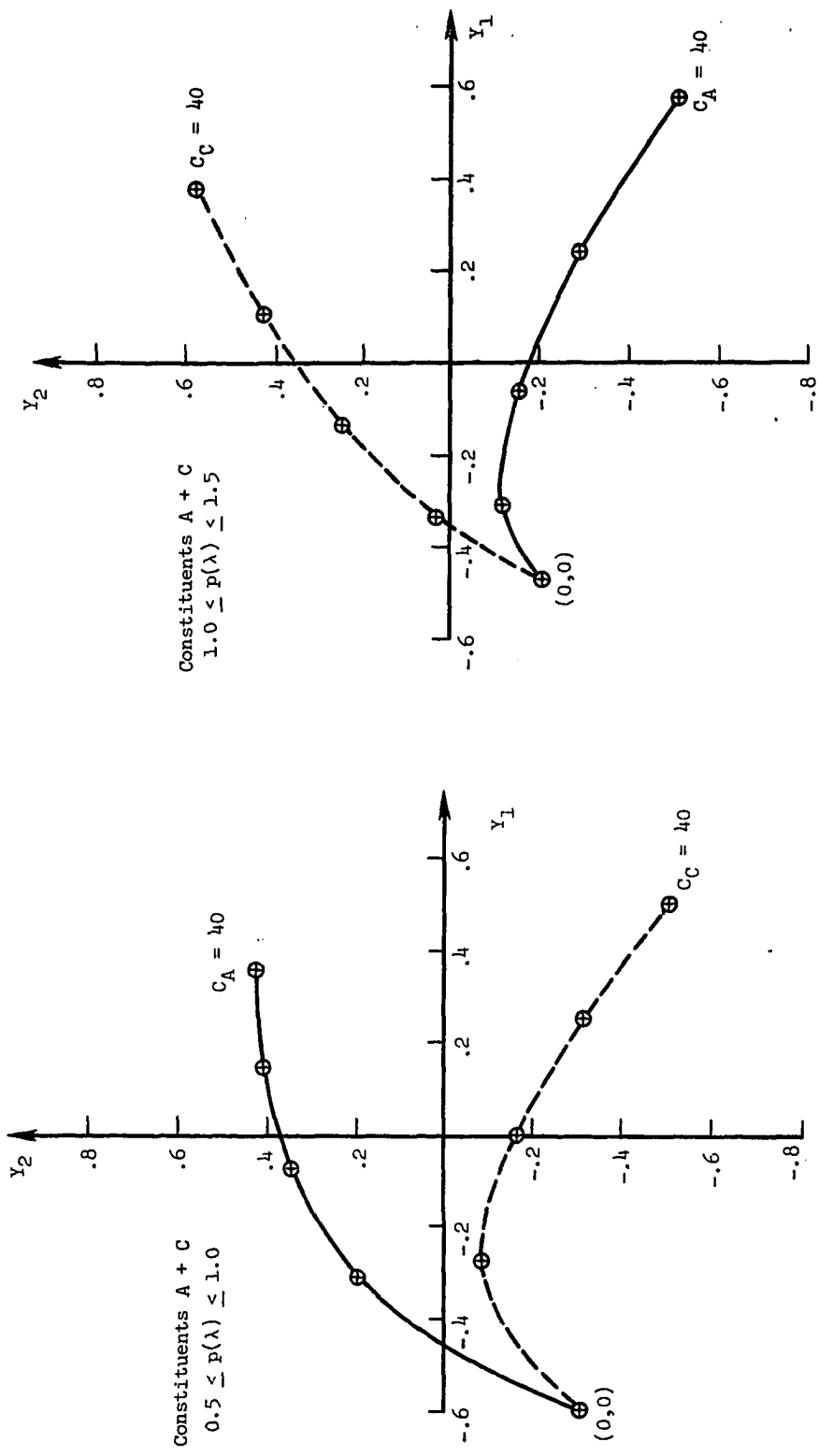

Figure 40.- Concluded.

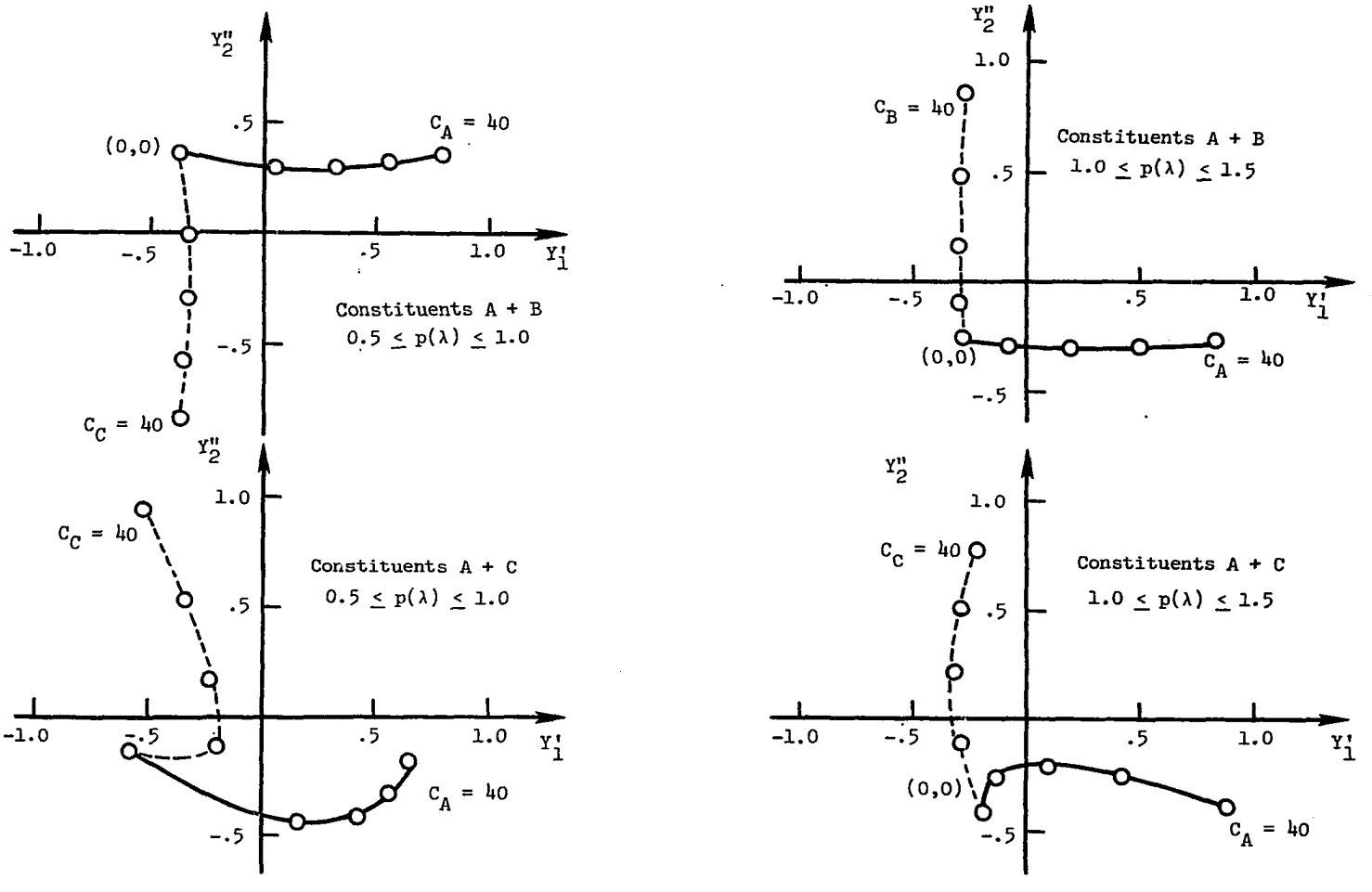

Figure 41.- Scalar multiples transformed into oblique axes system for spatially-independent, wavelength-dependent nonlinear constituents A + B, A + C.

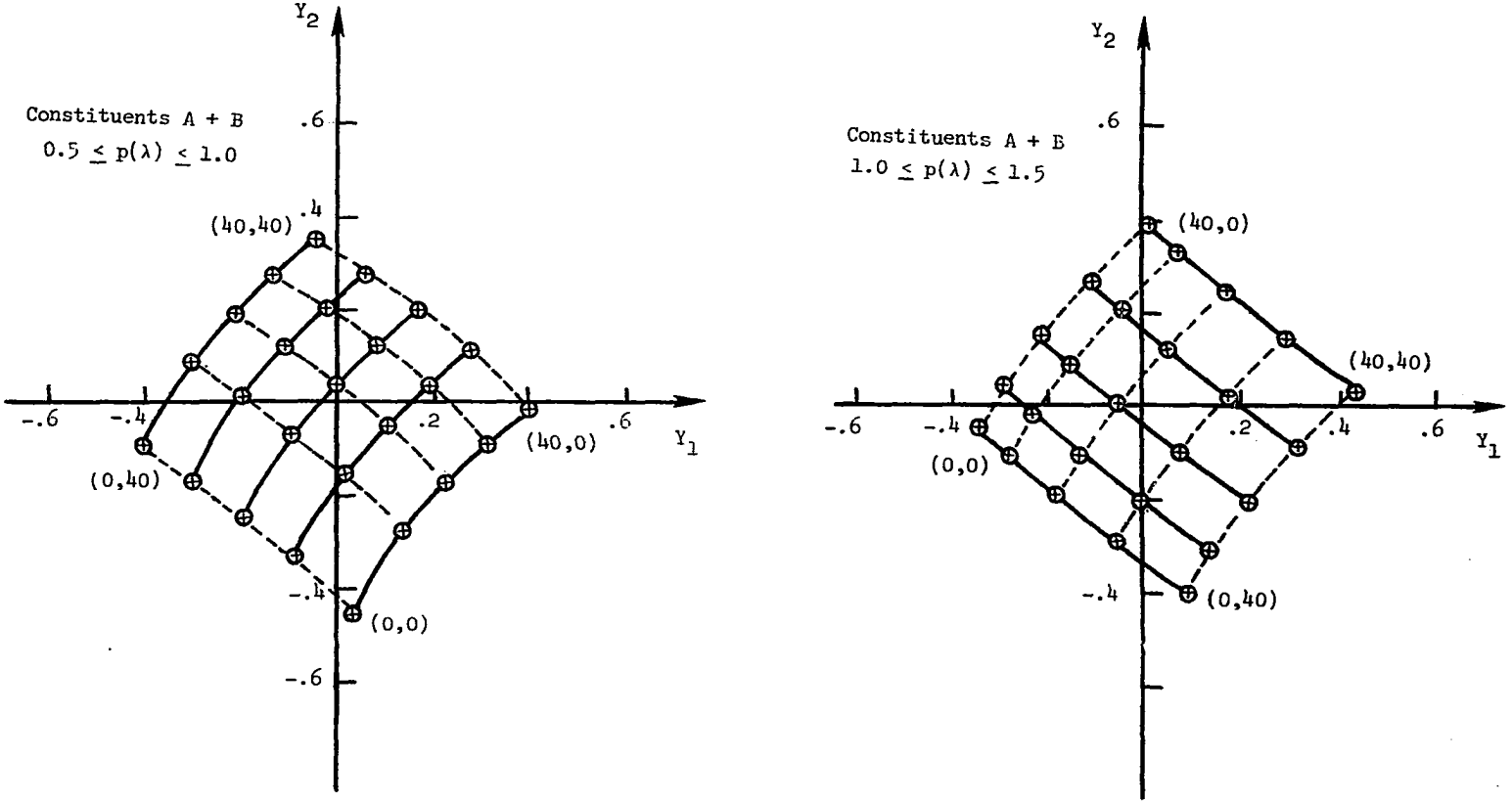

Figure 42.- Scalar multiples for mixtures (25 spectra) of wavelength-dependent nonlinear constituents A + B, A + C. Representative concentration pairs (C_A, C_B) or (C_A, C_C) are labeled.

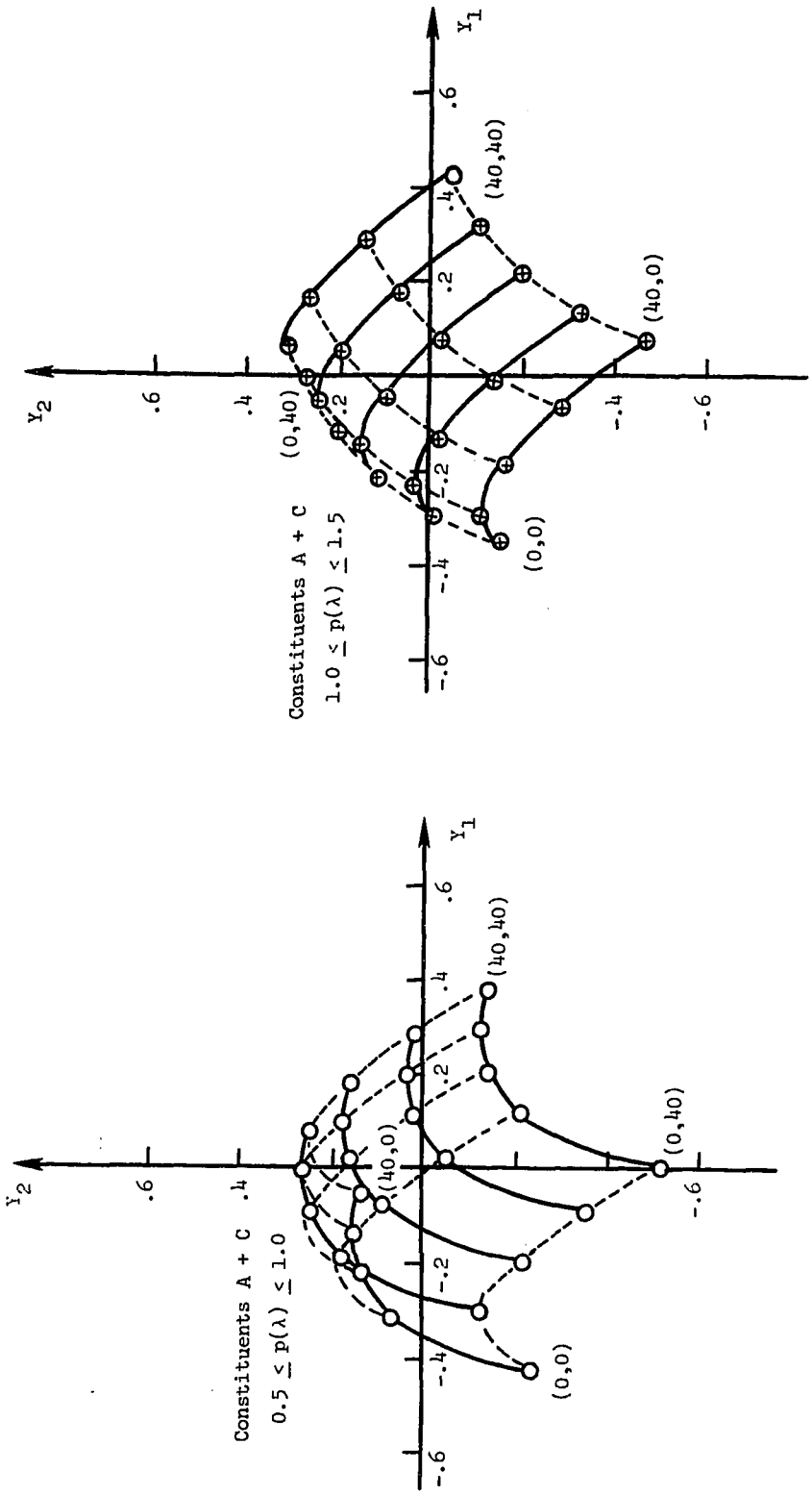

Figure 42.- Concluded.

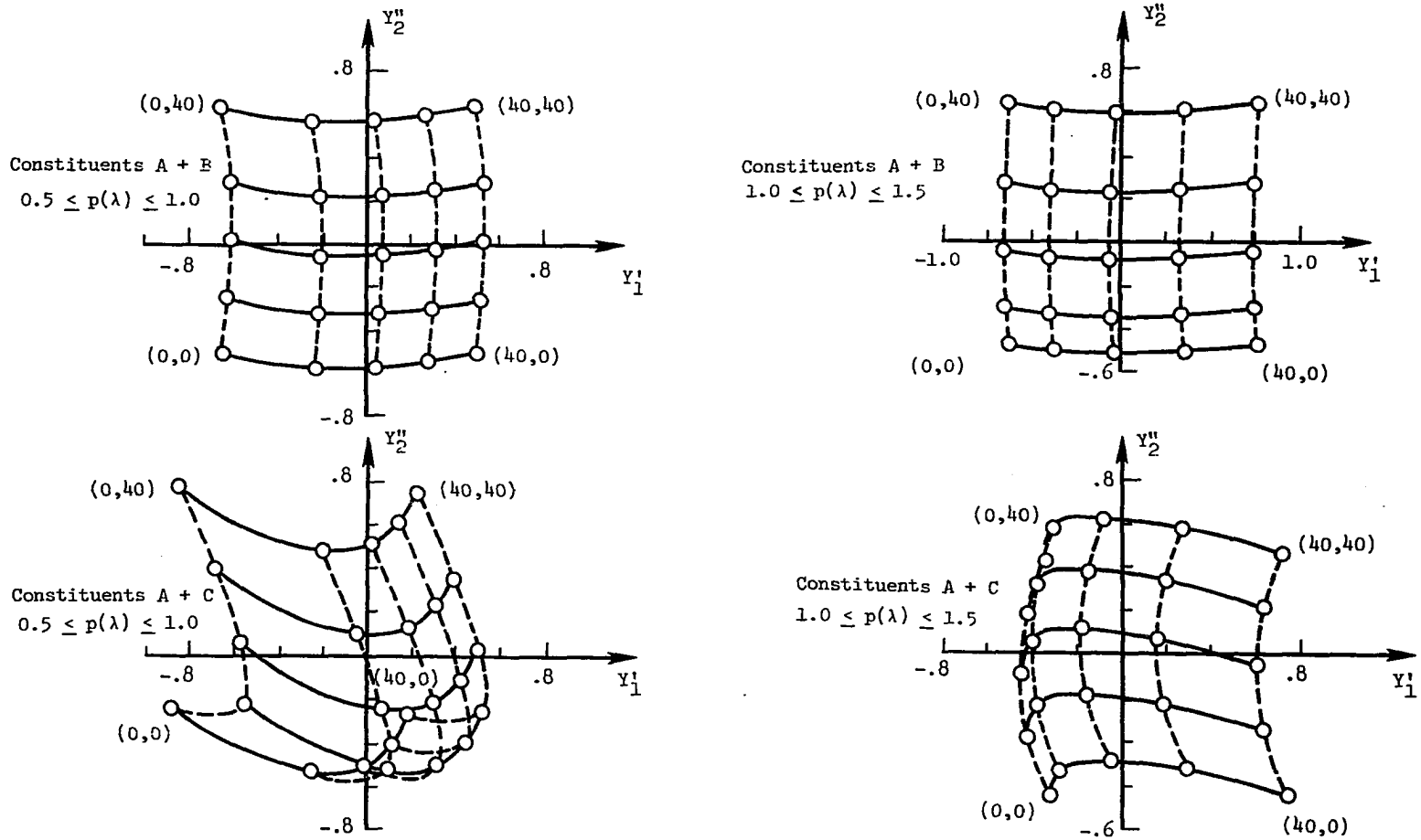

Figure 43.- Scalar multiples transformed into oblique axes system for mixtures (25 spectra) of wavelength-dependent nonlinear constituents A + B, A + C. Representative concentration pairs (C_A, C_B) or (C_A, C_C) are labeled.

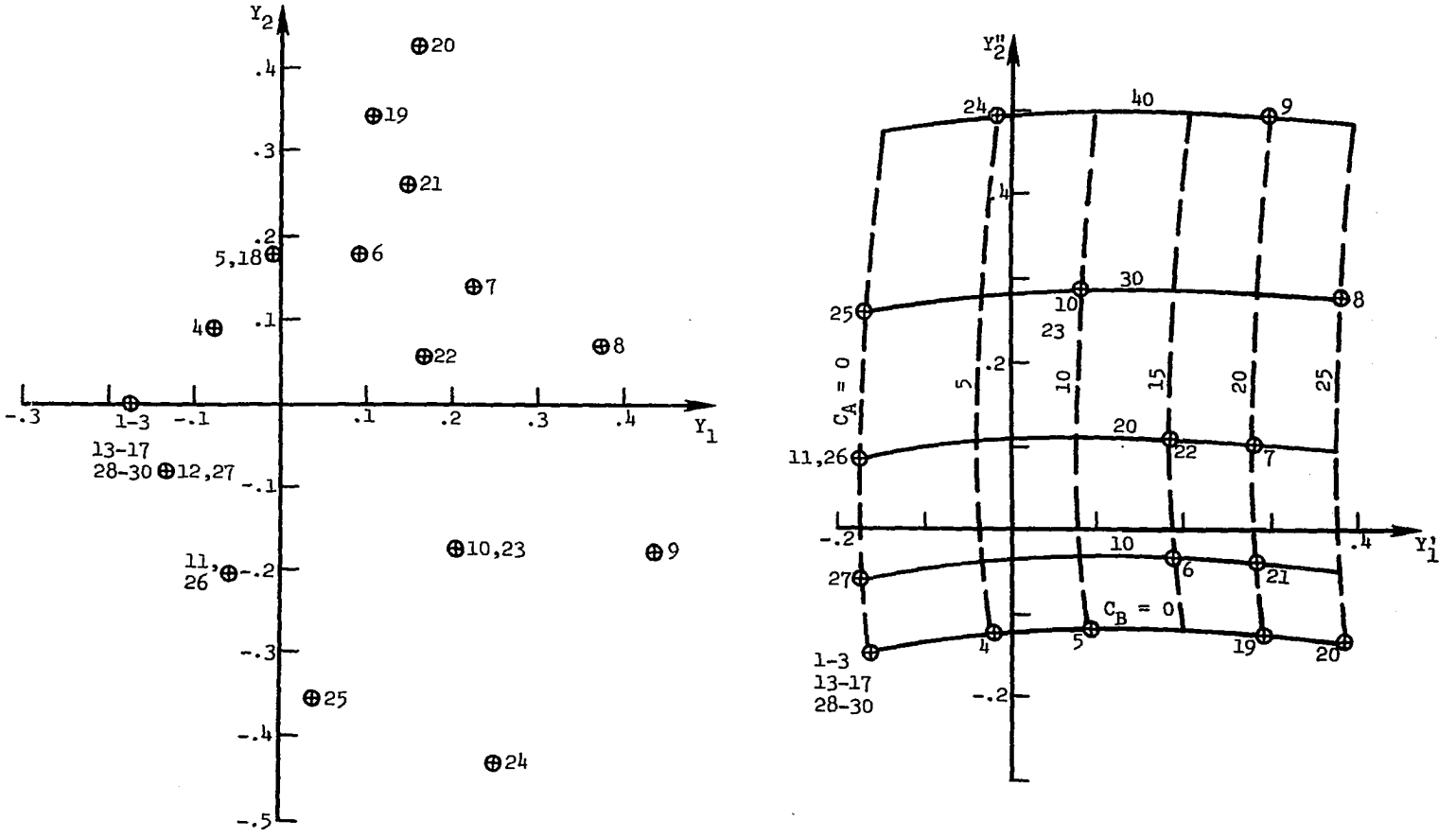

Figure 44.- (a) Scalar multiples in principal axes system and (b) transformed into oblique axes system for flight experiment involving hypothetical wavelength-dependent nonlinear constituents in water.

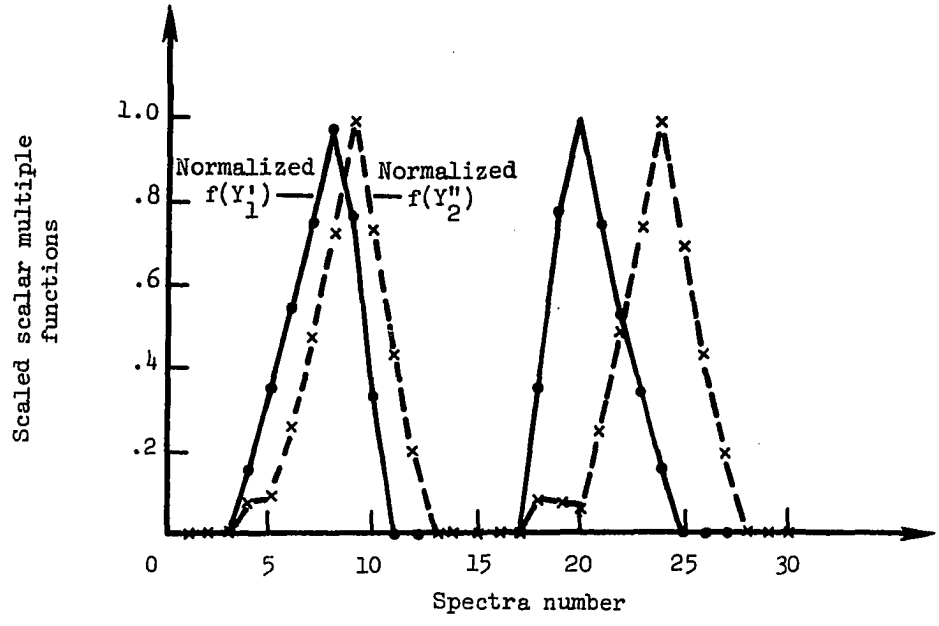

(a)

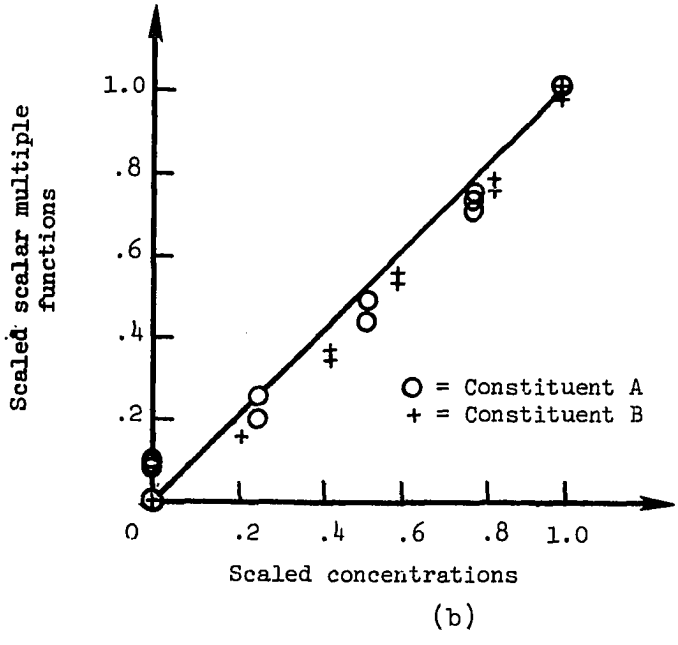

(b)

Figure 45.- (a) Scaled scalar multiple functions along hypothetical flight lines, (b) comparison with scaled concentrations. Constituents are wavelength-dependent nonlinear.

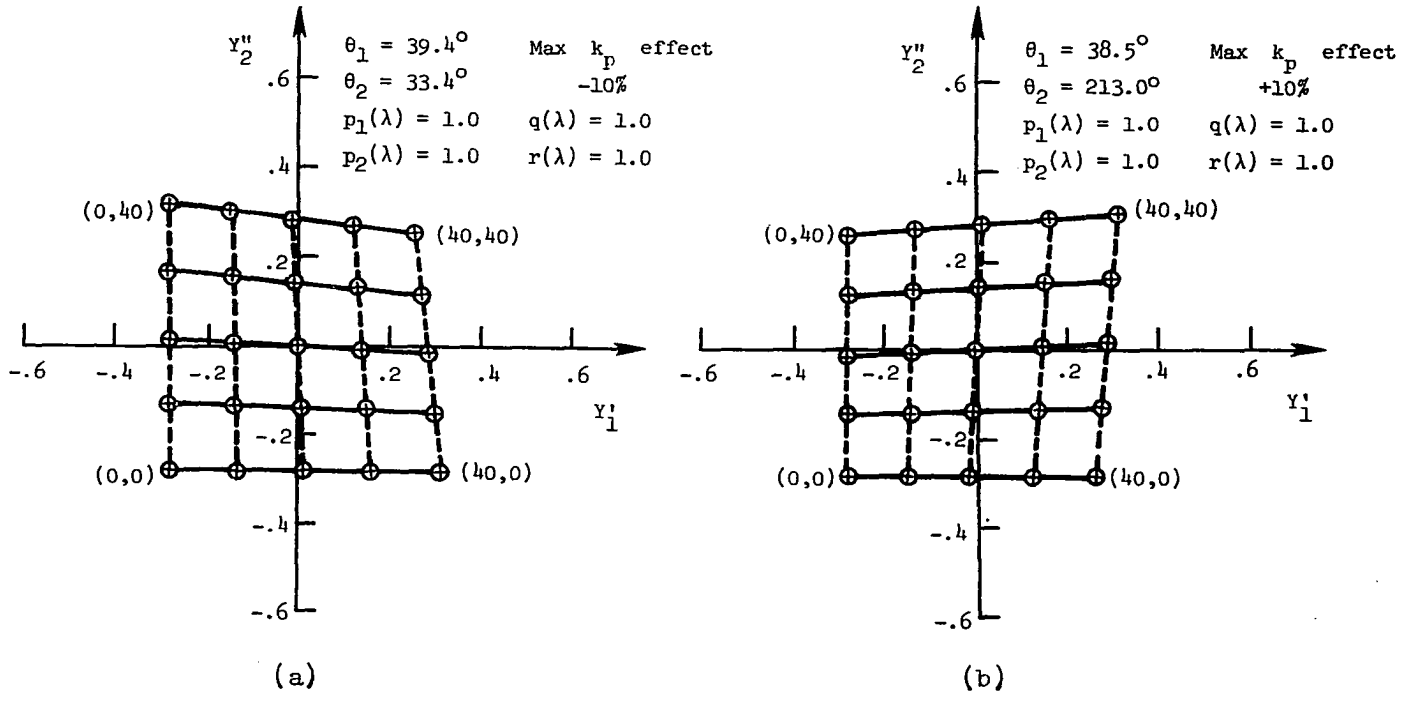

Figure 46.- Oblique axes scalar multiples for proportional nonlinear superposition. Constituents A + B, linear powers, variable interaction effect. Representative concentration pairs (C_A, C_B) are labeled.

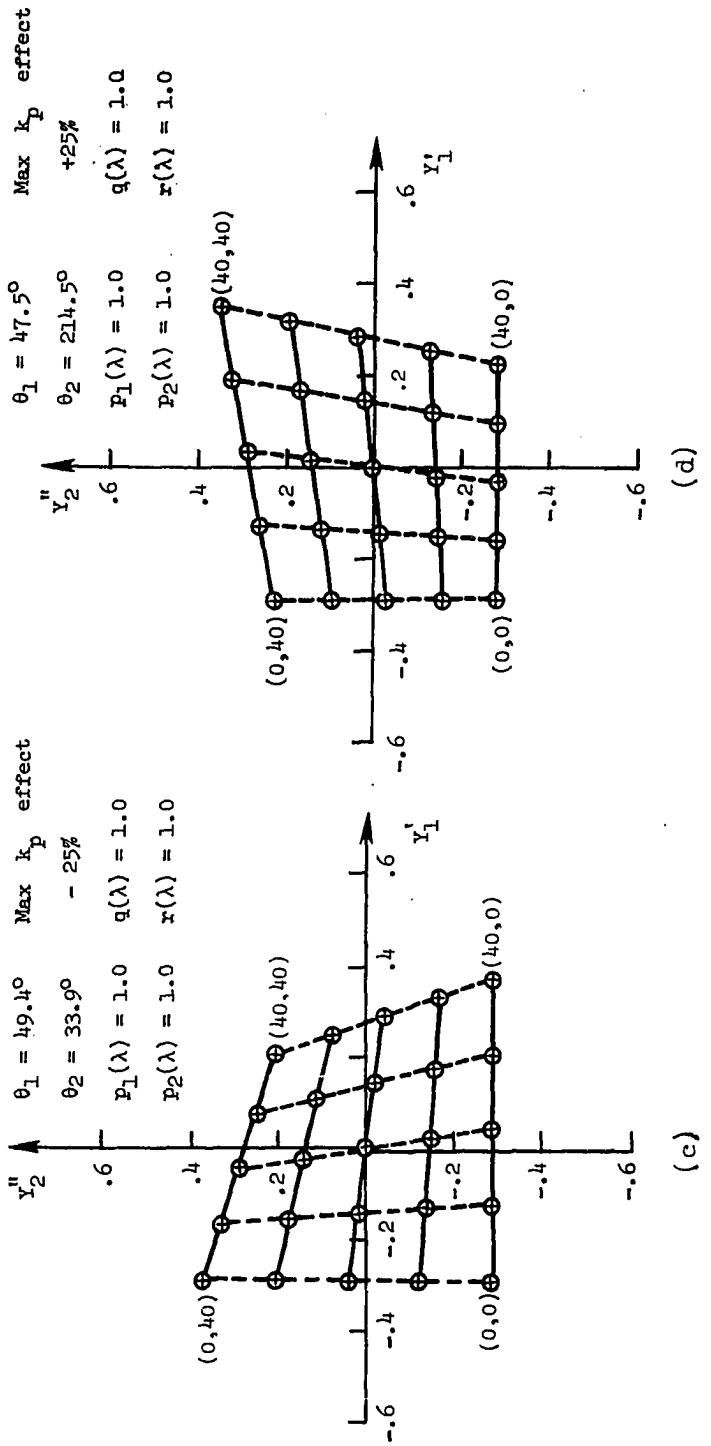

Figure 46.- Continued.

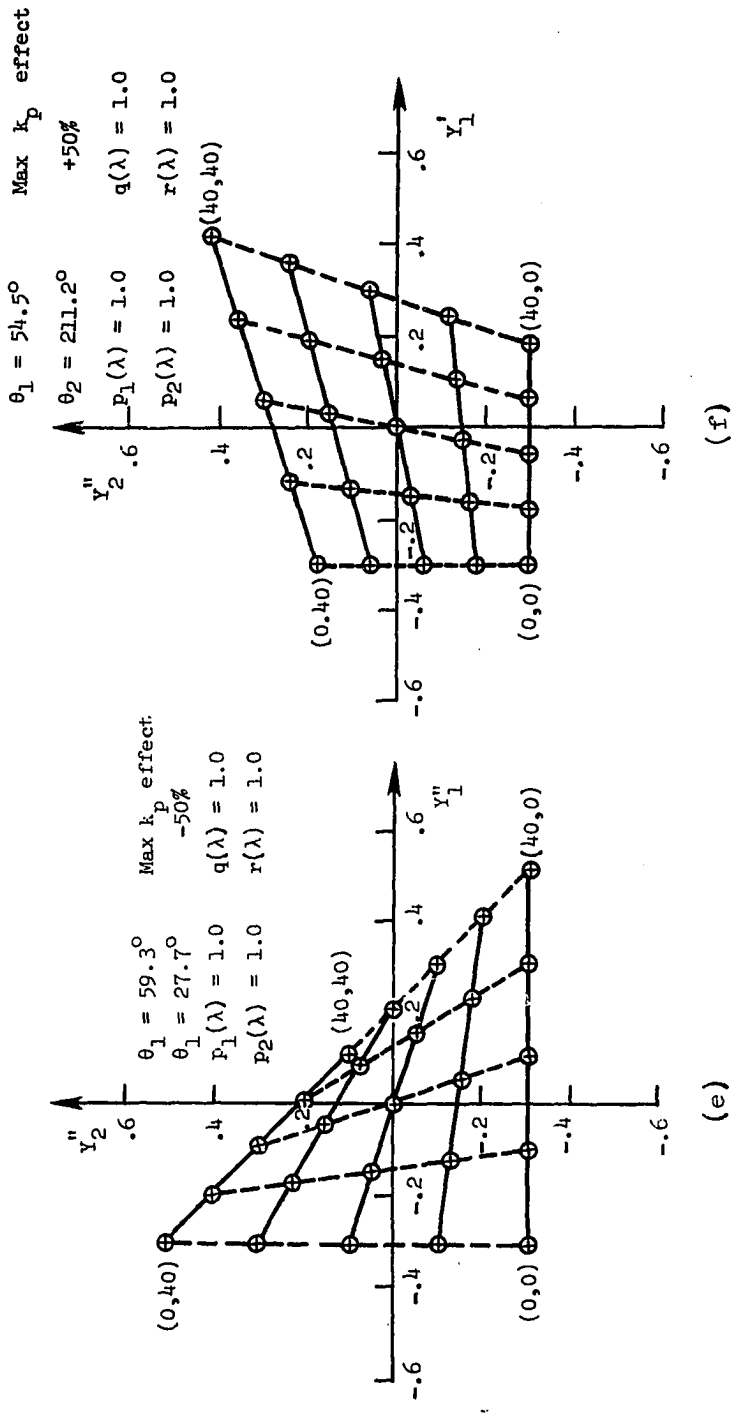

Figure 46.- Concluded.

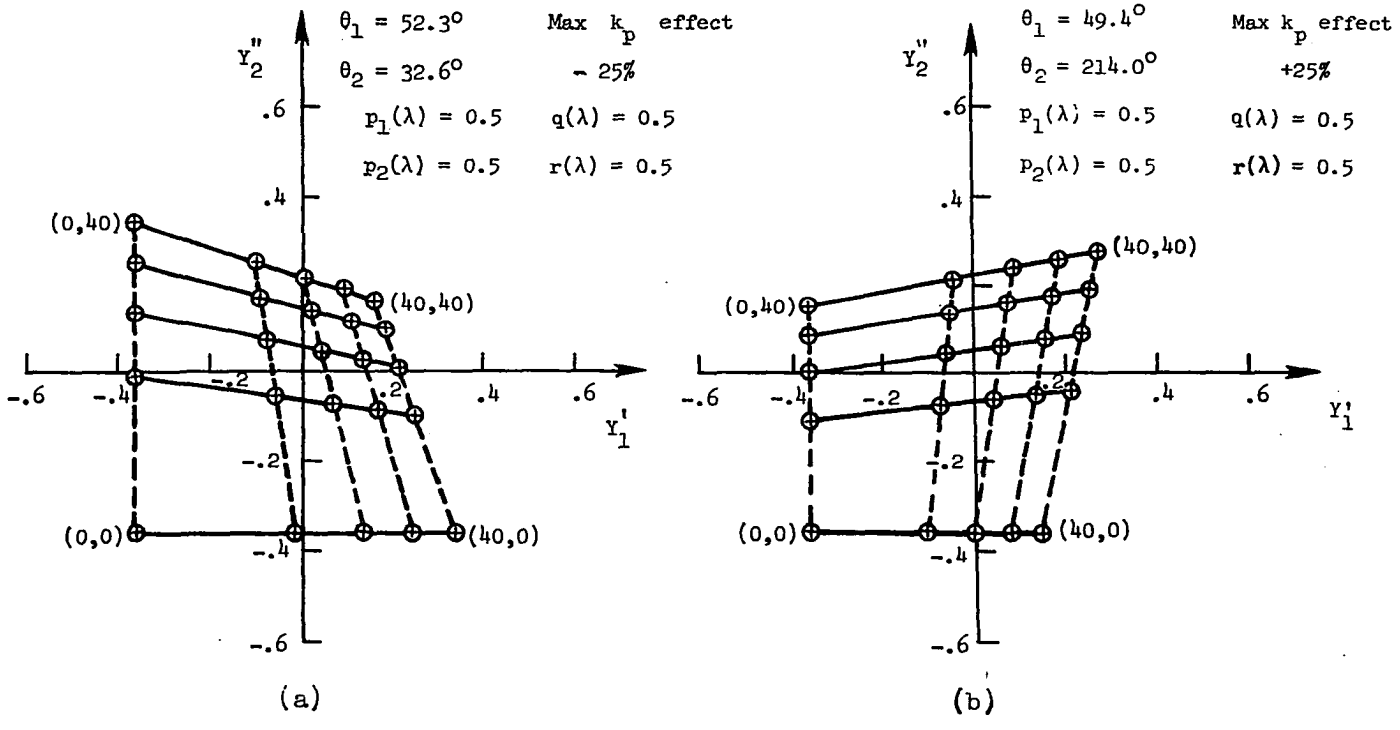

Figure 47.- Oblique axes scalar multiples for proportional nonlinear superposition. Constituents A + B, simple nonlinear powers. Representative concentration pairs (C_A, C_B) are labeled.

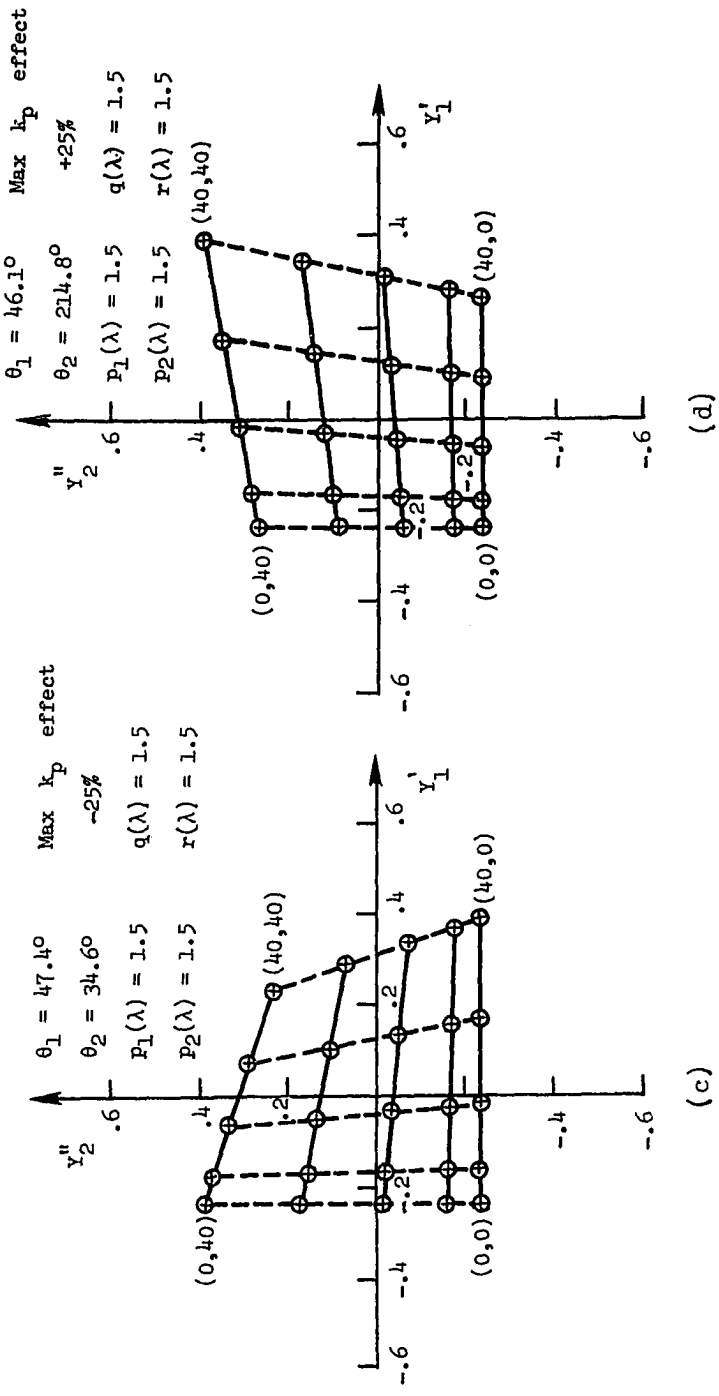

Figure 47.- Concluded.

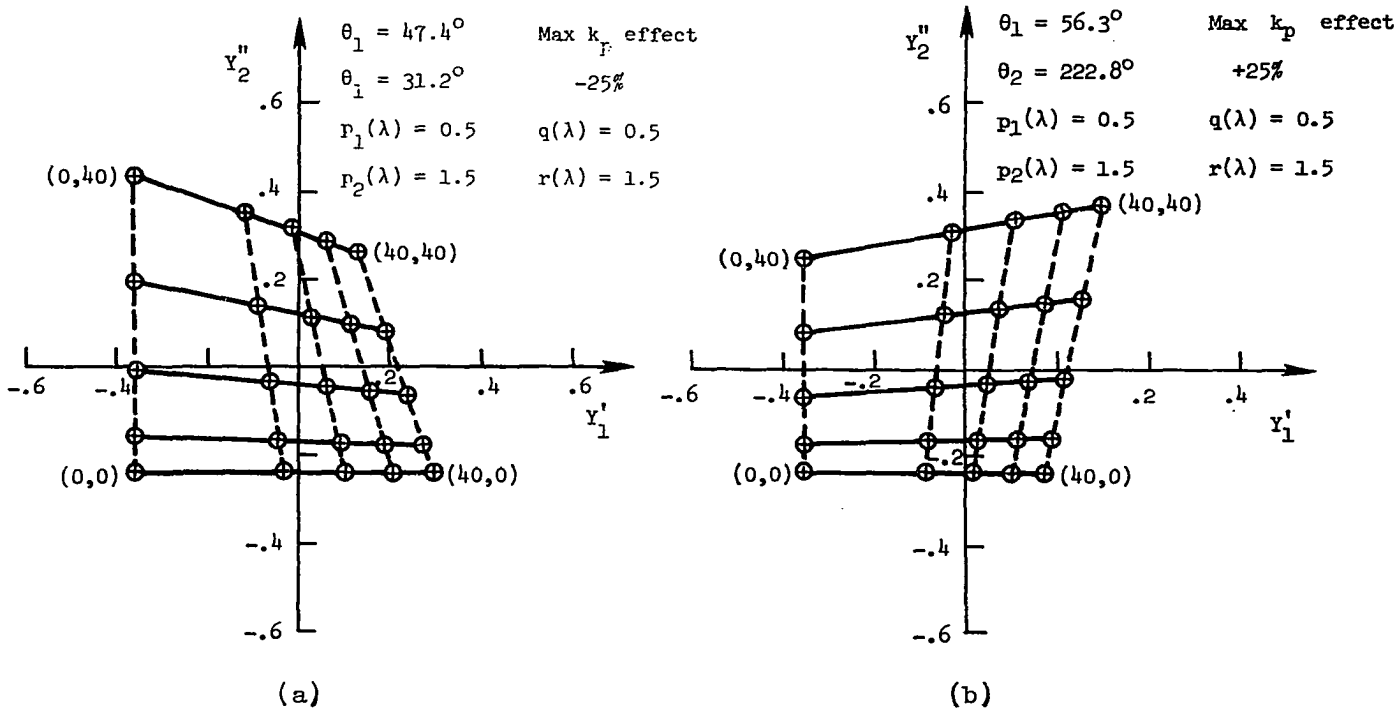

Figure 48.- Oblique axes scalar multiples for proportional nonlinear superposition. Constituents A + B, mixed simple nonlinear powers. Representative concentration pairs are labeled.

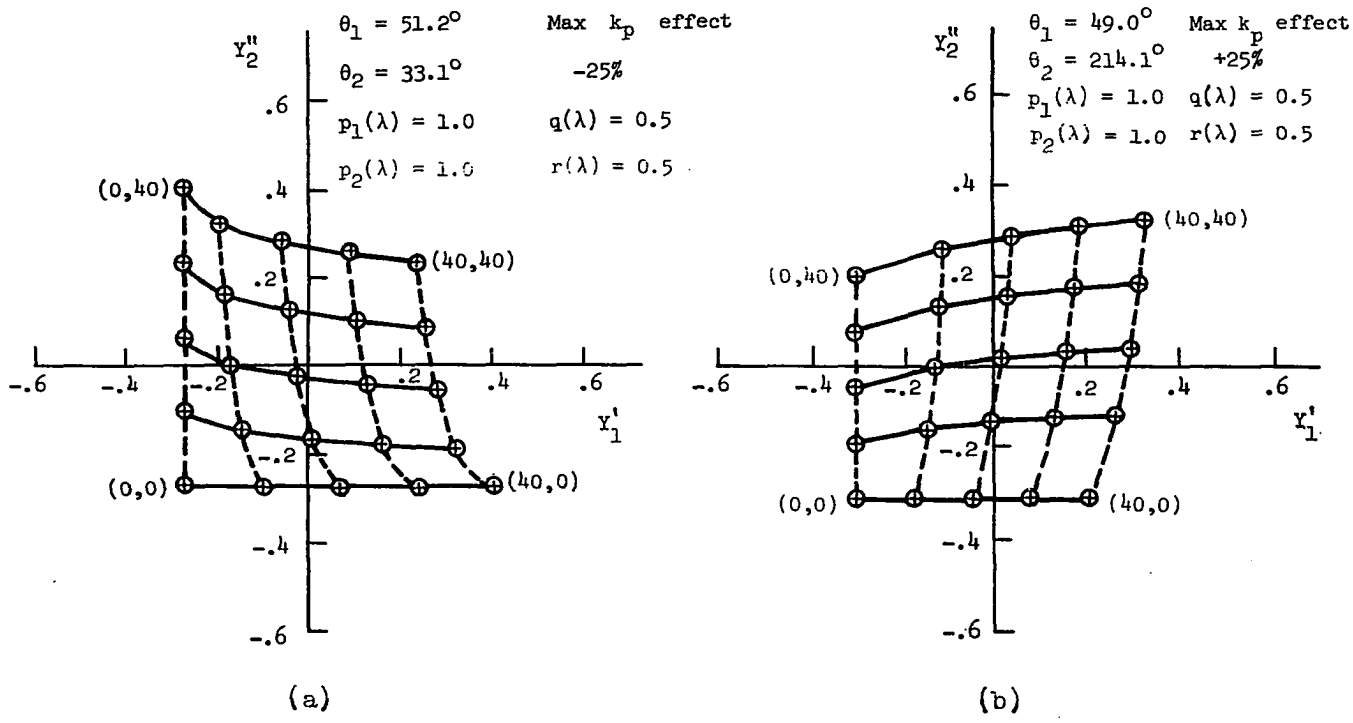

Figure 49.- Oblique axes scalar multiples for proportional nonlinear superposition. Constituents A + B, interaction term powers different from constituent term powers. Representative concentration pairs (C_A, C_B) are labeled.

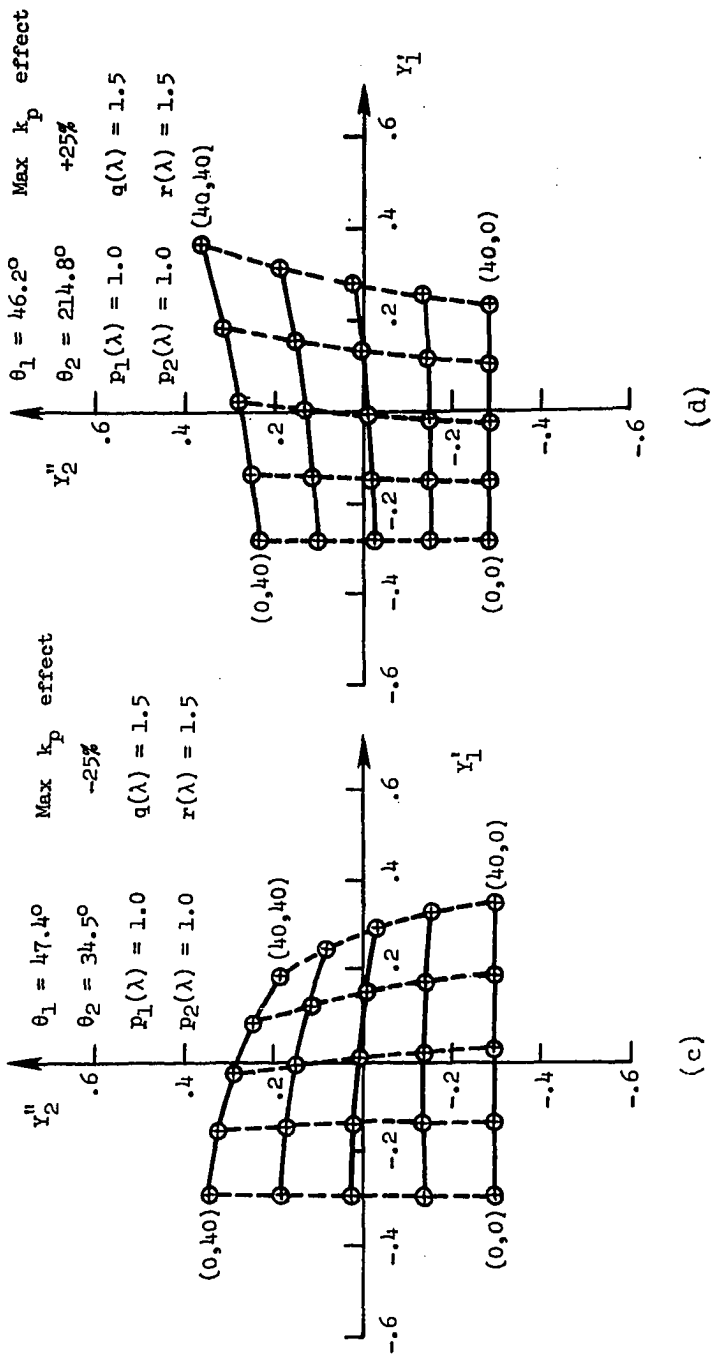

Figure 49.- Concluded.

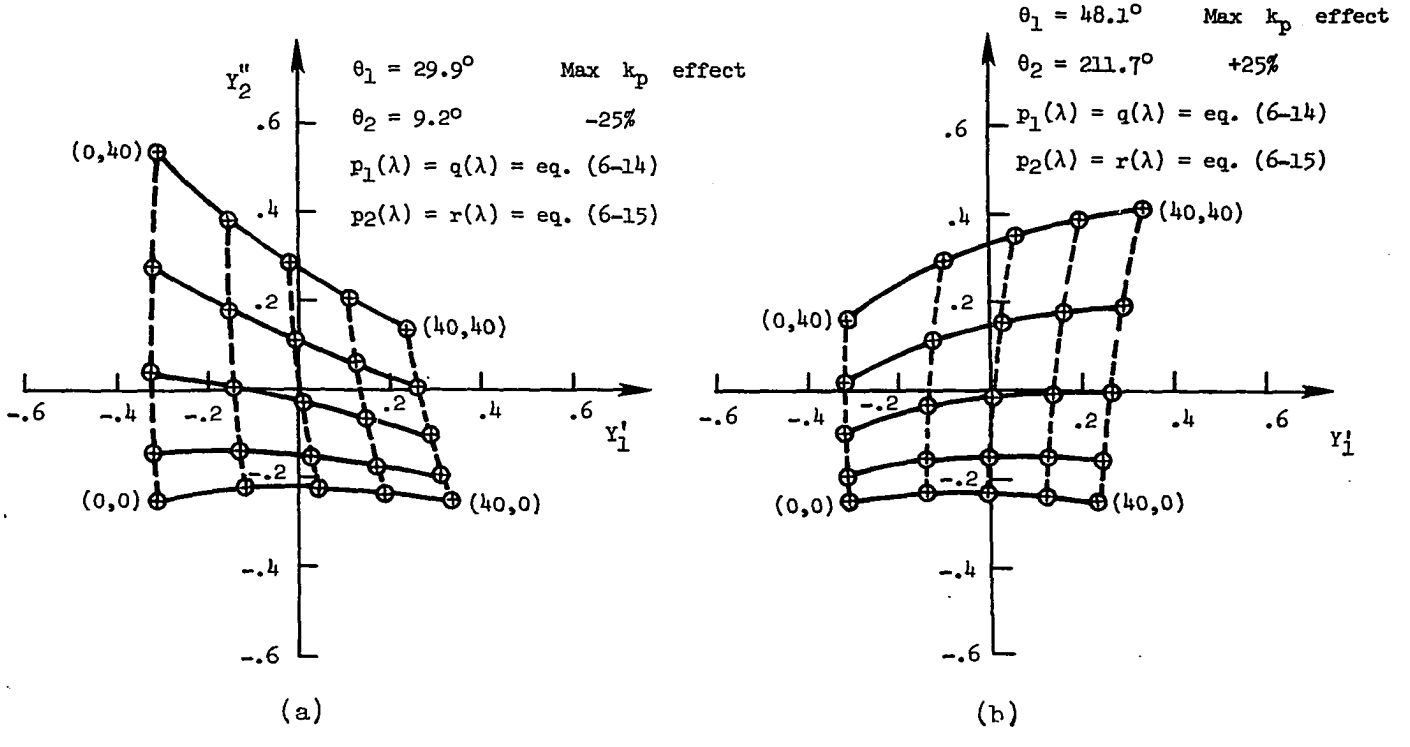

Figure 50.- Oblique axes scalar multiples for proportional nonlinear superposition. Constituents A + B, wavelength-dependent powers. Representative concentration pairs (C_A, C_B) are labeled.

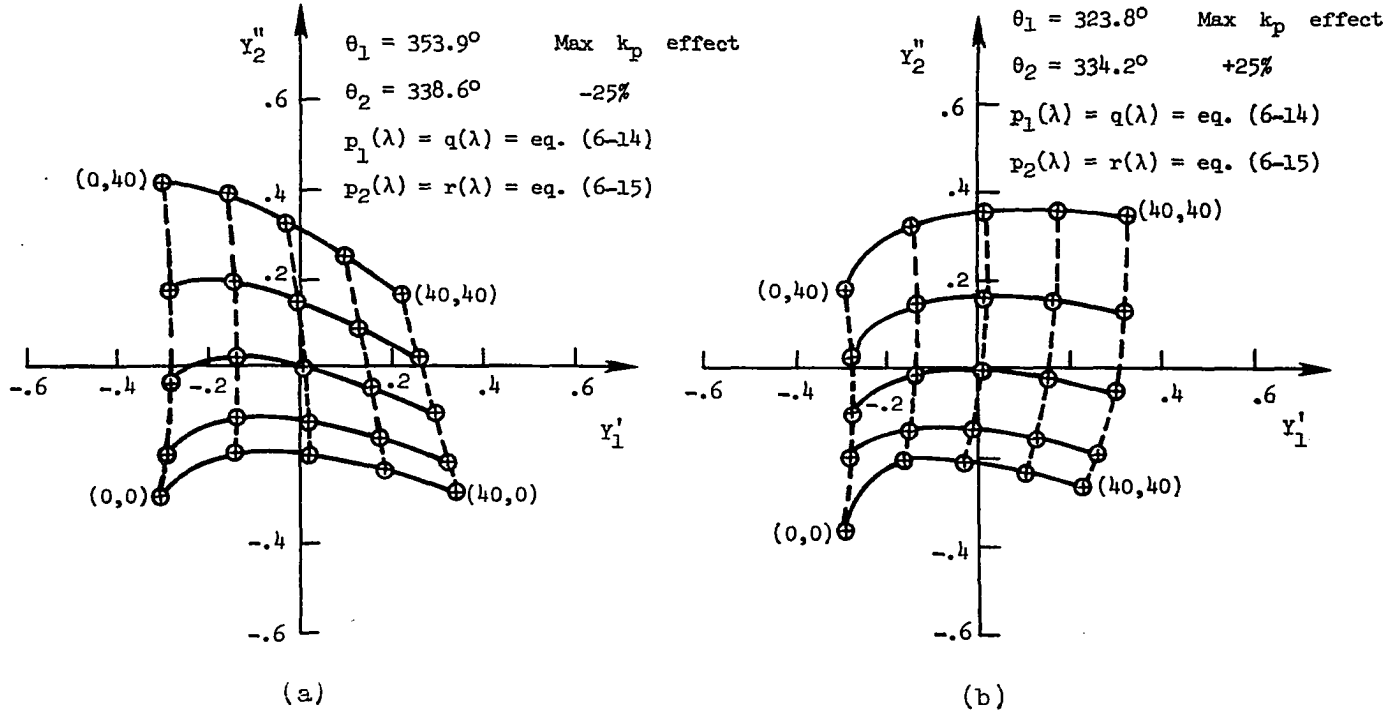

Figure 51.- Oblique axes scalar multiples for proportional nonlinear superposition. Constituents A + C, wavelength-dependent powers. Representative concentration pairs (C_A, C_C) are labeled.

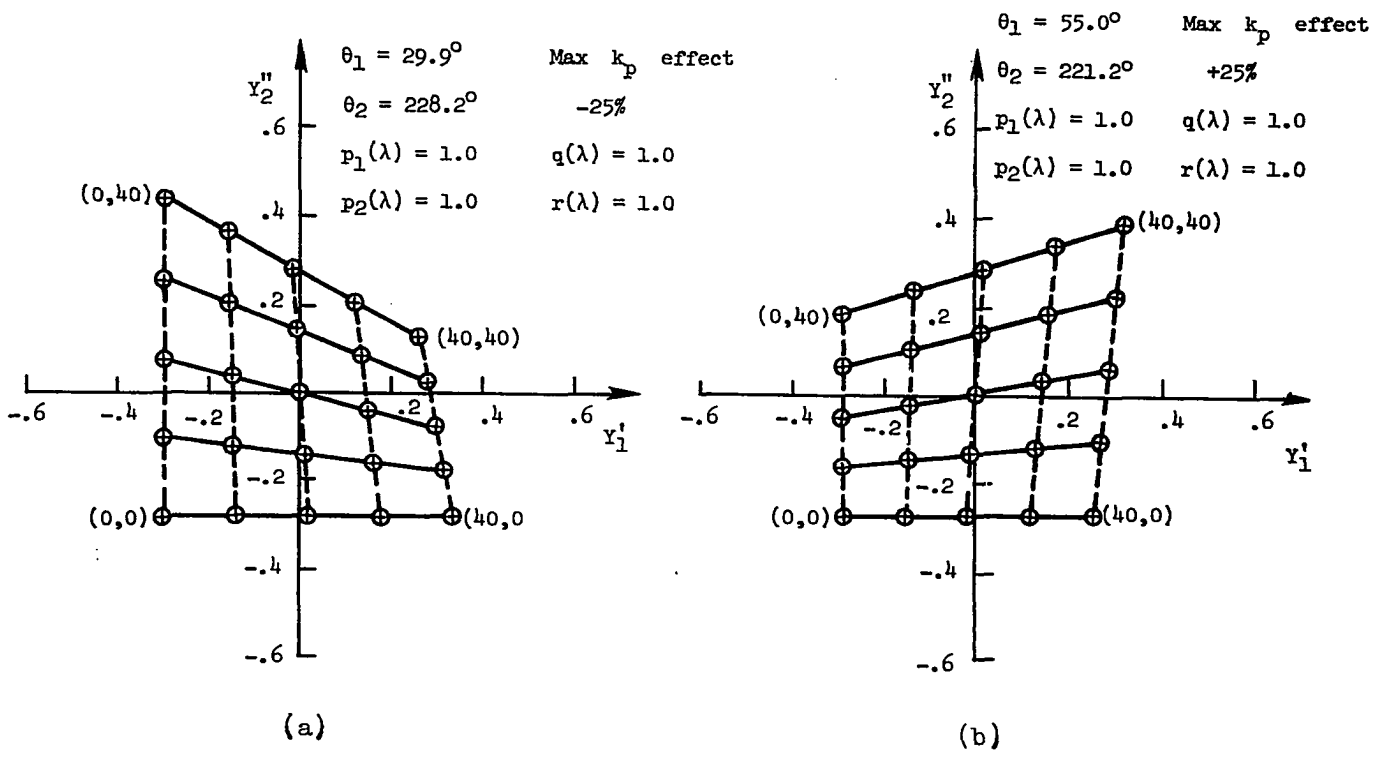

Figure 52.- Oblique axes scalar multiples for nonproportional nonlinear superposition. Constituents A + C, linear powers. Representative concentration pairs (C_A, C_C) are labeled.

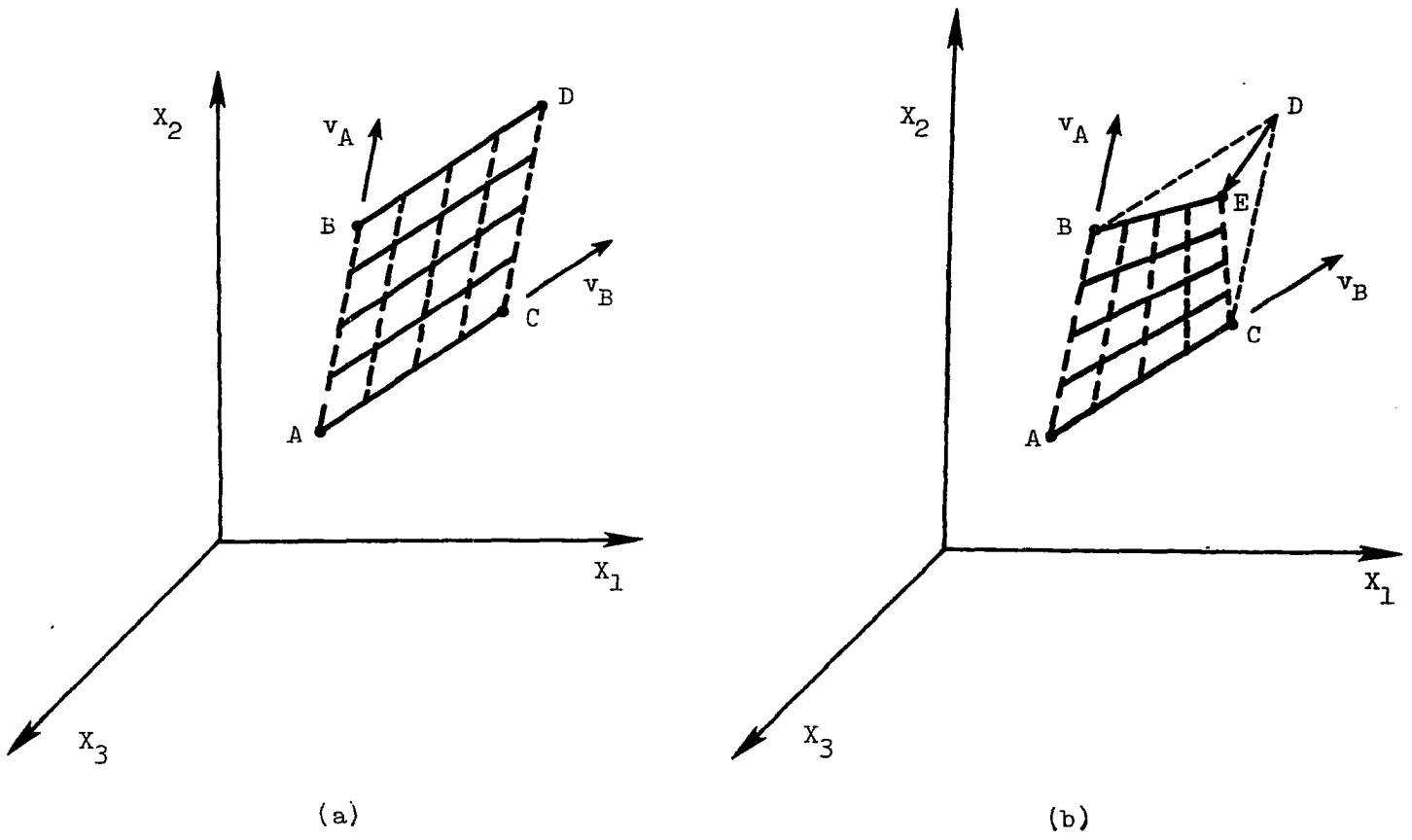

Figure 53.- Geometric interpretation of a two-constituent mixture using a three-band radiance plot of (a) linear, additive constituents, (b) proportional nonlinear superposition of linear constituents, and (c) nonproportional, nonlinear superposition of linear constituents.

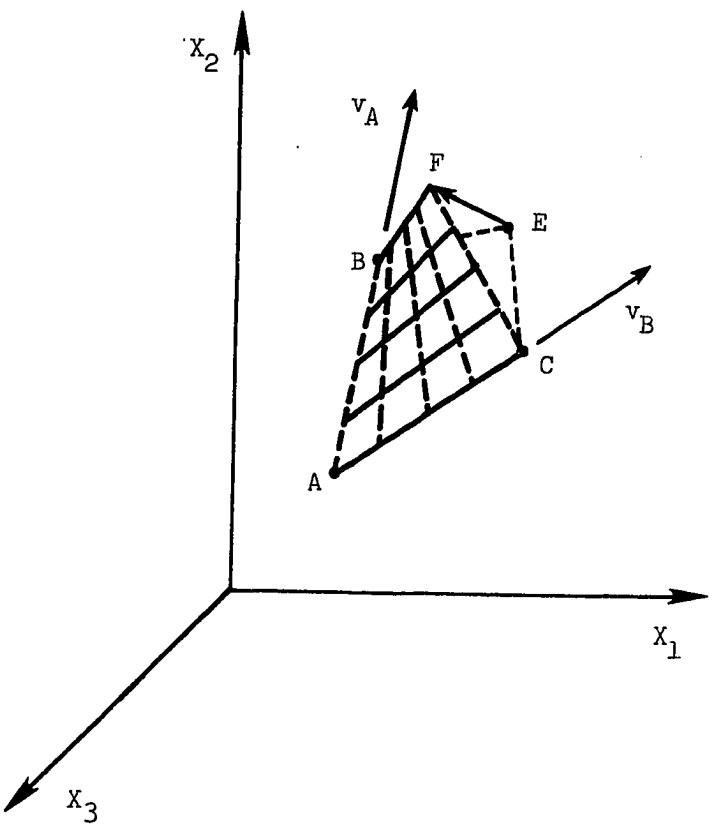

(c)

Figure 53.- Concluded.

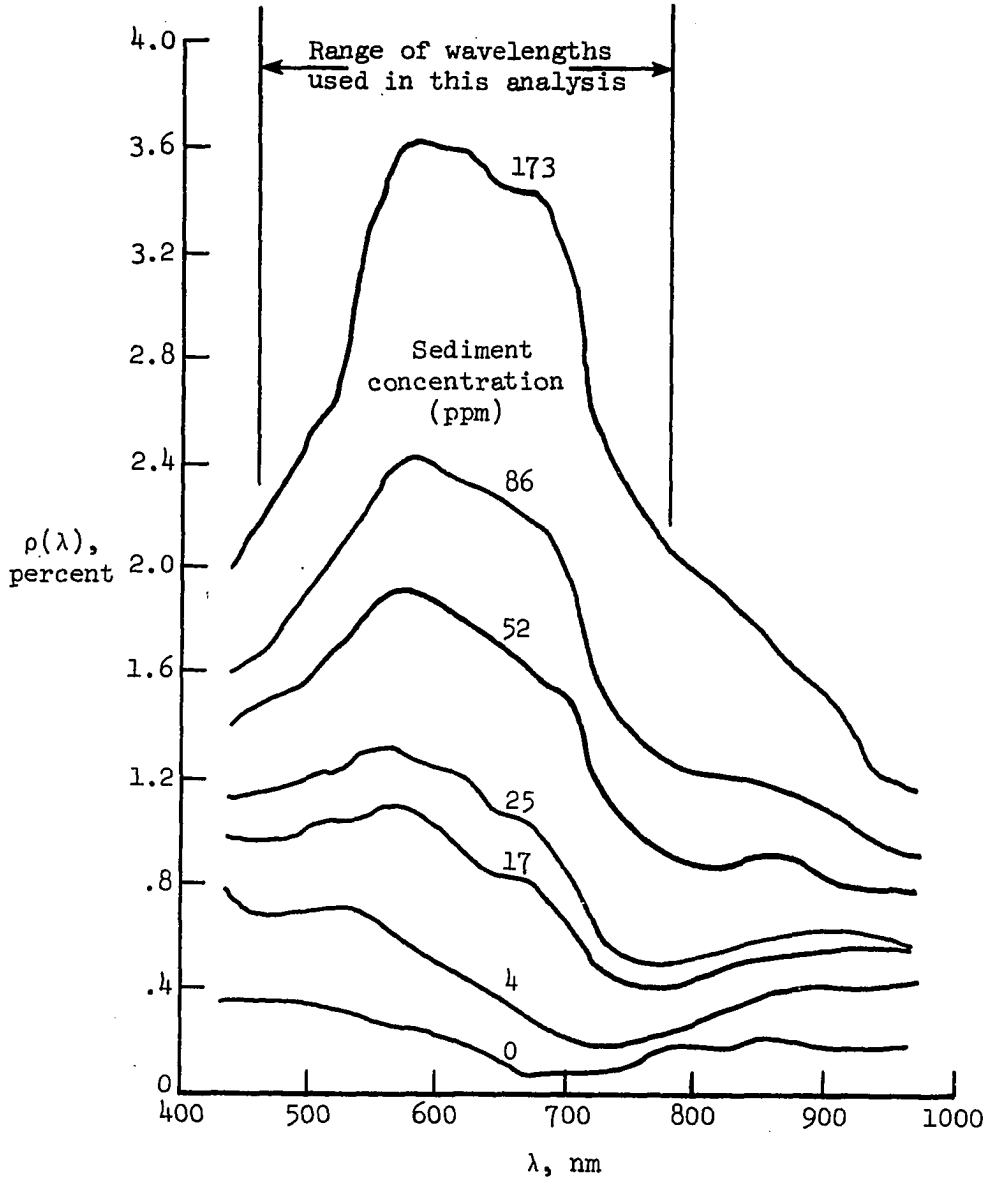

Figure 54.- Experimental reflectance spectra for Bermuda Hundred sediments. (After Whitlock et al 1978).

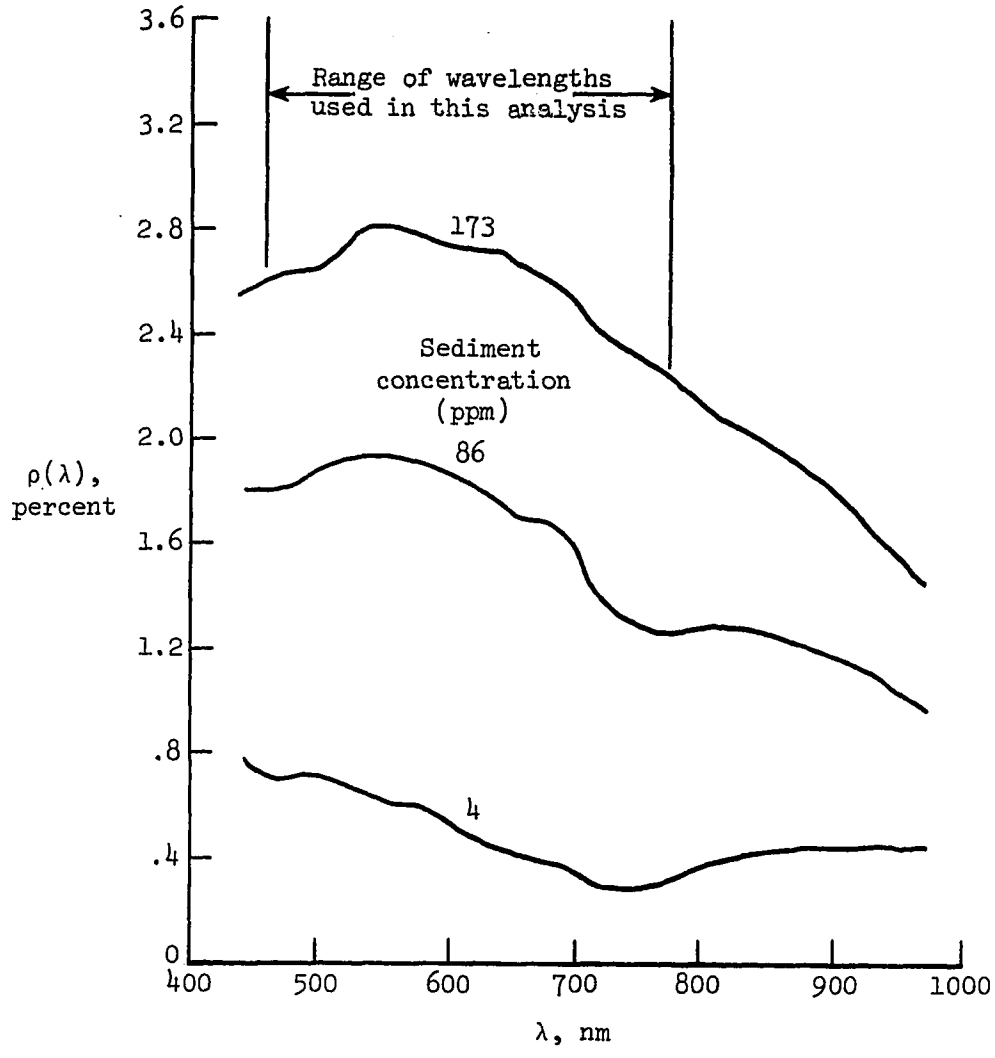

Figure 55.- Experimental reflectance spectra for Bailey Bay sediments. (After Whitlock et al 1978).

Mixture no.	Sediment mixture concentrations, ppm		
	Bermuda Hundred	Bailey Bay	Total
1	25	0	25
2	25	4	29
3	25	17	42
4	25	34	59
5	25	86	111
6	25	129	154
7	25	173	198

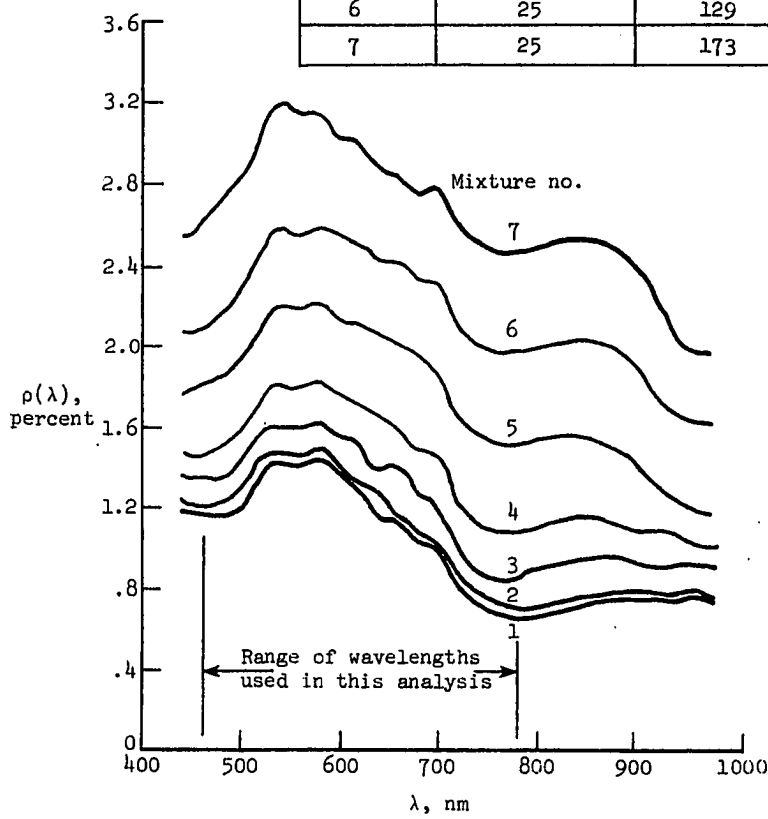

Figure 56.- Experimental reflectance spectra for mixture of Bermuda Hundred and Bailey Bay sediments. (After Whitlock et al 1978).

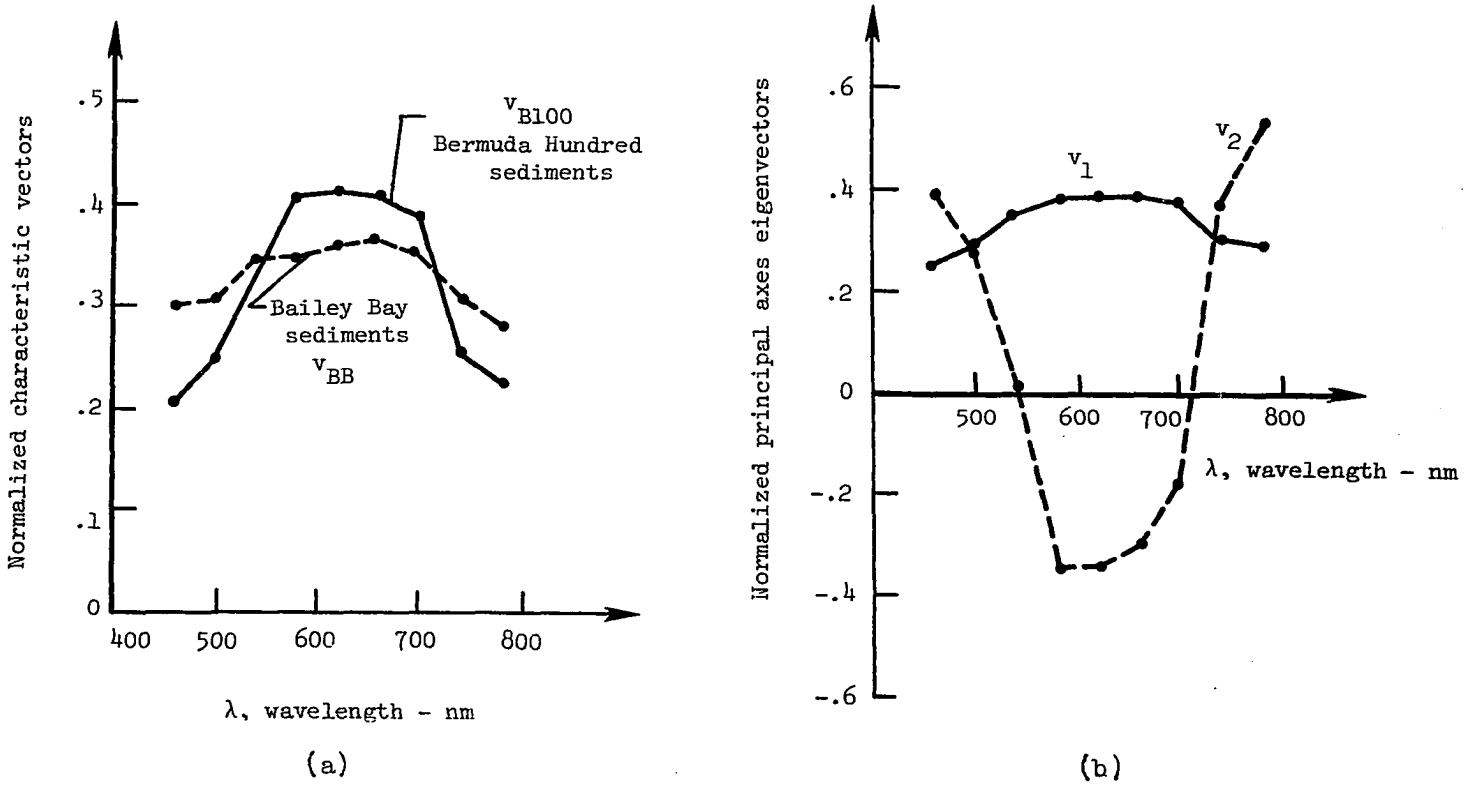

Figure 57.- (a) Characteristic vectors for reflectance data of Bermuda Hundred and Bailey Bay sediment classes and (b) principal axes eigenvectors for reflectances of complete Bermuda Hundred-Bailey Bay data set.

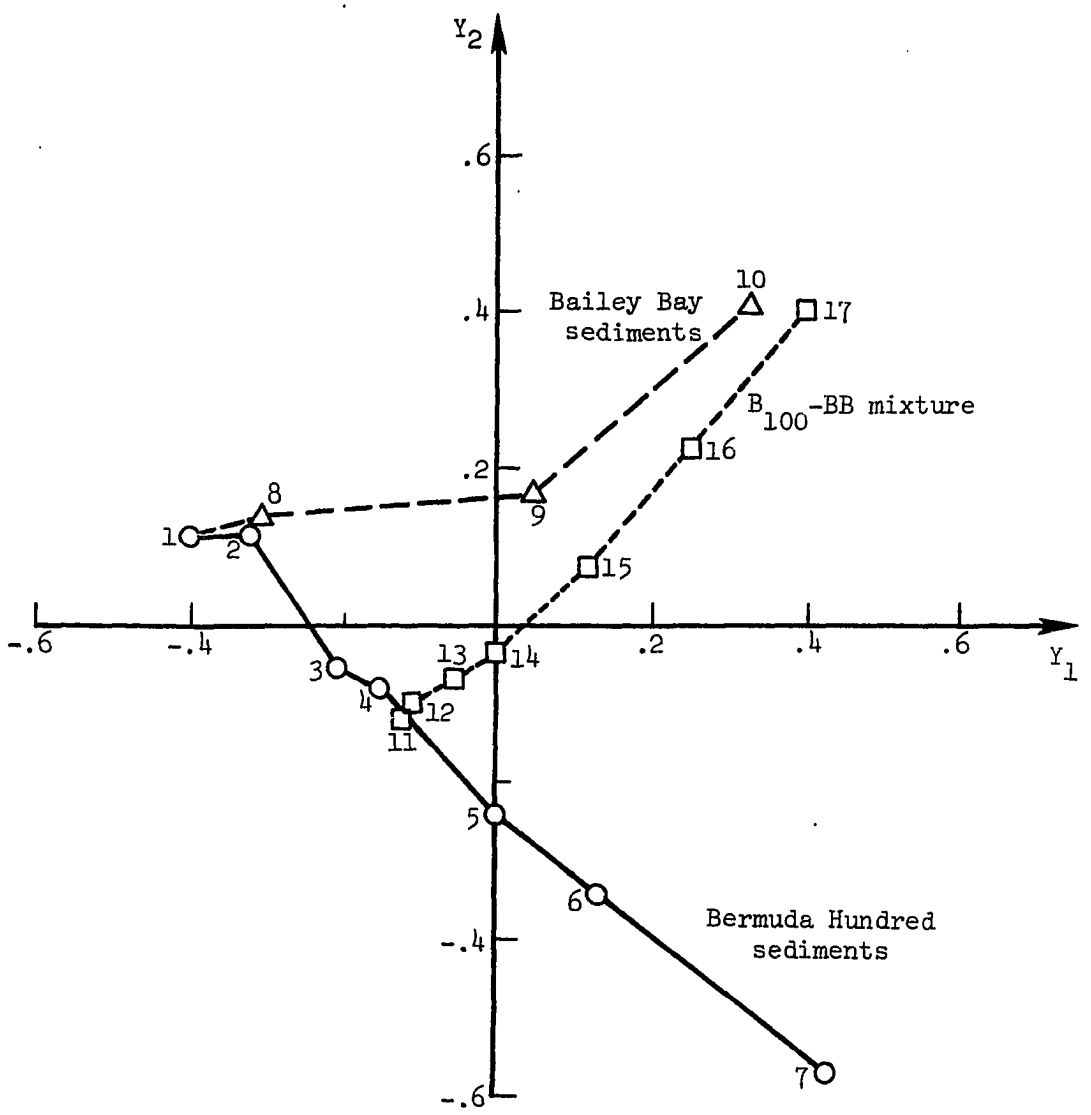

Figure 58.- Scalar multiples associated with first two principal axes eigenvectors. Spectra numbers are noted.

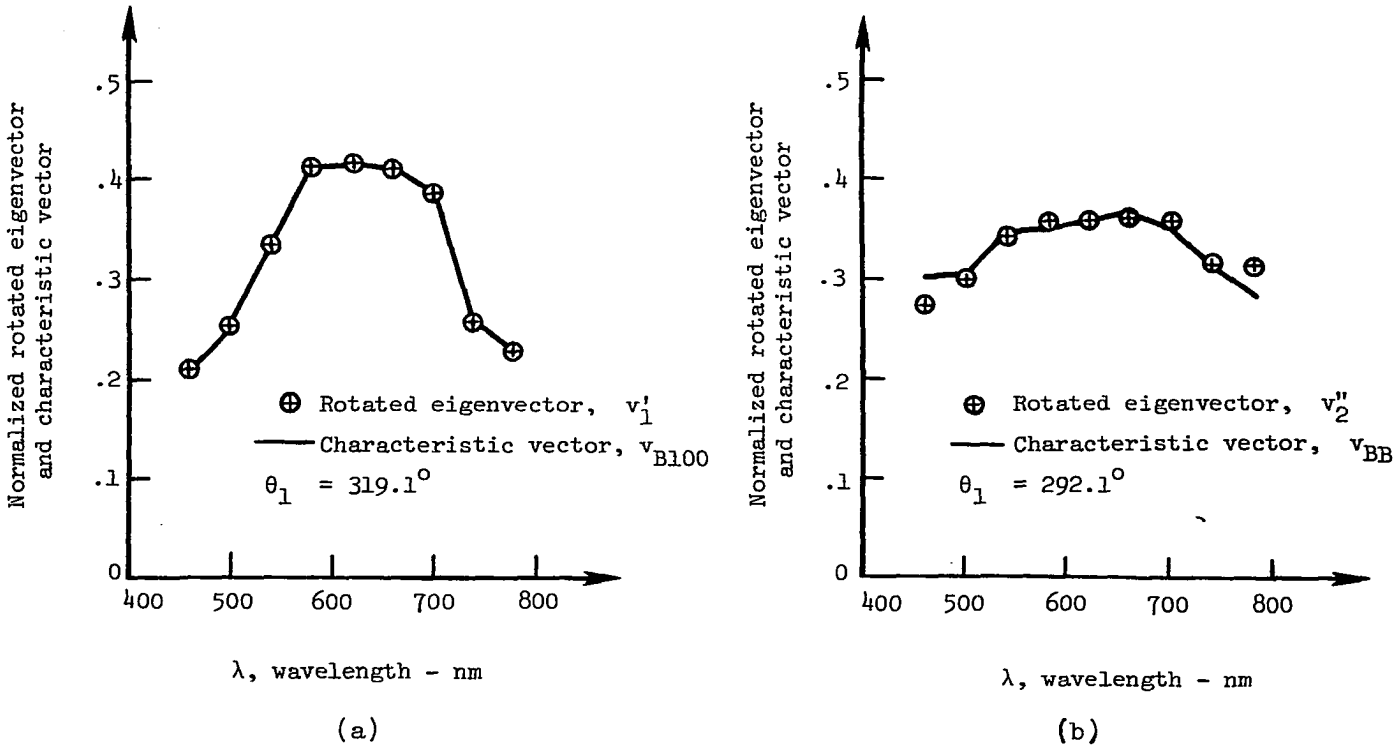

Figure 59.- Comparison between rotated principal axes eigenvectors and characteristic vectors for reflectance data from (a) Bermuda Hundred and (b) Bailey Bay sediments.

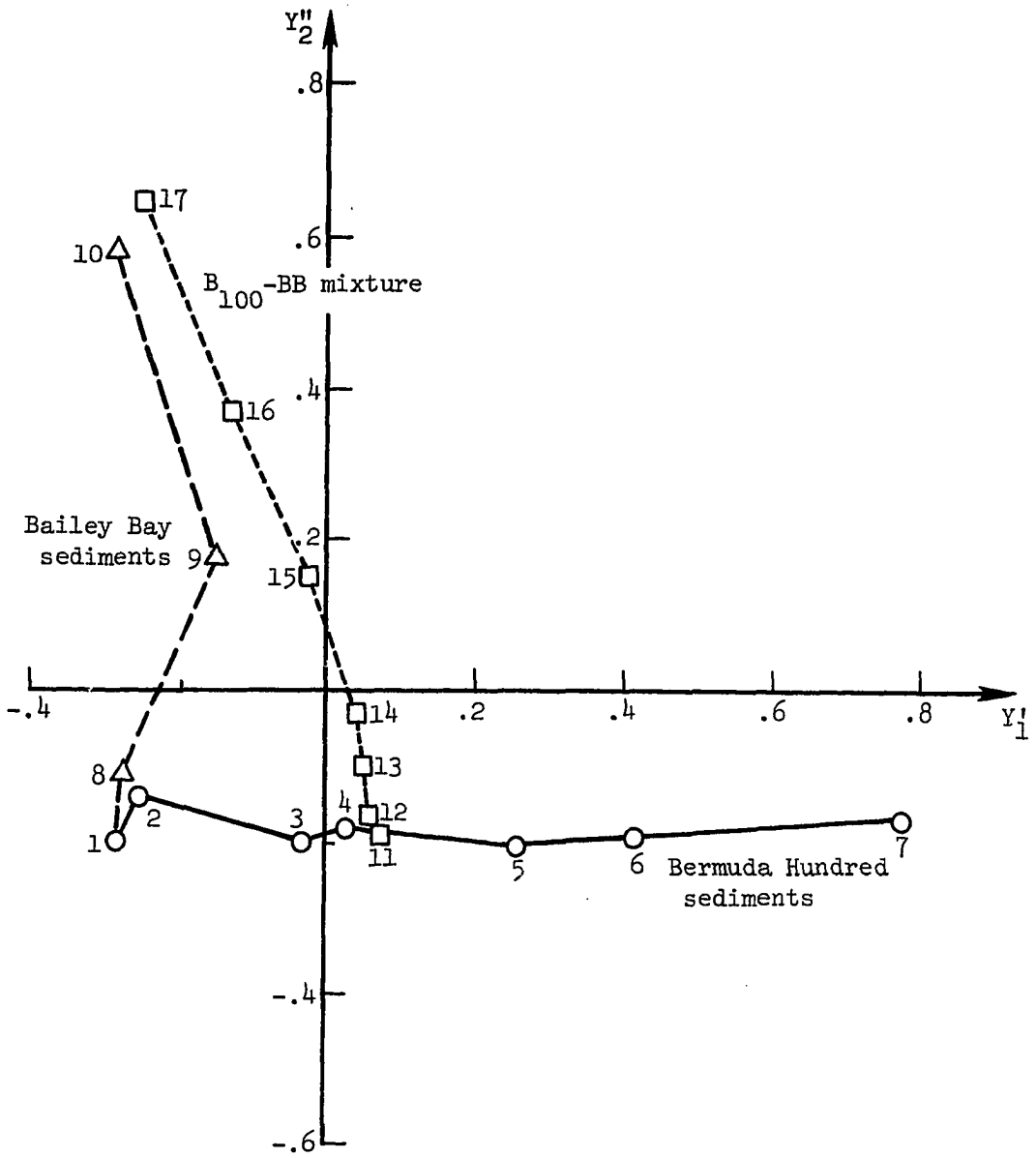

Figure 60.- Transformed scalar multiples in oblique axes system. Spectra numbers are noted.

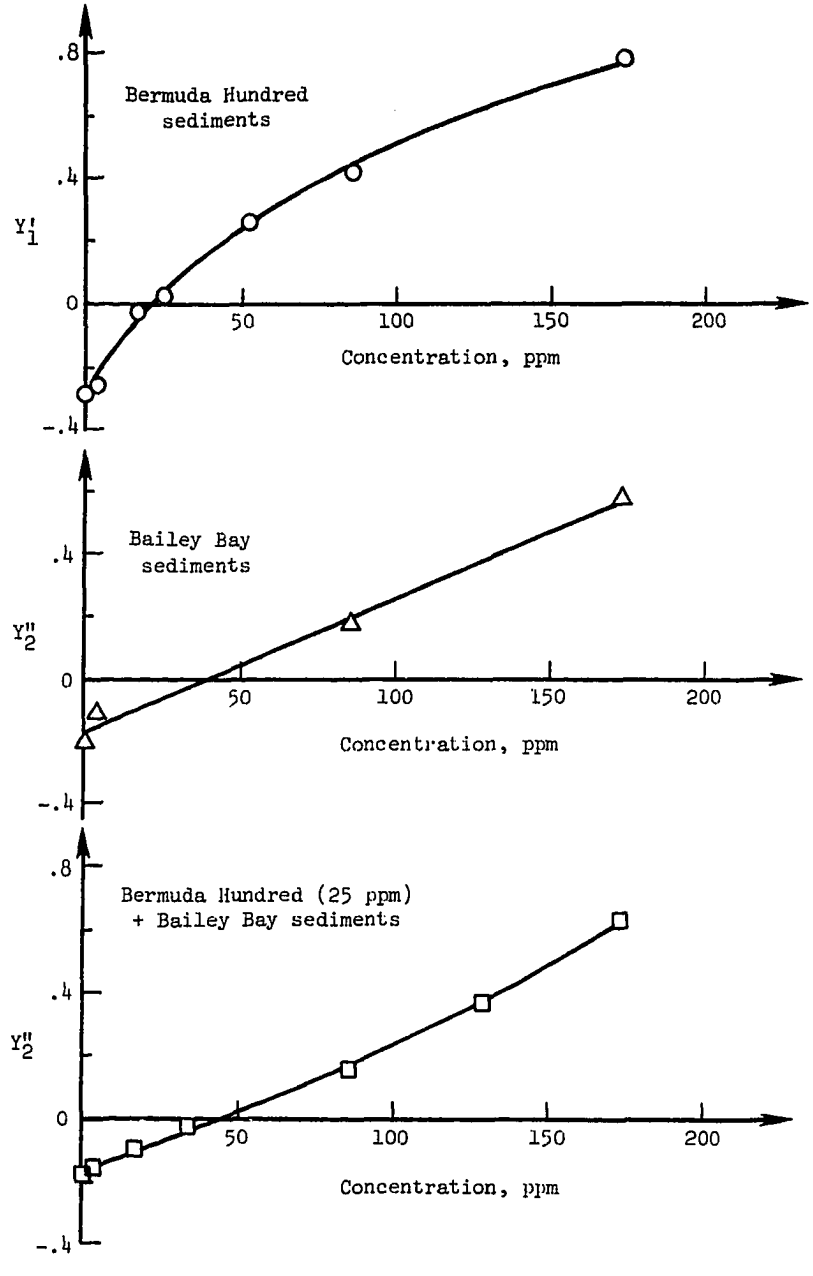

Figure 61.- Transformed scalar multiples as a function of constituent or mixture concentrations of Bermuda Hundred and Bailey Bay sediments.

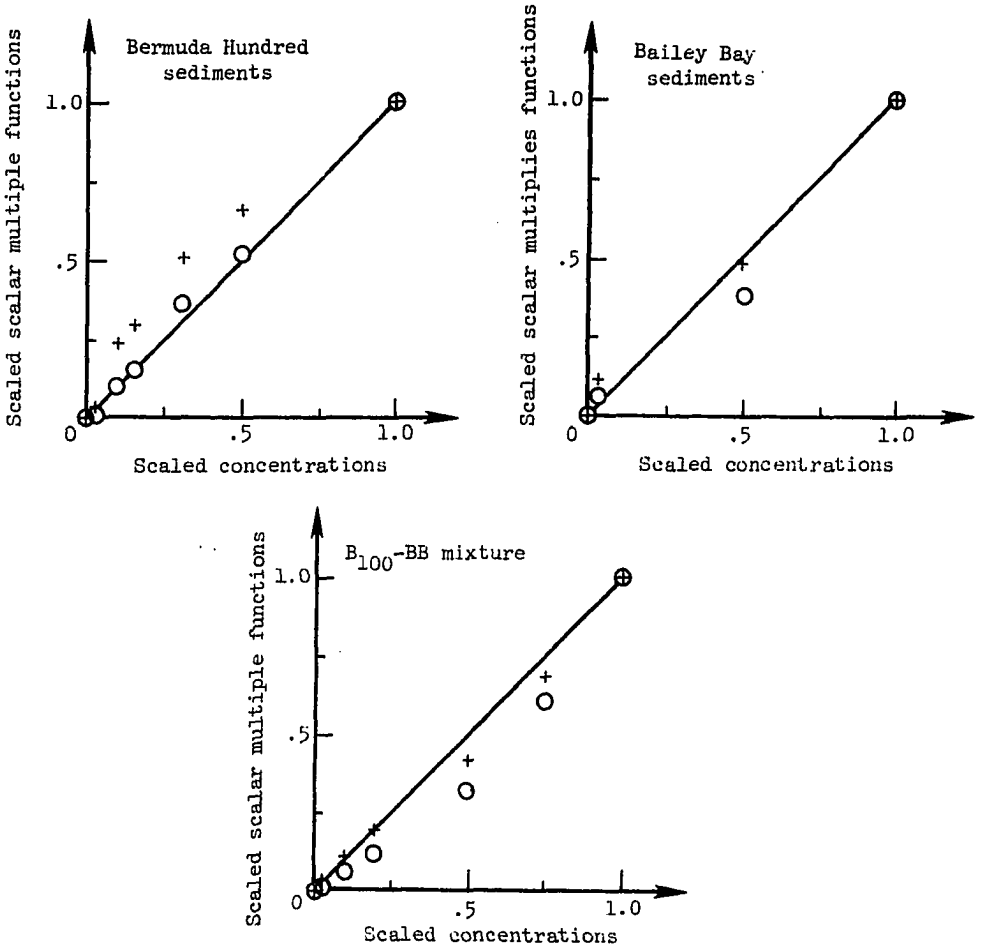

Figure 62.- Comparison between scaled scalar multiple functions and scaled concentrations for Bermuda Hundred-Bailey Bay sediments experiment. Crosses (+) are linear scaling approximations; circles (O) are simple nonlinear scaling approximations.

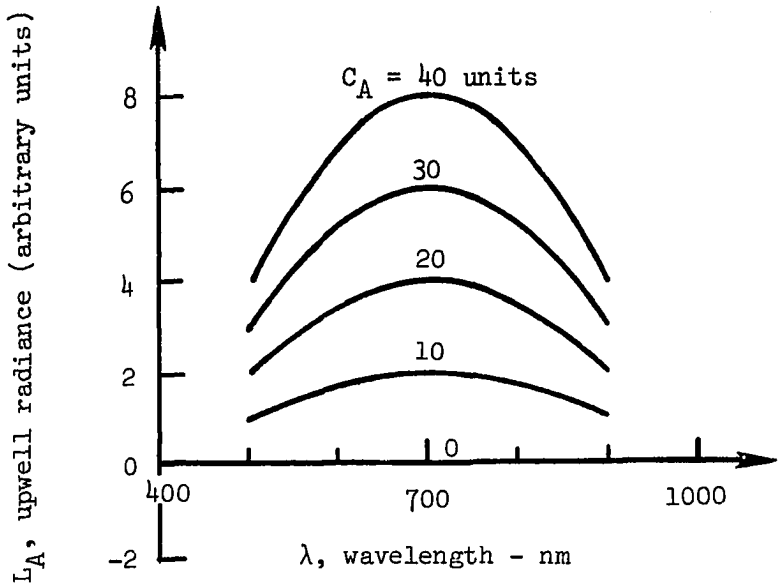

(a) 0% random noise

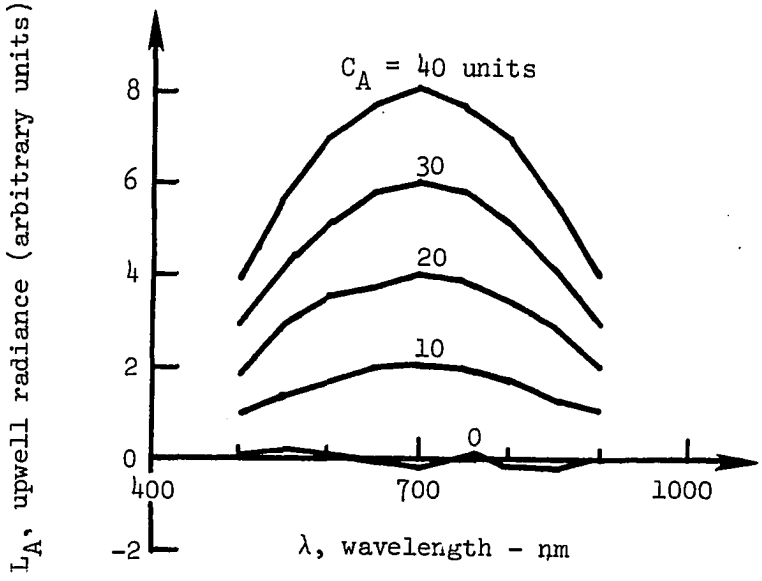

(b) 1% random noise

Figure 63.- Effects of several levels of random noise on spectra of linear constituent A.

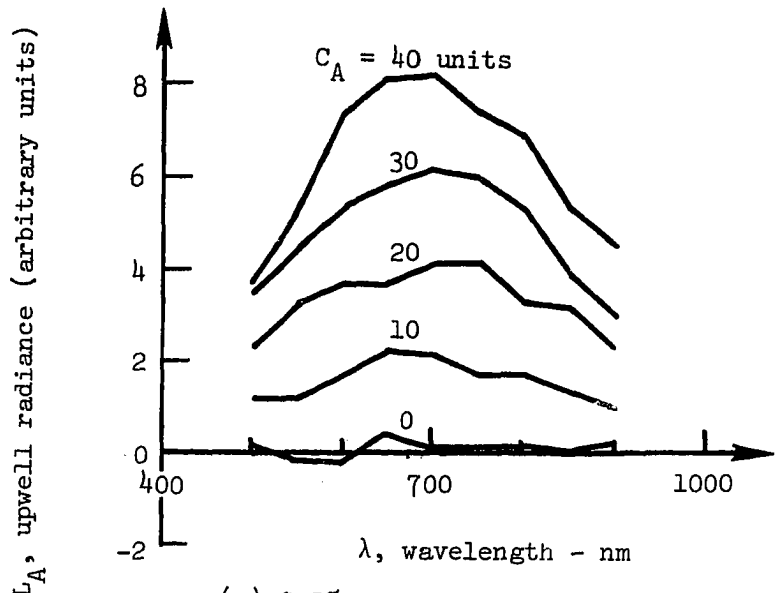

(c) 2.5% random noise

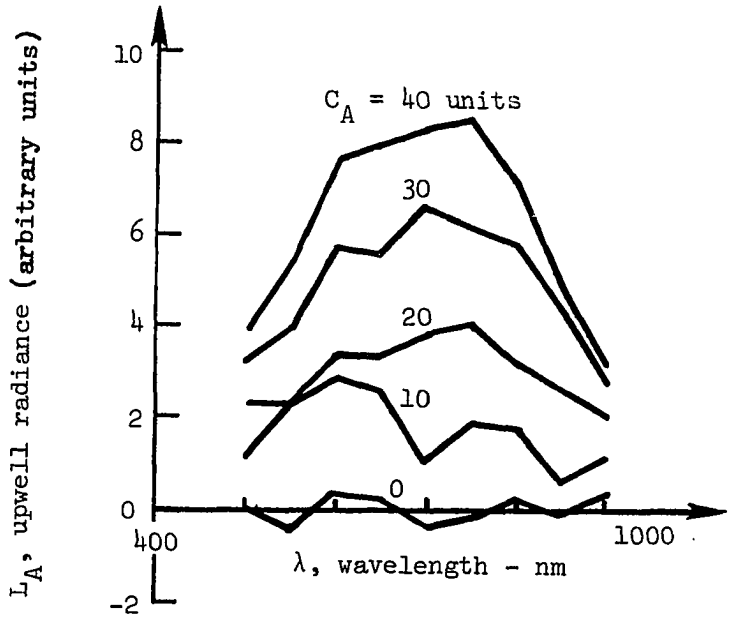

(d) 5% random noise

Figure 63.- Continued.

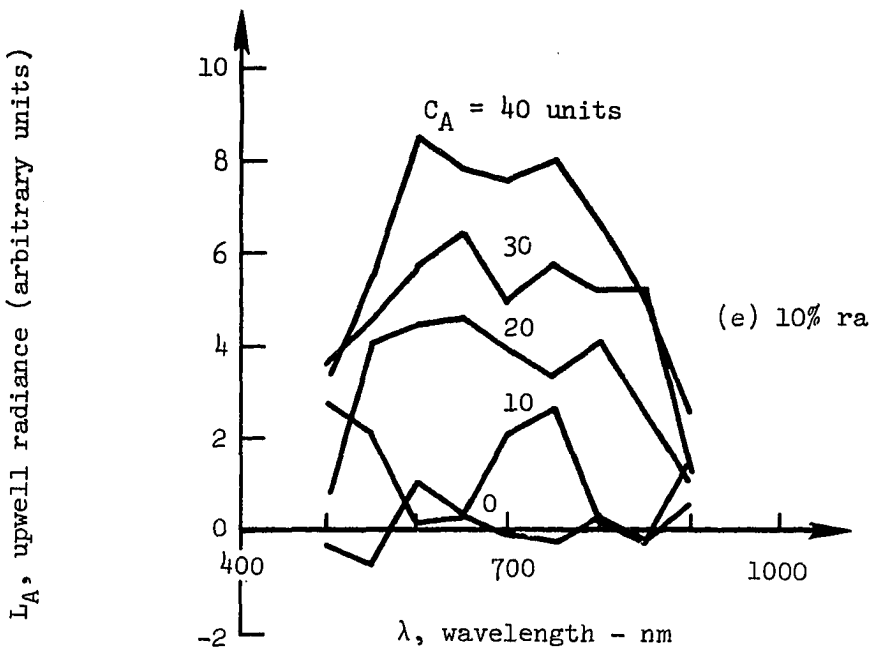

(e) 10% random noise

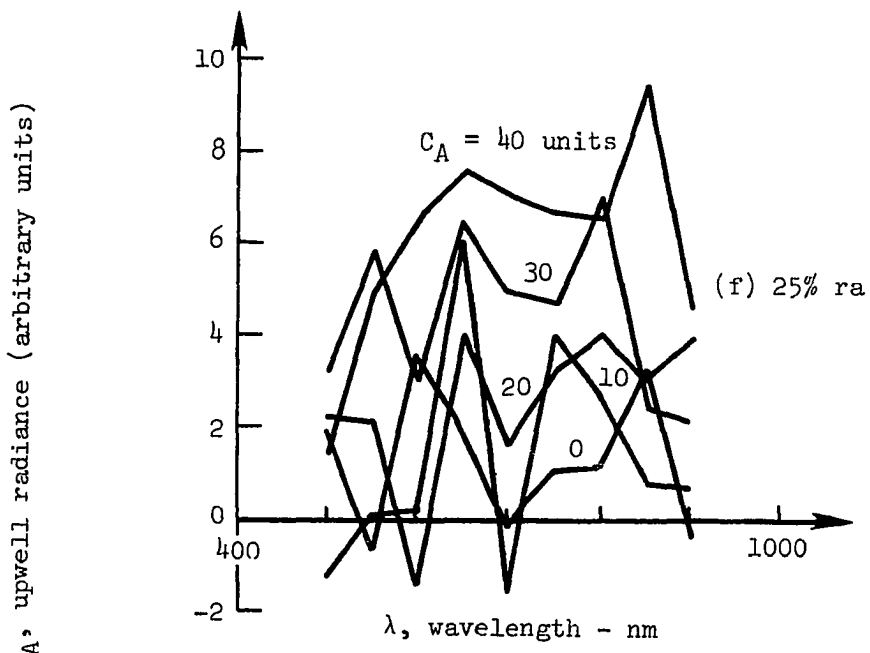

(f) 25% random noise

Figure 63.- Concluded.

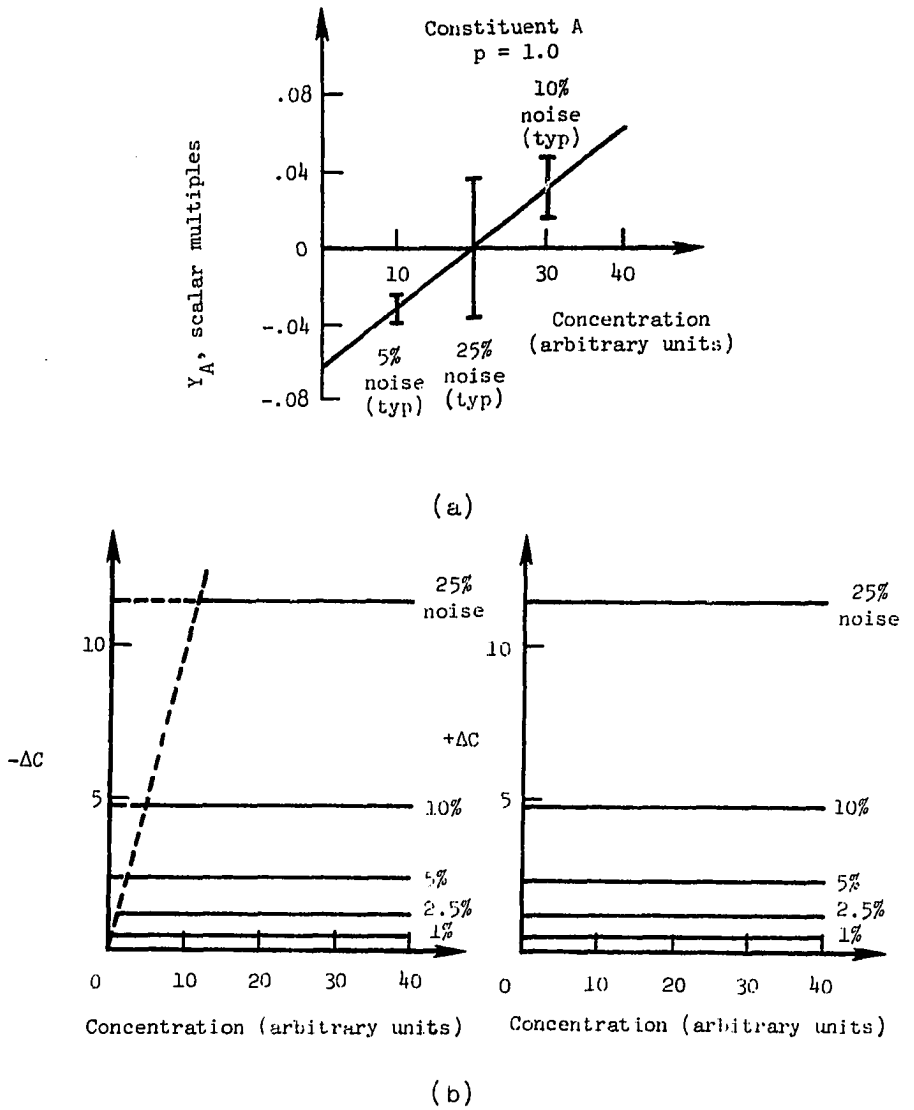

Figure 64.- (a) Scalar multiple-concentration relation for spectra of linear constituent A. (b) Concentration errors for linear constituent A associated with random noise-induced scatter in scalar multiples.

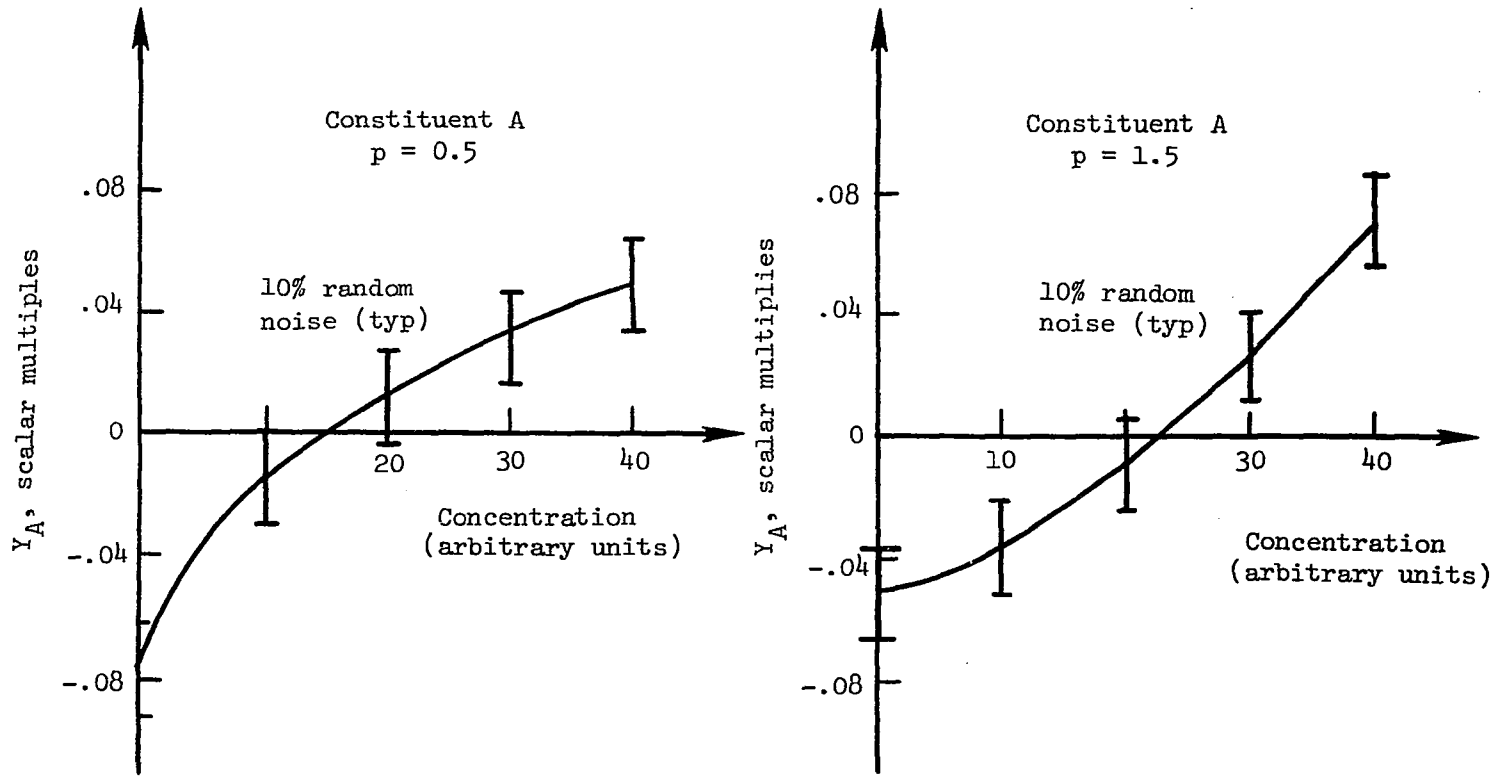

(a)

Figure 65.- (a) Scalar multiple-concentration relation for spectra of simple nonlinear constituents.

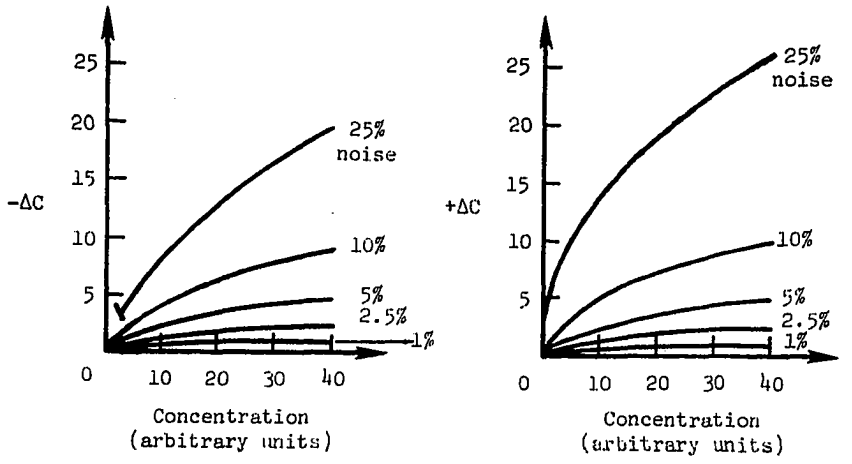

(b) Constituent A, p = 0.5

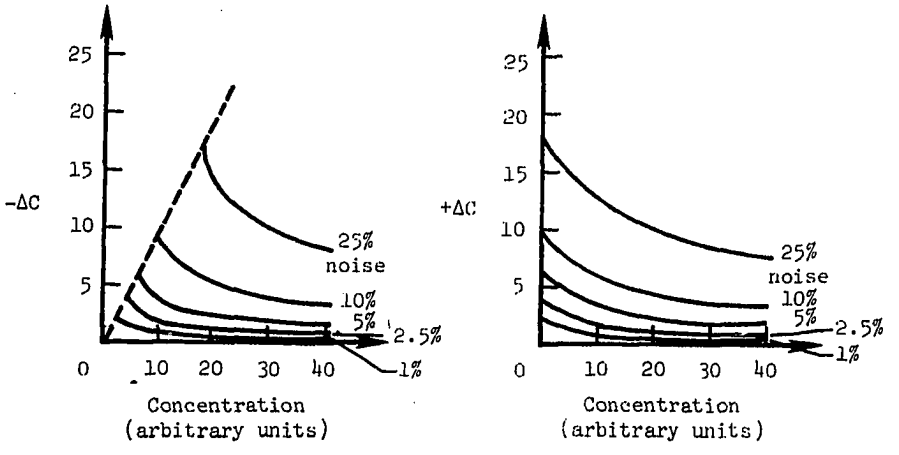

(c) Constituent A, p = 1.5

Figure 65.- (b), (c) Concentration errors associated with random noise-induced scatter in scalar multiples for simple nonlinear constituents.

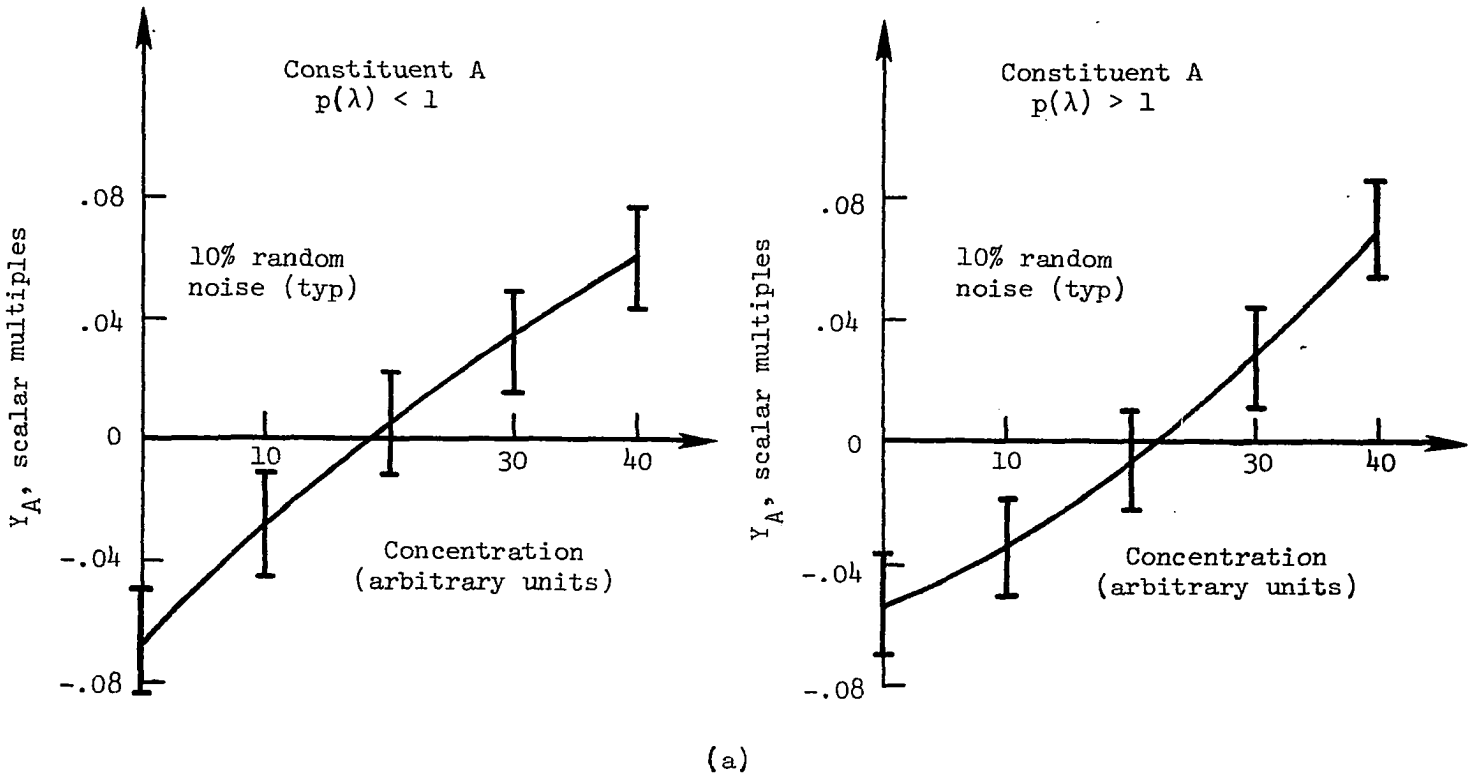

(a)

Figure 66.- (a) Scalar multiple-concentration relation for spectra of wavelength-dependent nonlinear constituents.

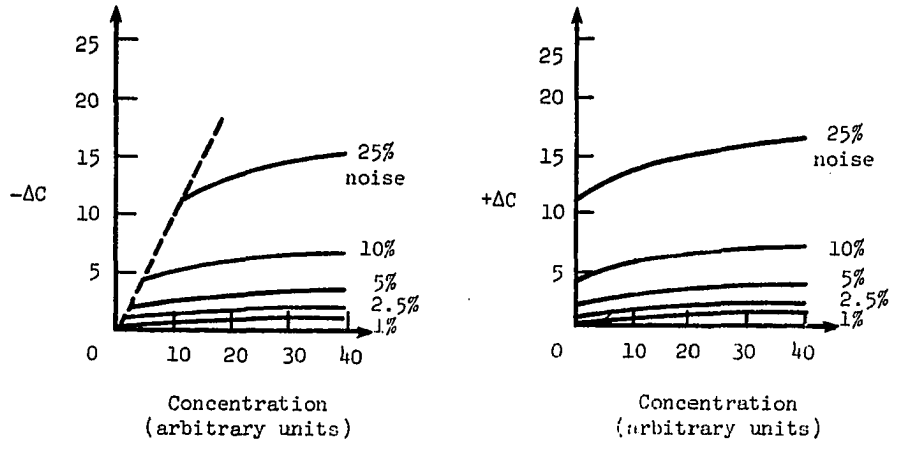

(b) Constituent A $p(\lambda) < 1$

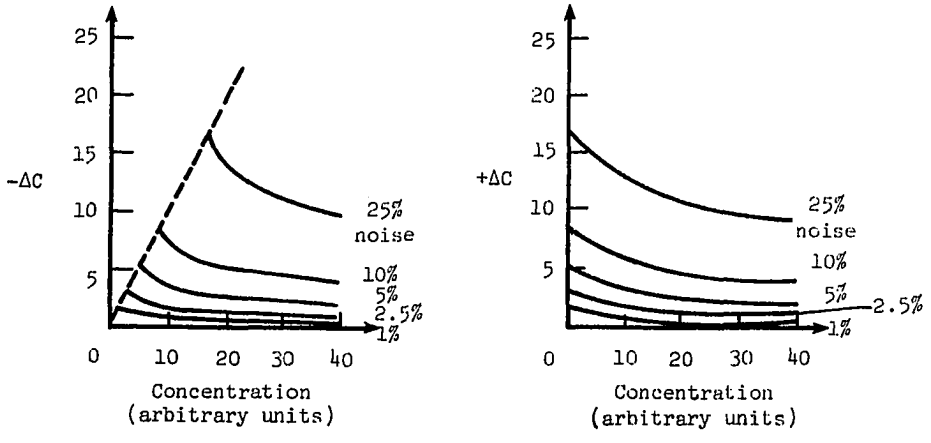

(c) Constituent A $p(\lambda) > 1$

Figure 66.- (b), (c) Concentration errors associated with random noise-induced scatter in scalar multiples for wavelength-dependent nonlinear constituents.

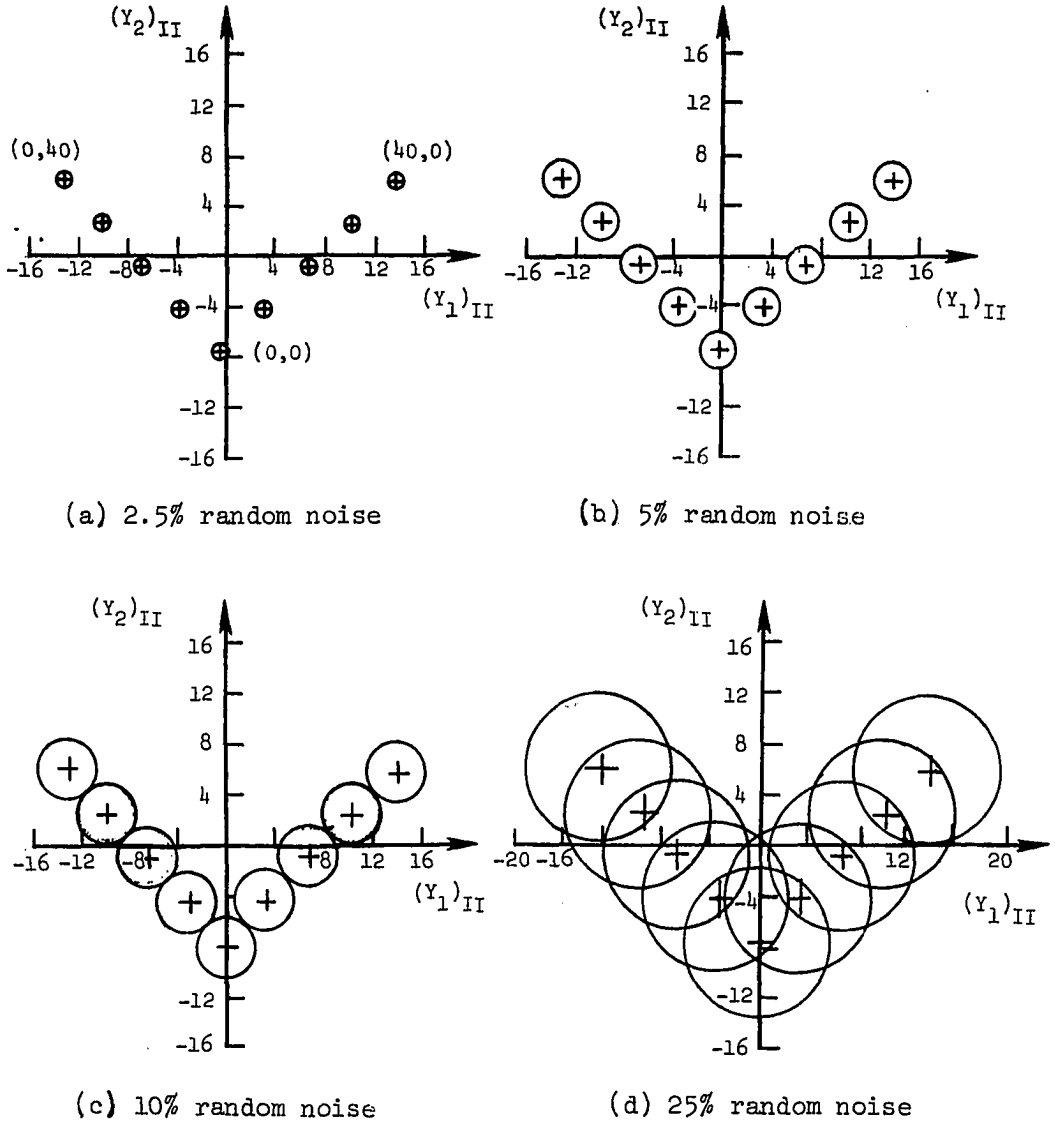

(a) 2.5% random noise

(b) 5% random noise

(c) 10% random noise

(d) 25% random noise

Figure 67.- Effects of random noise on principal component values of spatially-independent linear constituents A + B. Representative concentration pairs (C_A, C_B) labeled on (a) only.

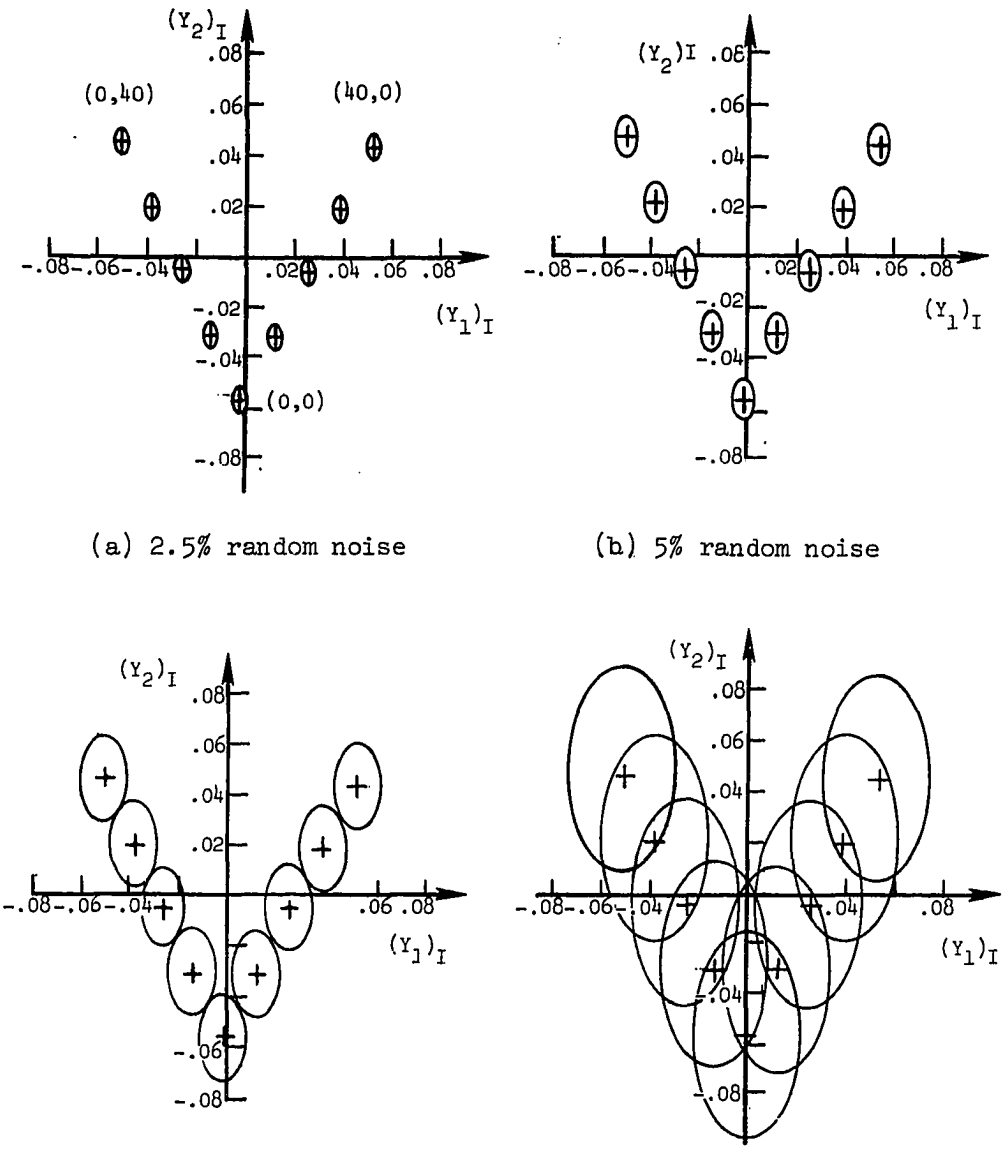

(a) 2.5% random noise

(b) 5% random noise

(c) 10% random noise

(d) 25% random noise

Figure 68.- Same as figure 67 except scalar coefficients presented in scalar multiple system.

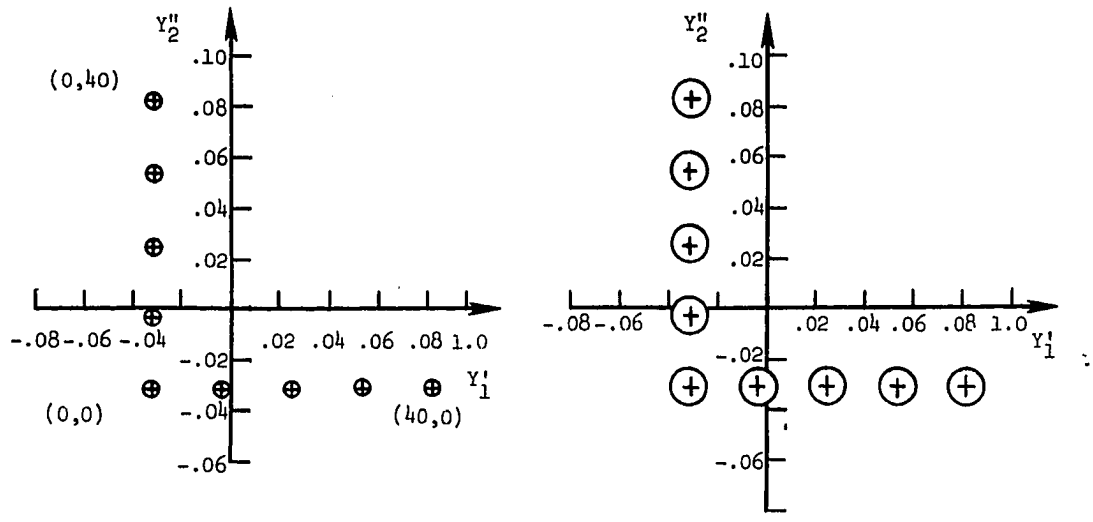

(a) 2.5% random noise

(b) 5% random noise

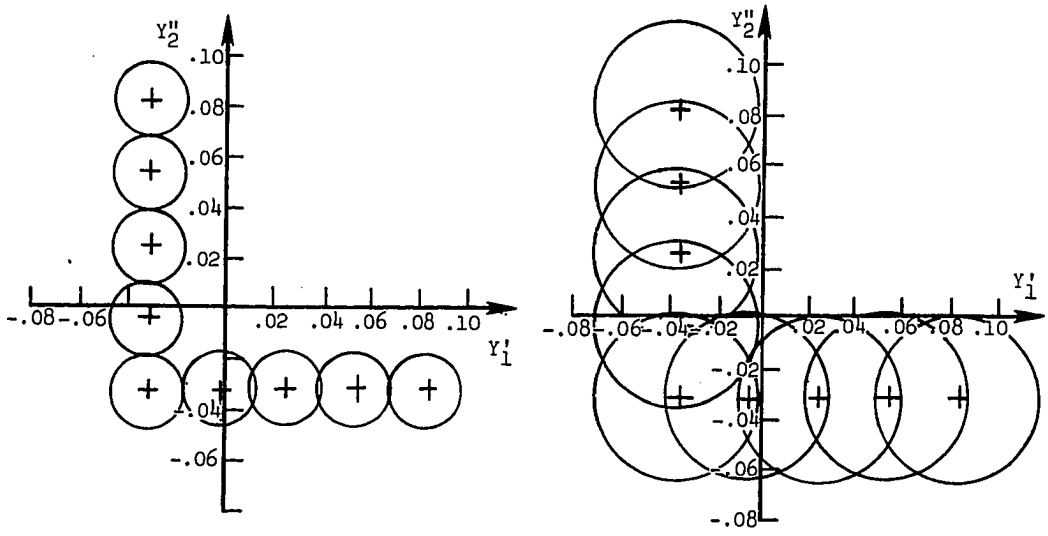

(c) 10% random noise

(d) 25% random noise

Figure 69.- Same as figure 68, except scalar multiples transferred into an oblique axis system. Representative concentration pairs (C_A, C_B) labeled on (a) only.

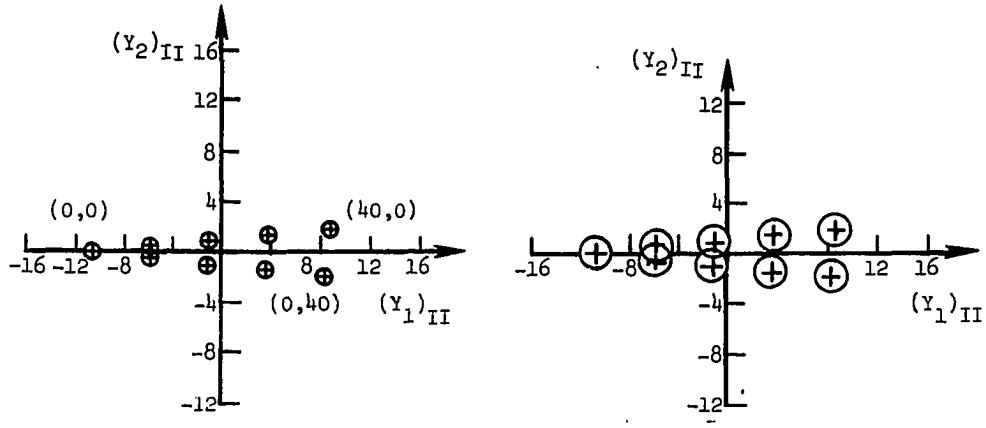

(a) 2.5% random noise

(b) 5% random noise

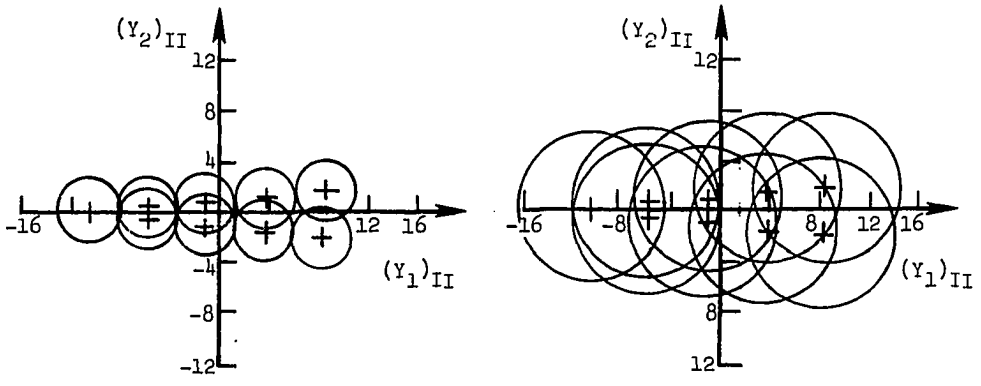

(c) 10% random noise

(d) 25% random noise

Figure 70.- Effects of random noise on principal component values of spatially-independent linear constituents A + C. Representative concentration pairs (C_A,C_C) labeled on (a) only.

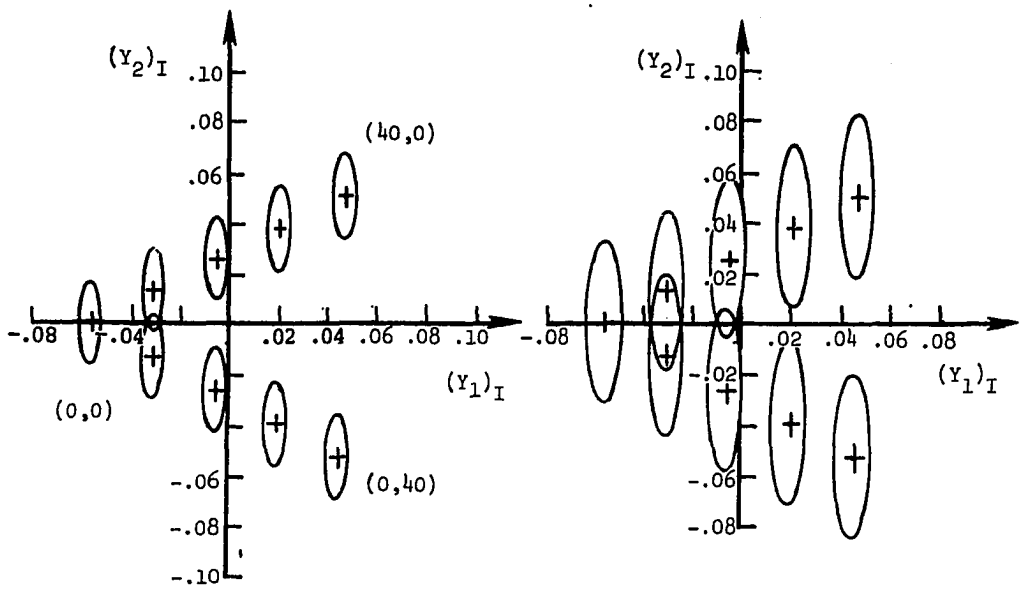

(a) 2.5% random noise

(b) 5% random noise

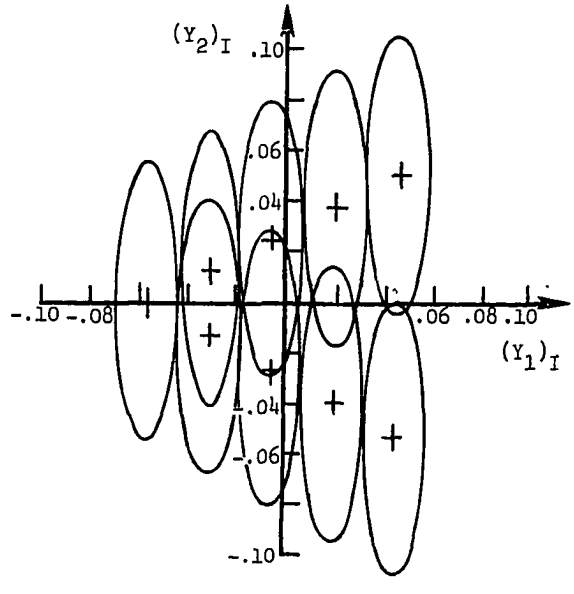

(c) 10% random noise

Figure 71.- Same as figure 70 except scalar coefficients presented in scalar multiple system.

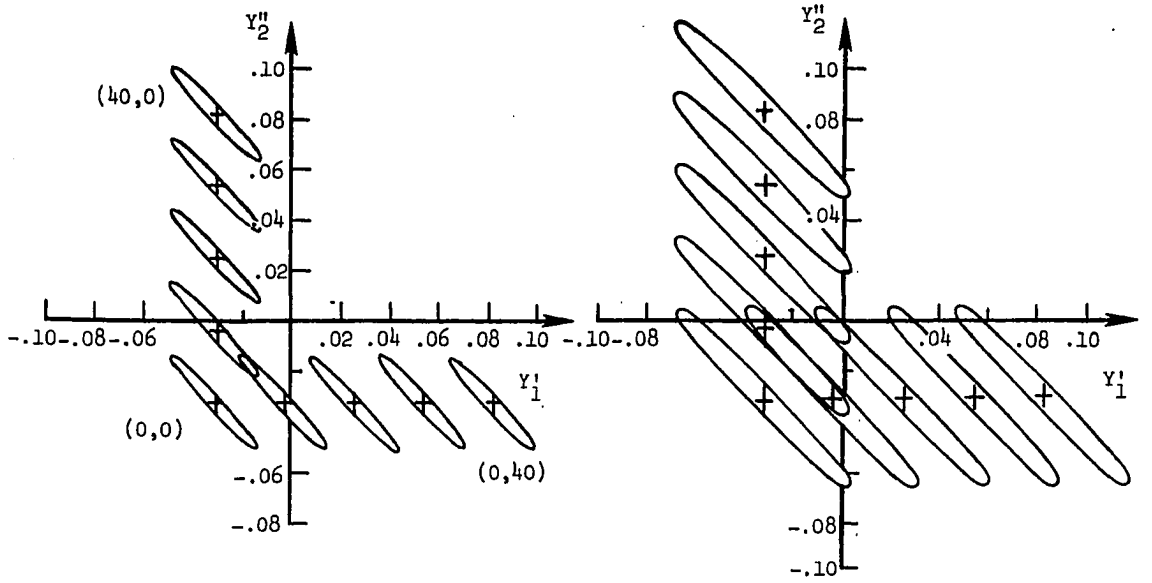

(a) 2.5% random noise

(b) 5% random noise

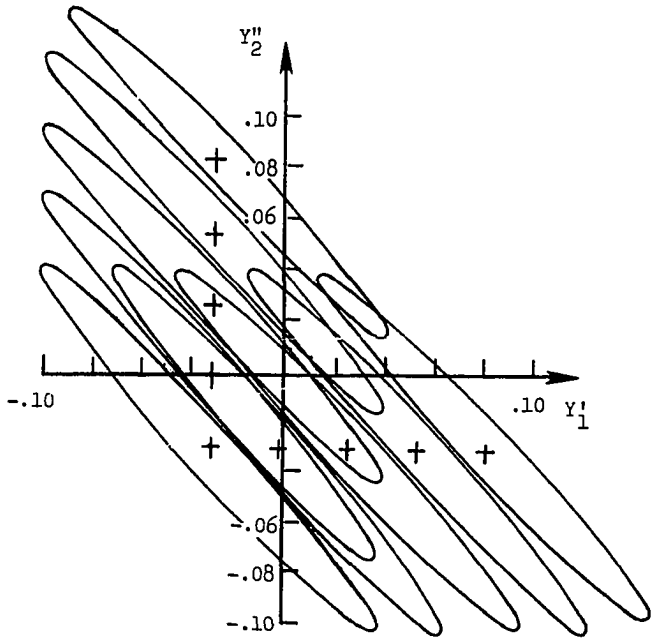

(c) 10% random noise

Figure 72.- Same as figure 71 except scalar multiples transferred into an oblique axis system. Representative concentration pairs (C_A, C_C) labeled on (a) only.

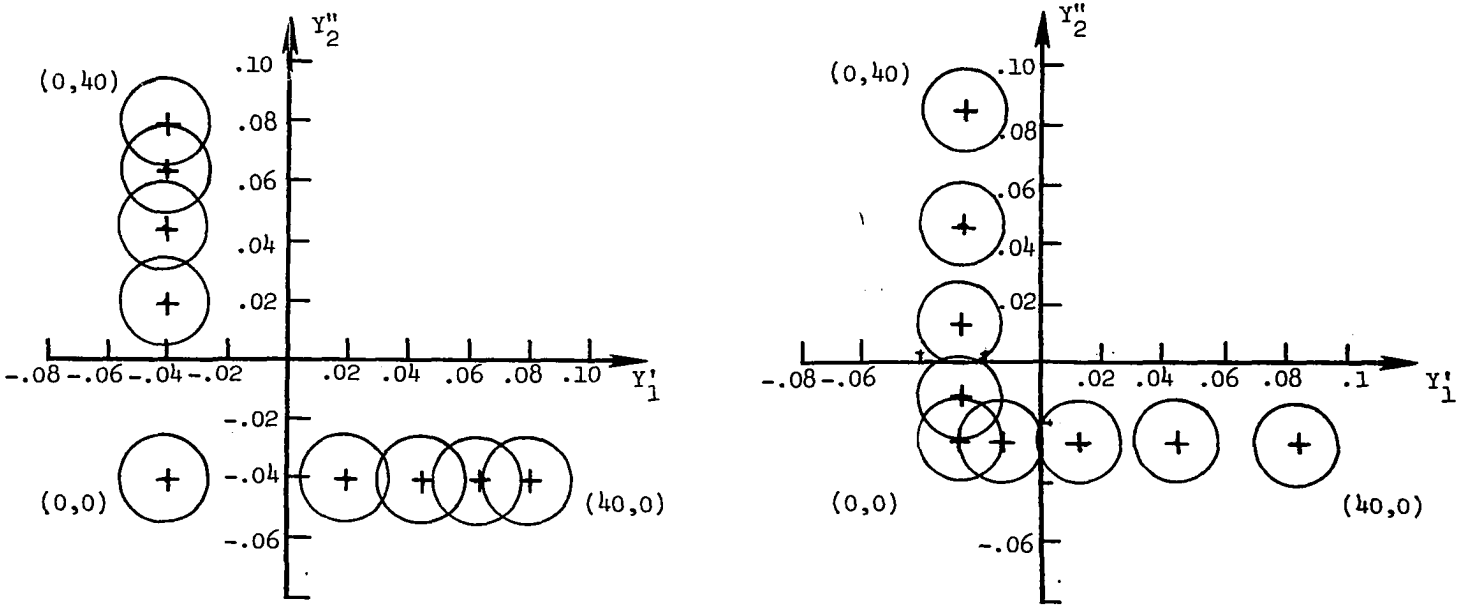

(a) 10% random noise
Constituents A + B p = 0.5

(b) 10% random noise
Constituents A + B p = 1.5

Figure 73.- Effects of random noise on transformed scalar multiples of spatially-independent, simple-nonlinear constituents A + B. Representative concentration pairs (C_A, C_B) labeled.

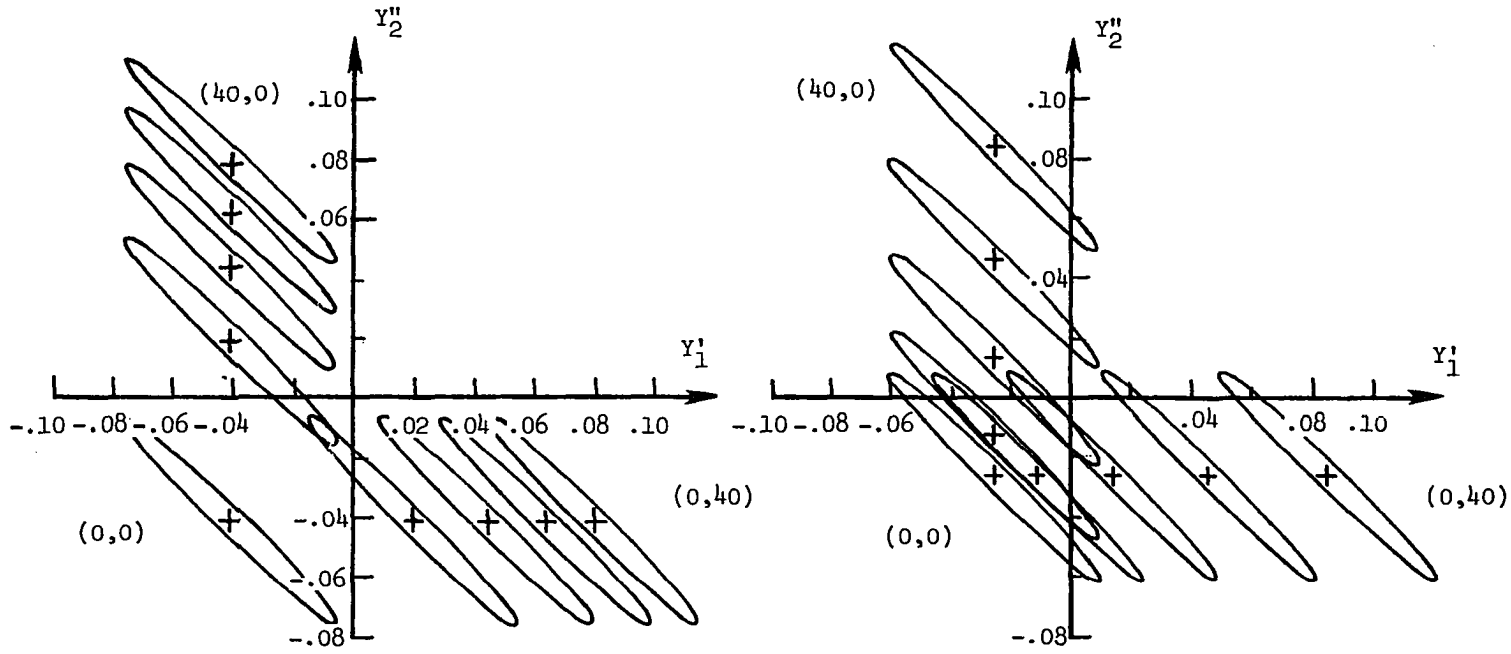

(a) 5% random noise
Constituents A + C p = 0.5

(b) 5% random noise
Constituents A + C p = 1.5

Figure 74.- Effects of random noise on transformed scalar multiples of spatially-independent, simple-nonlinear constituents A + C. Representative concentration pairs (C_A, C_C) labeled.

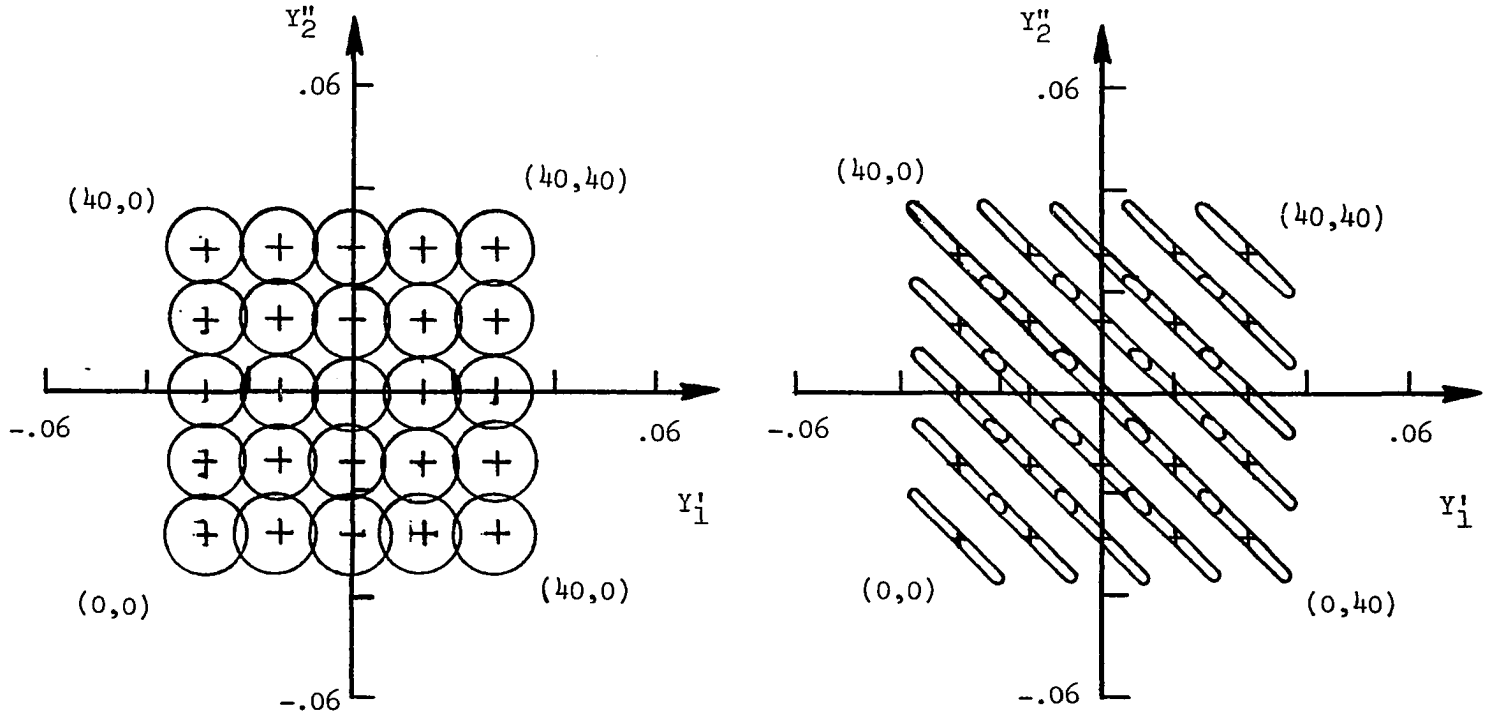

(a) Constituents A + B
10% random noise

(b) Constituents A + C
25% random noise

Figure 75.- Effects of random noise on transformed scalar multiples of mixtures of linear constituents (a) A + B and (b) A + C. Representative concentration pairs (C_A, C_B) or (C_A, C_C) are labeled.

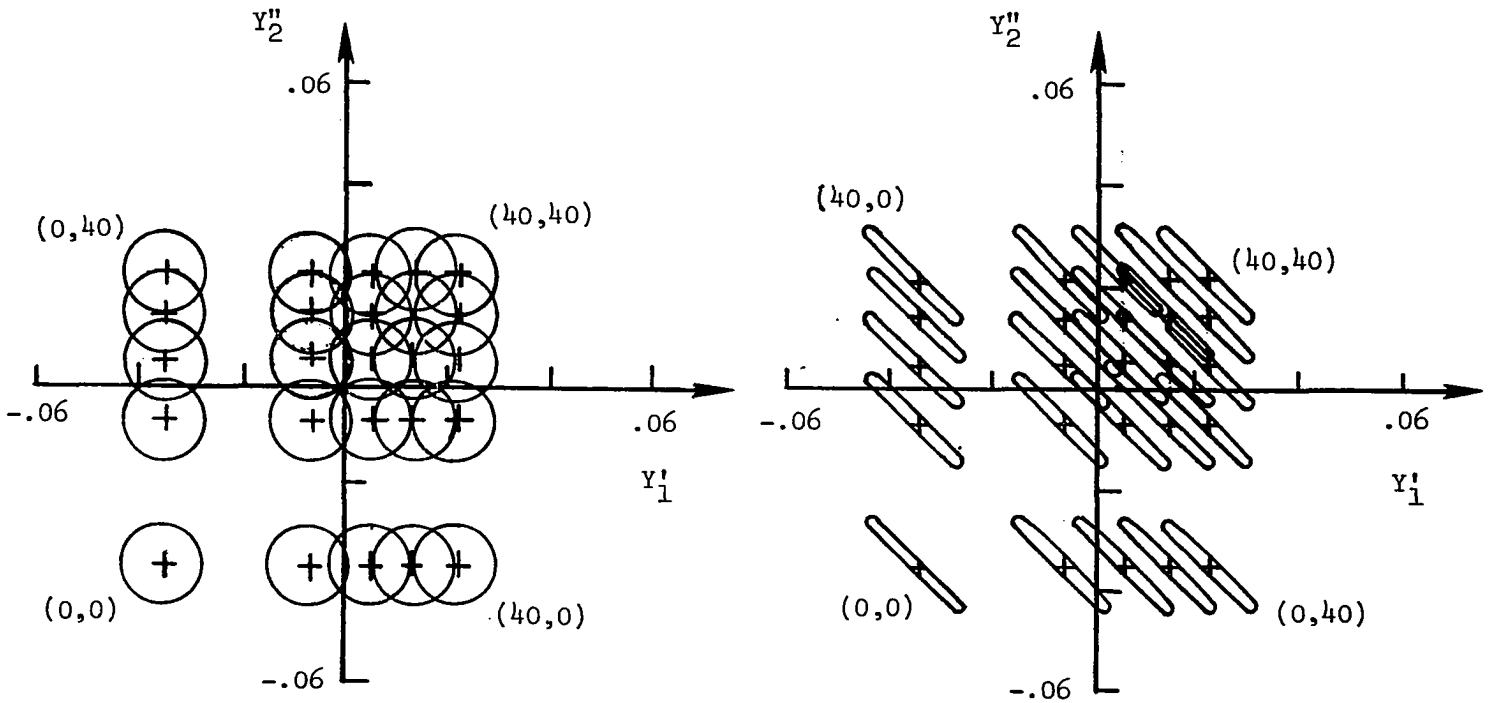

(a) Constituents A + B
10% random noise p = 0.5

(b) Constituents A + C
2.5% random noise p = 0.5

Figure 76.- Effects of random noise on transformed scalar multiples of mixtures of simple nonlinear constituents (a) A + B and (b) A + C. Power p = 0.5. Representative concentration pairs (C_A, C_B) or (C_A, C_C) are labeled.

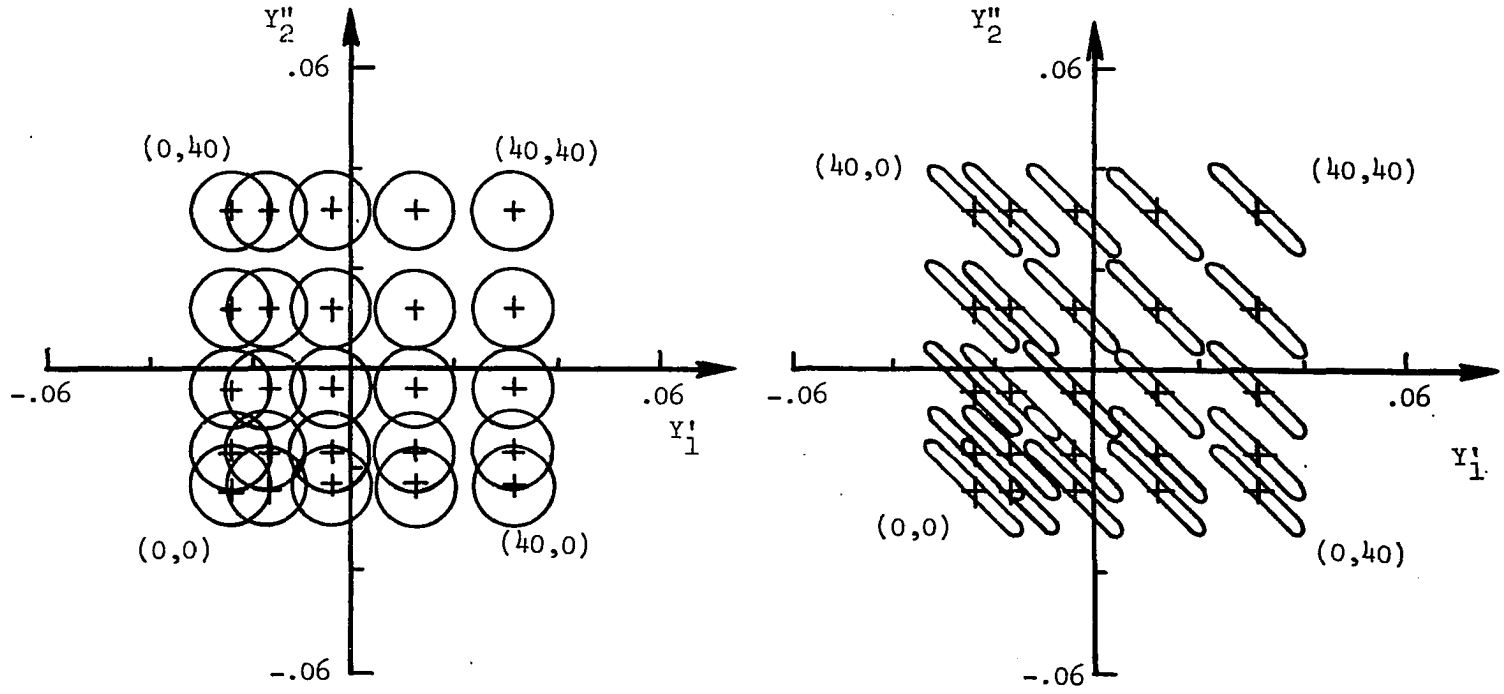

(a) Constituents A + B
10% random noise p = 1.5

(b) Constituents A + C
2.5% random noise p = 1.5

Figure 77.- Same as figure 76 except power p = 1.5.

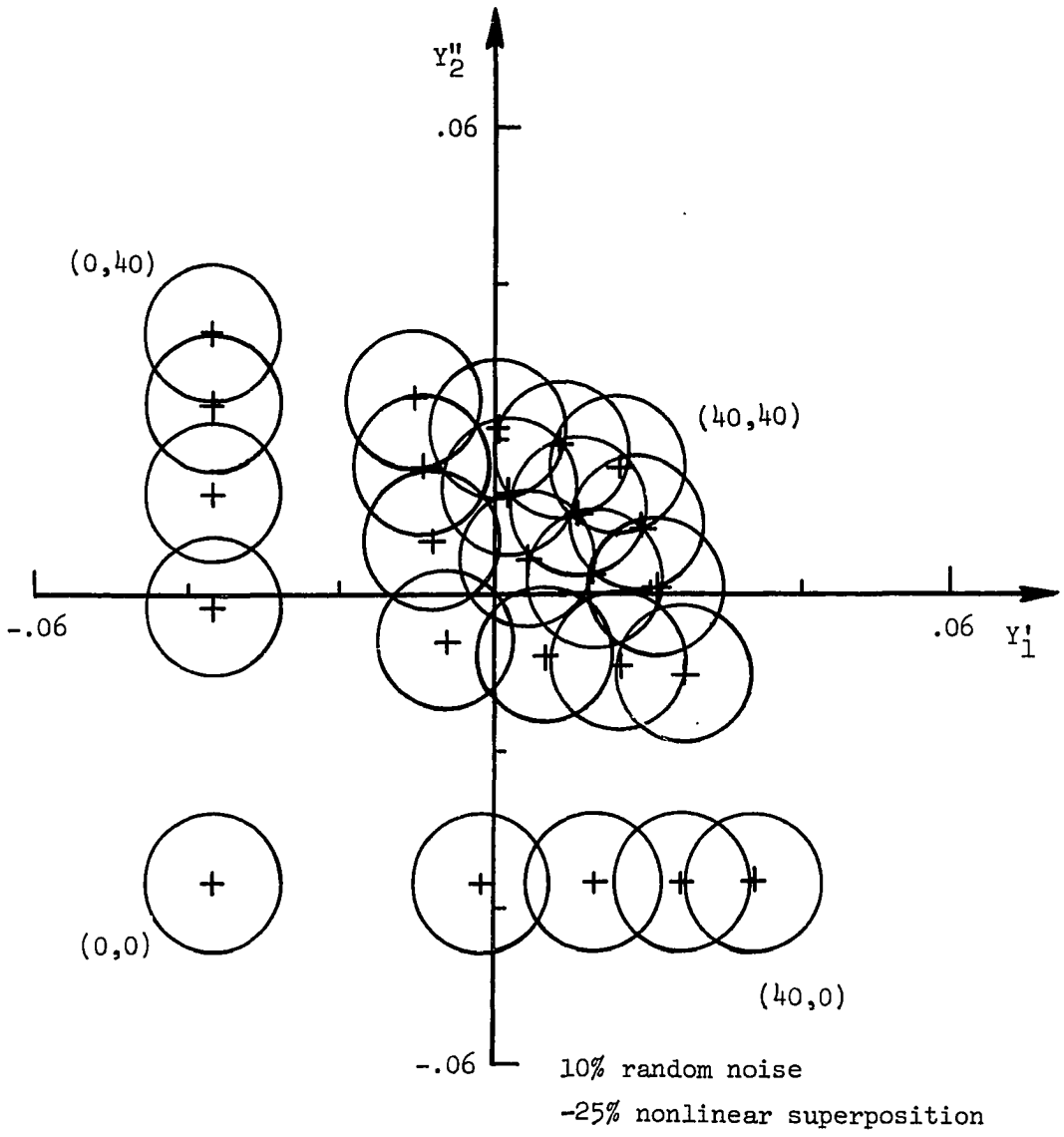

Figure 78.- Effects of random noise on transformed scalar multiples of nonlinear superposition mixture of simple-nonlinear constituents A + B. Representative concentration pairs (C_A,C_B) are labeled.

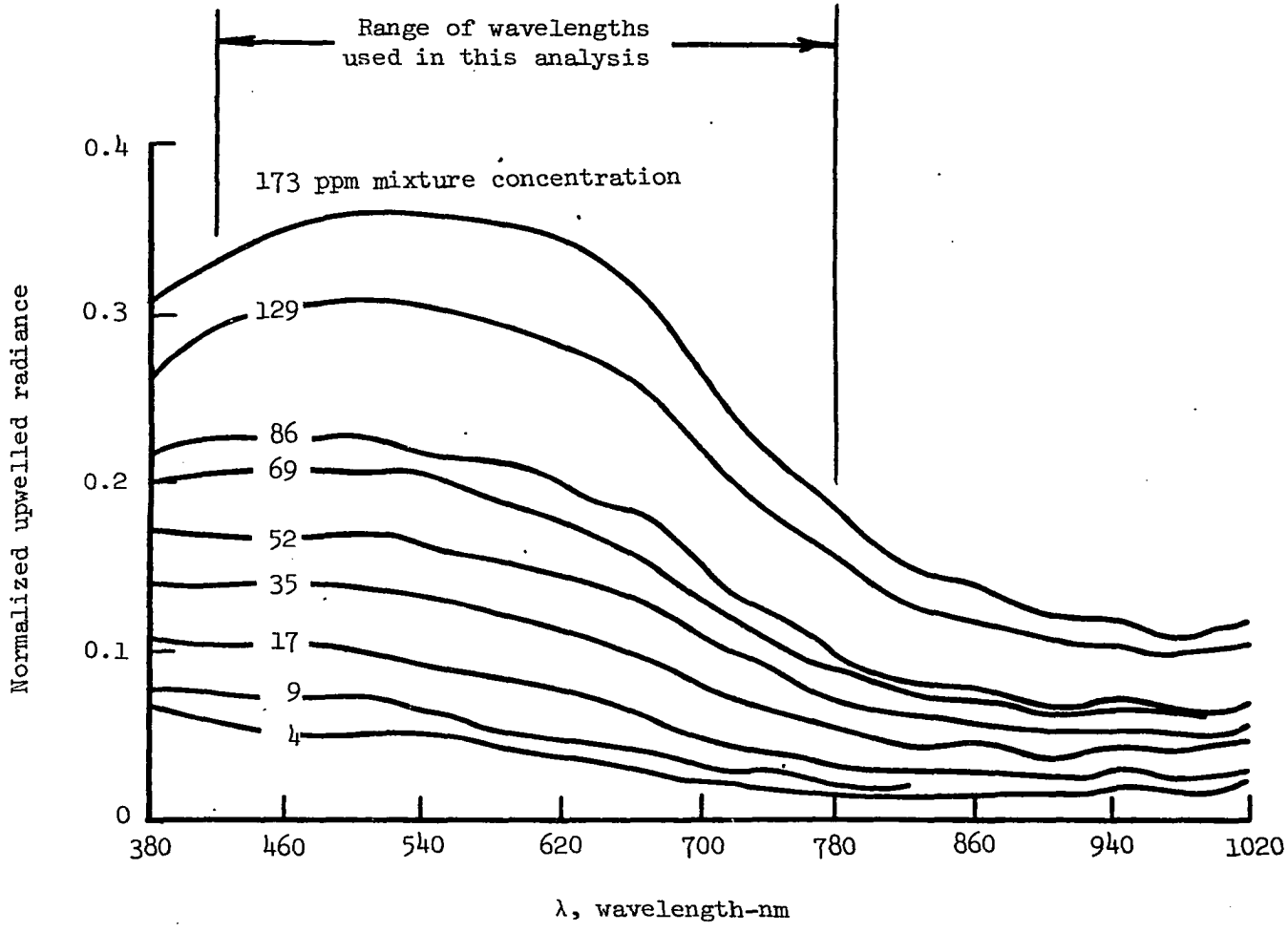

(a) Ball clay soil

Figure 79.- Measured normalized upwell spectra for (a) Ball clay soil and (b) feldspar soil. (After Whitlock 1977a).

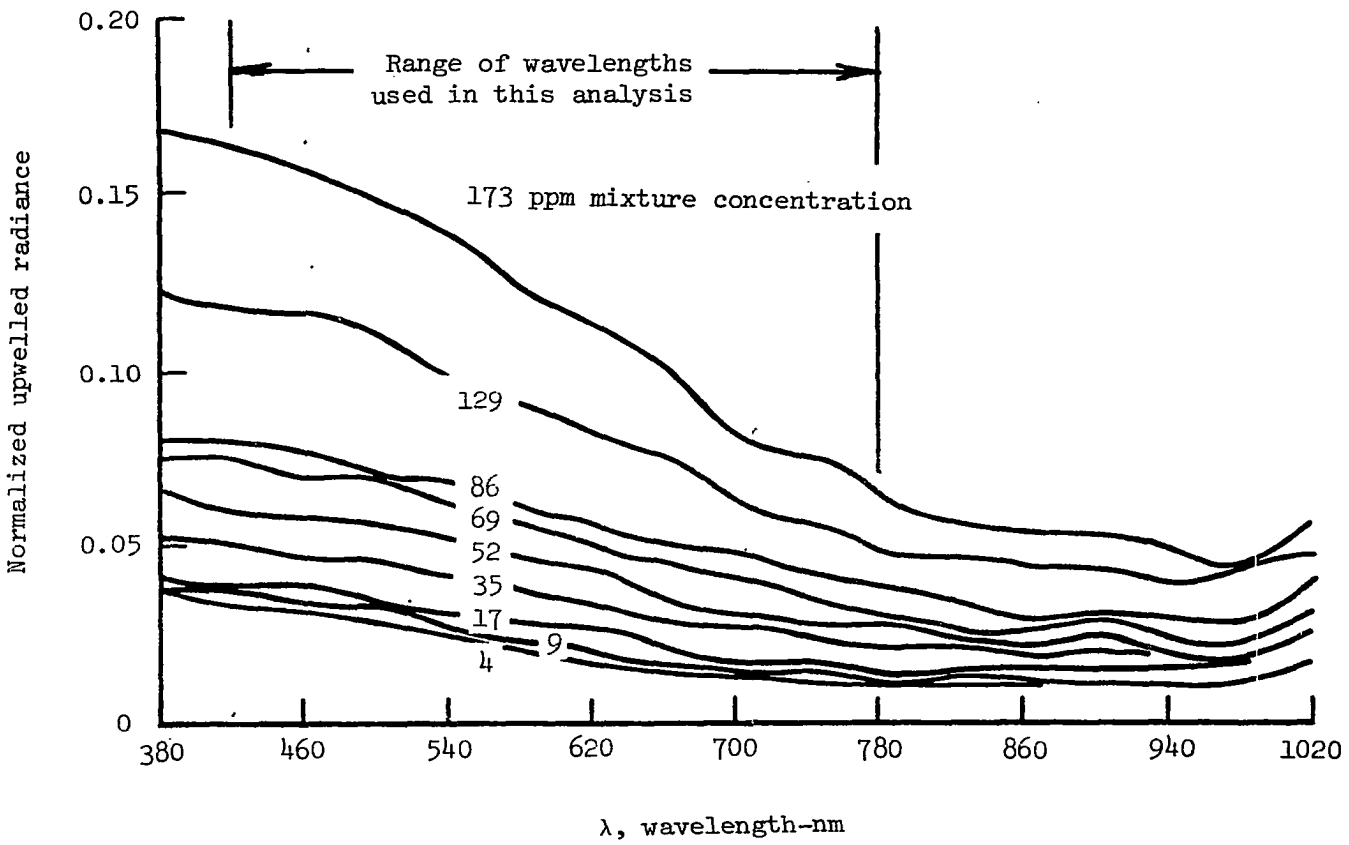

(b) Feldspar soil

Figure 79.- Concluded.

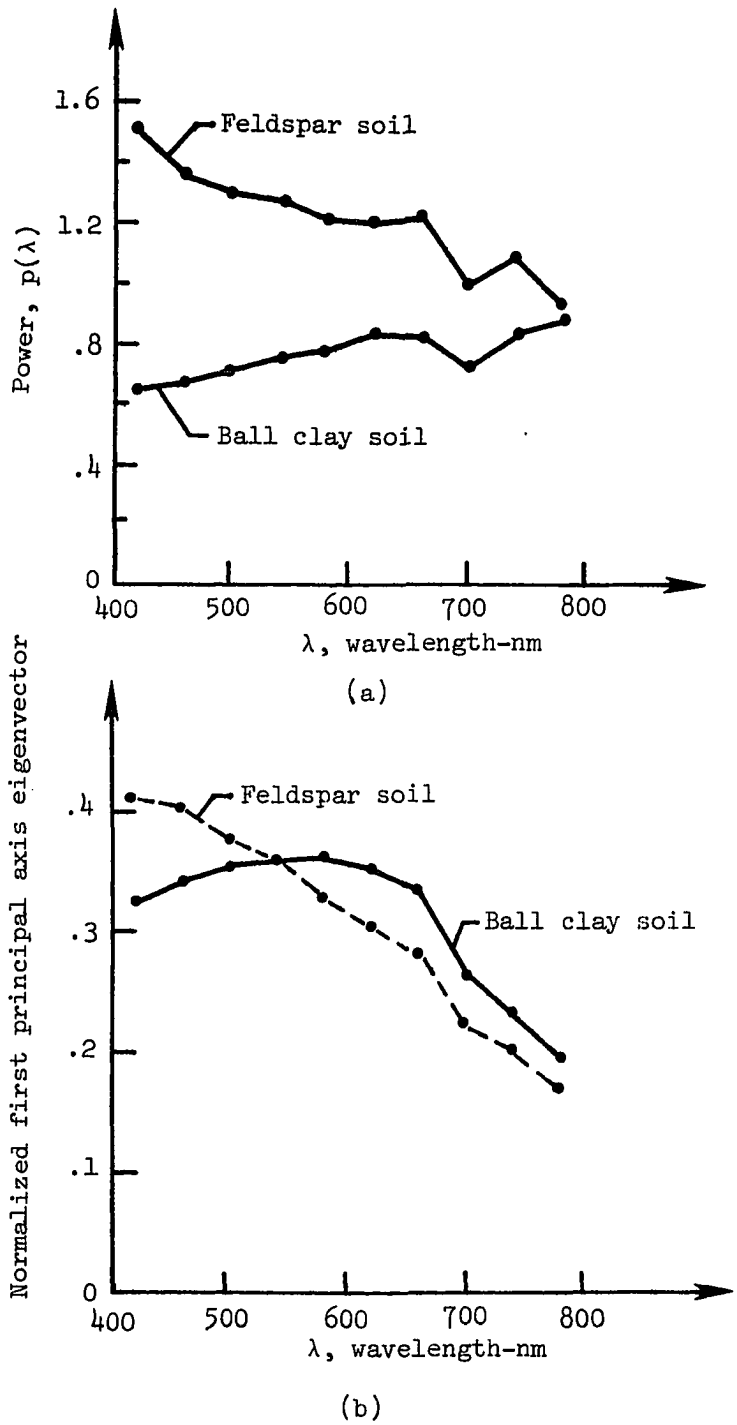

Figure 80.- (a) Spectral powers from power-law model regression fit to ball clay and feldspar soils constituent spectra. (b) Normalized first principal axes eigenvectors for same constituent spectra.

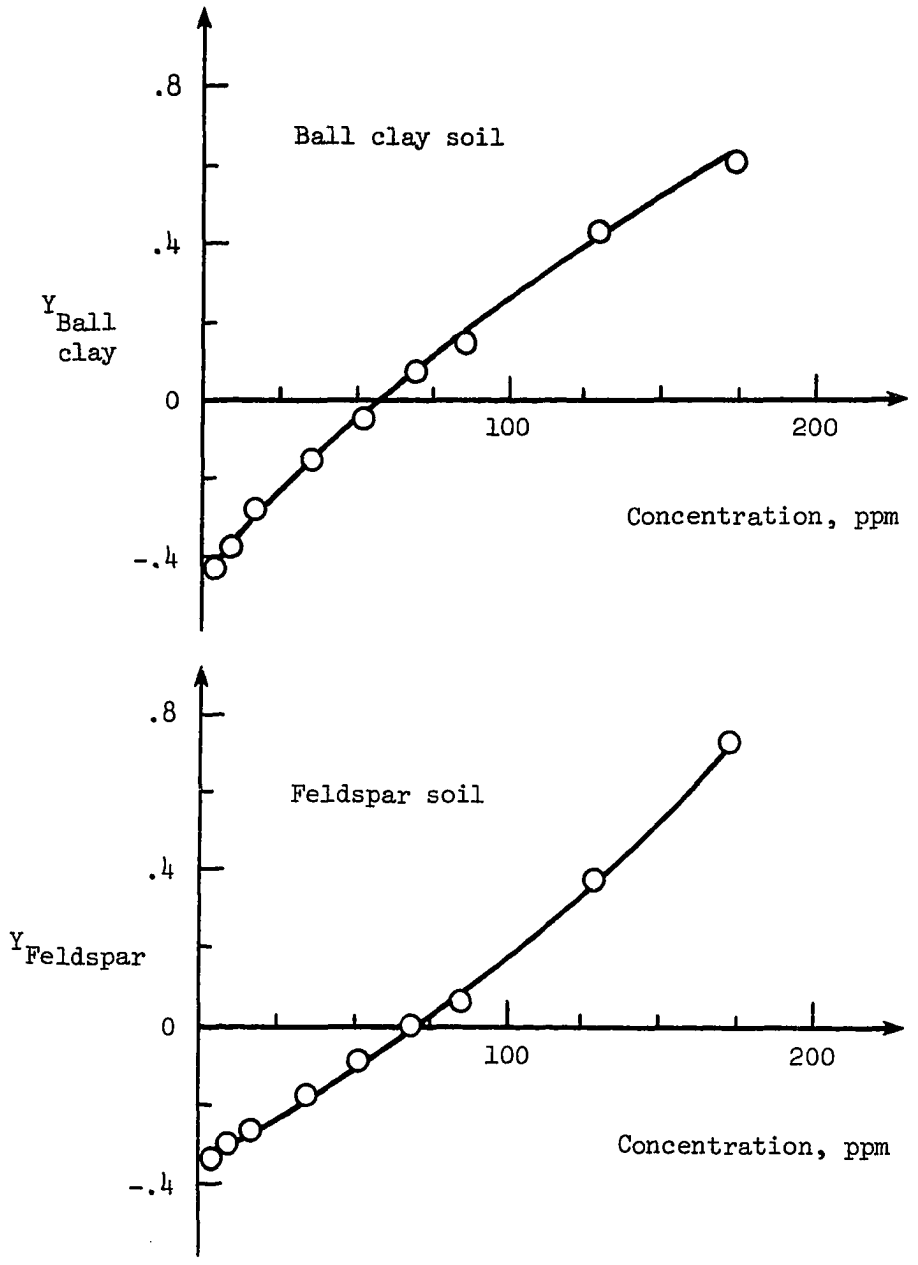

Figure 81.- Scalar multiples as a function of concentration for individual spectral measurements of Ball clay and feldspar soils.

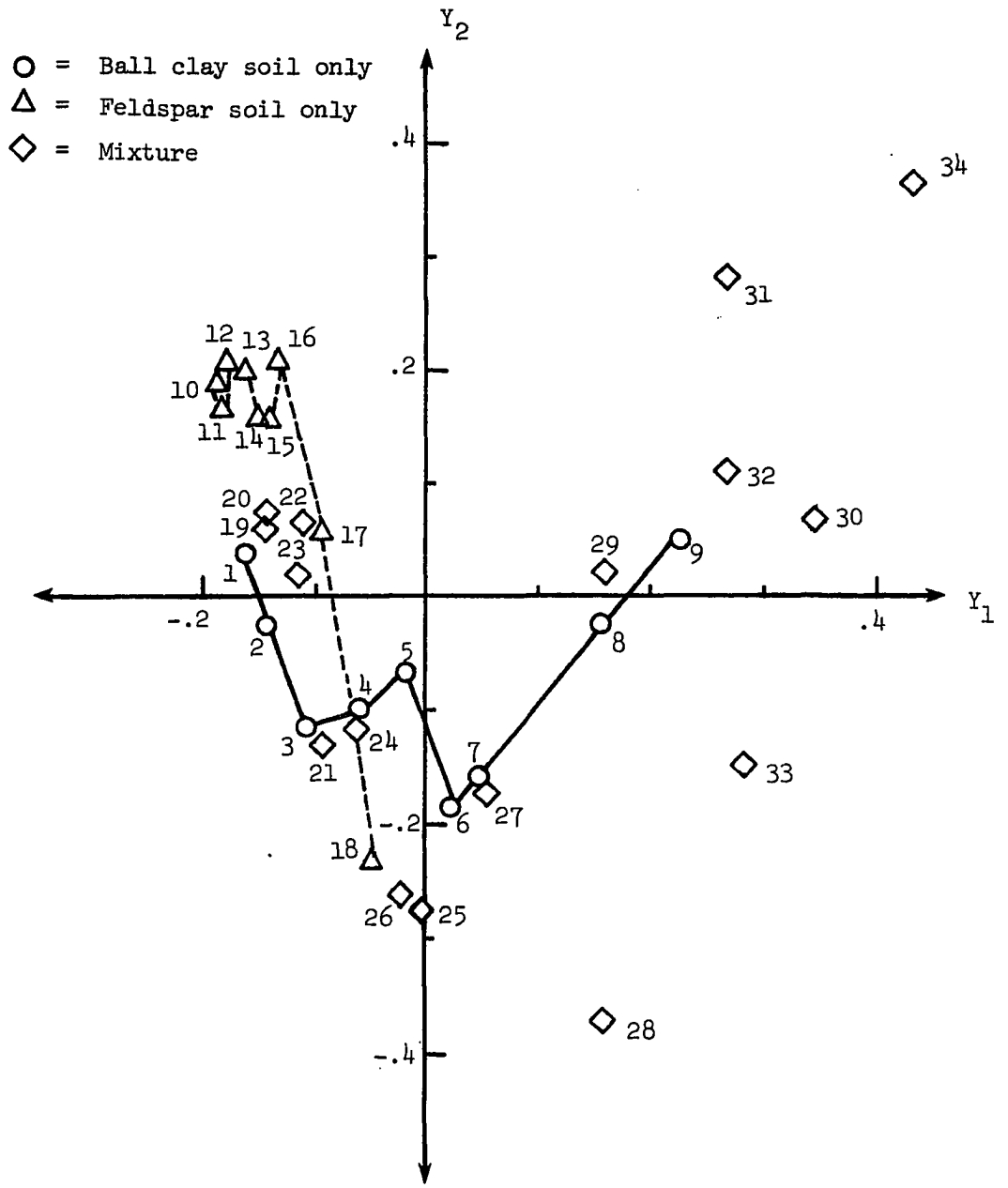

Figure 82.- Scalar multiples associated with first two principal axis eigenvectors for Ball clay-feldspar soils experiment data. Spectra numbers are noted.

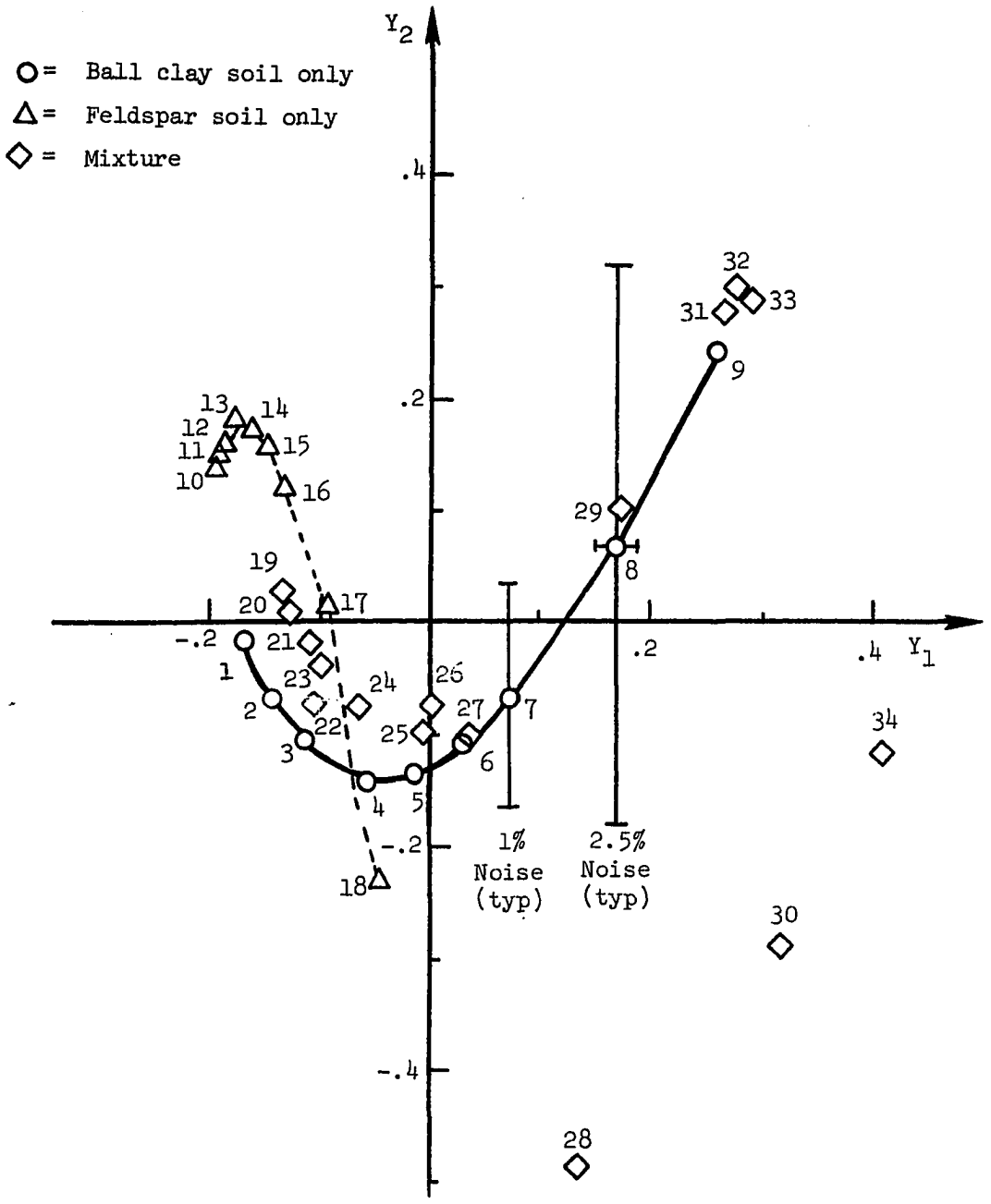

Figure 83.- Scalar multiples for characteristic vector analysis of processed (power fit and linear superposition) spectra for Ball clay-feldspar soils experiment. Spectra numbers are noted.

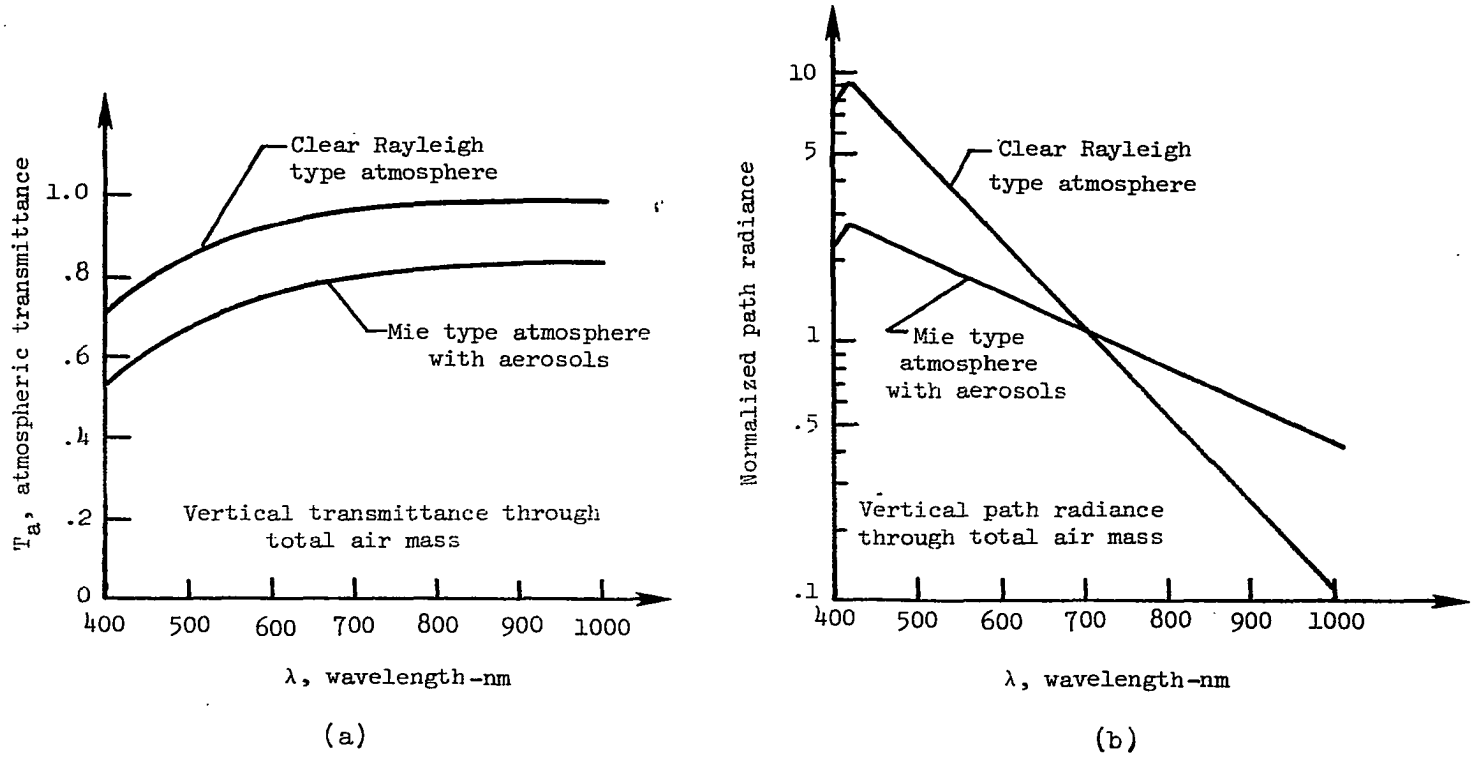

Figure 84.- Spectral vertical transmittance and normalized path radiance through total air mass.

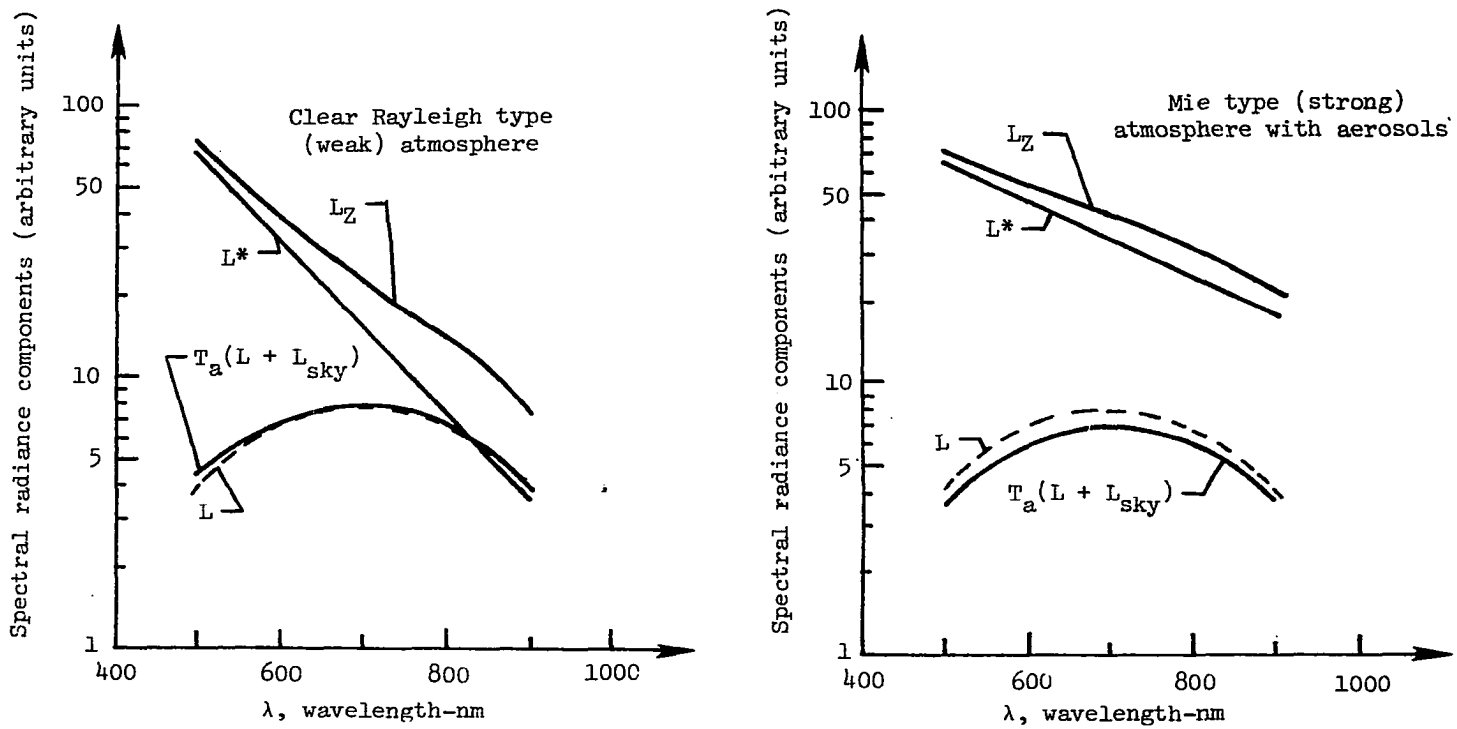

Figure 85.- Sample computed spectral radiance components for a weak and strong atmosphere as observed by a sensor above the atmosphere. (Upwell radiance, L, for linear constituent A, C_A = 40 units).

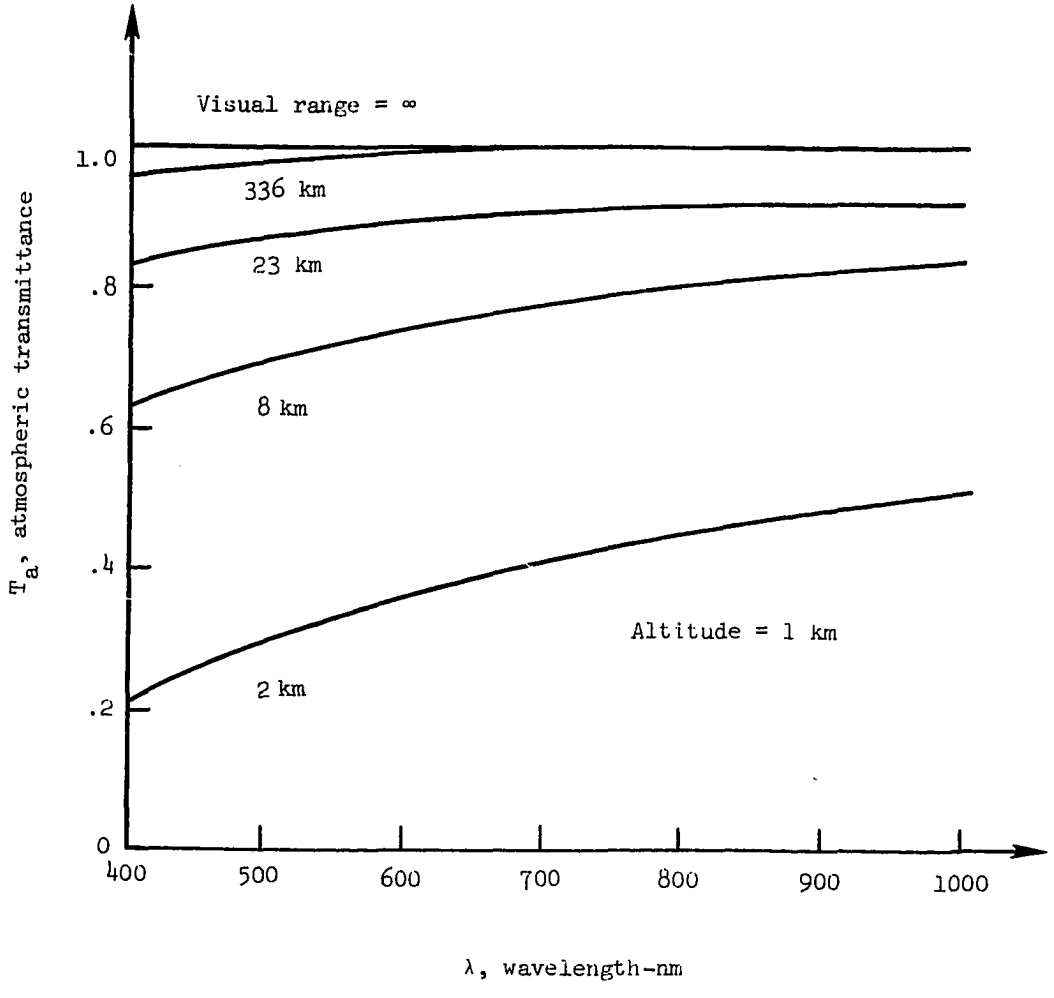

Figure 86.- Spectral atmospheric transmittance for varying visual ranges for nadir viewing for 1 km altitude.

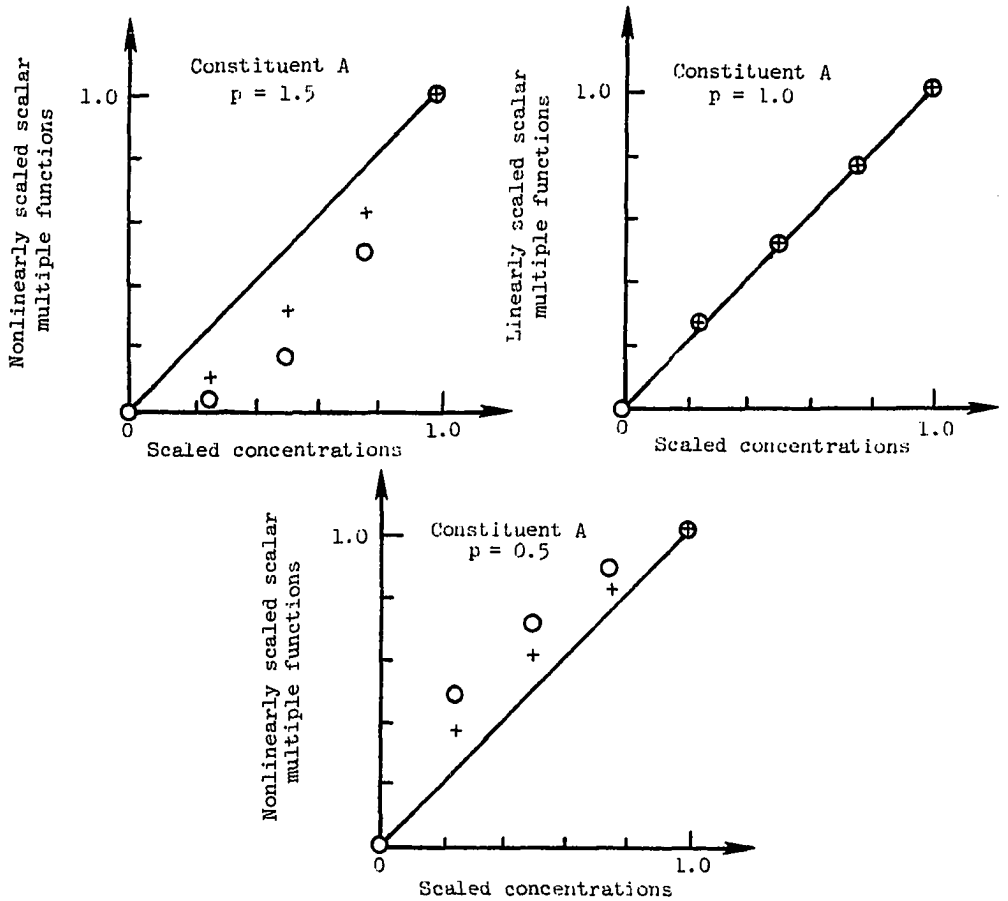

Figure 87.- Comparison between scaled scalar multiple functions and scaled concentrations for constituent A (variable powers) under the influence of variable atmospheres. Crosses (+) represent a weak-strong atmosphere variation. Circles (O) represent a strong-weak atmosphere variation.

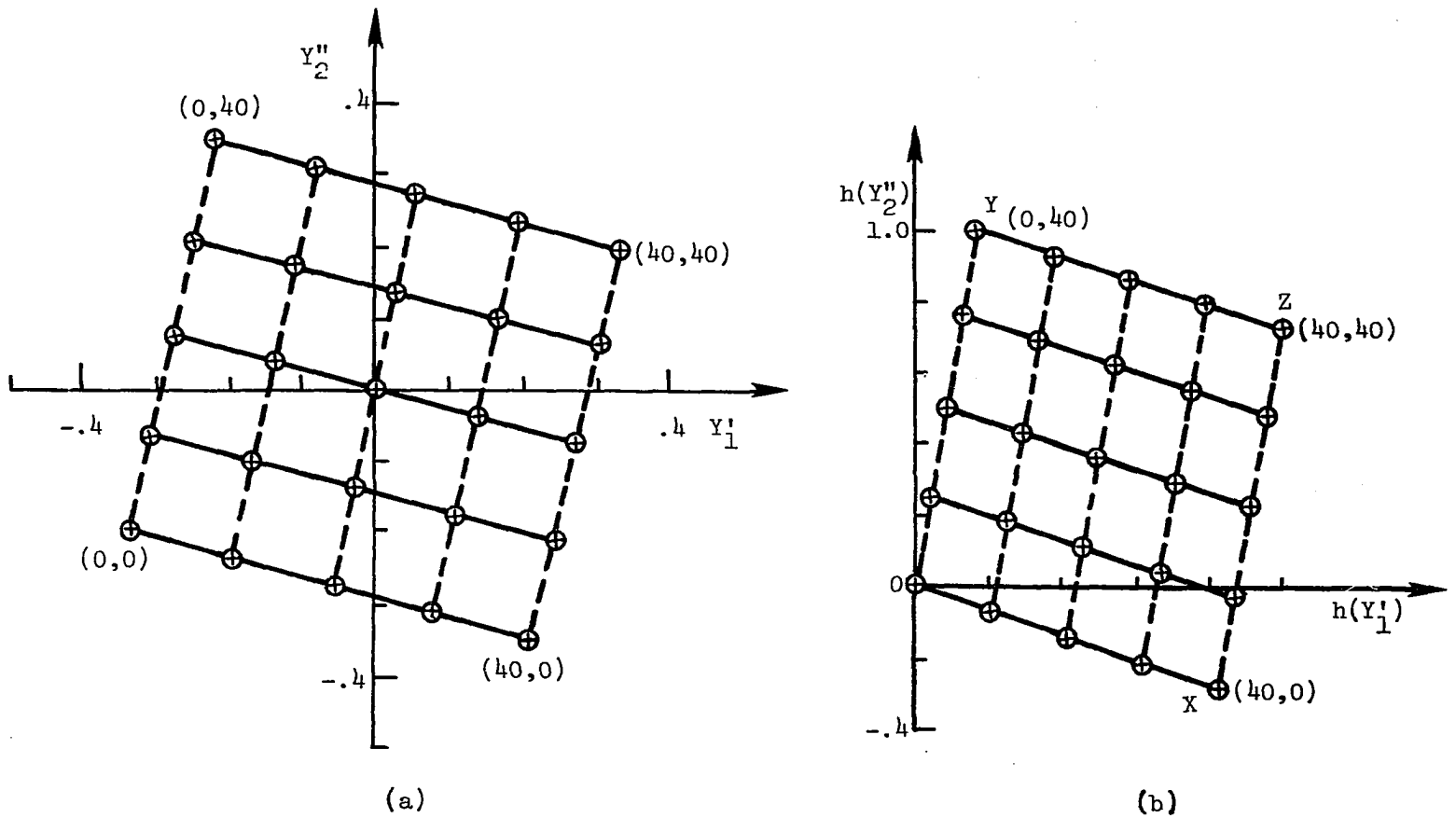

Figure 88.- (a) Transformed scalar multiples in oblique axes system for mixtures of linear constituents A + C for spectra modified by a strong atmosphere. Constituent concentrations (C_A, C_C) indicated. (b) Same example with linear scaling.

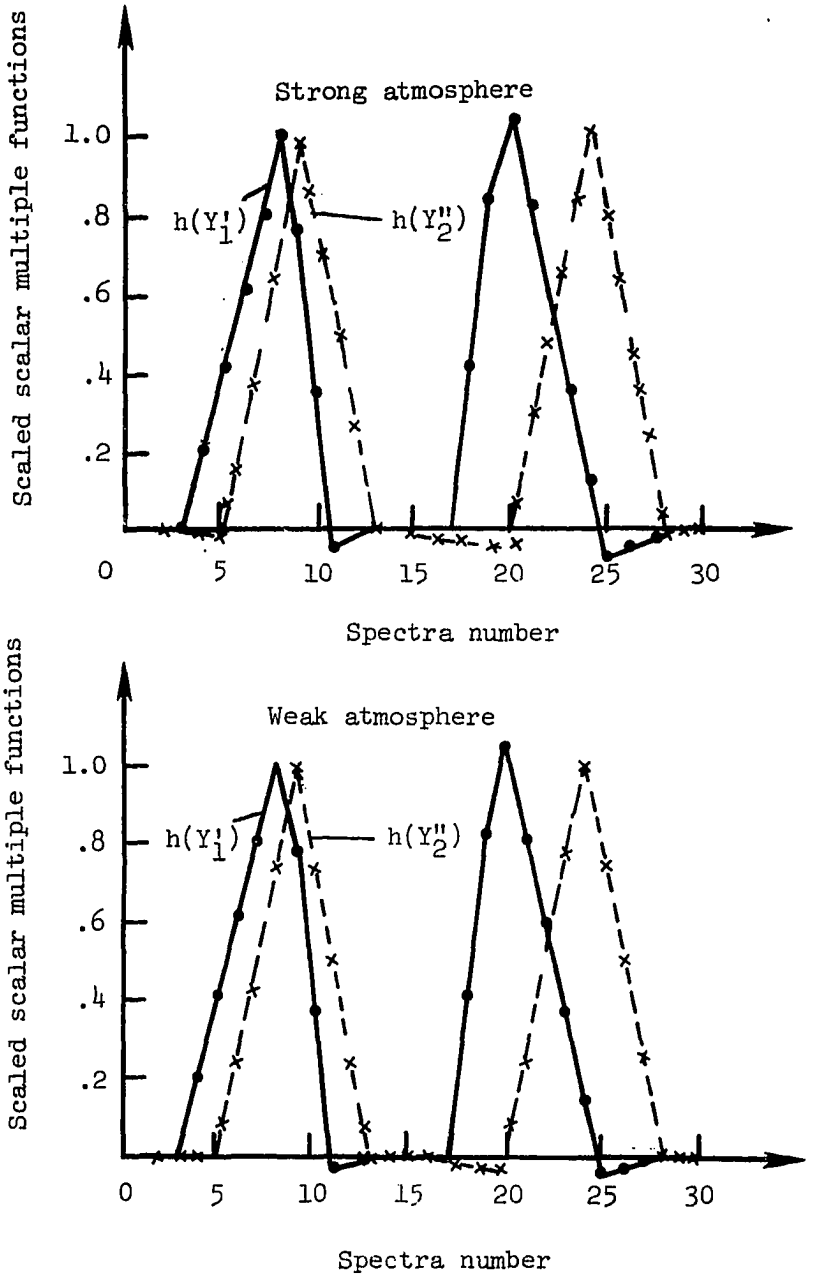

Figure 89.- Relative quantification scaling results for 30-spectra flight case for linear constituents A+B with (a) spectra modified by strong atmosphere and (b) spectra modified by weak atmosphere. Compare with figure 27b for no atmosphere.

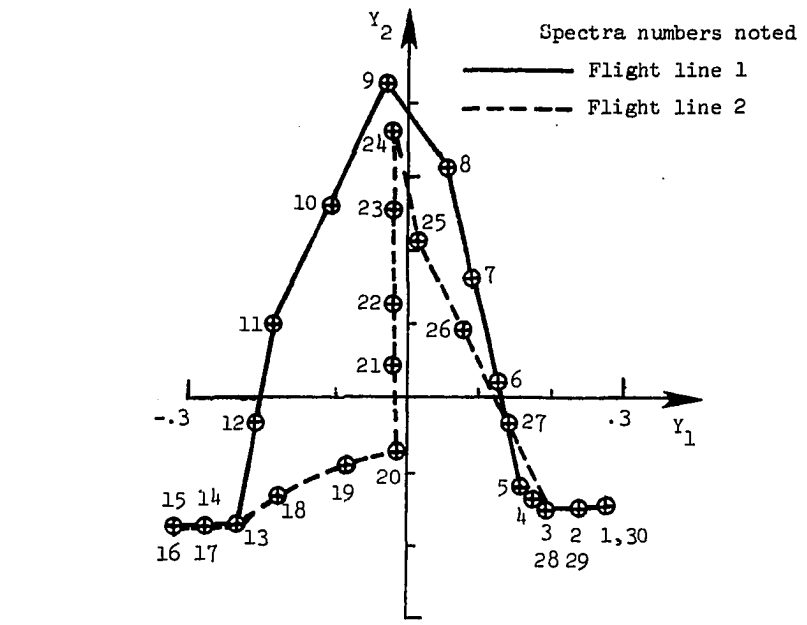

(a)

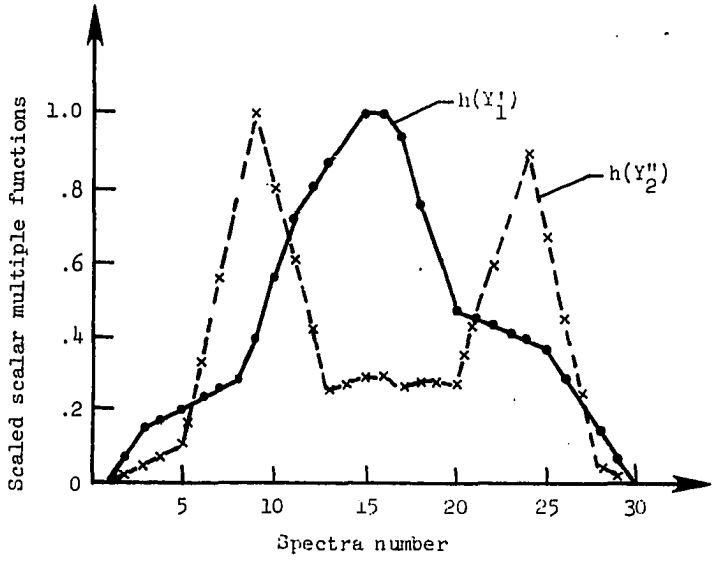

(b)

Figure 90.- (a) Scalar multiples for 30-spectra flight case using linear constituents A + B with variable strong-weak atmosphere. (b) Scaled (transformed) scalar multiple functions for same case. Compare with figure 27b for atmosphere-free case.

BIOGRAPHY

Theodore A. Talay

BORN:

February 13, 1946, Flushing, New York

EDUCATION:

B.A.E., June 1967, Rensselaer Polytechnic Institute
M.A.E., February 1970, Rensselaer Polytechnic Institute
Ph.D. Candidate, September 1978 to Present, Old Dominion University

POSITION:

NASA Langley Research Center, Research Aerospace Engineer (1970 - present)

HONORS AND AWARDS:

Five NASA awards for technical accomplishments and superior performance.

PUBLICATIONS:

1. Talay, Theodore A.: An Optimal System for Soft-Landing an Unmanned Mars Entry Vehicle. MAE Thesis, Rensselaer Polytechnic Institute, January 1970.

2. Talay, T. A.; Poole, L. R.; and Whitlock C. H.: The Effect of Suspension-Line Length on Viking Parachute Inflation Loads. LWP-985, September 1970.

3. Talay, T. A.; and Poole, L. R.: The Effects of Parachute System Mass and Suspension-Line Elastic Properties on the LADT #3 Viking Parachute Inflation Loads. LWP-1021, December 30, 1971.

4. Talay, T. A.; Morris, W. D.; and Whitlock, C. H.: An Advanced Technique for the Prediction of Decelerator System Dynamics. AIAA Paper 73-460, May 1973. Also published in Journal of Spacecraft and Rockets, vol. 10, no. 12, December 1973, pp. 817-819.

5. Whitlock, C. H.; Poole, L. R.; and Talay, T. A.: Post-Flight Simulation of Parachute Deployment Dynamics of Viking Qualification Flight Tests. NASA TN D-7415, 1973.

6. Talay, T. A.: Parachute Deployment Parameter Identification Based on a Post-Flight Analytical Simulation of Viking BLDT AV-4 Test. NASA TN D-7678, August 1974.

7. Whitlock, C. H.; and Talay, T. A.: The Influence of Surface Waves on Water Circulation of the Mid-Atlantic Continental Shelf. NASA TN D-7771, 1974.

8. Talay, T. A.; and Whitlock, C. H.: Wave Modeling and Experimental Activities in the Baltimore Canyon Region. Proceedings of BLM Conference on Marine Environmental Implications of Offshore Oil and Gas Development in the Baltimore Canyon Region of the Mid-Atlantic Coast, College Park, Maryland, December 2-4, 1974.

9. Talay, T. A.: An Introduction to the Aerodynamics of Flight. NASA SP-367, 1975. (Reprinted November 1977, January 1980).

10. Talay, T. A.: Theoretical Monochromatic Wave-Induced Currents in Intermediate Water with Viscosity and Nonzero Mass Transport. NASA TM X-3312, December 1975.

11. Whitlock, C. H.; and Talay, T. A.: Remote Sensing Observations of Industrial Plumes at Hopewell, Virginia. Presented at the EPA Kepone Seminar II, Easton, Maryland, September 20-21, 1977.

12. Talay, T. A.; Sykes, K. W.; and Kuo, C. Y.: Remote Monitoring of the Gravelly Run Thermal Plume at Hopewell and the Thermal Plume at the Surry Nuclear Power Plant on the James River. Presented at the 56th Annual Meeting of the Virginia Academy of Science, Blacksburg, Virginia, May 9-12, 1978. Also NASA TM 80124, July 1979.

13. Talay, T. A.: Remote Sensing of Thermal Plume Dynamics Near the Surry Nuclear Power Station on the James River. Presented at the 57th Annual Meeting of the Virginia Academy of Science, Richmond, Virginia, May 8-11, 1979.

14. Kuo, C. Y.; and Talay, T. A.: Remote Monitoring of a Thermal Plume. NASA TM 80125, July 1979.